UPDATE OF 'AIRCRAFT WAKE VORTICES: A STATE-OF-THE-ART REVIEW OF THE UNITED STATES R&D PROGRAM'

FINAL REPORT

Contract DTRS-57-85-C-00032

June 1985

Submitted to

U. S. DEPARTMENT OF TRANSPORTATION
TRANSPORTATION SYSTEMS CENTER
KENDALL SQUARE
CAMBRIDGE, MA 02142

by

Lockheed
Missiles & Space Company, Inc.
Huntsville Engineering Center
4800 Bradford Drive, Huntsville, AL 35807

LOCKHEED MISSILES & SPACE CO.
HUNTSVILLE ENGINEERING CENTER
4800 BRADFORD DRIVE
HUNTSVILLE, AL 35807

UPDATE OF 'AIRCRAFT WAKE VORTICES: A STATE-OF-THE-ART REVIEW OF THE UNITED STATES R&D PROGRAM'

by

DR. WILLIAM R. EBERLE

FINAL REPORT

CONTRACT DTRS-57-85-C-0032

JUNE 1985

Submitted to

U. S. DEPARTMENT OF TRANSPORTATION
TRANSPORTATION SYSTEMS CENTER
KENDALL SQUARE
CAMBRIDGE, MA 02142

PREFACE

One of the primary limitations for airport capacity in the United States is the phenomenon of aircraft wake vortices. In 1977, a document which described the state-of-the-art for vortex technolgy was published by the Department of Transportation[1]. That document was a compilation of the work of most of the major contributors in the field of wake vortex technology.

Since 1977, there have been some significant advances in the state-of-the-art of wake vortex technology resulting from additional analytical work and from the results of some major experiments. The intent of this document is to rewrite selected sections of the 1977 document to bring that document up to date with the current state-of-the-art of vortex technology. Sections 3.3 (Vortex Transport) and 3.4 (Vortex Demise) of the 1977 document have been replaced with corresponding sections in this report. Section 3.3 also presents some definitions of vortex terms which have not previously been formally defined. This report adds new Sections 3.5, 3.6, and 3.7. Section 6, which describes vortex sensors has been completely rewritten to reflect advances in vortex sensor technology since 1977. Section 9 has been added to the report. It is an insert on a topic which was not addressed in the old report and is therefore not a replacement of Section 9 of the old report. References in this report are given in two formats. Number references are given for references in the 1977 version of the report. Letter references refer to literature which was not included in the 1977 report and are listed at the back of this report.

This report was originally written with the intent of republication of an entire new document, which would replace the 1977 document. Therefore, this report is currently in draft form. It is not clear if or when a new document will be published, so this document will serve as an addition to the old document until an entire new document is publihed. There has been some recent work in the measurement of wakes from helicopters, but results from those tests are not included in this report.

The author expresses his appreciation to Dr. David C. Burnham of the U. S. Department of Transportation for his assistance in identifying and locating many of the most important documents related to vortex technology over the last ten years.

[1] Hallock, J. N. and W. R. Eberle, Editors, "Aircraft Wake Vortices: A State-of-the-Art Review of the United States R&D Program," FAA-RD-77-23, U. S. Department of Transportation, Cambridge MA, February 1977.

3.3 Vortex Transport
3.3.1 Definitions
3.3.1.1 Vortex Parameter Definitions
3.3.1.2 Vortex Model Definitions and Roles
3.3.1.3 Role of Analytic and Predictive Models in a WakeVortex Avoidance System
3.3.2 Basic Equations of Vortex Transport
3.3.2.1 Vortex Descent Out of Ground Effect
3.3.2.2 Vortex Transport by Mutual Induction in Ground Effect
3.3.2.3 Vortex Transport in Uniform Crosswind
3.3.3 Dominant Mechanisms in Vortex Transport
3.3.3.1 Influence of Crosswind on the Calculated Vortex Transport Time
3.3.3.2 Influence of Aircraft Parameters on the Calculated Vortex Transport Time
3.3.3.3 Influence of Aircraft Altitude on Calculated Vortex Transport Time
3.3.3.4 Effect of Vortex Decay
3.3.4 Secondary Vortex Transport Effects
3.3.4.1 Wind Shear Effect on Vortex Transport
3.3.4.2 Vortex Buoyancy
3.3.4.3 Comprehensive Vortex Transport Model
3.3.4.4 Comprehensive Vortex Transport Model Verification
3.3.5 Statistical Description of Vortex Transport
3.3.5.1 Background for vortex Statistics
3.3.5.2 Statistical Vortex Transport Data
3.4 Vortex Demise
3.4.1 Dissipative Wake Vortex Decay
3.4.2 Core-Bursting
3.4.3 Crow Instability
3.4.4 Statistical Model of Vortex Demise
3.4.5 Statistical Description of Vortex Demise
3.5 Meteorological Variability
3.6 Summary of Vortex Meteorological Effects

3.7 Recommendations for Future Work
3.7.1 Varying Altitude Considerations
3.7.2 Vortex Tilting
3.7.3 Statistical Distribution of Vortex Residence Time
3.7.4 Residence Time Prediction

6. VORTEX SENSORS
6.1 General Sensor Requirements
6.2 Sensor Characteristics
6.3 Description of Wake Vortex Sensors
6.3.1 Mechanical Techniques
6.3.1.1 Wind Sensors
6.3.1.2 Pressure Sensors
6.3.2 Acoustic Sensors
6.3.2.1 Active Acoustic Sensors
6.3.2.2 Doppler Acoustic Vortex Sensing System
6.3.2.3 Monostatic Acoustic Vortex Sensing System
6.3.2.4 Pulsed Acoustic Vortex Sensing System
6.3.3 Optical Techniques
6.3.3.1 Passive Optical Techniques
6.3.3.2 Scanning Laser Doppler Velocimter System
6.3.3.2.1 SLDVS Historical Development
6.3.3.2.2 SLDVS Vortex Measurement Experience
6.3.3.2.3 SLDVS Hardware Description
6.3.3.2.4 SLDVS Data
6.3.4 Electromagnetic Techniques
6.3.5 Combination Techniques
6.3.6 Future Sensor Development
6.4 Airborne Wake Vortex Detection

9. MATHEMATICAL AND STATISTICAL METHODS APPLICABLE TO VORTEX TECHNOLOGY
9.1 Statistics of Extreme Values
9.2 Kalman Filtering

3.3 VORTEX TRANSPORT

Vortex transport is the process by which each vortex moves in the vertical plane after vortex roll-up has been completed. Vortex transport is dominated by the effect of crosswind and by the mutual effect of each vortex upon the other vortex of the pair. The vortex transport process may be viewed as a deterministic phenomenon with a significant random component superimposed on the deterministic phenomenon. Accordingly, this description of vortex transport is organized to show both the deterministic aspect and the probabilistic aspect of vortex transport.

The understanding of vortex transport and vortex demise requires the definition of several terms. These definitions are presented first along with a definition of classes of vortex transport models and their roles in a Wake Vortex Avoidance System.

For the description of vortex transport, generalized deterministic vortex transport equations are presented first. The equations are presented as a set of differential equations which must be integrated numerically to yield vortex trajectories as functions of time. However, for a uniform crosswind, the numerical integration may be eliminated. Therefore, vortex transport in a uniform crosswind is presented next. The model for vortex transport in a uniform crosswind permits the characterization of vortex transport characteristics as functions of selected independent parameters, and a section which describes some of these characteristics is presented next. The reader who is primarily interested in vortex transport characteristics rather than the theory of vortex transport may wish to skip directly to that section. However, such readers are cautioned that the results presented cannot be thoroughly understood without an understanding of the theory by which those results are derived.

The probabilistic aspects of vortex transport are primarily related to pehnomena which may be described qualitatively, but for which good quantitative agreement between the mathematical models describing these phenomena and available experimental data has been difficult to achieve. Phenomenological descriptions and mathematical models for these phenomena have been formulated and are presented. An understanding of these phenomena is important for understanding the meteorological conditions under which long vortex residence times may occur.

Because vortex transport is a random phenomenon, an approach to the statistical description of vortex transport is presented. The approach presented is a classical statistical approach. In an operational environment, the statistics of extreme values will probably be useful for the description of vortex behavior. The statistics of extreme values is described in Section . However, it has not yet been directly applied to vortex behavior.

3.3.1 Definitions

3.3.1.1 Vortex Parameter Definitions

The definition of several terms is deemed appropriate for the clear understanding of the principles discussed in this report.

3.3.1.1.1 Vortex-Protected Corridor

If there is no vortex in a region near the ILS (i.e., the nominal trajectory used by landing aircraft and defined by the intersection of the localizer centerline with the glideslope centerline), there is no vortex hazard to following aircraft. The vortex-protected corridor (or vortex corridor) is defined as the airspace for which the absence of vortices is a sufficient condition for safe passage by a following aircraft. For the purposes of this report, the vortex corridor is defined as a corridor which extends 150 ft laterally on each side of the localizer centerline from the middle marker to the runway touchdown zone. The altitude of the vortex corridor extends approximately 250 ft upward from the surface. The altitude of the glide slope at the middle marker is normally approximately 200 ft. The 150-ft criterion is based upon the standard deviation of lateral aircraft position about the localizer centerline (3@ = 50 ft, Ref. A) at the middle marker and the lateral distance above which a vortex cannot significantly affect aircraft motion (ê 100ft, Ref. B). Since the primary focus of this report is vortex behavior in ground effect, vortex behavior when the aircraft is inbound from the middle marker is of primary concern.

3.3.1.1.2 Significant Times Related to Vortex Behavior

There are three significant times related to the behavior of the vortex pair. These are: (1) vortex transport time, which is the time (measured

from the time of aircraft passage) required for both vortices to be transported out of the vortex corridor; (2) vortex life time, which is the time from aircraft passage until both vortices disintegrate or decay sufficiently to be innocuous to following aircraft, regardless of the position of the vortices relative to the vortex corridor; and (3) vortex residence time, which is the time (measured from aircraft passage) during which a vortex is active in the vortex corridor.

For vortex transport, the downwind vortex almost always exits the vortex corridor before the upwind vortex. Therefore, the vortex transport time is almost always the time at which the upwind vortex exits from the vortex corridor. If the vortex disintegrates before it leaves the vortex corridor, the transport time is the time that the vortex would have left the vortex corridor if it had not disintegrated. Vortex life time is the time at which vortex demise occurs. There are three mechanisms by which vortex demise may occur. The first and second mechanisms are vortex bursting and mutual annihilation by Crow Instability (Ref.C). "Vortex disintegration is the term used for vortex demise by either of these two mechanisms because the vortex strength decreases rapidly and the vortex becomes innocuous over a relatively short period of time. The third mechanism is viscous decay by which the strength of the vortex decreases sufficiently so that it will not be hazardous to following aircraft. This usually occurs over a long period of time. "Vortex decay" is the term used for vortex demise by viscous decay. The term "vortex demise" is a general term which implies vortex disintegration or vortex decay.

Vortex residence time is the time at which vortex life in the vortex corridor ceases. It is the lesser of vortex transport time and vortex life time. The maximum transport distance is the maximum distance normal to the flight path to which either vortex is transported before vortex demise. It is especially important in the consideration of use of parallel runways.

5 In addition to the above times and distances which refer to the behavior of the vortex pair, there are several definitions which are used for a single vortex. Death time is the time at which a single vortex strength has been dissipated (either by vortex annihilation or by vortex decay) so as to be innocuous to following aircraft. Death position is the lateral position of the individual vortex at which vortex demise occurs.

3.3.1.2 Vortex Model Definitions and Roles

There are three general classes of models for describing vortex behavior. These are: (1) analytic models (deterministic and probabilistic), (2) empirical models, and (3) predictive models.

Analytic models of vortex behavior are based on the physics of fluid mechanics. Thus, analytical models may also be termed theoretical models. The degree of sophistication of various analytic models may vary. The models may be either deterministic or probabilistic. Deterministic analytic models are used primarily for research. They answer the question: "Given values for all independent parameters affecting vortex behavior, what is the behavior (i.e., values of dependent parameters) of the vortex pair?" The development and validation (by experimental means) of deterministic analytic models is extremely important. Such a model may be used for identification of the important mechanisms and parameters of vortex behavior and determination of the limit to which calculated vortex parameters will agree with actual vortex parameters. In addition, a good deterministic analytical model is required for probabilistic models and predictive models. The role of such a deterministic model in probabilistic models and predictive models is discussed in the following paragraphs.

In an operational environment, values for all of the independent parameters necessary to calculate vortex behavior may not be available. Examples are exact aircraft weight, exact aircraft position relative to the ILS, spanwise loading distribution, etc. In general, these parameters may vary from flight to flight for the same aircraft type. Therefore, the dependent vortex parameters may be determined probabilistically, depending on the probability distribution functions of the independent parameters. If the probability distribution functions of the independent parameters are known, the deterministic analytic model may be used to generate the probability distribution functions of the dependent vortex parameters.

One of the most important aspects of calculating or predicting wake behavior in the atmosphere is the uncertainty in the wind measurement caused by the difference of the wind at the point of the wind measurement at at the point at which the vortex parameters are being measured. One of the primary

factors which can make an "analytic" model probabilistic is wind uncertainty. Thus, wind uncertainty models are very important in the description of vortex behavior. Such models are discussed further in Section .

For the analytical models of vortex behavior (both deterministic and probabilistic) the values of the dependent parameters are based upon concurrent values of the independent parameters. By contrast, in this report, the term "predictive model" refers to any model which forecasts vortex behavior. The model may calculate vortex behavior based on forecast meteorological parameters or may forecast vortex behavior based on previous history of vortex behavior. It is noted that previous literature on vortex behavior (e.g., Refs. 48 and F) have used the term "predictive model" to describe vortex behavior based on concurrent values of independent parameters. However, in this report "predictive" is synonymous with forecasting. Since predictive models always imply forecasting, predictive models are always probabilistic. Future events can never be forecast with absolute certainty.

3.3.1.3 Role of Analytic and Predictive Models in a Wake Vortex Avoidance System

Both analytic models of vortex behavior (which yield calculated values of behavior) and predictive models have value in a WVAS. There are several purposes for the analytic model. First, there are many meteorological conditions for which vortex considerations do not constrain aircraft separations. An accurate analytic model allows identification of those meteorological conditions. The analytical model provides a theoretical basis for certification of spacings used. The model may be used in conjunction with empirically derived data. Certification criteria which are based on theoretical considerations and supported by empirical data have a greater credibility than criteria based on empirical data alone.

Second, in an operational WVAS, an analytic model is necessary for the selection of optimal spacing standards, based on current or forecast meteorological parameters. The Vortex Advisory System (VAS, Ref. G and discussed further in Section 9.1) allows either uniform 3-nautical-mile

spacing or 3/4/5/6-nautical-mile spacing (described in Section 1), but no intermediate spacing standards. An accurate analytic model would allow an intermediate spacing standard to be used.

Third, certification of aircraft spacing must provide protection from anomalous vortex behavior. Therefore, both theoretical and experimental approaches to vortex behavior are appropriate to identify the conditions under which extremely long vortex life can occur. An analytic model can be used to identify conditions of anomalous vortex behavior which may not be identified by experimental results alone because the anomalous conditions may not occur during the experiments.

The purpose of the predictive model in the Wake Vortex Avoidance System is to forecast wake vortex residence times and safe aircraft separation distances based on known aircraft parameters and meteorological conditions. The aircraft separation distances given by the predictive model serve to eliminate hazardous wake vortex encounters and at the same time increase the current runway capacity and minimize aircraft delays. The functional relationship of the predictive model to the overall Wake Vortex Avoidance System is sketched in Fig. 3-27. The predictive model uses prevailing weather conditions and aircraft parameters to compute and forecast the safe aircraft separation distances. Vortex sensors provide a feedback on the calculated and predicted values of wake vortex transport time and life time and serve as a check on the integrity of the system. The safe separation distance provided by the predictive model and by vortex sensors is used by air traffic controllers and pilots for maintaining safe and efficient terminal area operations. The spacing information can also serve as an important input to the ARTS-3 air traffic control system.

Since the analytic model plays a dominant role in the WVAS, it is essential that the reliability, accuracy, and operational characteristics of the analytic model be established. The purpose of this section on vortex transport is to summarize the best current understanding of vortex transport and to identify areas which require additional theoretical, analytical, or experimental work and are amenable to advances in the state-of-the-art in vortex technology by such work.

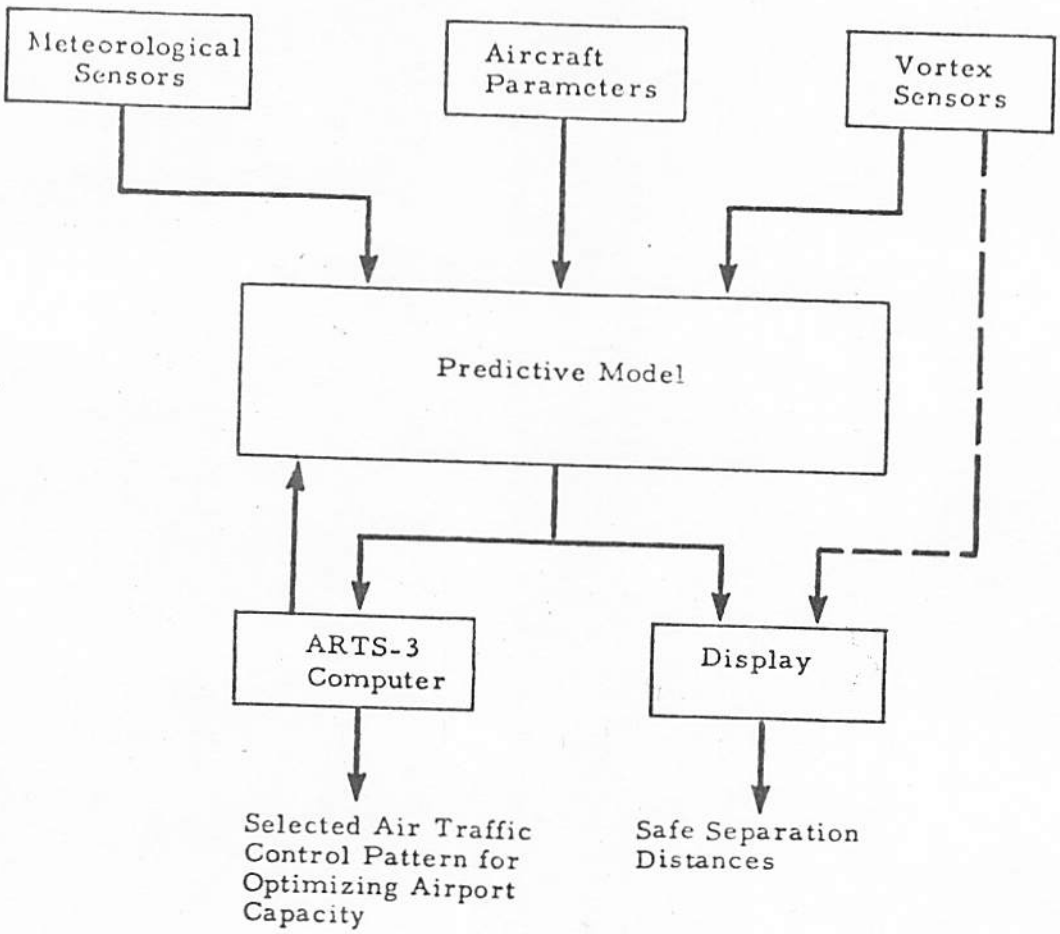

FIGURE 3-21 THE ROLE OF THE PREDICTIVE MODEL IN THE WAKE VORTEX AVOIDANCE SYSTEM

3.3.2 Basic Equations of Vortex Transport

There are two mechanisms by which a vortex pair ceases to reside in the flight corridor. The first - and most frequent - is the transport of the vortex out of the flight corridor caused by advection by the ambient wind or by interaction with the ground. The second mechanism is vortex demise by one of two catastrophic processes or vortex decay by viscous decay. After rollup is complete, viscous decay begins. The rate of decay is very slow during the first 30 to 60 seconds and accelerates thereafter. In this section it is assumed that the vortex is non-decaying (in the sense that vortex strength is constant) during the transport process. The demise of the vortex pair will be considered in the next section.

The foundation for the discussion on vortex transport is set by reviewing vortex transport out of ground effect. Then the stages of vortex development are reviewed to determine the maximum time for which the assumption of constant vortex strength is reasonable. With this background, a simple model of vortex transport is presented.

3.3.2.1 Vortex Descent Out of Ground Effect

Returning to the concepts presented in Section 3.1, a spanwise loading coefficient is defined as (cf., equation (3.23))

$$K = \frac{2}{b\Gamma_0'} \int_0^{b/2} \Gamma'(y)dy \tag{3.73}$$

Physically, K is the ratio of the actual lift for a given spanwise wing loading to the lift that would be generated with a uniform wing circulation, Γ_0'. From equations (3.20), (3.22), and (3.23),

$$L = \rho b K \Gamma_0' U_\infty \tag{3.74}$$

or

$$\Gamma_0' = \frac{W_A}{\rho b K U_\infty} = \Gamma \tag{3.75}$$

Expressed in terms of the lift coefficient (cf., equation (3.23))

$$\Gamma = C_L U_\infty \bar{c}/2K \tag{3.76}$$

and the separation distance between the two vortices is

$$b' = 2\bar{y} = Kb \tag{3.77}$$

Therefore, the vertical speed for the vortex pair is

$$\frac{dz}{dt} = -\frac{\Gamma}{2\dot{U}(2\bar{y})} = -C_L U_\infty/4\pi K^2(AR) \tag{3.78}$$

$K = \pi/4$ for an elliptically loaded wing, and $K = 0.5$ for the linear spanwise wing loading example discussed in Section 3.1. Representative values of vortex parameters for selected aircraft are shown in Table 3-2. The time, t_s, shown in Table 3-2 will be discussed later.

For the basic vortex transport calculations, the Rankine vortex model is used:

$$v(r) = \Gamma r/2\pi r_c^2 \qquad r < r_c \tag{3.79}$$

and

$$v(r) = \Gamma/2\pi r \qquad r > r_c \tag{3.80}$$

The basic assumption of vortex transport is that the transport velocity of each vortex is the velocity of the surrounding velocity field evaluated at the centroid of the vortex. The velocity field is composed of ambient wind and the velocity imposed by other vortices. Thus, equation (3.80) can be used to calculate the mutual induction of vortices upon each other if r_c is less than the separation distance between the vortices. Equation (3.78) comes from the Rankine vortex assumption. The vertical velocity of each vortex of the pair is given by the tangential velocity field of the other vortex at $r = 2\bar{y}$, the separation distance between the vortices.

TABLE 3-2. INFLUENCE OF SPANWISE LOADING ON THE INITIAL VORTEX PARAMETERS

Aircraft	Config.	U_∞ (m/sec)	C_L	K	b' (m)	$d\bar{z}/dt$ (m/sec)	t_s (sec)
B747	Takeoff	83	1.02	0.74	44.2	-1.8	195
AR = 6.96	Holding	113	0.66	0.80	47.8	-1.3	282
b = 59.7 m	Landing	75	1,23	0,70	41,8	-2,1	153
L-1011	Takeoff	85	1.07	0.78	36.8	-1.7	169
AR = 6.95	Approach	81	1.20	0.74	35.0	-2.0	134
b = 47.2 m	Landing	73	1,51	0,71	33,5	-2,5	104
DC-10	Takeoff	78	1.21	0.63	29.8	-2.8	83
AR = 6.95	Approach	74	1.20	0.62	29.3	-2.7	85
b = 47.2 m	Landing	70	1.37	0.62	29.3	-2.9	78
B-727	Takeoff	66	1.59	0.70	23.0	-2.4	77
AR = 7.20	Holding	105	0.60	0.67	22.1	-1.6	112
b = 32.9 m	Landing	64	1.64	0.67	22.1	-2.6	67

Vortex descent speed is directly proportional to vortex strength, and vortex descent speed decreases as the vortex strength decays. Therefore, before proceeding to develop the equation of vortex transport by the mutual induction of the vortex pair, vortex development is first examined to ascertain the time period for which the constant vortex strenth assumption is reasonably valid. After the wing vortex sheet has rolled up, the trailing system consists of a pair of vortices of finite rotational core area, but with a core radius a relatively small fraction of the vortex span. If the vortex pair is immersed in a still, homogeneous inviscid flow, the pair is convected downward at a velocity $\Gamma/2\pi b'$. The classical analysis shows that there is a closed recirculating mass of air, of roughly oval proportions, associated with the concentrated vortex pair, and that the cell is convected downward at a uniform speed, as given by equation (3.78). Flow exterior to the cell never enters it. Thus a long vortex pair, which may be regarded as substantially two-dimensional, will move downward in an unbounded fluid with constant velocity for all times.

In real flows, this situation does not persist indefinitely, and most experiments show that the rate of descent decreases and finally approaches zero, even out of ground effect. This is caused by diffusion of core vorticity by some combination of laminar and turbulent viscosity, and it will occur even in homogeneous (unstratified) flows. Much effort has gone into explaining and quantifying the effect, but the subject still remains controversial. A rational interpretation of the effect, coupled with careful observations, which greatly assists explanation of the effect, has been put forward by Maxworthy (ref. 40).

Maxworthy conducted experiments with vortex rings in water, using various visualization techniques to identify where the flow went. When the vorticity was relatively well distributed in the ring he observed that the outer flow was entrained into the back of the cell, causing an increase in the cell volume. At the same time a portion of the cell vorticity was shed into the wake, removing both vorticity and momentum from the cell. The combined effect was to increase the cell size and to reduce its propagation velocity.

The mechanism of mass entrainment is important for further development of the vortex transport. Figure 3-28 shows a sketch of the vortex flow field, in coordinates fixed at the core centers, so that the outer flow is represented by a uniform, but unsteady, flow from below. The cell has a well defined stagnation point, A, and over the front portion, a well defined cell boundary, A-B. Across this boundary, the pressure and velocity fields of inner and outer flows are continuous, the only discontinuity being between the inner vortical fluid and the outer irrotational flow. Because of both laminar and turbulent effects, the vorticity of the inner vortical flow is transferred to the outer flow, and as a consequence the total pressure of the flow is reduced. Thus after passing the maximum velocity point near B, the outer flow contained approximately by the stream tube, DC, is unable to recover sufficient velocity to rejoin the outer flow at the rear, but remains as part of the stationary cell. Thus, the cell size is increased. At the same time, a neighboring stream tube EF acquires a smaller amount of vorticity and suffers less pressure reduction so that it does depart from the cell at the rear, but at a lower than free stream total pressure. This portion develops into a wake behind the cell.

Thus, the same process causes entrainment of the outer flow into the cell and a detrainment (removal) of some of the cell vorticity and momentum. A further process occurs on the centerline of the cell, AX. Here vorticity is annihilated by diffusion from the left and right cells, Thus, three vorticity transfer mechanisms occur and the overall effect controls the cell dynamics.

Maxworthy showed that initially the vortex shedding to form the wake was extremely weak since the cell vorticity at the boundary was quite weak. Thus, although the cell grew in size, it did not lose momentum, and the impulse was conserved. In these circumstances, the main vorticity loss occurred along the centerline and was small, and there was minimal wake momentum loss. During the later stages in growth, when more vorticity is present near the boundary between the inner and outer flows, the wake develops. Vorticity and momentum are shed from the cell and thus the momentum in the cell decreases while the cell size increases. Both of these effects contribute to the reduction in speed and the final complete annihilation of the cell momentum for the two-dimensional vortex observed by

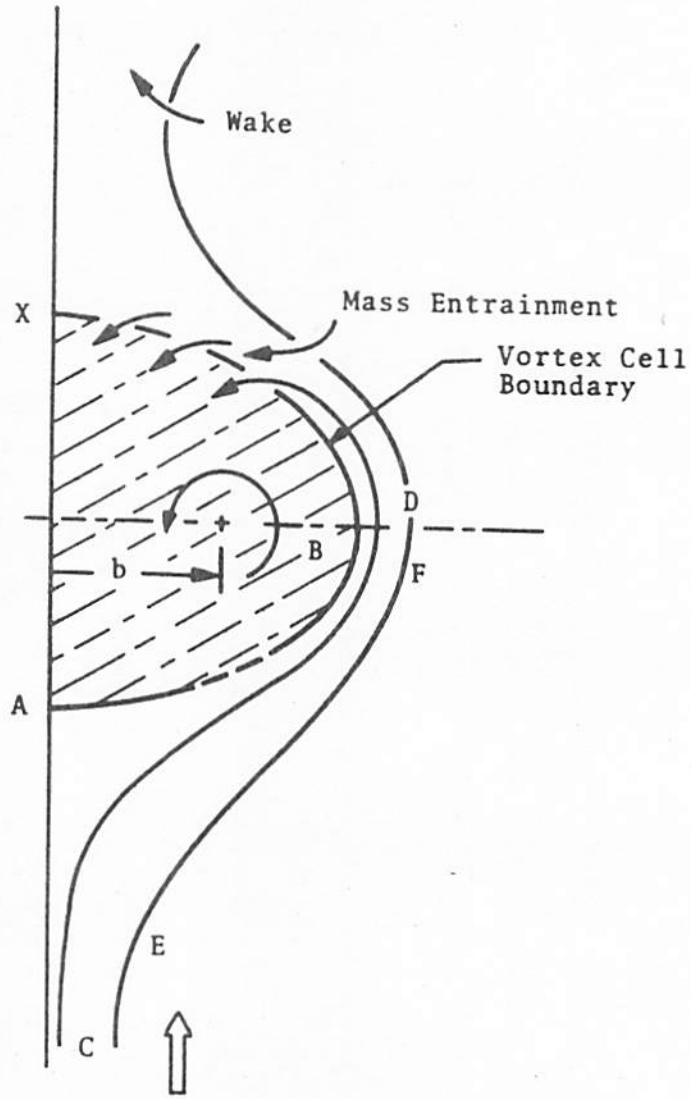

FIGURE 3-~~27~~ 28. VISCOUS EFFECTS ON VORTEX CELL

Maxworthy.. It is noted that for a three-dimensional vortex pair such as an aircraft wake, vortex annihilation caused by three-dimensional effects almost always precedes the two-dimensional vortex annihilation.

It must be noted that Maxworthy's experiments were conducted with vortex rings at extremely low Reynolds numbers for which the flow was certainly laminar. However, further unpublished flow visualization tests with finite wings also exhibited a detrained wake. These experiments were also performed at very low Reynolds numbers. It is, however, possible that during the later stages of development of an aircraft trailing vortex system that similar processes of mass entrainment and momentum detrainment occur. For laminar transfer, the time scales would be too long to be of interest, but if the transfer is assumed to be turbulent, it may be possible to account for some of the observed effects. Thus, it appears very probable that the later development of a vortex pair follows qualitatively the stages described by Maxworthy but with an additional initial stage. The three stages are postulated as shown in Figure 3-29.

Stage I - The Inviscid Cell: Here the vorticity is confined to well within the cell boundary. The cell boundary is defined as the streamline between the flow which remains with the vortex pair and that which remains with the ambient air. On the boundary itself there will be no laminar mass or momentum transfer (since there is no distortion), and turbulent transfer will have no net effect since both inner and outer flow have the same total pressure. In these circumstances, the core size is less than the cell size and the inviscid cell model will be a good representation of the dynamics. The time rates of change of cell size and vortex strength are zero; the propagation velocity, dz/dt, is constant.

Since the inviscid cell model (equation (3.58)) is the basic model to be used in the model for vortex transport in ground effect, it is important to make an approximation of the time for which the inviscid cell model is valid. Experimental measurements (refs. 19 and 41) indicate that the vortex core grows because of turbulent diffusion at the core boundary and can be predicted from Lamb's turbulent vortex model for the core growth as

$$r_c(t) = [r_c^2(0) + 5.04t\nu_T]^{1/2} \qquad (3.81)$$

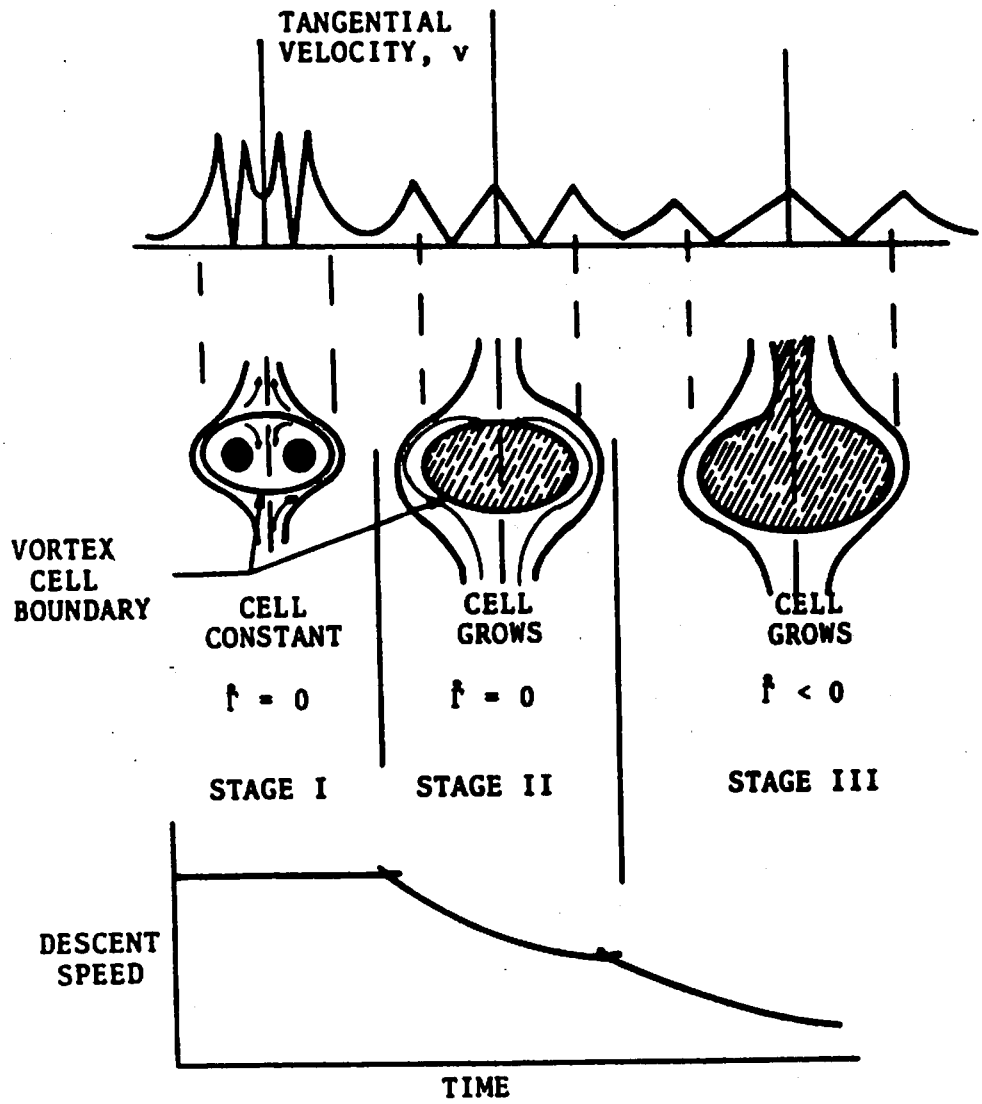

FIGURE 3-~~28~~ 29. VORTEX CELL STAGES

15

where $r_c(0)$ is the initial core radius and ν_T is the turbulent eddy kinematic viscosity. It follows that the time required for the core to grow sufficiently such that the cores overlap each other and vorticity detrainment is initiated is

$$t_s = \frac{\left(\frac{b'(t)}{2}\right)^2 - r_c^2(0)}{5.04\nu_T} \tag{3.82}$$

This expression can be reduced further using equations (3.76) and (3.77) and the empirical expressions relating the eddy kinematic viscosity coefficient and initial vortex core radius, $a_1 = \nu_T/\Gamma$, and $a_2 = r_c(0)/\bar{c}$ to obtain

$$t_s = \frac{K^3 b\,(AR)}{10.08 a_1 C_L U_\infty}\left[1-\left(\frac{2a_2}{K\,(AR)}\right)^2\right] \tag{3.83}$$

The parameter a_1 is approximately 10^{-3} based on model tests (ref. 41) and is an order of magnitude smaller for flight test measurements where the effects of atmospheric turbulence are present (ref. 19). The initial vortex core radius parameter, a_2, is a function of aircraft characteristics. For example, measurements conducted using the C-5A indicate that $a_2 \simeq 0.1$ and 0.2 for flaps-up and flaps-down flight configurations, respectively (ref. 19). For the DC-9, a_2 also ranges from 0.1 to 0.2 but appears to be independent of the flap setting (ref. 37).

The relationship given by equation (3.83) demonstrates that the constant initial wake vortex sink rate given earlier in equation (3.78) is valid up to a time t_s which is determined largely from aircraft parameters. The onset of the wake vortex slow down process has been calculated from equation (3.83) for representative aircraft assuming the constants $a_1 = 10^{-3}$ and $a_2 = 0.1$ in the holding configuration, and $a_2 = 0.2$ in the approach, takeoff, and landing configurations. The results are presented in the last column in Table 3-2 shown earlier. A significant variation can be noted in the predicted onset of the wake decay process which ranges from approximately 100 to 300 seconds in the holding

configuration and 80 to 200 seconds in the landing, takeoff, and approach configurations for the aircraft considered. The times are sufficiently long so that vortex strength may be considered to be constant for the transport process. However, if the vortex persists in the flight corridor for times greater than t_s in Table 3-2, vorticity decay must be included in any consideration of vortex transport past t_s.

Stage II- The Entraining Cell: As the core vorticity diffuses and approaches the cell boundary, the first process (of mass entrainment) occurs, and the cell grows; Γ = 0. The propagation velocity reduces slightly from the inviscid value because of greater vortex separation resulting from cell growth.

Stage III- The Decaying Cell: During the later stages, substantial mass entrainment and momentum and vorticity shedding occur, causing a wake to develop behind the vortex pair. Of course, various catastrophic instabilities usually develop before the complete decay has occurred.

This discussion has shown that vortex strength can be considered to be relatively constant for a significant period of time after aircraft passage. The next section presents the vortex transport equations in ground effect for a constant vortex strength.

3.3.2.2 Vortex Transport by Mutual Induction in Ground Effect

The primary mechanism of vortex transport is mutual induction--vortex motion caused by each vortex being immersed in the velocity field of the other vortex. The ground effect is included by "image vortices" as shown in Fig. 3-30. The image vortices are imaginary vortices whose presence creates the same effect as the ground plane (i.e., no mass transport across the ground plane), thereby obviating the need to otherwise model the ground plane.

The notation adopted is that Γ_1, Γ_2, Γ_3, and Γ_4 are the circulations of the vortices and (Y_1, Z_1), (Y_2, Z_2), . . . are the spatial coordinates of the vortices. The cross runway freestream velocity

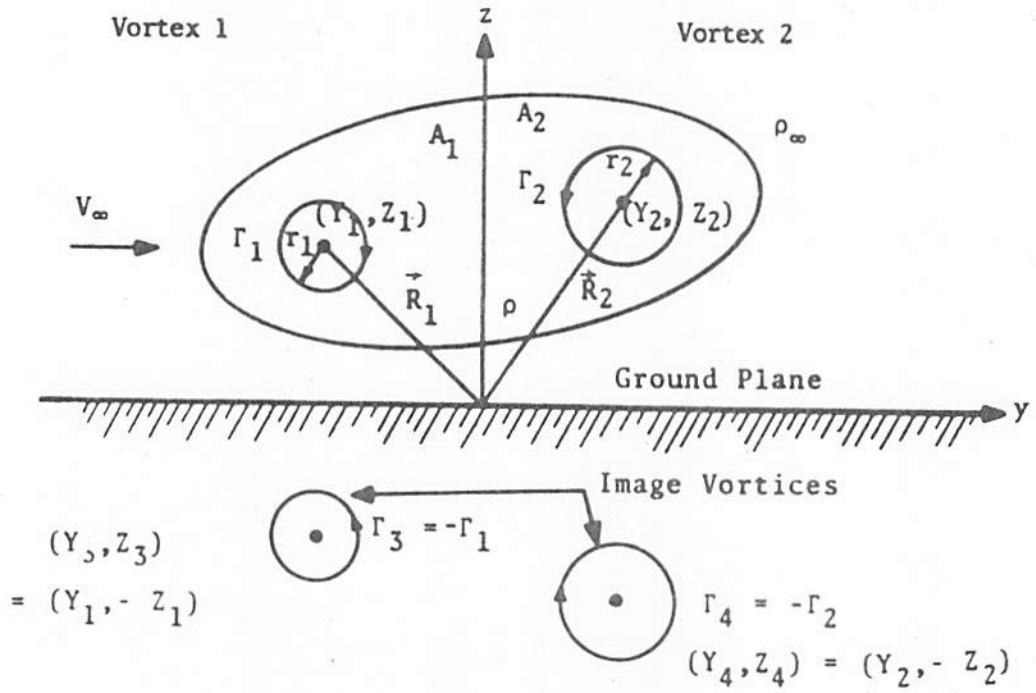

FIGURE 3-~~29~~ 30. GEOMETRY OF THE PREDICTIVE WAKE VORTEX TRANSPORT MODEL

component is V_∞. The coordinate system is a right-hand coordinate system with the positive x-axis out of the plane of the paper. Therefore Γ_1 is negative, and Γ_2 is positive.

By definition, for the image vortices

$$\Gamma_3 = -\Gamma_1 \tag{3.84}$$

$$\Gamma_4 = -\Gamma_2 \tag{3.85}$$

$$Z_3 = -Z_1 \tag{3.86}$$

$$Y_3 = Y_1 \tag{3.87}$$

$$Z_4 = -Z_2 \tag{3.88}$$

$$Y_4 = Y_2 \tag{3.89}$$

The advection of each vortex is caused by each vortex being immersed in the velocity field of the other vortices. Let V and W be the velocity components in the vortex field in the y and z directions, respectively. Both V and W are functions of position in the velocity field. The contribution to the velocity field by each vortex is given by the Rankine model (equation (3.79)). The velocity field at any point is given by the sums of the velocity fields of the individual vortices. A vortex does not contribute to the velocity field at its centroid. The contribution to the velocity field at the centroid of vortex 1 by vortex 3 is

$$V = \frac{-\Gamma_3}{2\pi(Z_1-Z_1)} = \frac{\Gamma_1}{4\pi Z_1} \tag{3.90}$$

$$W = 0 \tag{3.91}$$

The contribution to the velocity field at the centroid of vortex 1 by vortex 2 is

$$V = \left[\frac{\Gamma_2}{2\pi[(Z_2-Z_1)^2+(Y_2-Y_1)^2]^{1/2}}\right]\left[\frac{Z_2-Z_1}{[(Z_2-Z_1)^2+(Y_2-Y_1)^2]^{1/2}}\right] \tag{3.92}$$

The term in the first set of brackets is the tangential velocity (cf., equation (3.79)), and the term in the second set of brackets is the cosine of the angle between the tangential velocity and the positive y-axis. Similarly,

$$W = \left[\frac{\Gamma_2}{2\pi[(Z_2-Z_1)^2+(Y_2-Y_1)^2]^{1/2}}\right]\left[\frac{-(Y_2-Y_1)}{[(Z_2-Z_1)^2+(Y_2-Y_1)^2]^{1/2}}\right] \qquad (3.93)$$

The term in the first set of brackets is the tangential velocity and the term in the second set of brackets is the cosine of the angle between the tangential velocity and the positive z-axis. Similarly, the contribution to the velocity field at vortex 1 by vortex 4 (remembering $Y_4 = Y_2$ and $Z_4 = -Z_2$ and $\Gamma_4 = -\Gamma_2$) is

$$V = \left[\frac{-\Gamma_2}{2\pi[(Z_2+Z_1)^2+(Y_2-Y_1)^2]^{1/2}}\right]\left[\frac{-(Z_2+Z_1)}{[(Z_2+Z_1)^2+(Y_2-Y_1)^2]^{1/2}}\right] \qquad (3.94)$$

and

$$W = \left[\frac{-\Gamma_2}{2\pi[(Z_2+Z_1)^2+(Y_2-Y_1)^2]^{1/2}}\right]\left[\frac{(Y_2-Y_1)}{[(Z_2+Z_1)^2+(Y_2-Y_1)^2]^{1/2}}\right] \qquad (3.95)$$

Therefore, the total horizontal component of the induced velocity field at the centroid of vortex 1 is obtained by summing equations (3.90), (3.92), and (3.94), or

$$V_1(Y_1,Z_1) = \frac{\Gamma_1}{4\pi Z_1} + \frac{\Gamma_2}{2\pi}\left[\frac{Z_2-Z_1}{(Z_2-Z_1)^2+(Y_2-Y_1)^2} + \frac{Z_2+Z_1}{(Z_2+Z_1)^2+(Y_2-Y_1)^2}\right] \qquad (3.96)$$

and the total vertical component of the induced velocity field at the centroid of vortex 1 is the sum of equations (3.91), (3.93), and (3.95), or

$$W_1(Y_1,Z_1) = \frac{\Gamma_2}{2\pi}\left[\frac{-(Y_2-Y_1)}{(Z_2-Z_1)^2+(Y_2-Y_1)^2} + \frac{Y_2-Y_1}{(Z_2+Z_1)^2+(Y_2-Y_1)^2}\right] \qquad (3.97)$$

Similarly, for the velocity field at the centroid of vortex 2,

$$V_2(Y_2,Z_2) = \frac{\Gamma_2}{4\pi Z_2} + \frac{\Gamma_1}{2\pi}\left[\frac{Z_2+Z_1}{(Z_2+Z_1)^2+(Y_2-Y_1)^2} - \frac{Z_2-Z_1}{(Z_2-Z_1)^2+(Y_2-Y_1)^2}\right] \quad (3.98)$$

and

$$W_2(Y_2,Z_2) = \frac{\Gamma_1}{2\pi}\left[\frac{Y_2-Y_1}{(Z_2-Z_1)^2+(Y_2-Y_1)^2} - \frac{Y_2-Y_1}{(Z_2+Z_1)^2+(Y_2-Y_1)^2}\right] \quad (3.99)$$

When the effect of free stream crosswind is added,

$$\dot{Y}_1 = V_1(Y_1,Z_1) + V_\infty \quad (3.100)$$

$$\dot{Z}_1 = W_1(Y_1,Z_1) \quad (3.101)$$

$$\dot{Y}_2 = V_2(Y_2,Z_2) + V_\infty \quad (3.102)$$

$$\dot{Z}_2 = W_2(Y_2,Z_2) \quad (3.103)$$

It is noted that V_∞ may be a function of altitude. The vortex trajectories are obtained by integrating equations (3.100) through (3.103) with the initial values of the coordinates being the coordinates at which the roll-up process is completed. The integration forms the basic wake vortex transport predictive model. In the basic model, equations (3.100) through (3.103) are integrated using a fourth-order Runge-Kutta technique to determine vortex position as a function of time.

3.3.2.3 Vortex Transport in Uniform Crosswind

If the free stream crosswind, V_i, is uniform, the differential equations presented above can be integrated, and significant characteristics of vortex transport can be obtained. In the absence of wind shear, the vortices are of equal strength and descend together. Thus

$$\Gamma_2 = -\Gamma_1 = \Gamma \quad (3.104)$$

and

$$Z_2 = Z_1 = Z \tag{3.105}$$

Therefore,

$$\dot{Z}_1 = \dot{Z}_2 = \frac{-\Gamma}{2\pi(Y_2-Y_1)} + \frac{\Gamma}{2\pi}\left[\frac{Y_2-Y_1}{(2Z)^2+(Y_2-Y_1)^2}\right] \tag{3.106}$$

or by multiplying the numerator and denominator of the first term by $[(2Z)^2+(Y_2-Y_1)^2]$ and rearranging gives

$$\dot{Z}_1 = \dot{Z}_2 = \frac{-\Gamma}{2\pi(Y_2-Y_1)}\left[\frac{(2Z)^2}{(2Z)^2+(Y_2-Y_1)^2}\right] \tag{3.107}$$

The downward velocity goes to zero as Z goes to zero (i.e., near the ground), and equation (3.107) becomes the classic equation for vortex descent out of ground effect (equation (3.78)) as Z becomes large. Similarly, the horizontal component of vortex motion is

$$\dot{Y}_1 = V_\infty - \frac{\Gamma}{4\pi Z}\left[\frac{(Y_2-Y_1)^2}{(2Z)^2+(Y_2-Y_1)^2}\right] \tag{3.108}$$

$$\dot{Y}_2 = V_\infty + \left[\frac{\Gamma}{4\pi Z}\,\frac{(Y_2-Y_1)^2}{(2Z)^2+(Y_2-Y_1)^2}\right] \tag{3.109}$$

Y_1 and Y_2 approach V_∞ as altitude, Z, becomes large, indicating horizontal transport by the ambient wind for large altitude. These equations also show the phenomenon of vortices stalling in the flight corridor and permit the calculation of the crosswind which will cause stalling, as described below.

It has been observed that vortices tend to descend to an altitude of one half of their initial separation distance, b'. Near the ground, the vortices tend to separate, so that

$$(Y_2-Y_1)^2 >> (2Z)^2 \tag{3.110}$$

The vortex can be expected to stall in the flight corridor (i.e., $\dot{Y}_1 = 0$ or $\dot{Y}_2 = 0$) if

$$V_\infty \simeq \pm \frac{\Gamma}{-4\pi Z} = \pm \frac{\Gamma}{2\pi b'} \tag{3.111}$$

The vortex can be expected to stall in the flight corridor if the crosswind is approximately equal to the initial descent speed.

In the absence of a crosswind (i.e., $V_\infty = 0$), the vortex tranjectory is a hyperbola. In this condition, the vortex descent is symmetric with respect to a vertical plane. Hence,

$$Y_2 = -Y_1 = Y \tag{3.112}$$

From equations (3.107) and (3.109)

$$\dot{Y}/\dot{Z} = -(2Y)^3/(2Z)^3 \tag{3.113}$$

or

$$dZ/Z^3 = -dY/Y^3 \tag{3.114}$$

and hence,

$$1/Y^2 + 1/Z^2 = \text{Constant} = C \tag{3.115}$$

which is the equation of the hyperbola representing the vortex trajectory in the absence of a crosswind.

This result can be used to calculate the time for which a vortex remains in a flight corridor of width $2y_b$ for a constant crosswind. The coordinate system is referenced to the wind with the origin in the y-direction taken as the aircraft axis at the time of aircraft passage. The origin coincides with the runway centerline at the time of aircraft passage. This coordinate system is shown in Fig. 3-31(a). Since the coordinate system is fixed on the wind, the crosswind is zero relative to the coordinate system. From equations (3.109) and (3.112)

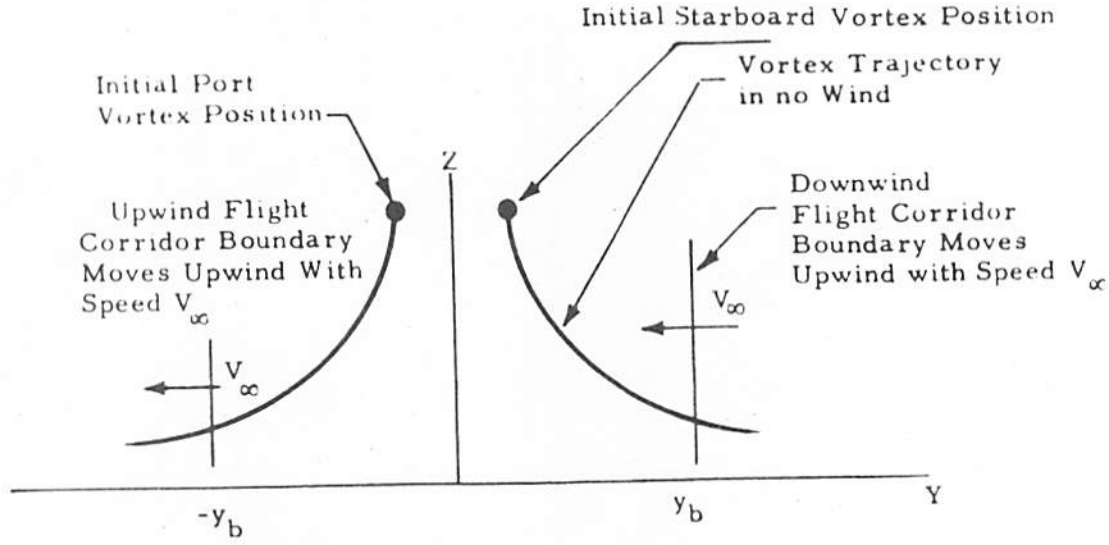

(a) Initial Vortex Geometry

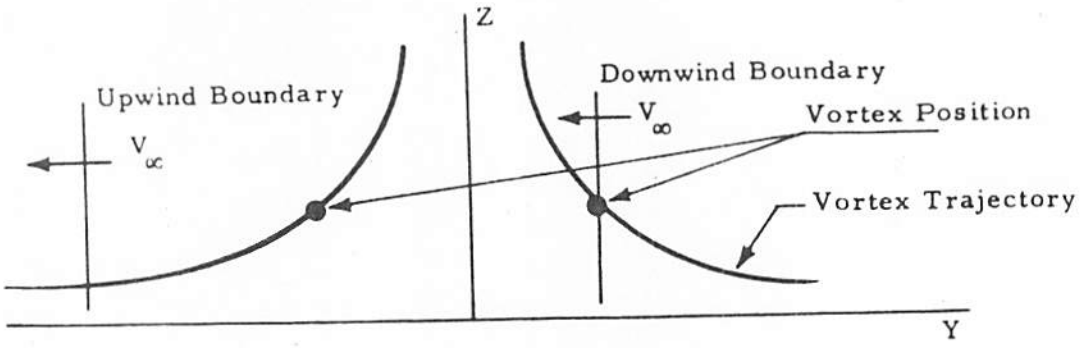

(b) Vortex Geometry at Time Downwind Vortex Leaves Flight Corridor

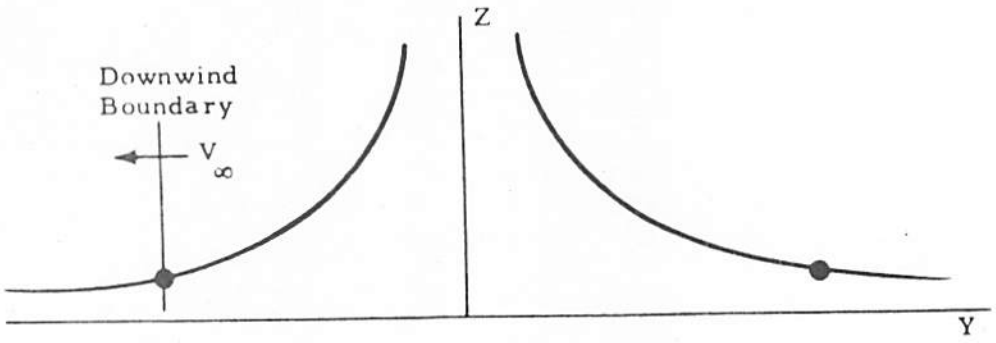

(c) Vortex Geometry at Time Upwind Vortex Leaves Flight Corridor

FIGURE 3-31. VORTEX GEOMETRY FOR VORTEX TRANSPORT TIME CALCULATION (Coordinate System is Fixed Relative to the Wind)

24

$$\dot{Y} = \frac{\Gamma}{4\pi Z}\left[\frac{Y^2}{Z^2+Y^2}\right] \tag{3.116}$$

Using equation (3.115) for Z,

$$\dot{Y} = \frac{\Gamma}{4\pi C}\left[\frac{CY^2-1}{Y^2}\right]^{3/2} \tag{3.117}$$

Where the value of C is calculated from equation (3.115) using the initial values of Y and Z (e.g., Y= b'/2 and Z = aircraft altitude). Integrating equation (3.117) gives

$$t+D = \frac{4\pi}{\Gamma C}\left[\frac{CY^2-2}{(CY^2-1)^{1/2}}\right] \tag{3.118}$$

where D is the constant of integration determined by Y = b'/2 at t = 0. If the lateral boundaries of the flight corridor are at $\pm Y$ at t = 0, at later time, t, the boundaries of the flight corridor (referenced to the wind-based coordinate system) are at

$$Y = -V_\infty t \pm y_b \,. \tag{3.119}$$

with a + or - denoting downwind or upwind flight corridor boundaries, respectively. Inserting equation (3.119) in (3.118)

$$\frac{(\pm y_b - Y)}{V_\infty} + D = \frac{4\pi}{\Gamma C}\left[\frac{CY^2-2}{(CY^2-1)^{1/2}}\right] \tag{3.120}$$

Let

$$F(Y) = \frac{4\pi}{\Gamma C}\left[\frac{CY^2-2}{(CY^2-1)^{1/2}}\right] - D + \frac{Y \mp y_b}{V_i} \tag{3.121}$$

Physically, F(Y) is the difference in the time at which the vortex reaches position Y and the time at which the boundary reaches position Y. Thus, the vortex is at the flight corridor boundary when F(Y) = 0. The various

solutions of the value of Y at which F(Y) = 0 are found by starting with Y é b'/2 as the initial solutions and performing a Newton iteration on equation (3.121). Once a value of Y is determined from the numerical solution of equation (3.121) for Y, the transport time may be determined directly by solving equation (3.119) for t. For the downwind vortex (Y > 0) and downwind boundary, there is only one solution. For the upwind vortex (Y < 0) crossing the upwind boundary, a solution may or may not exist (depending upon the magnitude of V_∞). Care must be taken when considering the upwind vortex crossing the downwind boundary; depending upon the magnitude of V_∞ either one solution exists or (for small V_∞) no solutions or two solutions exist.

In order to understand the dominant mechanisms of vortex transport, it is instructive to examine the conditions under which various solutions to equation (3.121) exist. Physically, it is desired to determine the conditions under which each of the vortices will exit from each of the vortex corridor boundaries.

For the downwind vortex (Y > 0) and downwind boundary (top sign on y_b), the definition of D in equation (3.118) for the initial condition (Y = b'/2 at t = 0) gives for t = 0

$$F(b'/2) = (b'/2-y_b)/V_\infty < 0 \qquad (3.122)$$

assuming that the vortex corridor width exceeds the vortex separation distance. As Y becomes large ($CY^2 >> 1$),

$$F(Y) \simeq \frac{4\pi}{\Gamma C}\sqrt{CY^2} + \frac{Y}{Y_\infty} > 0 \qquad (3.123)$$

There is, therefore, one solution of the downwind vortex crossing the downwind vortex corridor boundary (i.e., F(Y) = 0). The vortex geometry for this solution is shown in Fig. 3-31(b). This solution can be determined from Newton iteration on equation (3.121) with the initial "solution" being Y = b'/2. The transport time may be calculated with the solution value of Y by using Equation (3.118) or (3.119). By substituting the lower sign of

y_b for the upwind boundary, it may be shown mathematically (as well as from physical reasoning) that the downwind vortex cannot cross the upwind boundary.

For the upwind vortex ($Y < 0$) crossing the upwind boundary, the initial condition gives

$$F(-b'/2) = \frac{-b'/2+y_b}{V_\infty} > 0 \tag{3.124}$$

For large values of Y,

$$F(Y) \approx \frac{4\pi}{\Gamma C}\sqrt{CY^2} + \frac{Y}{V_\infty} = \frac{4\pi}{\Gamma\sqrt{C}}Y + \frac{Y}{V_\infty} \tag{3.125}$$

Therefore, since $Y < 0$,

$$F(Y) > 0 \quad \text{if} \quad V_\infty > \Gamma\sqrt{C}/4\pi \tag{3.126}$$

and

$$F(Y) < 0 \quad \text{if} \quad V_\infty < \Gamma\sqrt{C}/4\pi \tag{3.127}$$

for large values of Y. Therefore, if

$$V_\infty > \Gamma\sqrt{C}/4\pi \tag{3.128}$$

a solution to equation (3.121) does not exist, and the upwind vortex does not cross the upwind boundary. If

$$V_\infty < \Gamma\sqrt{C}/4\pi \tag{3.129}$$

the upwind vortex crosses the upwind boundary (cf. Fig. 3-31(c)). The value of Y may be determined by Newton interation on equation (3.121). The initial value of Y should be a negative value of about five wingspans.

For the condition of the upwind vortex crossing the downwind boundary,

$$F(-b'/2) = \frac{-b'/2-y_b}{V_\infty} < 0 \tag{3.130}$$

Similarly, for large absolute values of Y

$$F(Y) > 0 \quad \text{if} \quad V_\infty > \Gamma\sqrt{C}/4\pi \tag{3.131}$$

and

$$F(Y) < 0 \quad \text{if} \quad V_\infty < \Gamma\sqrt{C}/4\pi \tag{3.132}$$

If

$$V_\infty > \Gamma\sqrt{C}/4\pi \tag{3.133}$$

one solution exists and may be found by Newton interation on equation (3.121) beginning with Y = -b'/2. If

$$V_\infty < \Gamma\sqrt{C}/4\pi \tag{3.134}$$

either no solution or two solutions exist. It is necessary to determine if F(Y) is positive for any values of Y. The maximum value of F(Y) occurs when F'(Y) = 0. This occurs when

$$Y^2 = \frac{1}{C-[4\pi CV_\infty/\Gamma]^{2/3}} \tag{3.135}$$

Solving for F(Y) with this value of Y (denoted by Y_m) yields the number of times the upwind vortex crosses the downwind boundary. If

$$V_\infty < \Gamma\sqrt{C}/4\pi \tag{3.136}$$

and

$$F(Y_m) < 0 \tag{3.137}$$

there is no solution. Physically, the upwind vortex approaches the downwind boundary, but is transported upwind by its image vortex before it crosses the boundary. If

$$V_\infty < \Gamma\sqrt{C}/4\pi \tag{3.138}$$

and

$$F(Y_m) > 0 \tag{3.139}$$

two solutions exist. Physically, the upwind vortex crosses the downwind boundary, but is then transported upwind by its image vortex and reenters the vortex corridor through the downwind boundary. The values of Y for which the boundary crossings occur may be calculated by solving equation (3.121).

It is noted that the upwind vortex always remains in the vortex corridor longer than the downwind vortex. Therefore, the maximum vortex transport time is given by the upwind vortex crossing the downwind boundary if

$$V_\infty > \Gamma\sqrt{C}/4\pi \tag{3.140}$$

and by the upwind vortex crossing the upwind boundary if

$$V_\infty < \Gamma\sqrt{C}/4\pi \tag{3.141}$$

3.3.3 Dominant Mechanisms in the Vortex Transport Model

The general vortex transport model is an analytic tool which determines the lateral and vertical displacement of each vortex of the trailing vortex pair as a function of time for specified values of aircraft parameters and a given crosswind profile. An important output from the vortex transport model is the calculated vortex transport time, which is defined as the time after aircraft passage at which both vortices have been transported outside the corridor defined by boundaries ±150 ft from the runway centerline. Since it has been shown that vortices located outside the ±150 ft corridor do not pose a threat to following aircraft (cf. Section 1.2.1), the calculated vortex transport time is an indication of the safe separation time calculated for the aircraft type and prevailing meteorological parameters. Therefore, for an operational WVAS it is important to determine

the sensitivity of the calculated vortex transport time to variations in crosswind characteristics and aircraft parameters. The model presented above for vortex transport in a uniform crosswind is an excellent approach for such sensitivity calculations because it permits rapid calculation of transport time without the need for numerical integration.

The vortex transport model assumes a constant vortex strength, Γ, and assumes that the altitudes of the port and starboard vortices are equal. The vortex transport equations are (equations (3.107) through (3.109))

$$\dot{Z} = \frac{-\Gamma}{2\pi(Y_2-Y_1)} + \frac{\Gamma}{2\pi}\left[\frac{Y_2-Y_1}{(2Z)^2+(Y_2-Y_1)^2}\right] \tag{3.142}$$

and

$$\dot{Y} = V_\infty \simeq \frac{\Gamma}{4\pi Z}\left[\frac{(Y_2-Y_1)^{2_1}}{(2Z)^2+(Y_2-Y_1)^2}\right] \tag{3.143}$$

where

$$\Gamma = \frac{W_A}{\rho b K U_\infty} \tag{3.144}$$

where

Z = vortex altitude
Γ = vortex strength
Y_1 = port vortex lateral position
Y_2 = starboard vortex lateral position
V_i = crosswind
W_A = aircraft weight
ρ = air density
b = aircraft wing span
K = aircraft spanwise loading coefficient

and

U_∞ = aircraft airspeed.

Physically, the spanwise loading coefficient is the ratio of lift generated by the wing to the lift which would be generated if the wind loading (lift per unit span of the wing) were uniform at the value of spanwise loading at the wing root. The wing loading is proportional to the bound circulation, $\Gamma'(y)$, of the wing. The spanwise loading coefficient is

$$K = \frac{2}{b\Gamma_0'} \int_0^{b/2} \Gamma'(y)dy \qquad (3.145)$$

where

$\Gamma'(y)$ = bound circulation on the wind, and

Γ_0' = bound circulation at the wing root

For elliptically loaded wings,

$$K = \pi/4 \qquad (3.146)$$

which is the assumption made for calculated values of vortex parameters in this report.

Detailed derivations of equations (3.144) through (3.146) are presented in Section 3.1 of this report. (TO BE COPIED FROM SECTION 5.2 OF REF. L)

In order to understand the vortex transport phenomenon and in order to determine the effect of the more important parameters which affect vortex transport, it is instructive to examine the results of the vortex transport model for selected sets of independent parameters and to determine the sensitivity of vortex transport time to these selected independent parameters. Accordingly, the following paragraphs examine the sensitivity of the model to the basic input parameters including crosswind characteristics (crosswind as a function of altitude) and aircraft parameters (aircraft type, landing weight, altitude, and aircraft position relative to the ILS).

3.3.3.1 Influence of Crosswind on the Calculated Vortex Transport Time

The general vortex transport model developed above allows for variation of crosswind with altitude, and a transport model for uniform crosswind was developed from that. However, even for the uniform crosswind model, the

variation of crosswind with altitude is of significant concern. It can be shown that the most important crosswind value is the crosswind at the altitude which the vortex approaches asymptotically during its transport. This altitude is half of the initial vortex separation distance. Therefore, the difference between the wind at the altitude of crosswind anemometer and the asymptotic altitude of the vortex is of some concern, even when the uniform crosswind vortex transport model is used.

The calculated vortex transport time as a function of crosswind (defined as the wind vector component which is normal to the runway direction) is shown in Figs. 3-32, 3-33, and 3-34 for uniform, power law, and logarithmic crosswind profiles. The nominal values of aircraft parameters shown in Table 3-2 were used for calculation of the transport times. For low values of crosswind (< 4 ft/sec), the upwind and downwind vortices exit from the upwind and downwind vortex corridor boundaries, respectively. For high values of crosswind, both vortices exit from the downwind boundary. It is noted that the upwind vortex always leaves the vortex corridor later than the downwind vortex. Therefore, the vortex transport time can be calculated from the motion of the upwind vortex.

The calculated value of vortex transport time is shown as a function of crosswind at the reference altitude, $V_{z\ ref}$, and exponent, p, for a power-law profile in Fig. 3-33. The 20-ft altitude is used as the reference since available measurements are generally made at this altitude. The power-law exponents ranging from 0.1 to 0.4 are representative of the wind profiles observed during unstable to moderately stable atmospheric conditions. The power-law profile was chosen as the basic profile for use in this study because a previous study (ref. 49) showed that vortex trajectories calculated with the power-law wind profile matched measured vortex trajectories better than trajectories calculated with other profiles.

The curves in Fig. 3-33 appear to indicate a sensitivity of the vortex transport time to the 20-ft crosswind and to the value of the power-law exponents. However, a closer examination of the phenomenon reveals that the transport time is not sensitive to the shape of the wind profile, per se, but is sensitive to the value of the crosswind at an altitude higher than 20 ft.

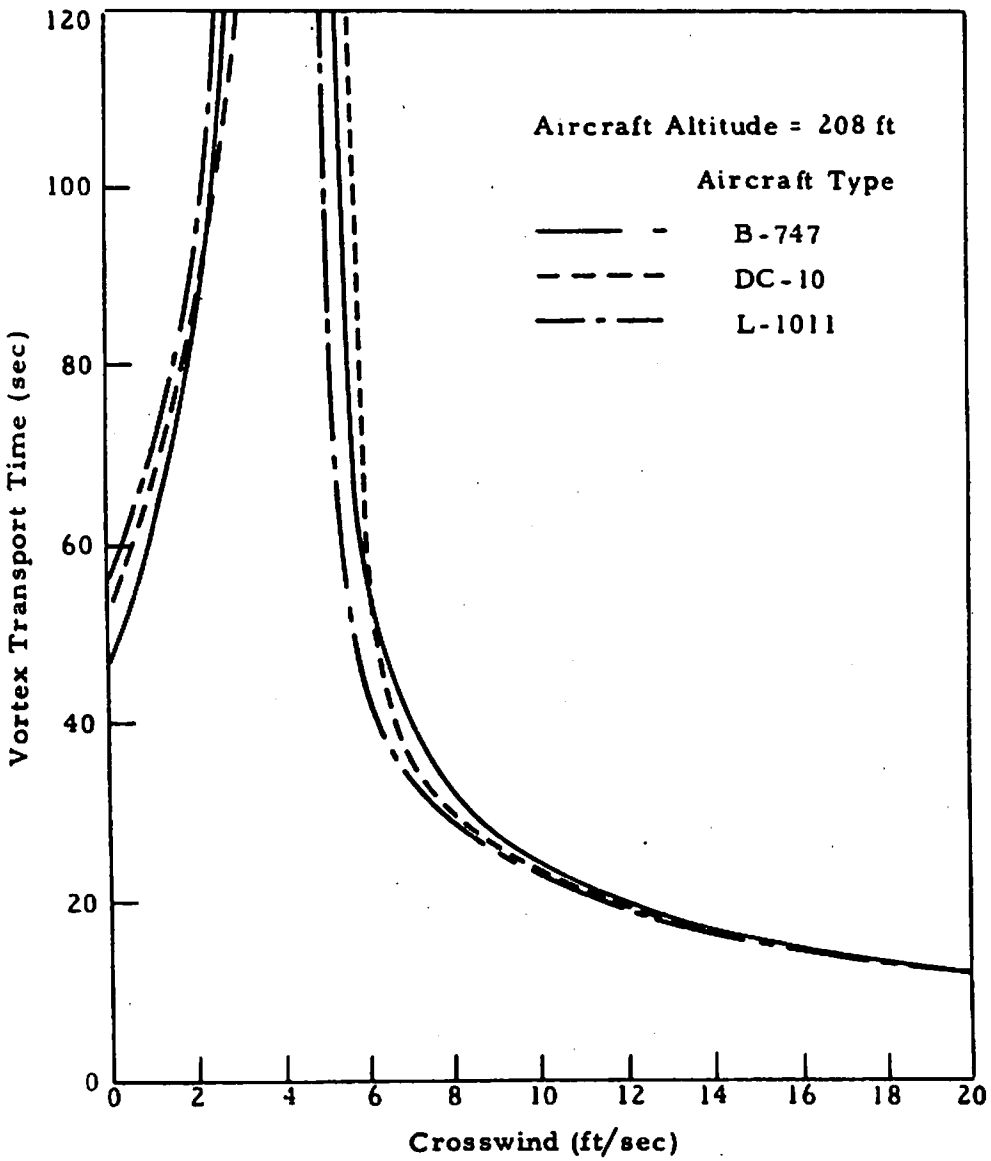

FIGURE 3-32. CALCULATED VORTEX TRANSPORT TIME FOR UNIFORM CROSSWIND

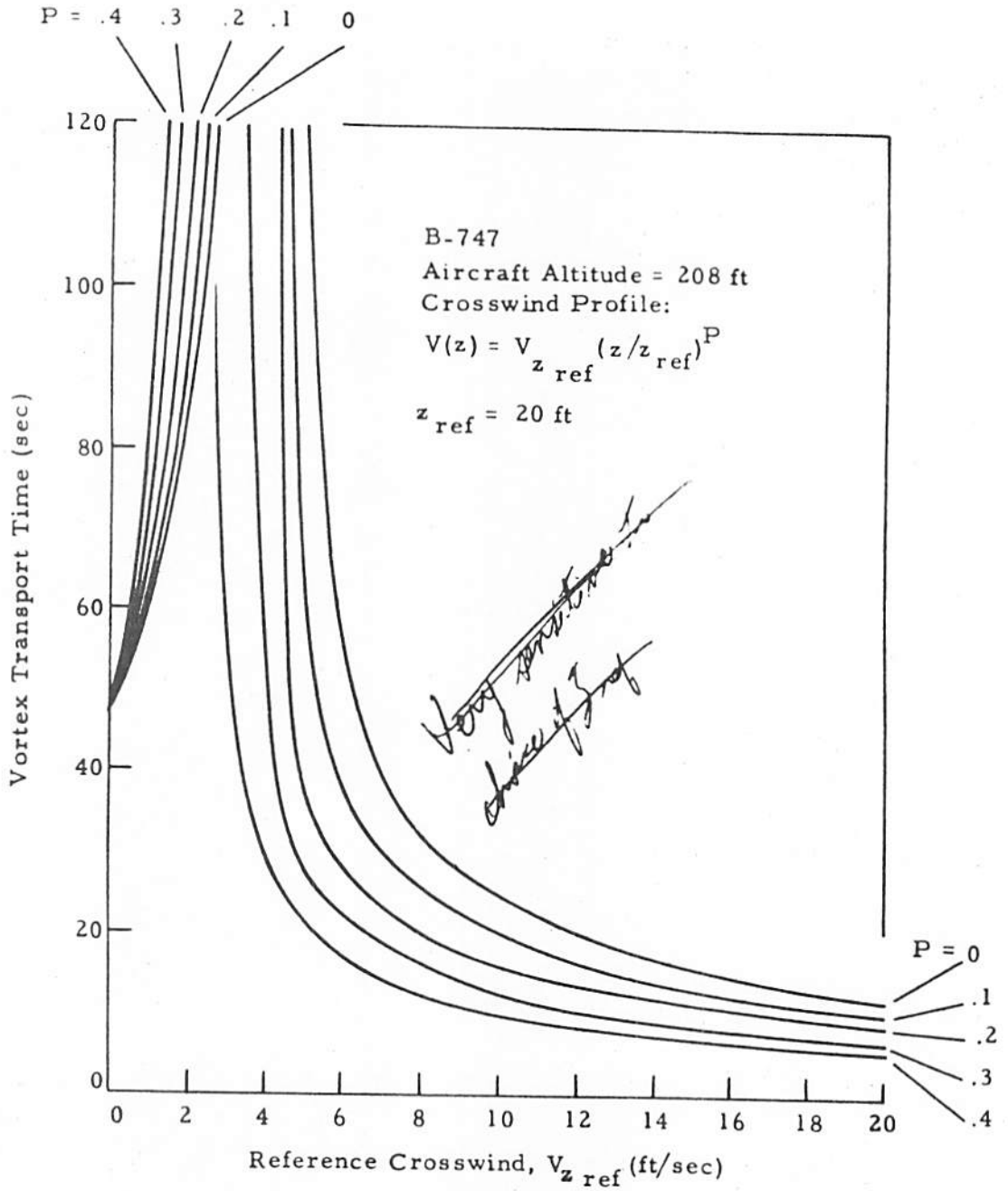

FIGURE 3-33. CALCULATED VORTEX TRANSPORT TIME FOR CROSSWIND DESCRIBED BY POWER-LAW PROFILE

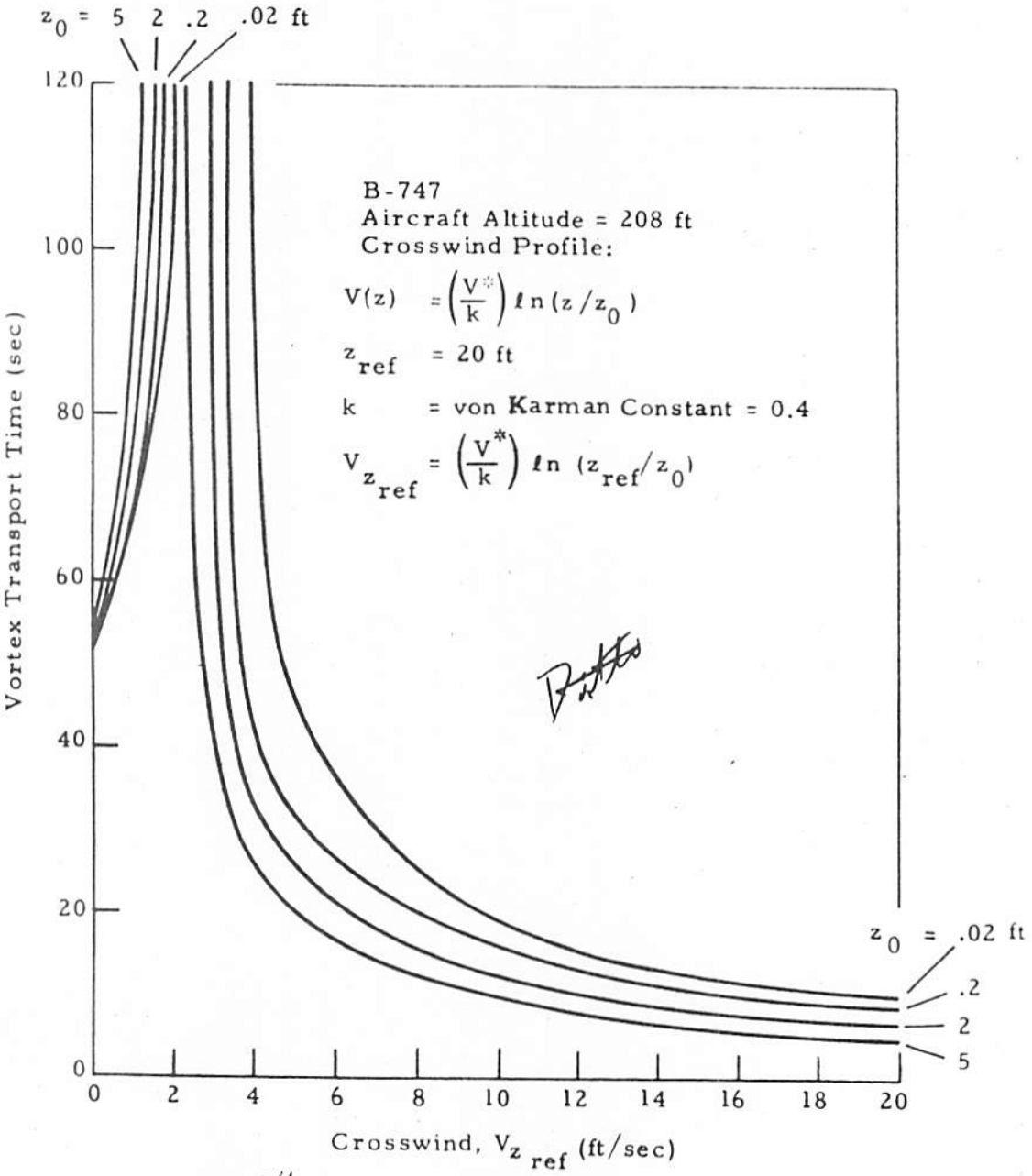

FIGURE ~~10~~ 3-34. CALCULATED TRANSPORT TIME FOR CROSSWIND DESCRIBED BY LOGARITHMIC PROFILE

35

Because the reference altitude was taken below the minimum altitude to which the vortex descends (i.e., approximately half the initial vortex separation distance), the effect of increasing the power-law exponent, p, is to increase the value of crosswind which the vortex experiences during its entire trajectory. The effect shown in Fig. 3-33 is essentially that of a difference in wind from the reference altitude to the asymptotic altitude (i.e., minimum altitude to which the vortex descends asymtotically) of the vortex pair. Figure 3-35 shows curves similar to Fig. 3-33, but with the reference altitude taken as 77 ft, which is the asymptotic altitude for an elliptically loaded B-747. For this condition the effect of the power-law exponent is almost negligible. Of particular significance is the fact that there is little dependence on the value of the exponent for large values of transport time. The spread in the lines of Figs. 3-33 and 3-35 is an indication of uncertainty in vortex transport time based on wind measured at the asymptotic altitude (i.e., Fig. 3-35) compared with uncertainty based on wind measured at the 20-ft altitude and extrapolated to higher altitudes on thebasis of a power-law exponent (i.e., Fig. 3-33). Figures 3-33 and 3-35 clearly show that the uncertainty in residence time decreases as the altitude of the wind measurement approaches the vortex asymptotic altitude.

The conclusion of this analysis is that direct wind measurement at the asymptotic altitude is preferable to wind measurement at another altitude with extrapolation to the asymptotic altitude.

3.3.3.2 Influence of Aircraft Parameters on the Calculated Vortex Transport Time

Variations in aircraft type, landing weight, altitude, and lateral displacement from the localizer centerline result in changes in the wake vortex transport time in the vortex corridor and are discussed below.

The calculated vortex transport time is shown for heavy and large jet transports in Figs. 3-32 and 3-36, respectively. The vortex transport time is relatively insensitive to aircraft type within each of the two broad aircraft groups (heavy and large), based upon the nominal values of aircraft parameters in Table 3-2. For a given initial altitude, vortex corridor width and crosswind, the vortex transport time is primarily a function of

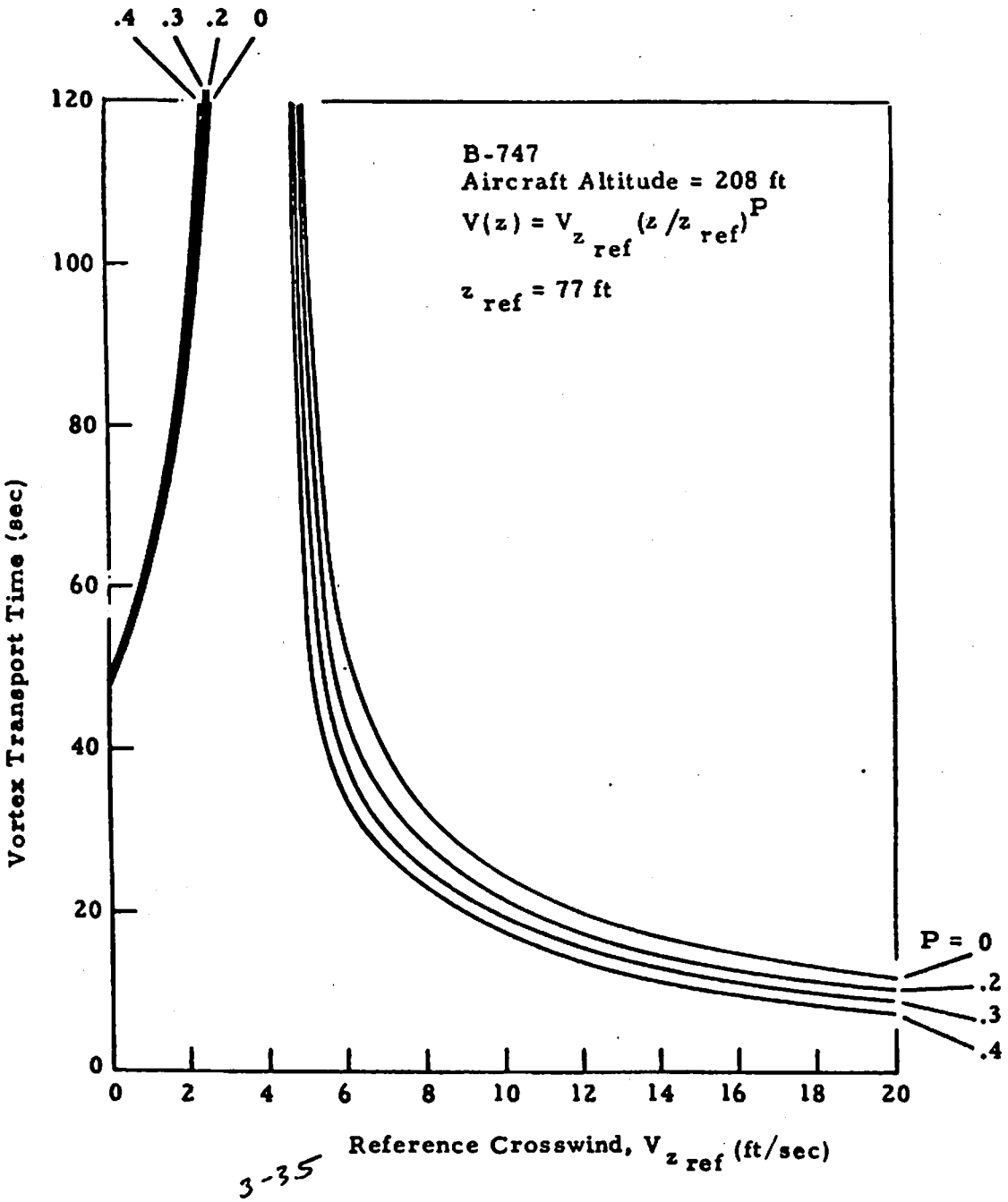

3-35

FIGURE 4. CALCULATED TRANSPORT TIME FOR CROSSWIND DESCRIBED BY POWER-LAW PROFILE WITH MODIFIED REFERENCE ALTITUDE

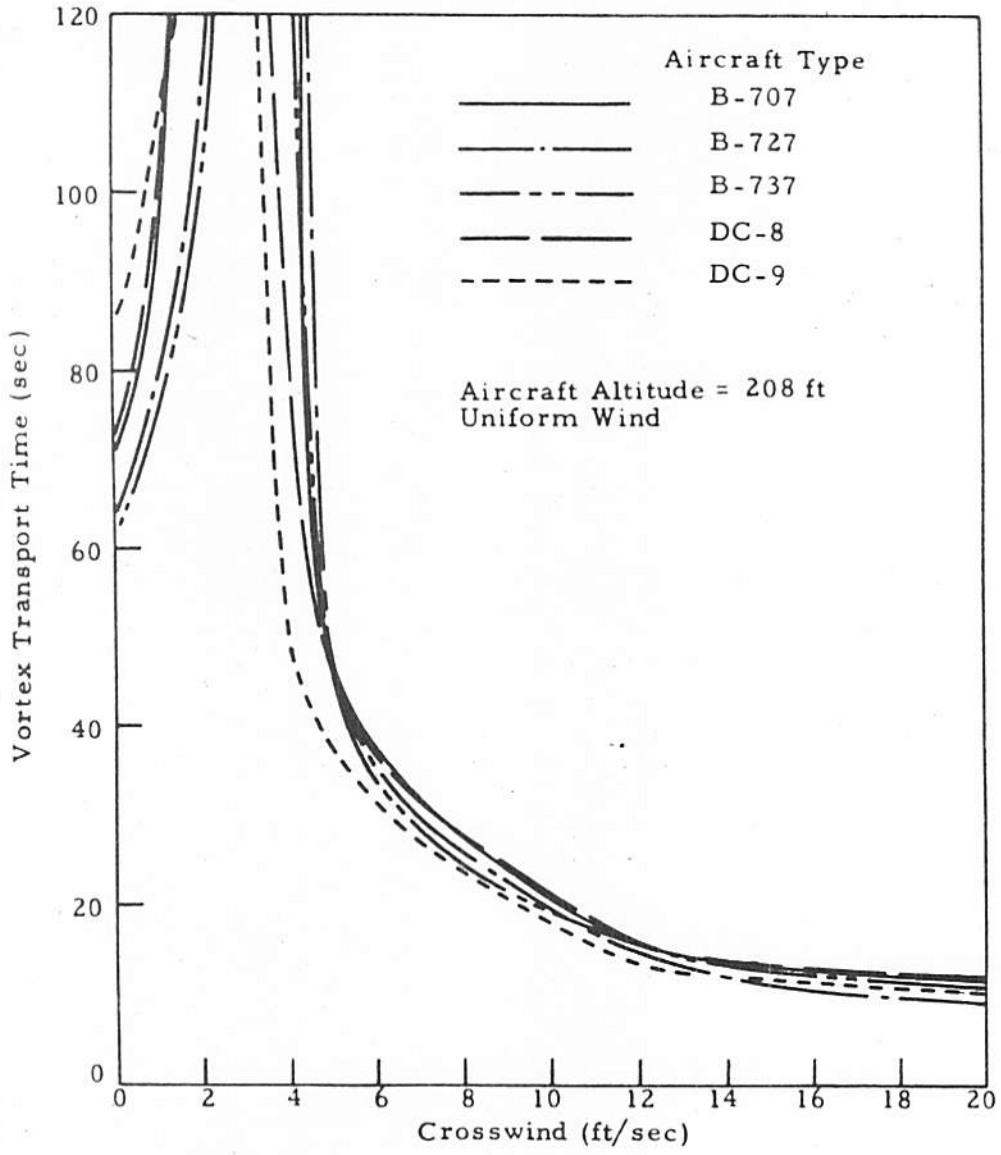

3-36

FIGURE ~~12~~. CALCULATED VORTEX TRANSPORT TIME FOR LARGE TRANSPORTS IN UNIFORM WIND

38

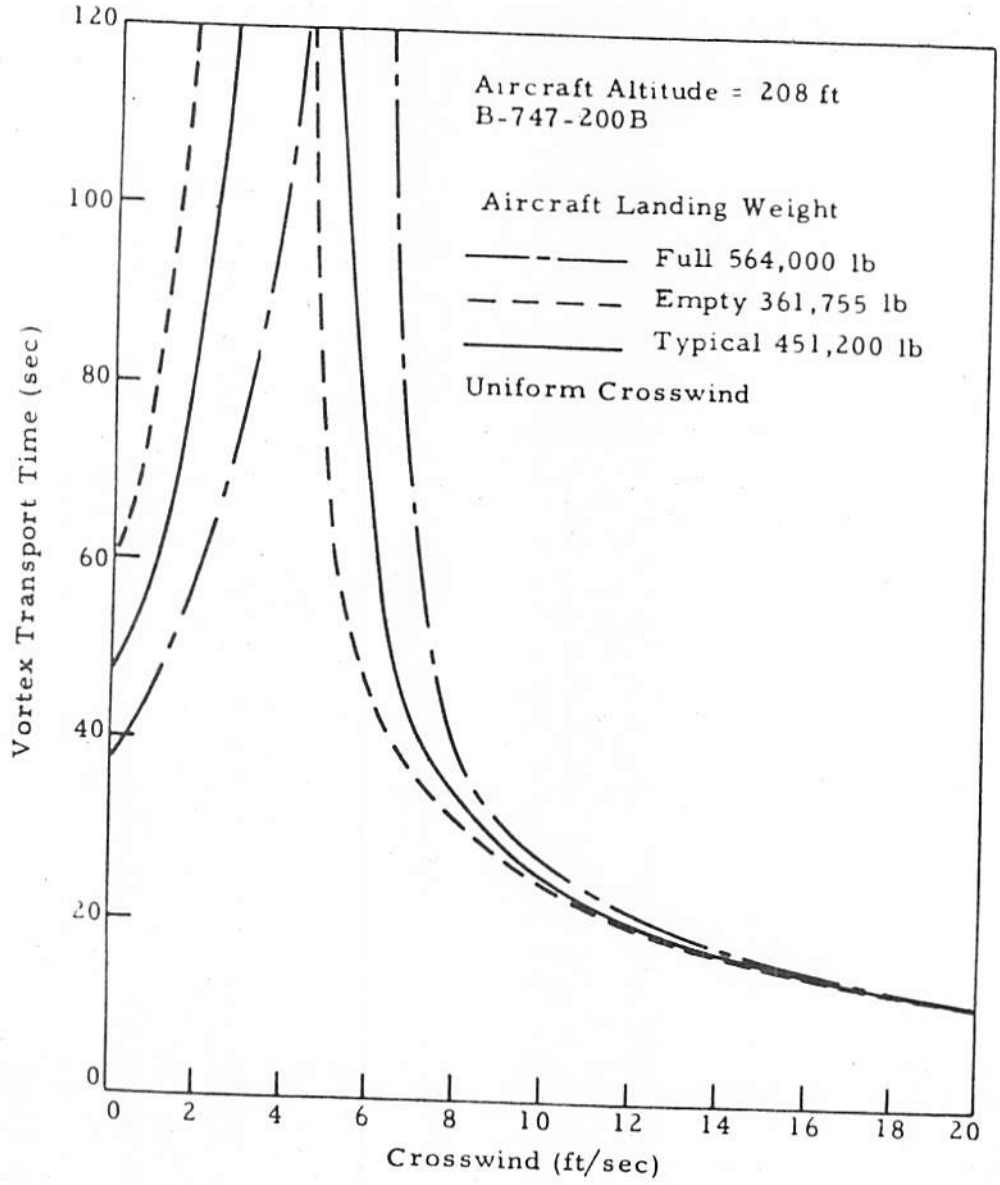

FIGURE 3-37. EFFECT OF AIRCRAFT LANDING WEIGHT ON CALCULATED TRANSPORT TIME

the vertical speed of the vortex pair. Equation (3.115) shows that the vortex trajectory in the wind-fixed coordinate system is a hyperbola which passes through the initial vortex position of the vortex, regardless of the speed at which the vortex moves along the trajectory. Therefore, for a given initial vortex position, the transport time is a function of the speed with which the vortex moves along the trajectory, which is proportional to the initial vertical speed of the vortex pair. This speed is given by equation (3.78) as

$$\frac{dZ}{dt} = - \frac{C_L U_\infty}{4\pi K^2 (AR)} \qquad (3.147)$$

where

C_L = lift coefficient ,and
(AR) = wing aspect ratio

The nominal values of each of the parameters affecting vertical speed (i.e., lift coefficient, C_L; approach air speed, U_∞; spanwise loading coefficient, K; and aspect ratio, (AR)) do not vary significantly between different aircraft types. This is shown in Table 3-2, which shows that vertical speeds of the vortex pair do not vary greatly between aircraft types. Therefore, it should be expected that transport times which are based upon nominal values of aircraft parameters should not be expected to be significantly different for different aircraft types. Figures 3-32 and 3-36 show some difference between wide-body aircraft (as a class) and narrow-body aircraft (as a class).

The influence of aircraft landing weight on the wake vortex transport time in the approach corridor for a given aircraft type is shown in Fig. 3-37. The results indicate that the vortex transport time is very sensitive to the aircraft landing weight at low crosswind conditions, i.e., < 7 ft/sec. If the crosswind is strong enough so that the vortex leaves the flight corridor before entering ground effect, aircraft weight has no effect on vortex transport time. If ground effect occurs within the vortex corridor, there are two mechanisms by which weight affects transport time. First, both the descent velocity and the velocity at which each vortex moves

horizontally (relative to the wind) in ground effect are directly proportional to aircraft weight for constant flight speed. The descent velocity (alternative form of the above equation) for an elliptically loaded wing is (cf. equation (3.28))

$$\frac{dZ}{dt} = -\frac{-8L}{\pi^3 \rho U_\infty b^2} \tag{3.148}$$

where

L = lift,
ρ = atmospheric density,
U_∞ = flight speed,
b = wing span.

Equation (3.147) is identical with equation (3.146) with

$$K = \pi/4 \tag{3.149}$$

for an elliptically loaded wing and

$$L = \frac{1}{2}\rho C_L b^2 U_\infty{}^2/(AR) \tag{3.150}$$

The asymptotic velocity at which the vortex moves horizontally with respect to the wind in ground effect may be shown to be (i.e., let $Y >> Z$ in Equation (3.116), let $Z = b'/2$, let $Y_0 = \pi b/8$ for elliptic wing loading, and let vortex strength, $\Gamma = 4L/\pi\rho U_\infty b$ (Section 3.1)

$$\dot{Y} = \frac{L}{\pi^2 \rho U_\infty b}\left[\frac{64}{\pi^2 b^2} + \frac{1}{Z_0{}^2}\right] \tag{3.151}$$

where Z_0 is the initial vortex altitude. This velocity reduces to the magnitude of the initial descent velocity as Z_0 becomes large. Because of this effect, an increase in the aircraft landing weight decreases the vortex transport time when the crosswind is below the critical value of crosswind (i.e., the value of crosswind below which the upwind vortex exits from the upwind boundary) because the increased horizontal velocity of the upwind

vortex acts with the wind in removing the vortex from the flight corridor. An increase in aircraft weight increases the vortex transport time when the crosswind is above the critical value of crosswind because the increased horizontal velocity acts against the crosswind in removing the vortex from the flight corridor.

Second, an increase in the landing weight increases the critical value of crosswind at which the vortex stalls in the approach corridor, and which also discriminates between upwind and downwind exit of the upwind vortex. In general, the upwind vortex exits the corridor from the upwind boundary if (equation (3.140))

$$V_\infty < \Gamma\sqrt{C}/4\pi \tag{3.152}$$

and from the downwind boundary if

$$V_\infty > \Gamma\sqrt{C}/4\pi \tag{3.153}$$

Since for a given aircraft configuration the vortex strength is directly proportional to aircraft weight, the critical value of the crosswind which discriminates between upwind and downwind exit of the vortex is directly proportional to aircraft weight.

The above discussion indicates that variations in aircraft weight have a much greater effect on vortex transport time than differences between aircraft types (within a class of wide-body or narrow-body aircraft).

The influence of aircraft altitude at the middle marker position on the wake vortex transport time is shown in Fig. 3-38. The results show that the vortex transport time is relatively insensitive to normal variations in aircraft altitude. (Experienced pilots can generally stay on the glideslope within 1 division or dot on the glideslope indicator.)

The influence of aircraft lateral displacement on the wake vortex transport time in the vortex corridor is shown in Fig. 3-39. Variations in aircraft lateral displacement about the localizer centerline indicate a noticeable 20 to 80-sec variation in the vortex transport time at low

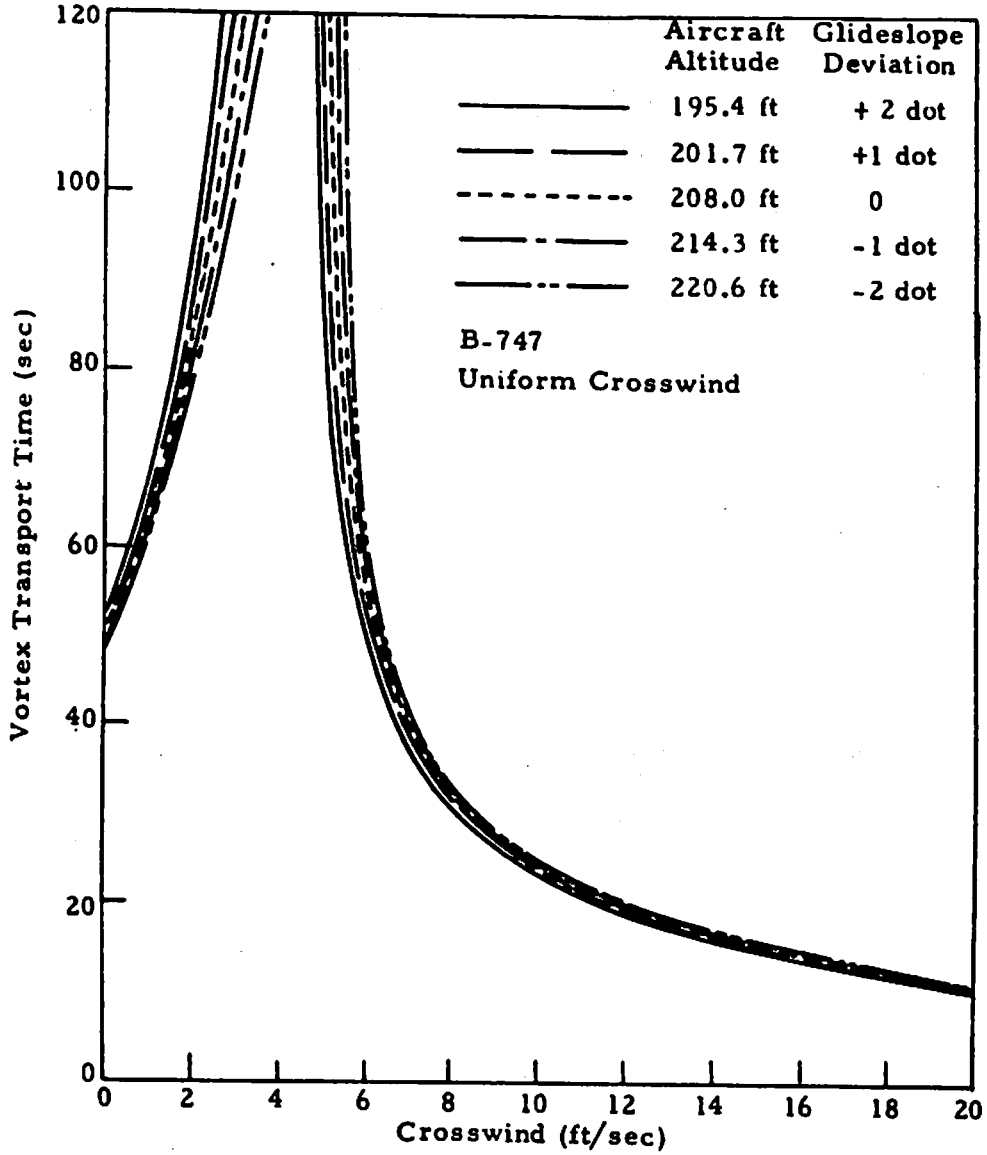

FIGURE ~~4~~ 3-38. INFLUENCE OF AIRCRAFT ALTITUDE AT THE MIDDLE MARKER ON VORTEX TRANSPORT TIME

43

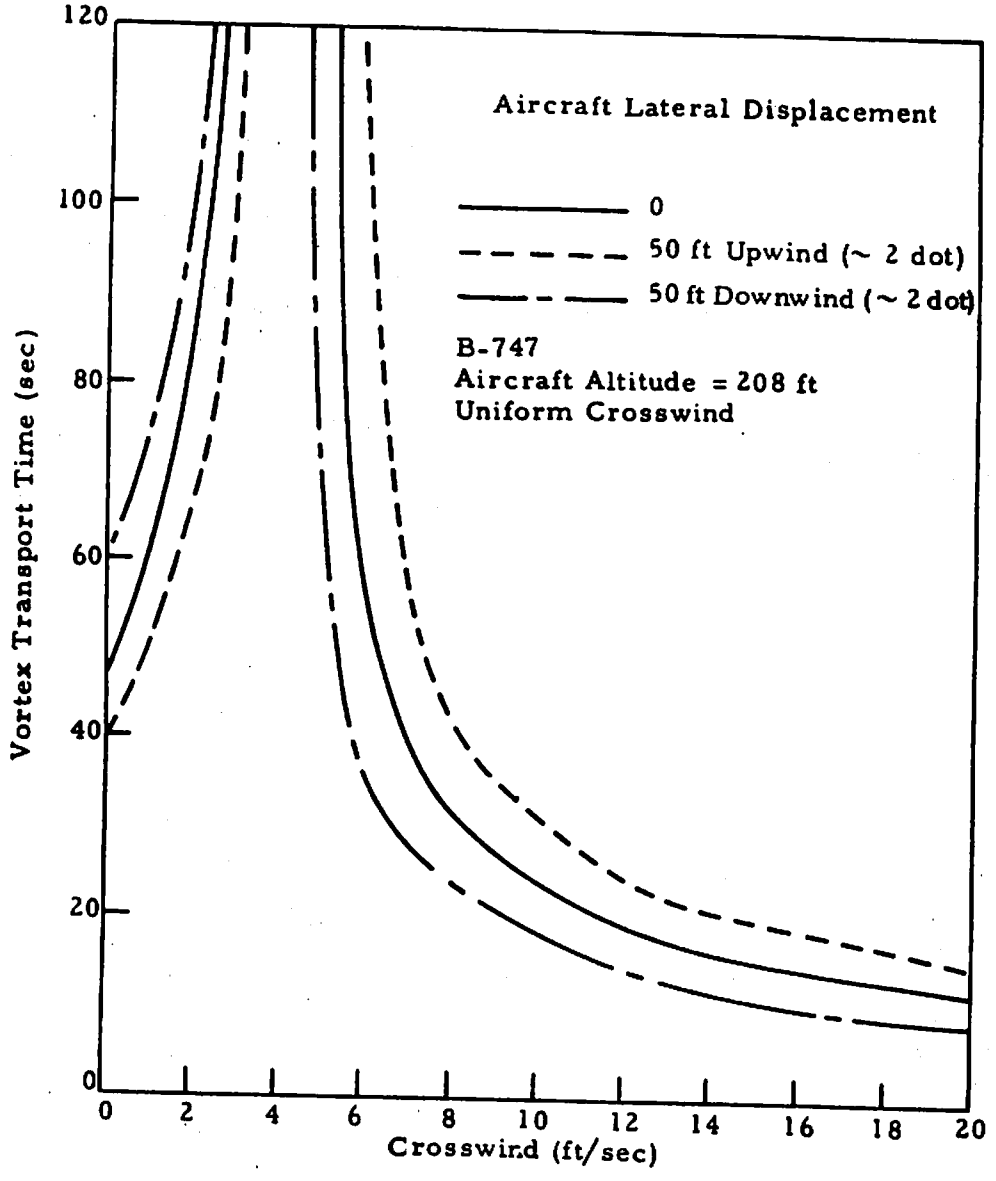

FIGURE ~~15~~ 3-39. INFLUENCE OF AIRCRAFT POSITION FROM LOCALIZER CENTERLINE ON VORTEX TRANSPORT TIME

74

crosswind velocities. For higher crosswind velocities, the effect of aircraft displacement on vortex transport time is small. It is noted that the ±50 ft deviation from the localizer centerline is a ±3σ variation (Ref. H).

From the results shown above, variations in aircraft weight and lateral displacement from the localizer centerline can exert a significant influence on the calculated vortex transport time in the vortex corridor. Since the calculated vortex transport time in the WVAS is based on nominal values of aircraft parameters, this can be an important consideration. For example, the vortex of a B707-120 at minimum operating weight, spanwise loading coefficient of 0.8, 5 knots above nominal landing speed, and 10 ft above and 20 ft to the side of the ILS at the middle marker has a vortex strength of 1895 ft^2/sec and a transport time of 113 sec for no crosswind. By contrast, a B-707-320C at maximum landing weight, spanwise loading coefficient of 0.75, 5 knots below nominal landing speed, and centered on the ILS has a vortex strength of 4246 ft^2/sec and a transport time of 47 sec for no crosswind. The corresponding values for the nominal values of aircraft parameters shown in Table 3-2 is a vortex strength of 3135 ft^2/sec and a transport time of 66 sec.

In addition to the direct effect of unknown values of aircraft parameters (i.e., parameters for which values would not be known in an operational environment) by virtue of the effect on vortex descent rate, unknown values of aircraft parameters also affect vortex transport time in the determination of the corridor boundary from which the upwind vortex exits. For constant crosswind, the upwind vortex for the B-707-120 described above will exit the upwind boundary for crosswinds less than 3 ft/sec and will exit the downwind boundary for crosswinds greater than 3 ft/sec. By contrast, for B-707-320C described above, the critical value of crosswind is 6.4 ft/sec. For the nominal condition (Table 3-2), the critical value of crosswind is 4.5 ft/sec. In a constant crosswind of 5 ft/sec, the B-707-120 would have a calculated transport time of 231 sec (although life time would prevent residence time from being that long).

Since the calculated vortex transport time is sensitive to aircraft weight, the above results suggest that an indirect determination of the

aircraft weight through measurement of the vortex descent rate in the early part of the vortex trajectory may be a useful input to the WVAS. Aircraft weight can also be determined by pressure sensors under the flight path (ref. I). The pressure sensor senses the downwash of the aircraft as it passes the sensor. Also, a good measurement of initial vortex descent rate would be a good indicator of vortex strength. Therefore, a good measurement of the initial vortex descent rate would permit a reasonably accruate calculation of the vortex transport time. In principle, an early estimate of vortex transport time would have some value in a WVAS because a following aircraft could be given an early warning if there was a reasonable chance that the vortex preceeding it would not clear the vortex corridor before its projected landing.

3.3.3.3 Influence of Aircraft Altitude on Calculated Vortex Transport Time

One of the most important influences on vortex tranport time is the influence of initial aircraft altitude. All aircraft altitudes between 20 ft (the altitude of the wing at touchdown) and 200 ft (the middle marker) are of concern because every aircraft must traverse this entire altitude range in landing, and a following aircraft is sufficiently low that it may encounter a vortex in ground effect. From equations (3.139) and (3.140), the upwind vortex exits the flight corridor from the downwind vortex corridor boundary if

$$V_\infty < \Gamma\sqrt{C}/4\pi = \frac{\Gamma}{4\pi Y_0}\left[1+Y_0^2/Z_0^2\right] \tag{3.154}$$

and from the upwind vortex corridor boundary if

$$V_\infty > \Gamma\sqrt{C}/4\pi = \frac{\Gamma}{4\pi Y_0}\left[1+Y_0^2/Z_0^2\right] \tag{3.155}$$

The value of the critical crosswind velocity which discriminates between downwind and upwind exit of the upwind vortex is a strong function of Z_0 at low altitudes (i.e., $Y_0/Z_0 > 1$). Therefore, a crosswind which would cause the upwind vortex to rapidly exit the flight corridor for an aircraft altitude of 200 ft can cause the vortex to stall in the flight corridor for

an aircraft altitude of less than 50 ft. Figure 3-40 shows vortex transport time as a function of crosswind for initial vortex altitudes of 200, 120, 80, and 40 ft.

In interpreting Fig. 3-40, it must be remembered that it is assumed that the vortex roll-up process occurs out of ground effect and that the vortex then descends into ground effect. However, it is expected that when the vortex roll-up occurs in ground effect, the ground has a significant effect on the roll-up process. Little analytical or experimental work on the roll-up process in ground effect or on vortex demise mechanisms which may exist when roll-up occurs in ground effect has been done. Limited measurements (ref. H) indicate that vortices generated at altitudes less than a quarter of a wing span dissipate rapidly. It is expected that vortex life time is a monotonic decreasing function of altitude as the altitude at which the vortex was generated decreases from less than half of a wing span. (Unpublished data tends to corroborate this statement.)

3.3.4 Secondary Vortex Transport Effects

The basic equations of vortex transport have been presented in Section 3.3.2. These equations are based upon transport by mutual induction and by the effect of crosswind. In addition to these dominant effects, there are also some secondary effects which exert significantly less influence on vortex transport, are less understood both theoretically and experimentally, and seem to be far more random in the effect on vortex transport. Nevertheless, they are significant effects which warrant discussion in this document.

Vortex tilting as a result of wind shear is discussed first. This is followed by a discussion of vortex buoyancy and an extension of the vortex transport equations presented previously to include the effects of vortex buoyancy.

3.3.4.1 Wind Shear Effect on Vortex Transport

The tilting or banking of the vortex pair (i.e., one vortex descending relative to the other vortex) has been observed experimentally at altitude (ref. 42) and in ground effect (ref. 43), as well as in operational

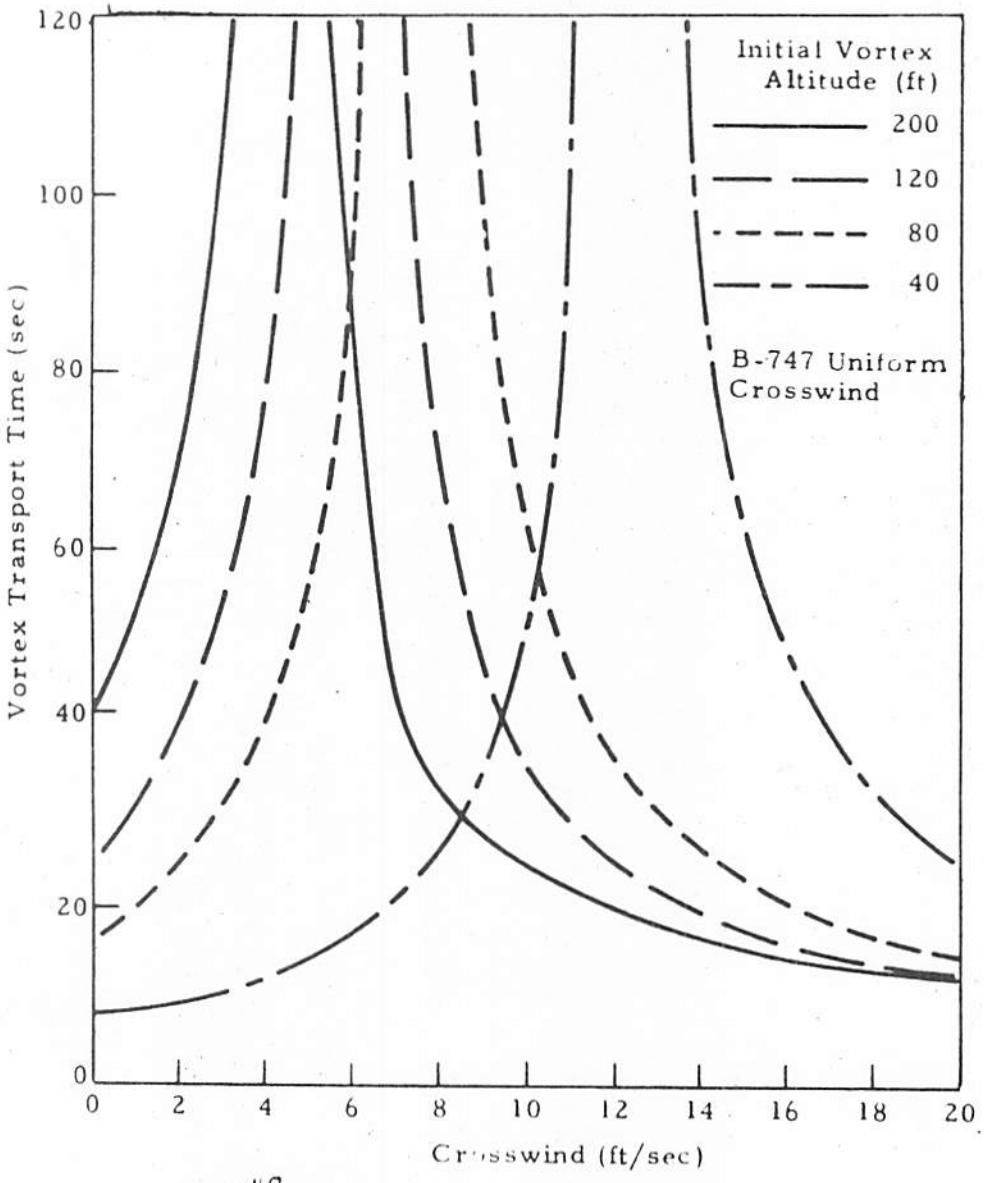

FIGURE ~~15~~ 3-40. INFLUENCE OF INITIAL VORTEX ALTITUDE ON VORTEX TRANSPORT TIME

situations (refs. 44 and 45). Occasionally in the light aircraft tests, long segments of the wake were observed to roll past the vertical resulting in bank angles exceeding 90 degrees. As will be shown below, it appears that crosswind shear or crosswind shear gradients are responsible for the observed rolling tendency of wakes.

The geometry of vortex transport in wind shear is shown in Fig. 3-41. Crosswind shear (change in crosswind with respect to altitude) in the vicinity of the wake implies an ambient, coherent vorticity field alined parallel with the vorticity associated with the vortex pair. Interactions between the two vortical flows could produce opposite changes in the circulations of the counterrotating wake vortices. Thus, the velocities induced by each vortex on the other (the descent speeds) would be unequal and wake roll, manifesting itself as an altitude mismatch between vortices, could occur for the descending pair.

There is a lack of definitive experimental evidence or agreement about which direction the wake will roll under given shear conditions--apparently because of the relatively weak deterministic influences of shear on wake roll. Four possible mechanisms by which wind shear can produce vortex tilting are presented below. These mechanisms show the existence of mechanisms for vortex tilting in both directions (i.e., upwind vortex descending relative to the downwind vortex and upwind vortex ascending relative to the downwind vortex). The lack of definitive experimental evidence may be due to the interaction of all of these mechanisms, with none of them being dominant or very strong. For light shear, it is possible that random vertical atmospheric convection of each of the vortices could overwhelm any shear-induced motions, resulting in atmospherically influenced, random roll directions. Full-scale aircraft wake measurements by Tombach et al (ref. 43) show a definite negative correlation between the sense of the shear and the sense of the tilting, so that the upwind vortex (the shear being produced in the sense of that of a boundary layer) descends relative to the downwind vortex a large percentage of the time, especially when the shear strength becomes significant. On the other hand, measurements reported by Brashears et al (ref. 45) show tilting in both directions, with a preference for tilting in the opposite sense to that noted by Tombach et al whenever the shear was relatively strong. The

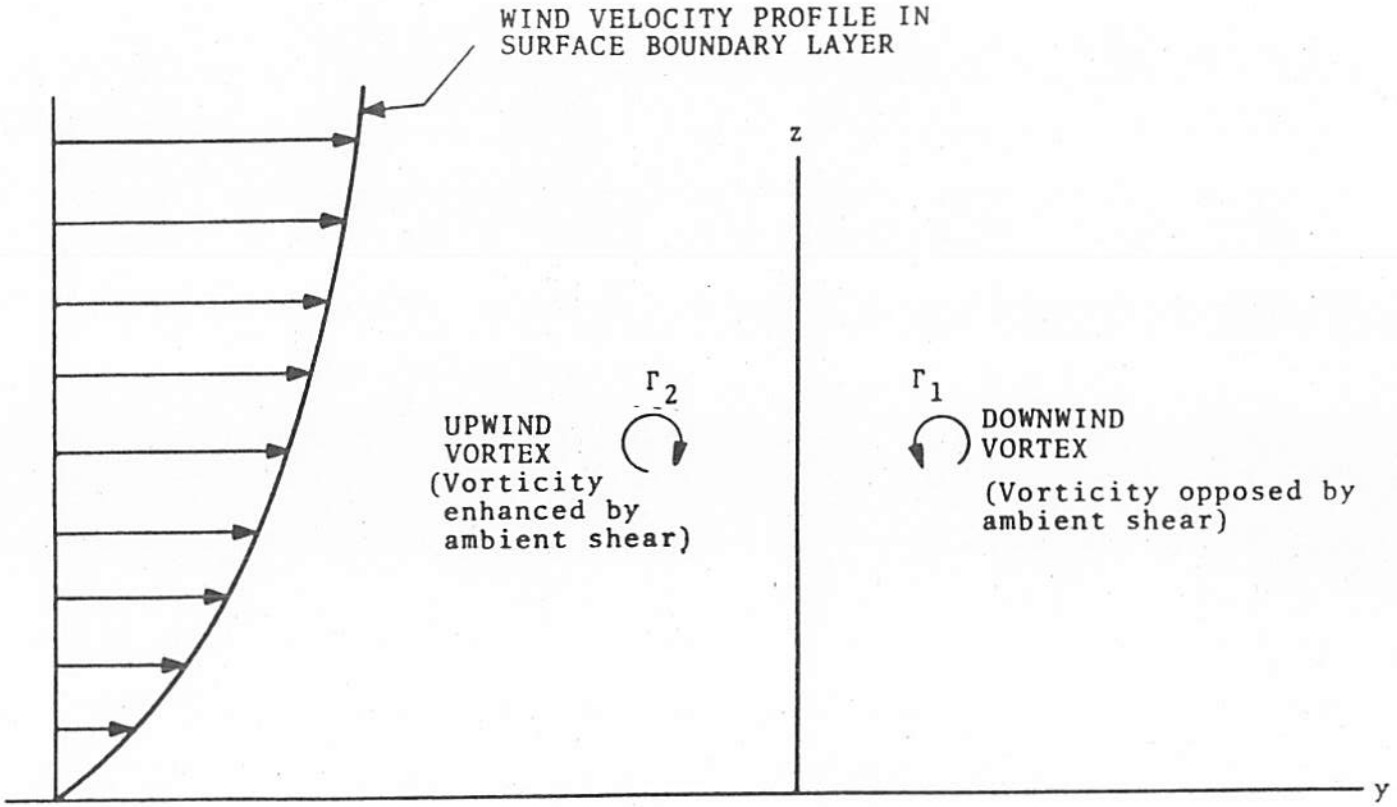

FIGURE 3-~~30~~ 41. VORTEX STRUCTURE IN CROSSWIND SHEAR

Brashears et al data also show, for weak shears, a tendency toward tilting in the same sense as that noted by Tombach. In this case however, random effects could dominate the weak deterministic influence of the shear. In fact, the Brashears et al data show the least tendency for tilting at a nonzero value of shear, where the opposite strong shear and weak shear tendencies are balanced out. The pulsed acoustic vortex sensing system at Heathrow (Ref. I) showed similar results with wake tilting in both directions, with a preference for the downwind vortex descending relative to the upwind vortex whenever the shear was relatively strong. The Heathrow data also show, for weak shears, a tendancy toward tilting in the opposite sense to the strong shear situation. The data indicated the least tendency for tilting at a nonzero value of shear, where the opposite strong and weak shear tendencies are balanced out.

Although an explanation for this behavior is not apparent, it may be related to the interaction of the various phenomena that may contribute to vortex tilting as described below. Variations in ground effects and differences in aircraft scale between the two sets of data may be a factor. It is noted, however, that Tombach's data are based on a small aircraft (AeroCommander), whereas the Brashears data are based on large and heavy jet transports. Therefore, the ratio of the vorticity in the wind shear to the vorticity of the wake vortices is significantly less for the Tombach data than for the Brashears data. If wake tilting is caused by the vorticity of the wind shear, the difference in the magnitudes of the vortcity ratios could have a significant effect.

Vortex tilting is an important phenomenon because of another dramatic (and operationally more significant than the tilting per se) aspect to wake behavior which occurs simultaneously with vortex tilting. Whenever the wake banks, the upper (generally downwind) vortex appears to break up well ahead of the other vortex, often leaving one vortex drifting alone for some time before it decays. In the overhead view in Fig. 3-42, the upper vortex shows signs of decay at 15 seconds and has completely broken down by 30 seconds; the lower vortex still persisted, apparently unmodified, when the last picture in the sequence was taken at 45 seconds. The single remaining vortex does not attempt to link with its image below the ground as has been observed when both vortices approach the ground, but rather invariably

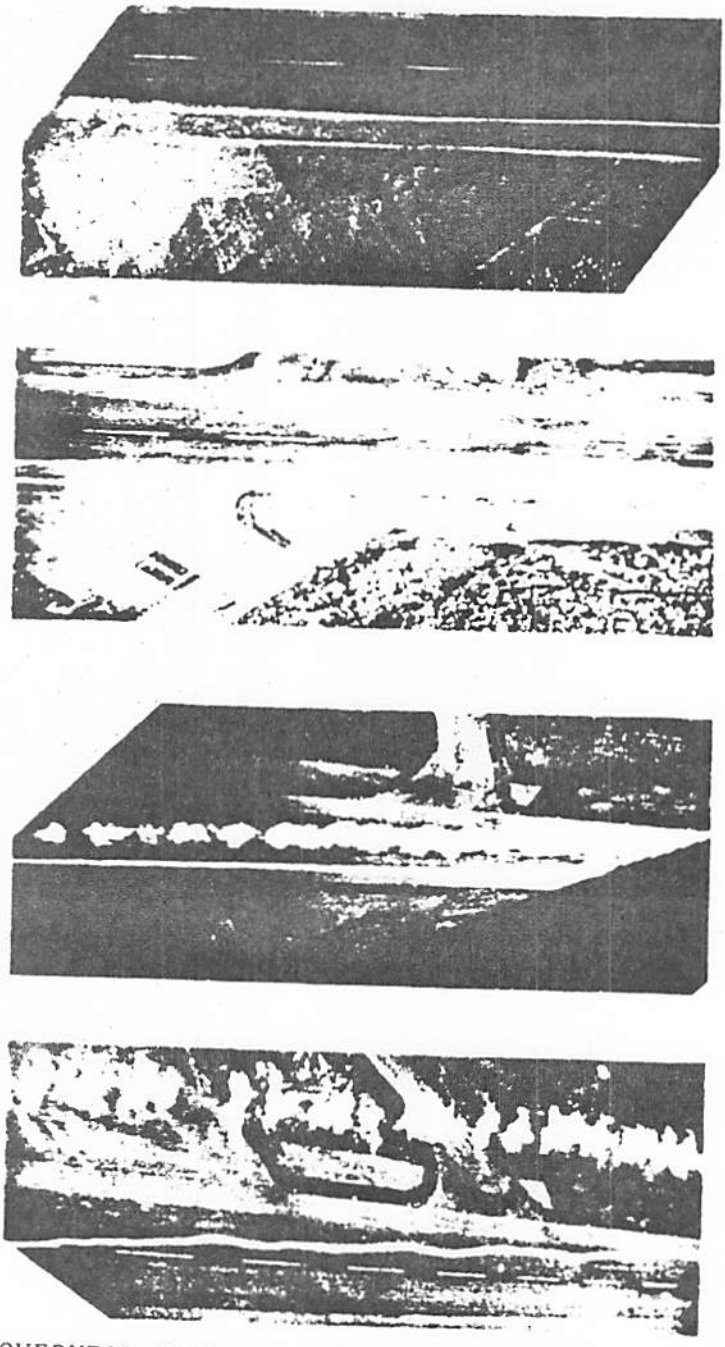

FIGURE 3-42. OVERHEAD VIEW OF AEROCOMMANDER 560F WAKE BEHAVIOR IN WIND SHEAR. WAKE GENERATED ONE SPAN ABOVE GROUND. WIND SHEAR 0.08 S-1; WIND FROM AIRCRAFT'S LEFT; I.E., FROM BOTTOM OF PICTURE. THE LEFT VORTEX DESCENDS TOWARD THE GROUND; THE RIGHT ONE RISES AND BREAKS UP. THE PHOTOGRAPHS WERE TAKEN FROM AN AIRCRAFT CIRCLING OVERHEAD, THUS THE ANGLE OF OBSERVATION IS SLIGHTLY DIFFERENT IN EACH PICTURE.

52

experiences vortex breakdown. It is likely that the downwind vortex breaks up first because its vorticity is opposed by the vorticity of the natural atmospheric wind shear, whereas the vorticity of the upwind vortex is augmented by the vorticity of the natural atmospheric wind shear.

It is noted that wind shear is a strong function of atmospheric stability and is therefore well correlated with atmospheric turbulence. In fact, the existence of atmospheric turbulence tends to inhibit wind shear by the transfer of momentum in the vertical direction. Thus, wind shear effects are more likely to occur in low turbulence conditions than in high turbulence conditions. This is operationally significant because the wind shear effects are most likely to coincide with long vortex life because the effects of atmospheric turbulence for decreasing vortex life are probably not present when wind shear effects occur.

Analytical studies of the mechanisms involved in wake tilting and in wind shear effects on wakes have not produced conclusive results. Potential flow analysis of a vortex pair at infinite altitude has shown that, in a uniform crosswind shear, the recirculating cell about the upwind vortex cell (the cell whose vorticity is enhanced by the shear) enlarges and the downwind cell (the cell whose vorticity is opposed by the shear) contracts, as shown in Fig. 3-43. Continued analysis along these lines (ref. 45) showed that additional cell contraction around the downwind vortex was brought about by the proximity of the ground. For a sufficiently large amount of cell contraction about the downwind vortex, the interior flow (and vorticity) could presumably be detrained, resulting in the rather abrupt dissipation of that vortex. The upwind vortex would be further isolated from the exterior flow by the enlargement of its cell, and hence, its vorticity would be "protected." These effects (if in fact real) are in qualitative agreement with experimental observations of vortex breakup in shear flow (ref. 43) such as in the example in Fig. 3-42.

Both of these analyses modeled the steady potential flow in the vicinity of a vortex pair resulting from superposition of vortex-induced motion, crosswind shear, and, in the case of ground effect from the induced flows of the image vortices. Resulting streamlines were calculated and mapped. The wake tilting is an unsteady phenomenon however, and thus, the limitations of such steady analyses should be recognized.

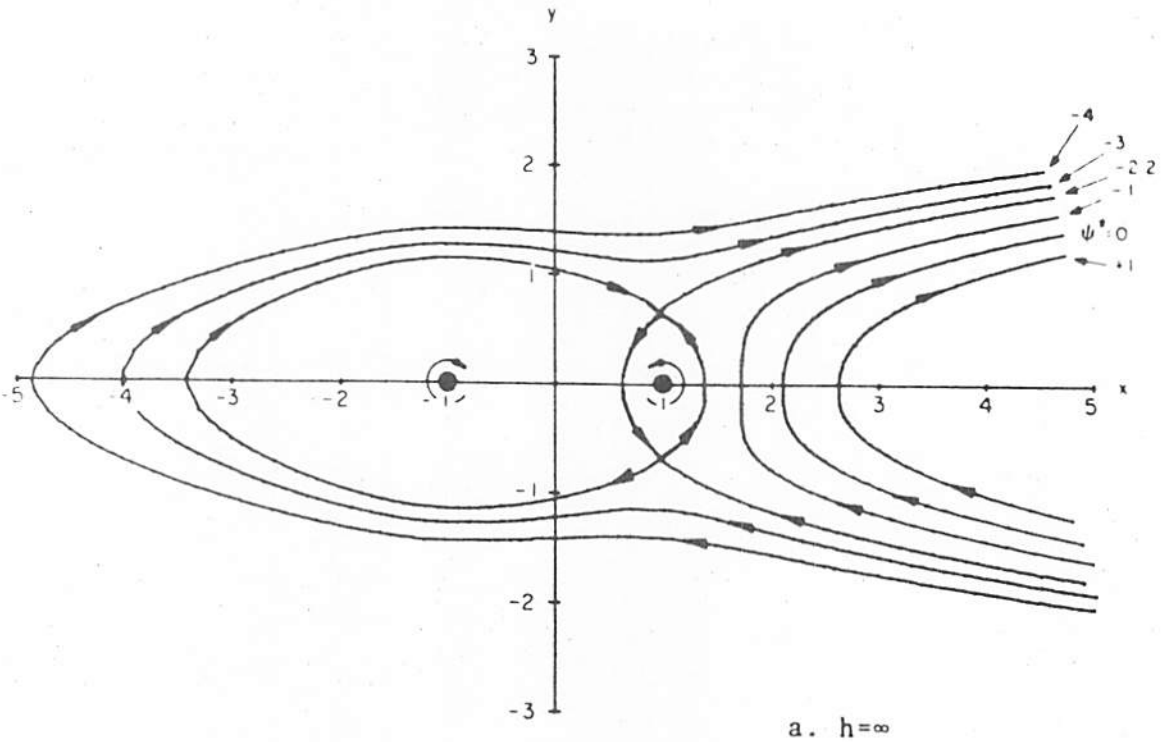

a. h=∞

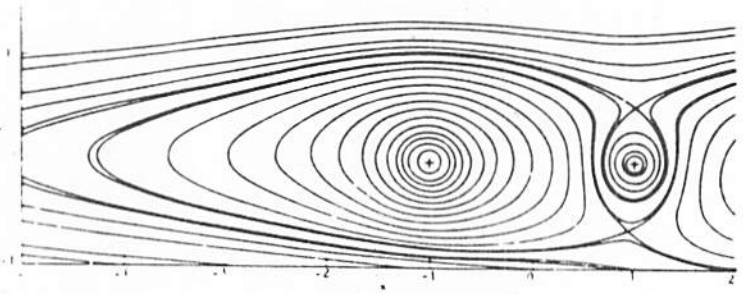

b. h=0.5 b_v

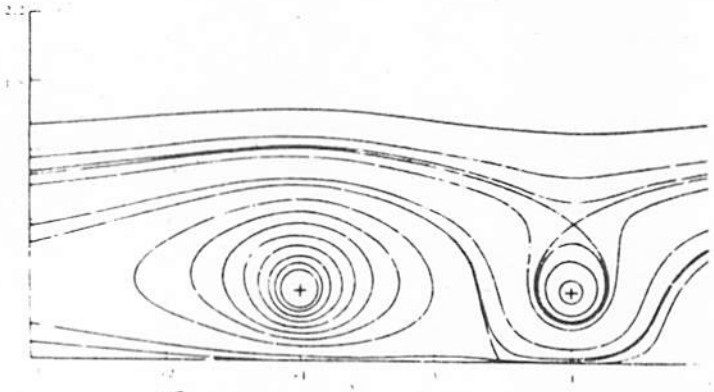

c. h=0.25 b_v

FIGURE 3-43. STREAMLINES IN THE VICINITY OF A VORTEX PAIR IN SHEAR AT (A) INFINITE ALTITUDE, AND (B,C) IN GROUND EFFECT. FOR SHEAR IN THE SENSE OF A BOUNDARY LAYER FLOW, THE CROSSWIND IS FROM THE LEFT. THE "DOWNWIND" VORTEX RECIRCULATION CELL BECOMES SMALLER THAN THE UPWIND CELL FOR SUCH A SITUATION.

54

There are four mechanisms which could cause vortex tilting, three of which are associated with wind shear. It is noted that the wind shear has vorticity associated with it. A common form of the wind velocity profile is

$$v(z) = v_0(z/z_0)^p \tag{3.156}$$

with the value of p ranging from 0 for a very unstable atmosphere to approximately 0.4 for a very stable atmosphere. The vorticity associated with this shear is

$$\Gamma_a(z) = \frac{\partial v(z)}{\partial z} = v_0\, p\, (z/z_0)^{p-1} \tag{3.157}$$

Since generally $0 < p < 1$, vorticity associated with shear decreases for increasing altitude.

The first mechanism by which wind shear could cause vortex tilting is that the vorticity augments the vorticity of the upwind vortex and decreases the vorticity of the downwind vortex. This effect is shown in Fig. 3-41. Thus the upwind vortex becomes stronger than the downwind vortex, and by mutual induction (cf. Section 3.3.2.1) the downwind vortex descends faster than the upwind vortex. Thus, the upwind vortex appears to rise relative to the downwind vortex.

Section 3.3.3.2 shows that the altitude at which a vortex trajectory levels out increases as vortex strength increases. Thus, if wind shear increases the strength of the upwind vortex it will level out at a higher altitude than the downwind vortex and so will appear to rise relative to the downwind vortex. This is an effect which will occur only in ground effect. Since vortex tilting has been observed out of ground effect, this cannot be the only effect of wind shear on vortex tilting, but may be a contributing effect in ground effect.

The third mechanism by which wind shear can affect vortex tilting was identified by Burnham (ref. 44) and explains tilting in the opposite direction to that explained above. Qualitatively, Burnham's approach can be

seen in Fig. 3-44(a). As seen by equation (3.156), the vorticity of the atmosphere decreases with increasing altitude. In a simple manner, Burnham described the atmosphere as two layers of uniform wind with small vortices distributed along the boundary. As the wake vortices approach the ground, they transport the vortices caused by wind shear up as shown in Fig. 3-44(b). The transported wind shear vortices now act on the wake vortices. They increase the rate of descent of the upwind vortex and decrease the rate of descent of the downwind vortex, causing the upwind vortex to descend relative to the downwind vortex.

In fact, the vorticity associated with wind shear is distributed throughout the lower part of the atmosphere rather than at discrete locations as described above. The modeling of the atmosphere with many vortices representing wind shear would consume large quantities of computer time. Nevertheless, the principal of wake vortices transporting low altitude atmospheric vorticity to higher altitudes and then being acted upon by the transported atmospheric vorticity is valid. This approach certainly explains the possibility of wind shear causing the upwind vortex to descend relative to the downwind vortex.

Burnham correctly observes that wind shear vortices would not affect the aircraft vortex vertical motion at all if they were uniformly distributed in space. As shown by equation (3.156), uniform distribution of vorticity in space does not occur, and the effect described is credible.

A fourth explanation for vortex tilting, which is not associated with wind shear, is presented in Ref. D. The wind profile of a vortex near the ground is as shown in Fig. 3-45(a) with a shear layer near the ground modeled to satisfy the conditions of zero velocity at the ground and continuity with the vortex velocity at the boundary layer thickness, z_{BL}. As shown in Fig. 3-45(b), the vorticity associated with the boundary layer is transported upward in a manner similar to that discussed above for atmospheric vorticity. However, in this case, the sign of the transported vorticity is different for the two vortices. The transported vorticity causes the wake vortices to decrease their descent speed. Atias and Weihs use this phenomenon to explain vortex bouncing. However, if for some reason such as non-uniform ground roughness, the transport processes were different

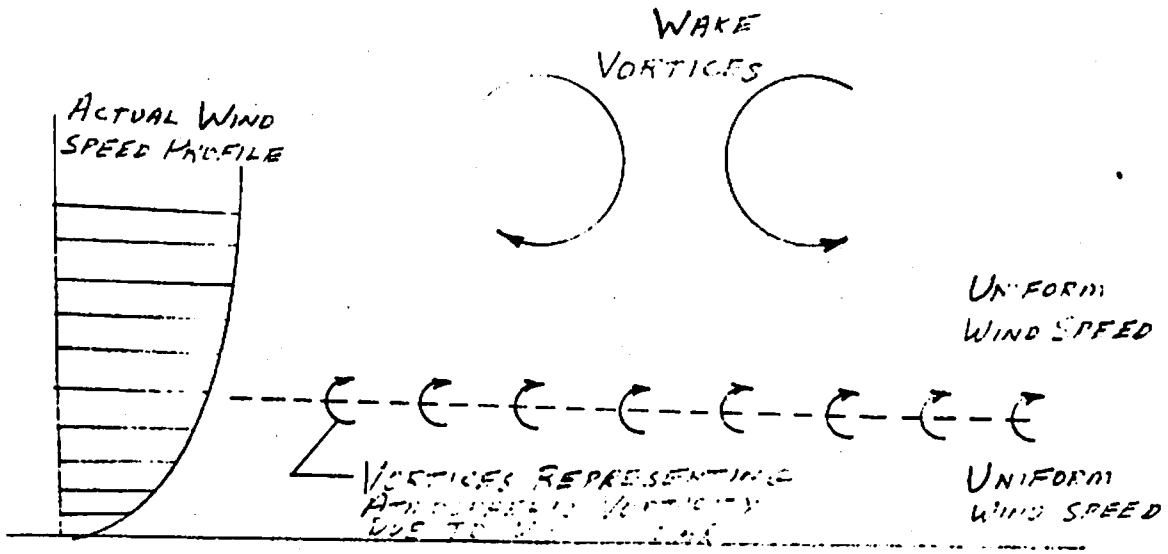

(a) RELATIONSHIP OF WAKE VORTICES AND ATMOSPHERIC VORTICITY DUE TO WIND SHEAR

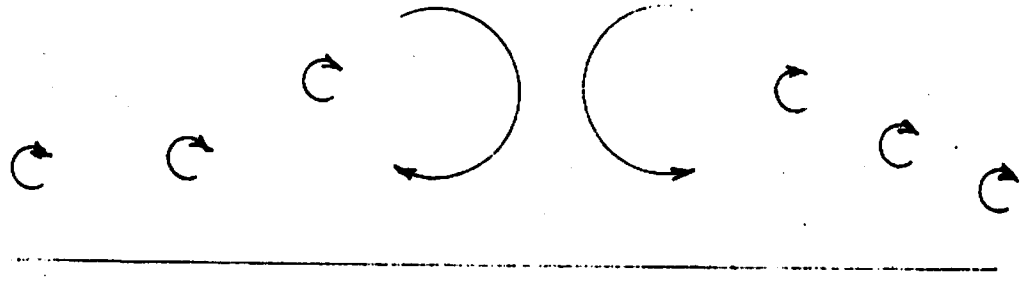

(b) DISPLACEMENT OF ATMOSPHERIC VORTICITY BY WAKE VORTICES

FIGURE 3-44. WIND SHEAR EFFECT ON WAKE VORTICES CAUSING UPWIND VORTEX TO DESCEND

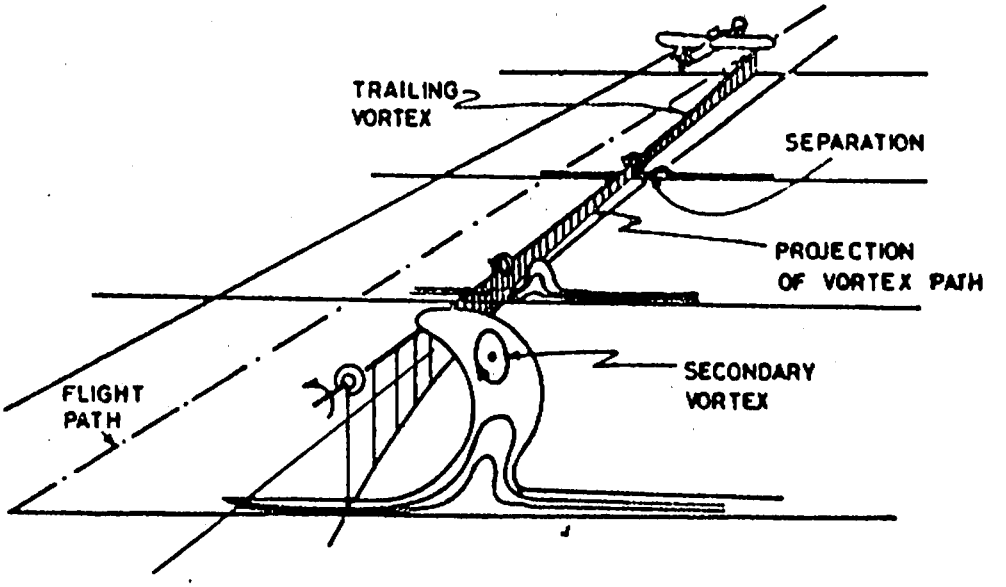

FIGURE 3-45 SCHEMATIC DEPICTION OF TRANSPORT OF ATMOSPHERIC BOUNDARY LAYER VORTICITY

for each of the two vortices, this phenomenon could cause one of the vortices to rise relative to the other vortex. Vortex tilting in either sense could be the result.

It appears that the factors causing vortex tilting are neither intuitively obvious nor have they been sufficiently illuminated by full-scale, atmospheric flight tests, or theoretical analysis. The most significant aspect of wake tilting from an operational standpoint is the occurrence of the solitary vortex. It is undoubtedly some manifestation of flow asymmetry associated with wind shear, turning flight, etc., which produces the conditions for the creation of the solitary vortex, which so far has eluded proper understanding. Such long-lived vortices could present operational hazards since they appear to be rare events and, as such, the conditions for their occurrence may not be predictable. Further investigation of this phenomenon would be enhanced by a large data base which would contain may vortex trajectories and a versile data management system (such as the Statistical Analysis System) which would allow isolation of the particular aircraft flybys for which vortex tilting occurs.

3.3.4.2 Vortex Buoyancy

Vortex buoyancy is the aerostatic force imposed on the vortex by virtue of the difference in density between the air contained within the vortex and the surrounding ambient air. There are three sources of this density difference: The first is a result of the static underpressure of the vortex (cf., Fig. 3-13). The second is the result of entrainment of hot exhaust gases from the engines. The third is the result of descent through a non-adiabatic atmosphere. The first two effects give the vortex a positive (upward) buoyancy force. The third may give a positive or negative force depending on the temperature lapse rate of the surrounding atmosphere. The magnitude of these effects on vortex motion is small compared with mutual induction.

Positive buoyancy causes the vortices to approach each other by virtue of a mass of air with vorticity having a velocity relative to the surrounding air. The Kutta-Joukouski force on a body with circulation and velocity through a fluid gives

$$F = -\rho(\dot{Z}-W)\Gamma \tag{3.158}$$

where the force is in the positive z-direction, and (Z-W) is the velocity of the vortex relative to the surrounding air. Therefore since Γ_1 is negative (Fig. 3-29), the force resulting from buoyancy is in the positive y-direction. Similarly, the force on vortex 2 is in the negative y-direction.

For the first effect, the momentum equation for cylindrical flow gives

$$\frac{dp}{dr} = \frac{\rho v^2}{r} = \frac{\rho \Gamma^2}{4\pi^2 r^2} \tag{3.159}$$

where the second part of the equation is valid outside the core for the Rankine vortex (equation 3.80)). Assuming adiabatic conditions in the core,

$$p\rho^{-k} = p_\infty \rho_\infty^{-k} = \text{Constant} \tag{3.160}$$

where k is the ratio of specific heats, and

$$\frac{k p_\infty \rho^{k-1}}{\rho_\infty^{k}}\, d\rho = \frac{\rho \Gamma^2}{4\pi^2 r^3}\, dr \tag{3.161}$$

Integrating between the limits of infinity and r,

$$\rho(r) = \rho_\infty^{k-1} - \frac{k-1}{k}\frac{\rho_\infty^{k}}{p_\infty}\frac{r^2}{2\pi r^2}^{\frac{1}{k-1}} \tag{3.162}$$

As an example of the magnitude of the effect, for the flight conditions for a landing B-727 (Table 3-2) and an assumed core radius of 0.6 m, the density is 0.72 kg/m compared with an ambient density of 1.23 kg/m^3. The upward buoyant force is

$$F = 2\pi g \int_0^\infty [\rho_\infty - \rho(r)]r\,dr \tag{3.163}$$

In practice the integral would be taken from the core radius, r_c, because equation (3.158) is based upon the Rankine vortex assumption, and therefore, is only valid for $r > r_c$.

Engine-exhaust extrainment is another aircraft variable which can affect the vortex transport process through variations in the vortex buoyancy. The density variation caused by exhaust entrainment is

$$\rho = \rho_\infty T_\infty / T \tag{3.164}$$

where T is the temperature of the air in the core of the vortex and T_∞ is
the ambient air temperature. The buoyant force produced by exhaust entrainment is also given by equation (3.162).

The third cause of buoyancy is vortex descent through a nonadiabatic atmosphere. The interface between the wake fluid and the exterior atmosphere is only a dividing streamline; it does not support shear or pressure. In the presence of atmospheric turbulence or turbulence in the wake, the streamline is perturbed, and some mixing between the interior wake fluid and the exterior atmosphere occurs. When the mixing is small, as it is when the wake is young and the turbulence is low, the wake fluid retains its identity and its physical properties as it moves about through the atmosphere. One consequence is the creation of aerostatic forces as the wake moves into regions of varied temperature and density. For example, an upward (or buoyant) force is developed on those segments of a wake descending into stable stratified atmosphere if there is little or no mixing of the ambient air with the wake fluid. Results of experiments on wake buoyancy are presented by Tombach (ref. 46) in which he showed that a wake descending into a stable atmosphere acquired buoyancy, until at some later time, turbulent mixing between the wake and the atmosphere became significant enough to erode the temperature difference between them. Increasing ambient turbulence shortened the period during which buoyancy was acquired, and as a consequence of more rapid mixing, resulted in more rapid decay of both buoyancy and vortex descent.

The aerostatic forces are a result of an increase in the temperature of the fluid in the wake oval, caused by adiabatic compression as the oval descends into a denser atmosphere. An atmospheric temperature

stratification other than adiabatic (neutral) will result in a temperature difference, and hence a density difference, between the wake and the atmosphere. Buoyancy will thus be created for wakes descending into a stable atmosphere (the most common situation) with no mixing. Theoretical models with no mixing (ref. 47) indicate that the buoyancy so acquired accelerates wake descent and decreases vortex-spacing. The experimental observations discussed above indicate, however, the possibility of a retarding tendency caused by buoyancy, but may be a consequence of entrainment rather than of buoyancy.

Overall, the effects of aerostatic forces on vertical wake motions appear to be of smaller order than the dissipitive mechanisms associated with turbulence, which could overwhelm the buoyancy effect, and thus, result in the difficulties experienced in properly isolating the influence. A comprehensive discussion of both theoretical and experimental observations on the descent of a wake in a stratified fluid is given in ref. 47.

The predominant effect of atmospheric stability appears to be the indirect one associated with the vertical air currents resulting from atmospheric mixing. In a stable atmosphere, this mixing is suppressed, resulting in reduced vertical air motions and reduced effects on vertical wake motions. In unstable conditions, vertical atmospheric activity and resulting wake motions are amplified. Such motions may be either upward or downward, largely depending on the radiative absorbtivity of the ground below; thus unpredictable variations of wake ascent or descent relative to the descent rate derived from mutual induction alone can result under such unstable atmospheric conditions. This is one of the primary sources of random vortex motion superimposed on the deterministic effects of non-turbulent crosswind and mutual induction.

The effects of atmospheric stratification on initial wake descent rates are shown schematically in Fig. 3-~~33~~46. For a stable atmosphere, the wake descends initially at a speed which is consistent with the inviscid analytical model. Random influences become more evident for less stable conditions. The figure applies only to vertical wake motion during the first few moments after the wake has been fully formed. Subsequent vertical wake motions are influenced by buoyancy, turbulence, and the continued

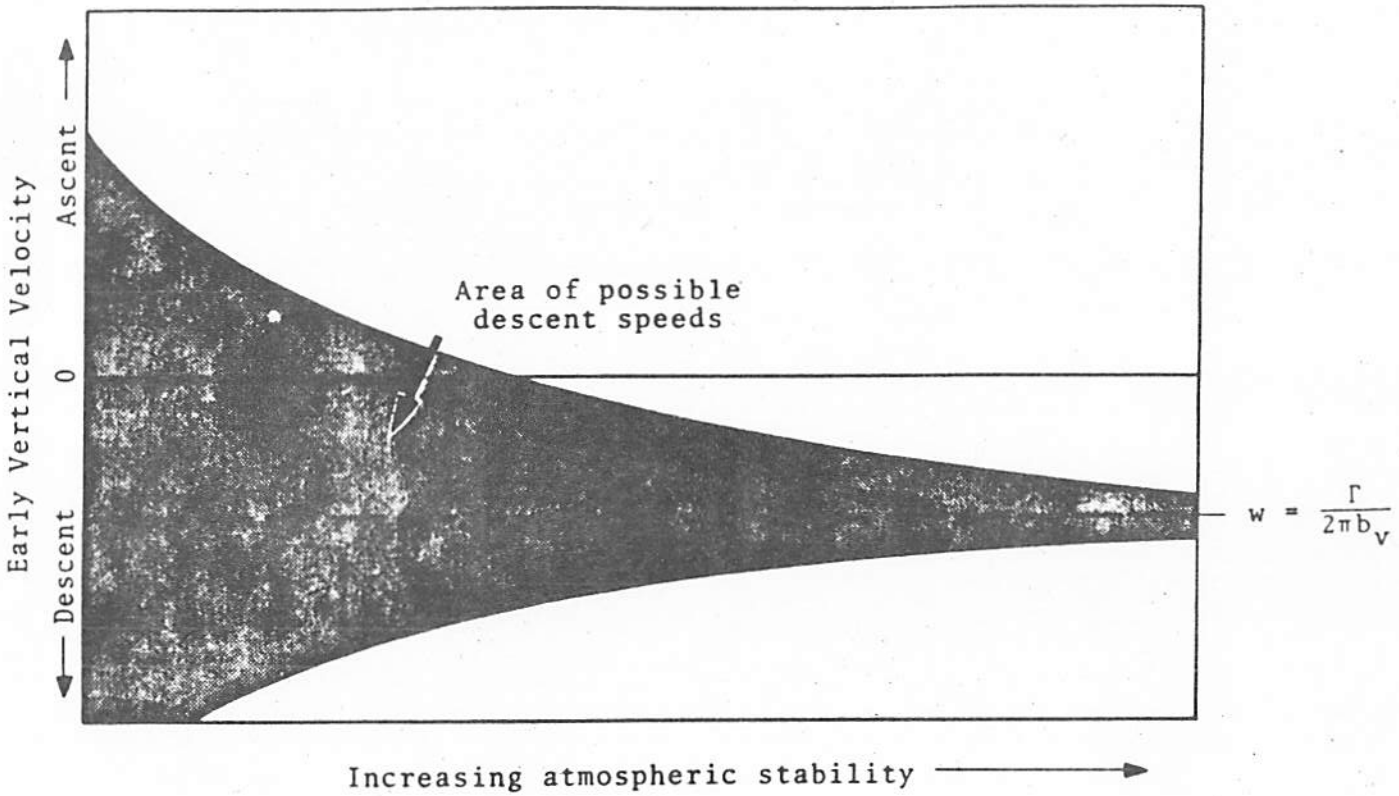

FIGURE 3-~~35~~ 46. SCHEMATIC REPRESENTATION OF OBSERVED RELATIONSHIP BETWEEN ATMOSPHERIC STABILITY AND WAKE DESCENT AT EARLY TIMES. IN UNSTABLE CONDITIONS, THE DESCENT IS RELATIVELY INDETERMINATE, PROGRESSIVELY INCREASING STABILITY RESULTS IN DESCENT MORE CLOSELY APPROACHING THE VORTEX INDUCED WAKE SPEED.

random action of vertical air motions (which are accentuated for less stable conditions). Not all of these factors can be quantified presently however.

Vertical air motions often become quite pronounced under the influence of thermal activity near the ground. Extreme vertical convolutions of wakes can occur because of convection by these air motions. Under these conditions, the wake (and the vortex pair) is stretched and distorted into a highly nonlinear configuration where mutual and self-induced vortex velocities act to amplify the process. Figure 3-47 shows such a wake generated near the ground under conditions of high atmospheric thermal activity. The impossibility of dealing with such a resultant wake structure on anything but a statistical basis is clearly evident. However, it remains to be shown that such a convoluted wake could pose a hazard in operational conditions. There is reason to believe that such a wake structure does not pose a hazard because of the limited exposure time which an encountering aircraft would experience.

All wake motions near the ground do not exhibit such extreme behavior. Under stable atmospheric conditions and reduced thermal activity, the wake and the vortex pair undergo more orderly motions which are fairly well understood and can be approximated analytically. These conditions are also the ones of greatest operational interest because these same factors are conducive to wake persistence. Wakes generated or moving into ground effect are subjected to the influences of the induction velocities generated by the underground or image vortices. The vertical motion of the wake gradually and predictably slows and eventually stops at about one-half the vortex spacing above the ground, and simultaneously, the vortices move apart.

3.3.4.3 Comprehensive Vortex Transport Model

A comprehensive wake vortex transport model based on the phenomena described in the preceding sections has been formulated (refs. 48 and 49). The most important of these phenomena is mutual induction which includes image vortices to provide for the effect of the ground as well as the effect of crosswind. This comprehensive model adds the effects of buoyancy to the effects of mutual induction and crosswind. When buoyancy conditions are present (i.e., the density of the vortex cell differs from that of the

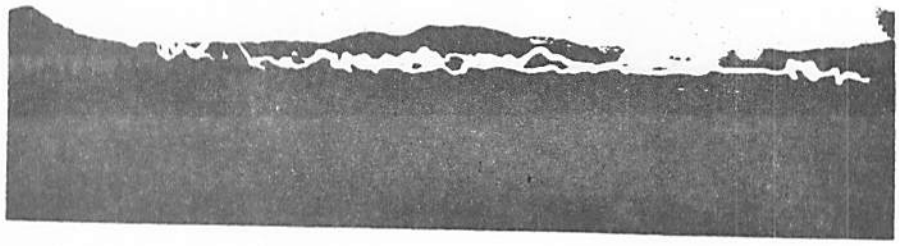

FIGURE 3-~~34~~ 47. VORTICES IN GROUND EFFECT.

65

ambient atmosphere), there are two forces which impose an acceleration on the vortex. The resulting velocity causes the vortex transport velocity to differ from that described in Section 3.3.2. The vortex transport model is a modification of the transport model presented in Section 3.3.2. It calculates the vortex transport velocity resulting from the acceleration and superimposes that velocity on the vortex transport velocity because of mutual induction.

The mass of the vortex per unit length is

$$\iint_{A_1} \rho \, dA = \bar{\rho} A_1 \tag{3.165}$$

where A_1 is the cell cross-sectional area associated with the vortex and ρ is the average mass density within A_1. The first force is the buoyancy force given by

$$F = (\rho_\infty - \bar{\rho}) A_1 g \tag{3.166}$$

and acts in the positive vertical direction. The second force is the Kutta-Joukowski force which is the force caused by a body with rotation moving relative to a fluid. Let V_1 and W_1 be the components of the sum of the velocity fields of vortices 2,3, and 4 (cf., Fig. 3-29) at the centroid of vortex 1. Let Y_1 and Z_1 be the transport velocity components of vortex 1. For pure advection presented in the basic vortex transport predictive model, $Y_1 = V_1 + V_\infty$ and $Z_1 = W_1$; this will not always be true in the generalized case considered in the comprehensive transport model. Let V_2, W_2, Y_2, and Z_2 have similar meanings for vortex 2.

The vector form for the Kutta-Joukowski force is

$$\bar{F} = \rho_\infty \bar{V}_r \times \bar{\Gamma} \tag{3.167}$$

where V_r is the free-stream velocity relative to the vortex. The horizontal component of the Kutta-Joukowski force on vortex 1 is

$$F_h = \rho_\infty (W_1 - \dot{Z}_1) \Gamma_1 \tag{3.168}$$

(Γ_1 is negative.) The vertical component is

$$F_v = -\rho_\infty[(V_1-V_\infty)-\dot{Y}_1]\Gamma_1 \tag{3.169}$$

Similarly for vortex 2, the buoyancy force is

$$F = (\rho_\infty-\bar{\rho})A_2 g \tag{3.170}$$

The horizontal component of the Kutta-Joukowski force is

$$F_h = \rho_\infty(W_2-\dot{Z}_2)\Gamma_2 \tag{3.171}$$

where F_2 is positive, and the vertical component is

$$F_v = -\rho_\infty[(V_2+V_\infty)-\dot{Y}_2]\Gamma \tag{3.172}$$

The change in the transport velocity of a vortex over a time period Δt is caused by three effects: (a) acceleration caused by application of buoyancy and Kutta-Joukouski forces, (b) displacement of the vortex within the velocity fields of the other vortices, and (c) change in the velocity field of the other vortices because of their displacement. The second and third effects are the mutual advection effects discussed in Section 3.3.2. Let starred quantities denote vortex transport parameters because of buoyancy and Kutta-Joukowski forces. The star denotes vortex transport because of the first transport effect only. Then

$$Y_1^* = \frac{\rho_\infty(W_1-\dot{Z}_1)\Gamma_1}{\bar{\rho}A_1} \tag{3.173}$$

and

$$Z_1^* = \frac{(\rho_\infty-\rho)A_1 g-\rho_\infty[(V_1+V_\infty)-\dot{Y}_1]\Gamma_1}{\bar{\rho}A_1} \tag{3.174}$$

Then in the numerical integration process, both the velocity caused by the first transport effect and the total transport velocity are calculated

$$\dot{Y}_1^*(t+\Delta t) = \dot{Y}_1^*(t)+\ddot{Y}_1^*(t)(\Delta t) \tag{3.175}$$

and the total vortex transport velocity is

$$\dot{Y}_1^*(t+\Delta t) = \dot{Y}_1^*(t+\%t)+V_1(t)+V_\infty \tag{3.176}$$

and the vortex position is

$$Y_1(t+\Delta t) = Y_1(t)+\dot{Y}_1(t)(\Delta t) \tag{3.177}$$

Similarly,

$$\dot{Z}_1^*(t+\Delta t) = \dot{Z}_1^*(t)+\ddot{Z}_1^*(t)(\Delta t) \tag{3.178}$$

$$\dot{Z}_1^*(t+\Delta t) = \dot{Z}_1^*(t+\Delta t)+W_1(t) \tag{3.179}$$

and

$$Z_1(t+\Delta t) = Z_1(t)+\dot{Z}_1(t)(\Delta t) \tag{3.180}$$

In practice, these equations are integrated with a fourth-order Runge-Kutta integration technique. In the absence of buoyancy, the starred quantities become zero, and equations (3.175) and (3.178) become equations (3.100) and (3.101), respectively. Similar equations are also written for vortex 2.

It is noted that the Kutta-Joukowski force cannot exist without buoyancy. The Kutta-Joukouski force results from a relative velocity between the vortex and the air in which it is immersed. The only mechanism in the model by which such a relative velocity can be generated is buoyancy since the basic assumption of the transport model is that the vortex transport velocity is identical to the velocity field at the vortex centroid.

3.3.4.4 Comprehensive Transport Model Verification

A comparison of predicted vortex tracks and vortex tracks obtained from photographic data of smoke entrained in the vortex is presented in Fig. 3-48 (ref. 50). The crosswind profiles assumed for the calculated vortex track are a mean power-law model based on data measured before aircraft passage, a linear interpolation based on data measured before aircraft

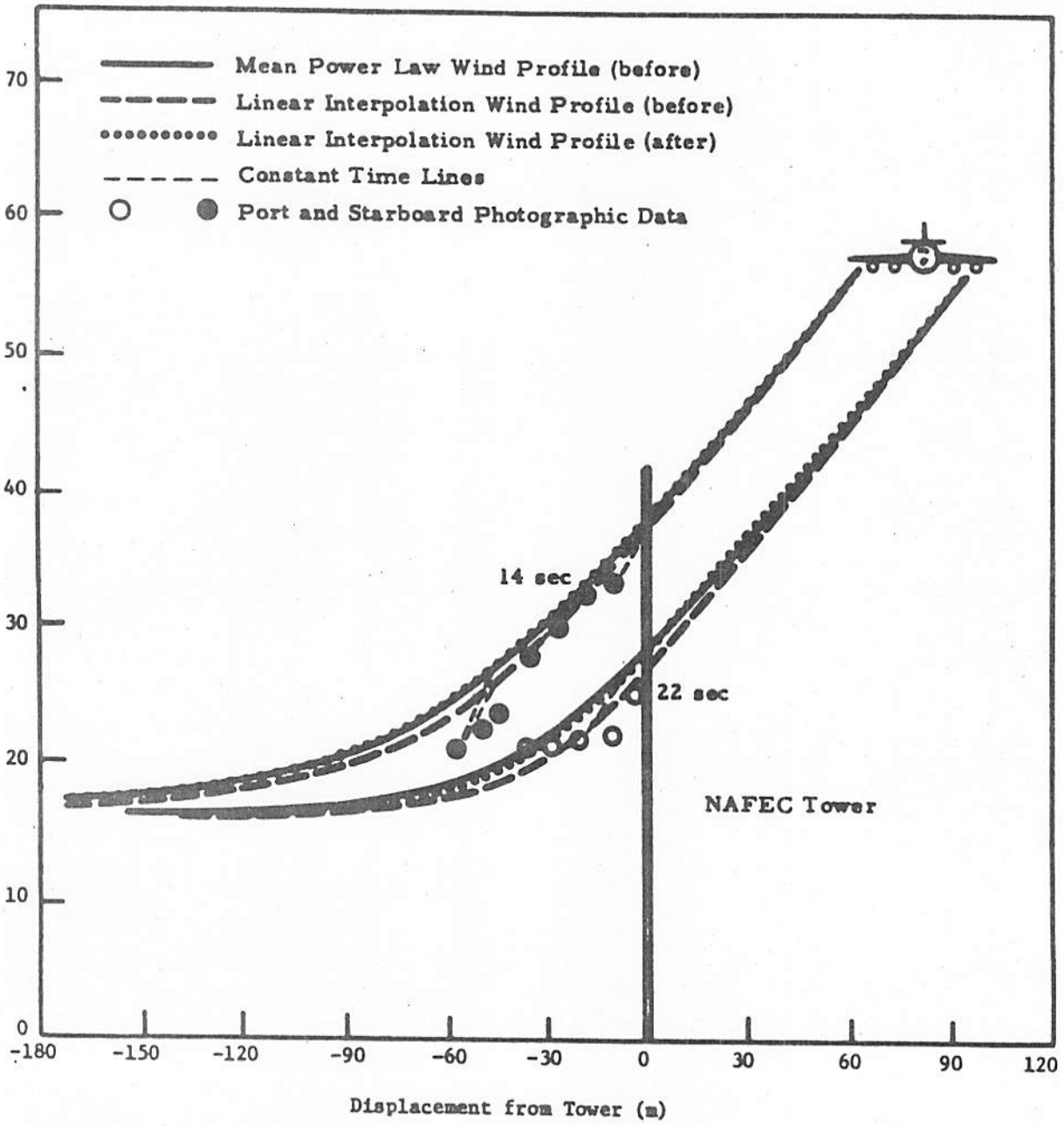

FIGURE 3-~~35~~ 48. COMPARISON OF PREDICTIVE VORTEX TRACKS WITH PHOTOGRAPHIC DATA FOR NAFEC B-707 RUN 17, 10/18/72.

passage, and a linear interpolation based on data measured after aircraft passage.

Figure 3-48 shows the importance of proper input of aircraft parameters as initial conditions to the integration of equations (3.100) through (3.103). The measured vortex positions are the same for the top and bottom. The predicted vortex track for the top uses an assumed value of spanwise loading coefficient of Ü/4, the value for an elliptically loaded wing. The predicted vortex track for the lower figure uses the more appropriate value (calculated from actual spanwise loading) of 0.63.

In the late 1970's, there were several extensive vortex measurement programs in which many vortex trajectories were measured and analyzed. These measurement programs permit comparison of experimental data and calculated vortex trajectories on a statistical basis. The results of these extensive vortex measurement programs are presented in Section .

3.3.5 Statistical Description of Vortex Transport

3.3.5.1 Background for Vortex Statistics

As described earlier, the vortex transport process may be described as a deterministic process with a significant stochastic component imposed upon it. This is also true for the processes of vortex demise to be described in Section 3.4. For this reason, both vortex transport and vortex demise must be treated statistically. Historically, the vortex research and development program began by treatment of the detministic aspects of vortex transport and demise, and it was later before data bases of size sufficient to permit meaningful statistical analysis were available.

The current status of the statistical treatment of vortex transport and demise is tht statistical approaches have been applied to certain sets of vortex data, but a unified overall statistical approach to the vortex problem is still evolving. Analytical statistical models of vortex behavior have been developed for vortex demise, and these models are presented in Section 3.4.4. Although these models have been developed for vortex demise, they could be adapted to vortex transport. Therefore, in this state-of-the-art summary of vortex technology, these statistical models are described under the subject of vortex demise because of their historical origins.

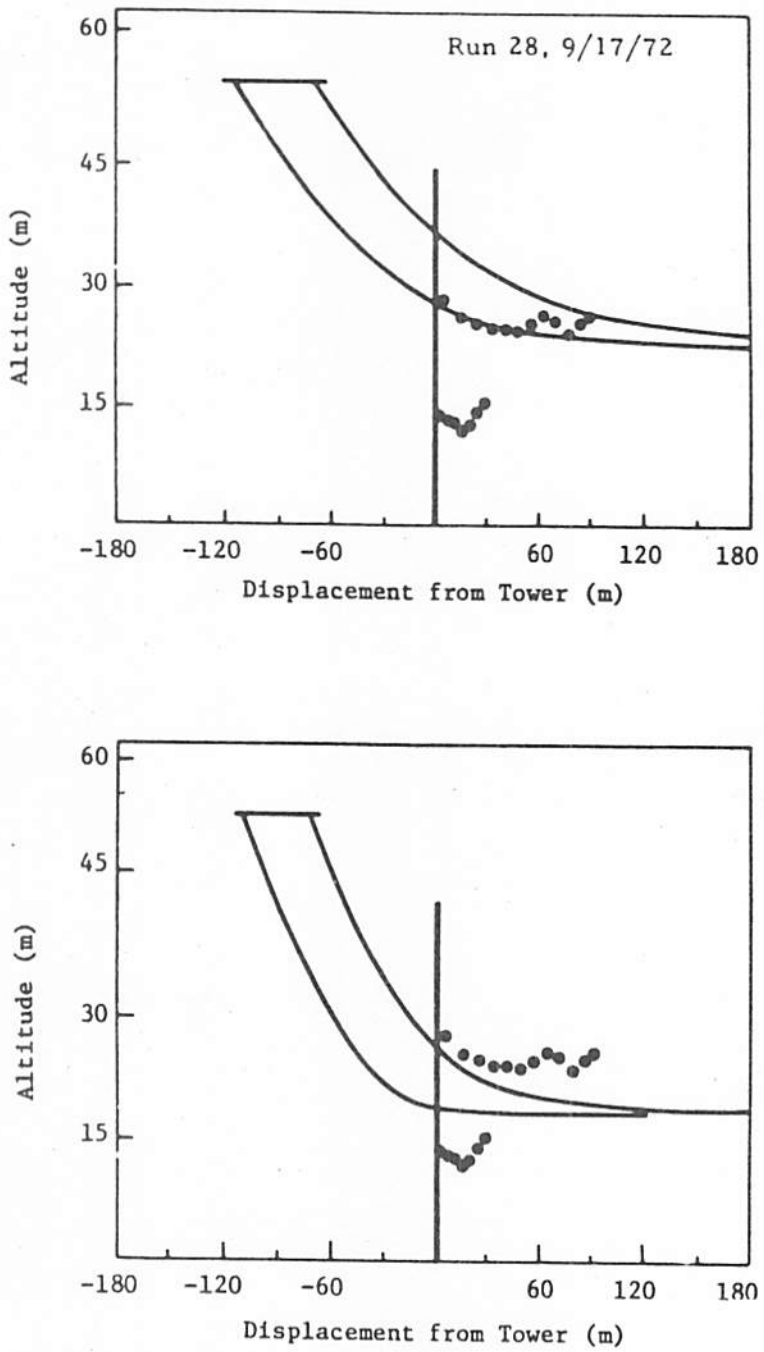

FIGURE 3-~~36~~ 49. WAKE VORTEX TRAJECTORY COMPUTED BY THE PREDICTIVE WAKE VORTEX TRANSPORT MODEL FOR A B-747 TOWER FLYBY (NAFEC RUN 28 9/17/72) WITH ELLIPTIC LOADING (TOP K = $\pi/4$) AND WITH FLAP EFFECTS (BOTTOM K = 0.63)

71

However, such models are relevant for vortex transport, although their adaptation to vortex transport remains to be accomplished.

The second aspect of the statistical treatment of vortex transport and demise is the presentatin fo vrotex data in statistical formats. There are several ways in which this can be done, and various authors have chosen various approaches i the statisticl presentation fo vortex data. Formants which have been used for the description of vortex transport may also be appropriate for the description of vortex demise, and conversely, formats which have been used for vortex demise may also be appropriate for the description fo vortex transport. The pruposes of the presentation of statistical data in this state-of-th-art summary is the presentation fo the various formats in which vortex statistical data have been presented in the vortex literature and a general overview of the nature of statistical vortex data. It is understood, however, that statistical approaches to vortex behavior are still evolving and that certain approaches which are presented here may be relevant to data other than that for which they are presented.

The statistical approaches presented in this section are presented i the form of classical statistics. However, it is likely that the statistics of extreme values will be a very useful form for the presentation and analysis of vortex statistics. The statistics of extreme values is associated with the analysis of random events of low probability and has been applied to structural fatigue and to air quality. However, it has not yet been applied to vortex problems. The statistics of extreme values is discussed in Section .

This section uses the terms "probability distribution function" and "probability density function" in their classical statistical contexts. In classical statistics, the probability distribution function, or probability function, $F(x)$, of random variable, X, is the probability that $X < x$, or

$$F(x) = P[X < x] \tag{3.181}$$

and has the properties that

$$F(-\infty) = 0, \qquad F(\infty) = 1 \tag{3.182}$$

The probability density function, f(x), is the derivative of the probability function with respect to x and is the probability that the random variable X lies between values x-Δ and x+Δ. The probability density function has the properties

$$F(-\infty) = 0, \qquad f(\infty) = 0 \tag{3.183}$$

and

$$\int_{-\infty}^{\infty} f(x)dx = 1 \tag{3.184}$$

For the statistics of vortex behavior, the probability that residence time or life time exceeds a certain value is often of interest. Therefore, in order to be consistent with probability functions as they are used in classical statistics, the descending probability function, F'(x), of the random variable, X, is defined as the probability that X > x and has the properties that

$$F'(-\infty) = 1 \qquad F'(\infty) = 0 \tag{3.185}$$

If the random variable, X, can only hve positive values, then

$$F'(0) = 1 \quad \text{and} \quad F'(\infty) = 0 \tag{3.186}$$

Then the probability density function is

$$f(x) = -d[F'(x)]/dx \tag{3.187}$$

3.3.5.2 Statistical Vortex Transport Data

The preceding paragraphs have set the background for the statistical treatment of vortex phenomena. The following paragraphs present some of the ways i which vortex residence time data have been presented in the literature. A presentation of some of the ways in which vortex life time data has been presented in the literature is given in Section 3.4.5

Figure 3-50, taken from ref. J, shos the probability density function of residence time as measured by the Groundwind Vortex Sensing System at O'Hare Airport. Results are shown for B-727 and B-747 aircraft. Figure 3-51 presents similar data for wide body three engine aircraft. Ref. J presents data for several more types of aircraft. In these figures, the shaded areas indicate residence time limited by vortex demise in the flight corridor, and the clear areas of the bars indicate residence time limited by vortex transport. Figure 3-52 shows the same information as Figure 3-51, but the data are presented in the form of a descending probability distributin function, rather than as a probabiity density function as in Figure 3-51. Figure 3-52 shows the probability that the vortex will be in the flight corridor at the time shown on the horizontal axis.

Obviously, vortex residence time is a function of crosswind. Figures 3-53 and 3-54 from ref. J show the statistical distribution (probability density function) of vortex residence time for several bands of crosswind for the B-747 and B-727, respectively. As expected, vortex residence time is a strong function of crosswind with the longes residence times occurring for 2 knots < V < 4 knots. In order to show that it is the crosswind which limits vortex residence time, the same data for all aircraft are plotted in Figure 3-55 for several bands of headwind. In general, the distribution of vortex residence times is not a strong function of headwind.

The data used for Figures 3-50 through 3-55 were obtained for baselines at 1550 ft and 1330 ft from the runway threshold. Therefore, the aircraft were approximately 130 ft above the ground at this point. As shown in Section 3.3.3.3, the crosswind at which the vortex stalls i the flight corridor is a strong function of the altitude of aircraft passage. Therefore, the data shown in Figures 3-50 through 3-55 would be different if it were measured at a different baseline for which the nominal aircraft altitude would be different.

Figure 3-56, taken from ref K, shows dat similar to that shown in Figure 3-52, but with the data presented on a linear scale. The data of Figure 3-56 are based on measurements taken at Kennedy International Airport in 1975.

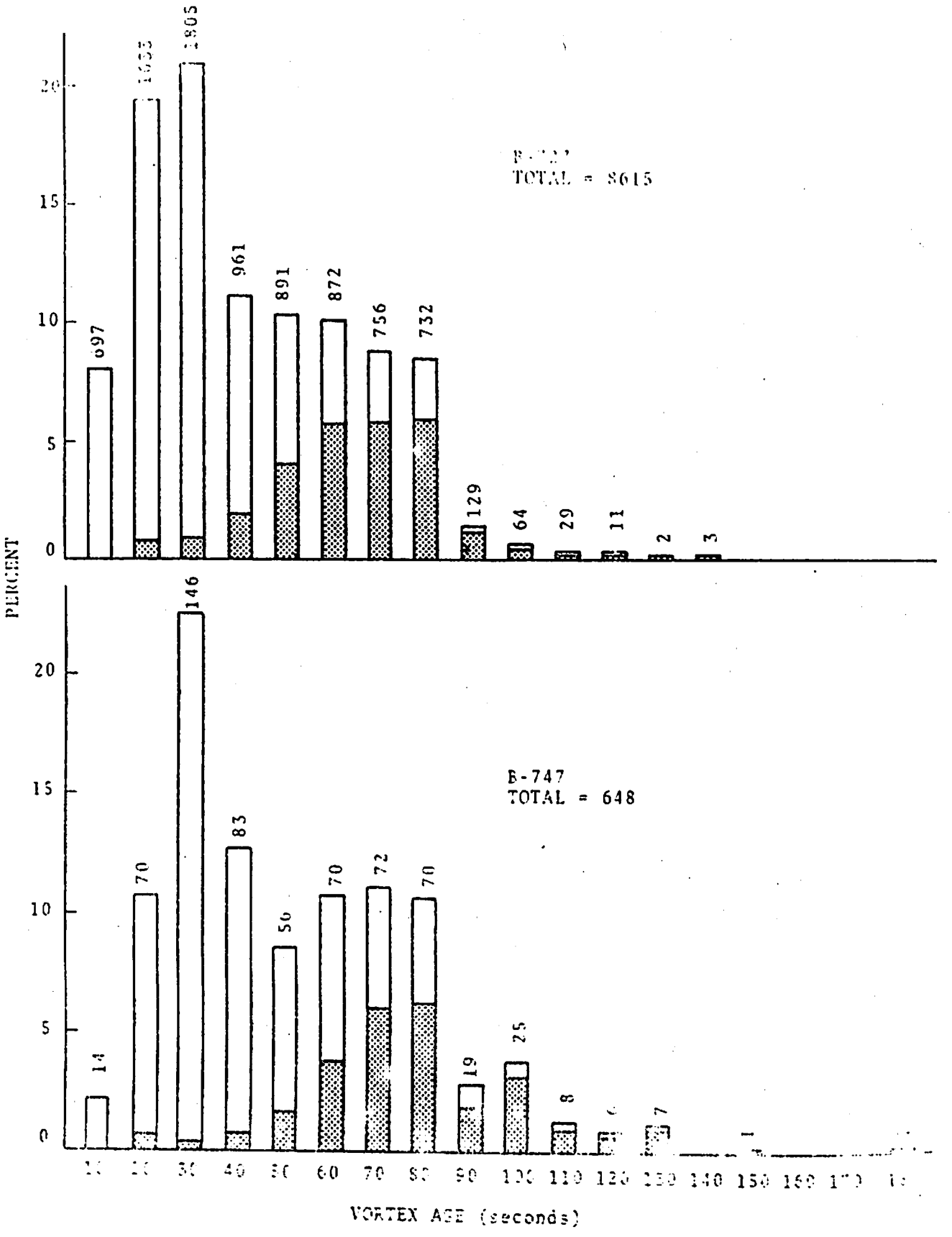

FIGURE 3-30. RESIDENCE TIME DATA FOR B-727 (TOP) AND B-747 (BOTTOM) AIRCRAFT

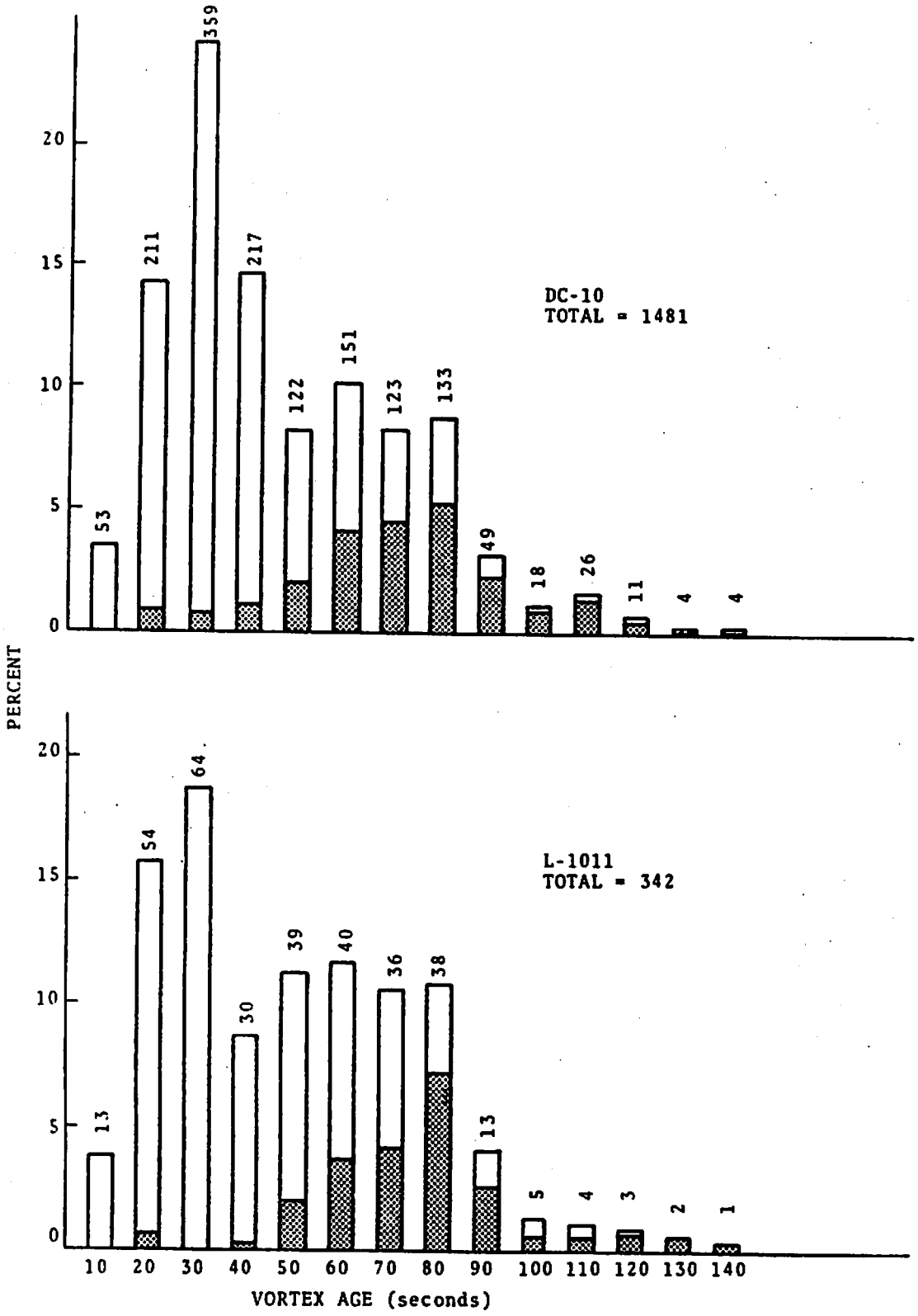

FIGURE ~~6~~ 3-5. RESIDENCE TIME DATA FOR DC-10 (TOP) AND L-1011 (BOTTOM) AIRCRAFT

76

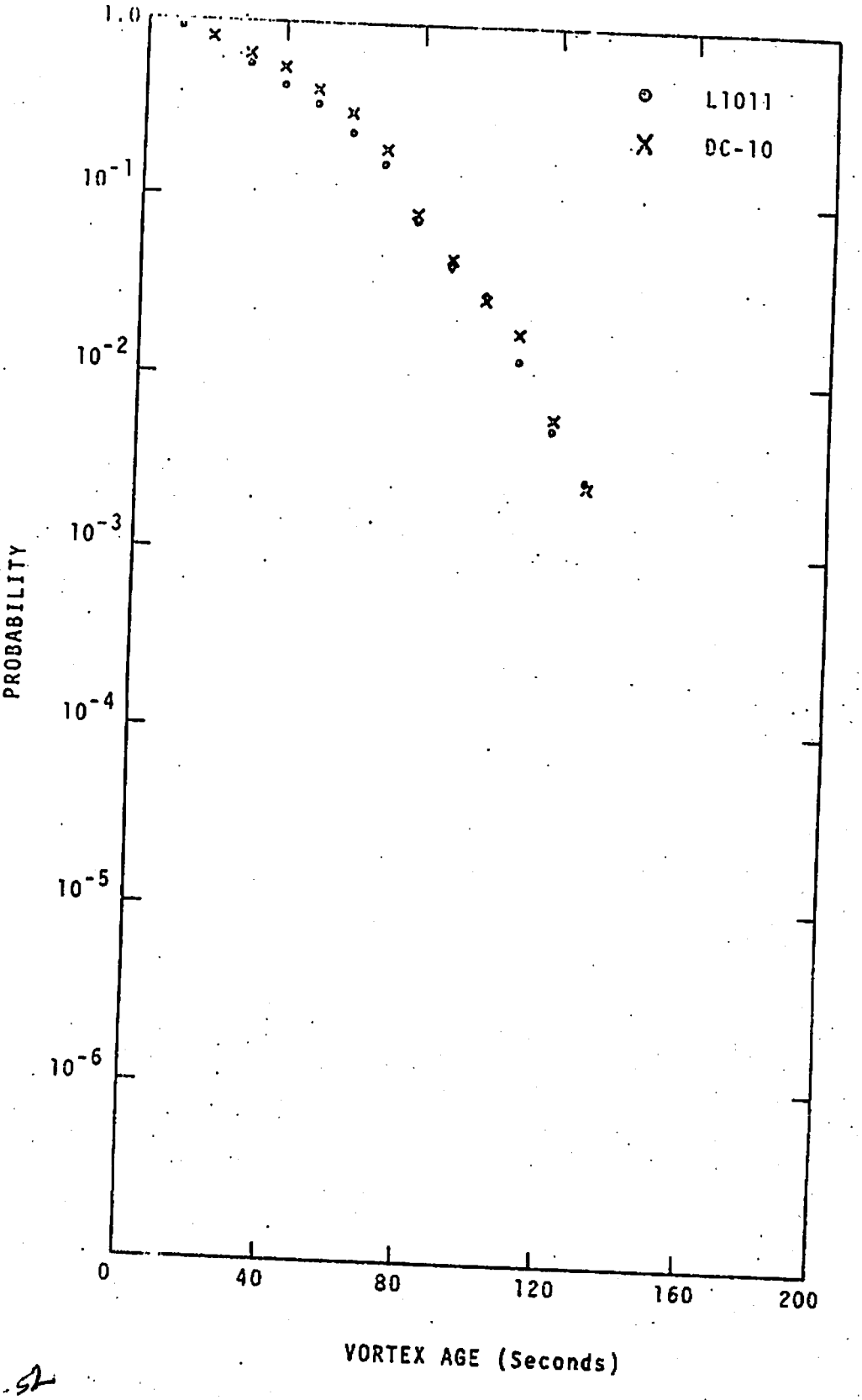

FIGURE 3-52. PROBABILITY FOR A VORTEX TO REMAIN IN THE SAFETY ZONE LONGER THAN A GIVEN TIME FOR L-1011 AND DC-10 AIRCRAFT

77

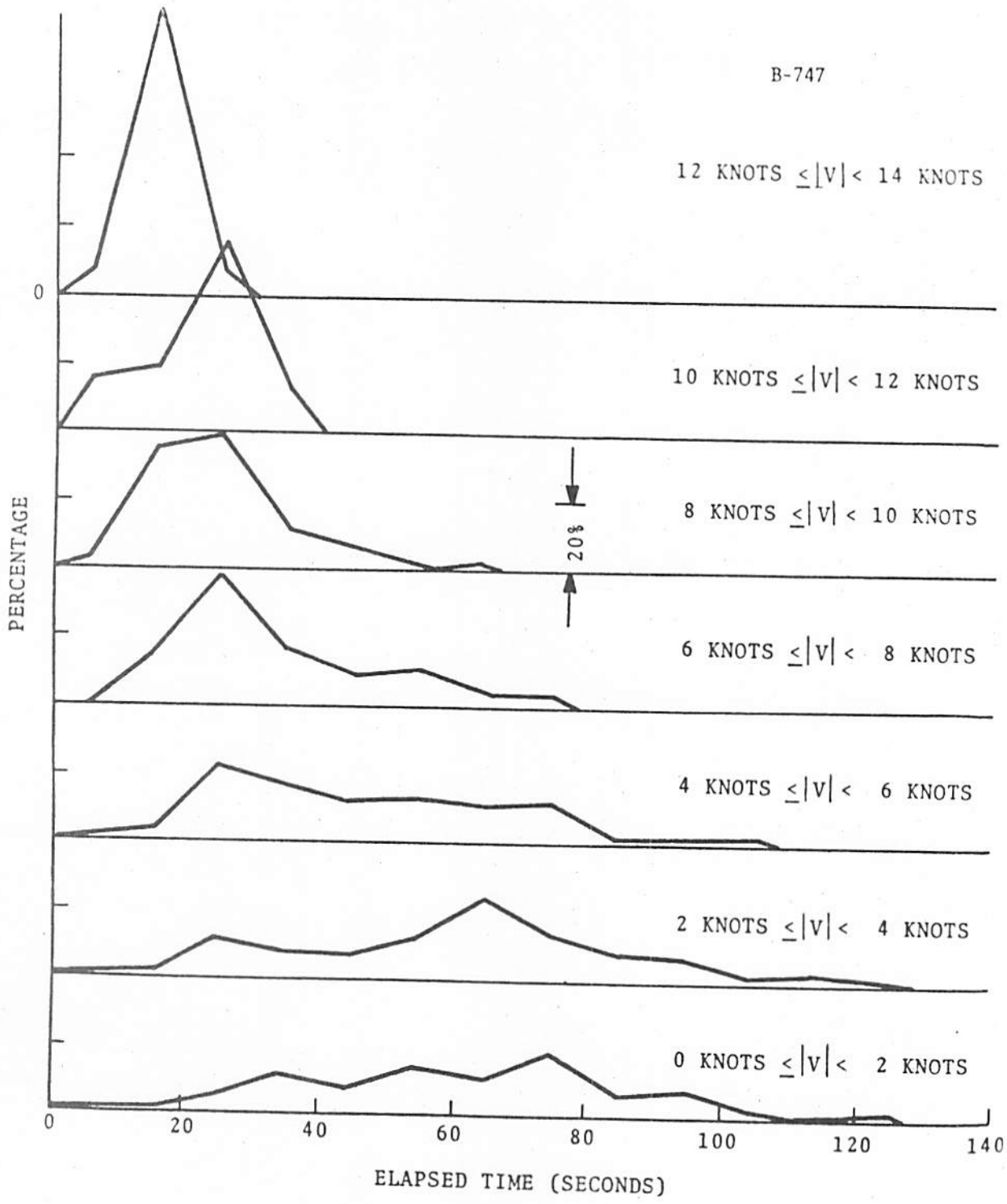

FIGURE 47. PROBABILITY DENSITY FUNCTION OF ~~PERCENTAGE~~ OF B-747 VORTICES THAT REMAINED IN SAFETY CORRIDOR AS A FUNCTION OF CROSSWIND

3-52

78

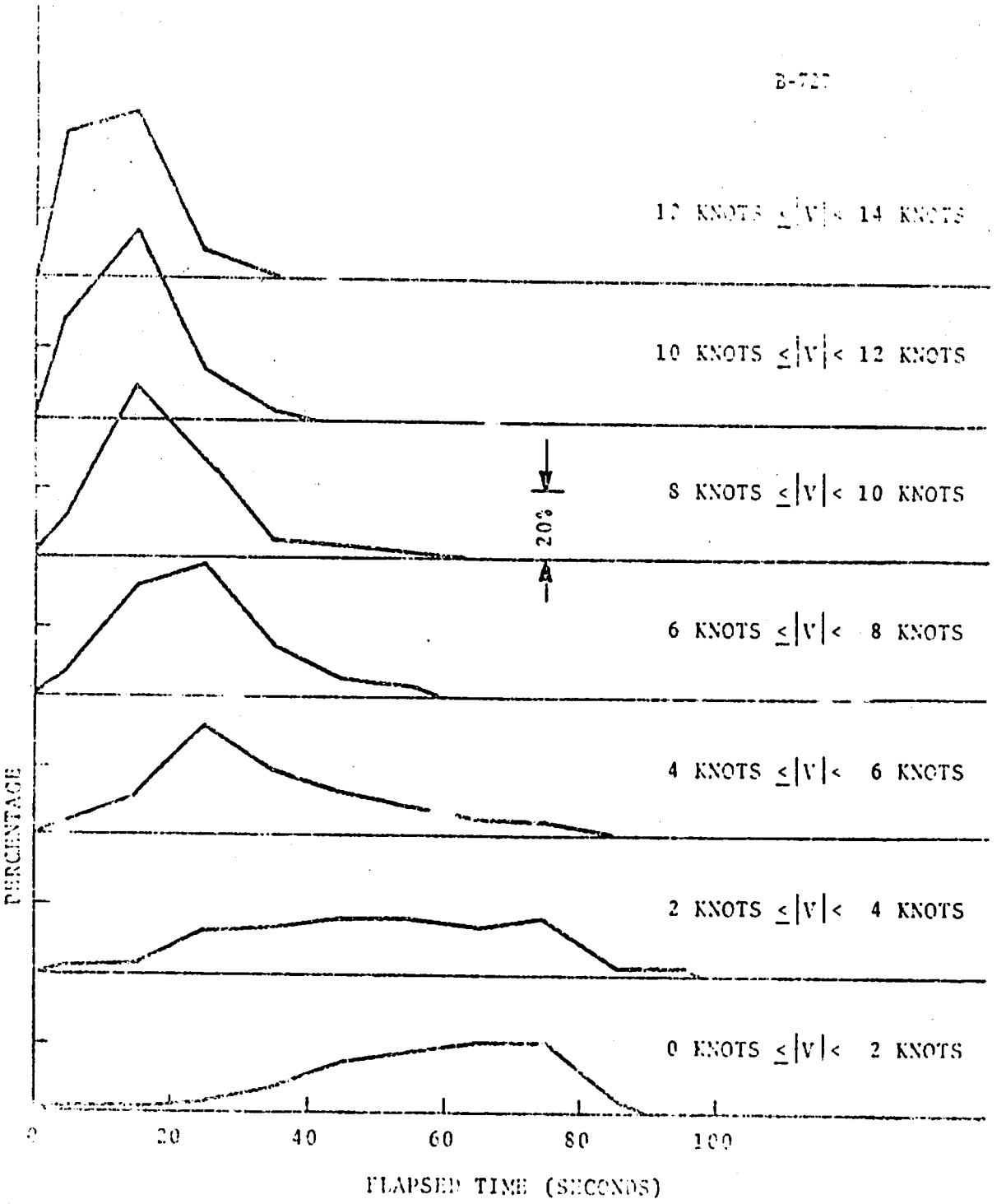

3-54 PROBABILITY DENSITY FUNCTION

FIGURE 41. [redacted] OF B-727 VORTICES THAT REMAINED IN SAFETY CORRIDOR AS A FUNCTION OF CROSSWIND

79

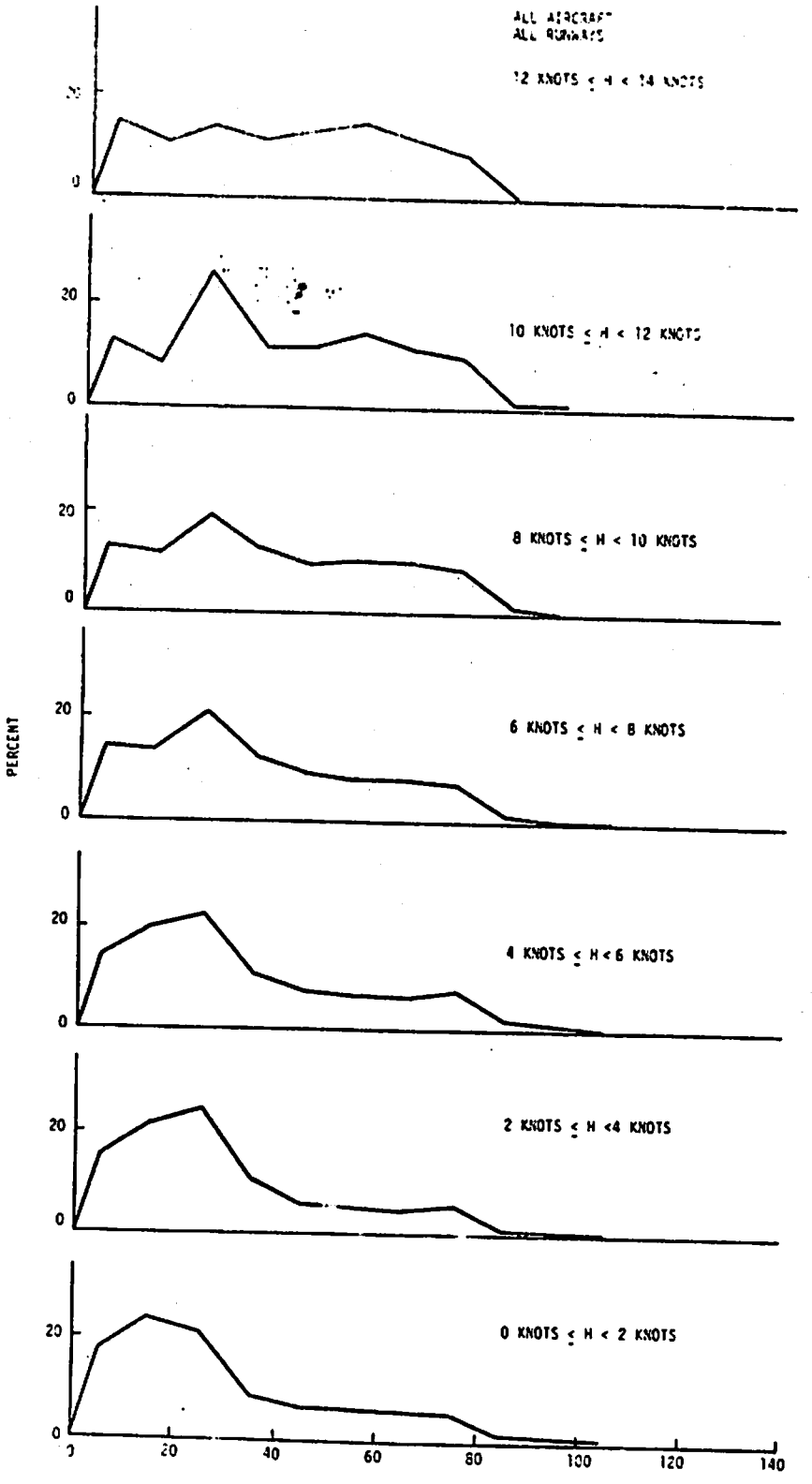

FIGURE 4. PROBABILITY DENSITY FUNCTION ~~PERCENTAGE~~ OF VORTICES THAT REMAINED IN SAFETY CORRIDOR AS A FUNCTION OF HEADWIND COMPONENT

3-55

80

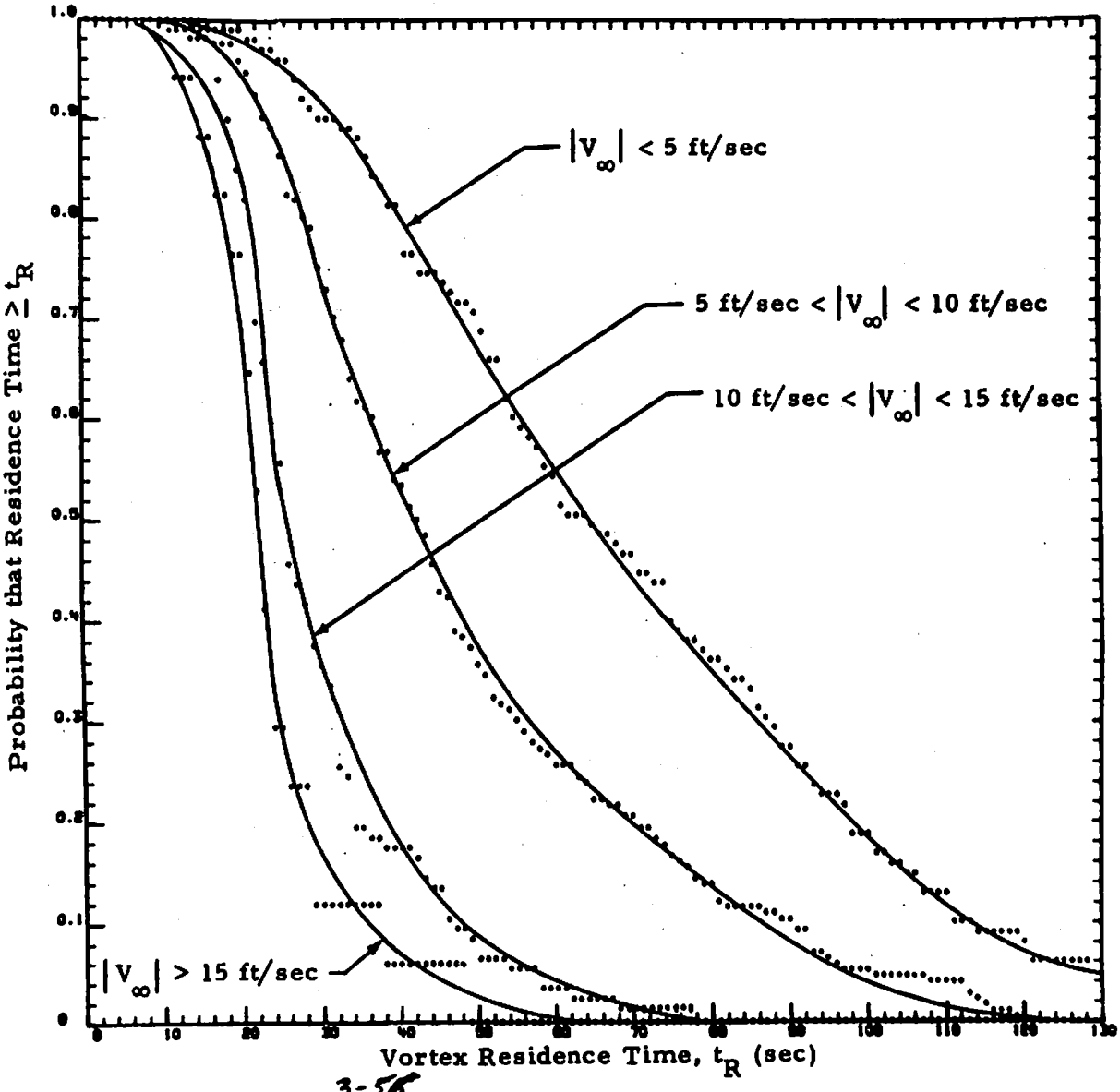

3-56

FIGURE 68. PROBABILITY DISTRIBUTION FUNCTION FOR MEASURED VORTEX RESIDENCE TIME AT BASELINE 1

81

Measured Residence Time at Baseline 2 (sec)

F
A
B

Figures 3-57 and 3-58 show vortex residence time as a function fo crosswind for data measured at Kennedy International Airport in 1975. the calculated data shown by the labeled lines are transport times calculated from nominal values of aircraft parameters, and the mesured data indicated by points are measured residence times, which may be limited by either transport or by life time. The shaded area in each figure represents the range of transport times which could occur as a results of normal, but unmeasured, variations in the aircraft parameters. The weight and airspeed limits from which the data in the shaded area were calculated arte shown i the table below. The minimum weight is the empty weight plus one hour of fuel for the smallest model of the type. The maximum weight is the maximum certificated landing weight of the larges model of the type.

Variations in Aircraft Parameters Used to Calculate Shaded Areas of Figures 3-56 and 3-57

	B-747	B-727
Minimum Aircraft Weight (lb)	331,412	88,893
Maximum Aircraft Weight (lb)	630,000	154,500
Minimum Approach Airspeed (ft/sec)	229.2	204.2
Maximum Approach Airspeed (ft/sec)	246.2	221.2

In addition to weight and airspeed variations, there was an allowable ±20 ft deviation from the glideslope and an allowable ±30 ft deviation from the localizer centerline for the determination of the shaded area. The shaded area is of operational significance because it shows that even for a very sophisticated vortex transport model, the variation of aircraft parameters which are generally unknown in an operational environment can cause a long transport time for a large range of crosswinds.

In Figures 3-57 and 3-58, the shaded area does not include uncertainties in crosswind measurement, which is the difference between crosswind at the anemometer location and crosswind at the vortex measurement baseline. For the experimental measurements of ref. K, the crosswind for

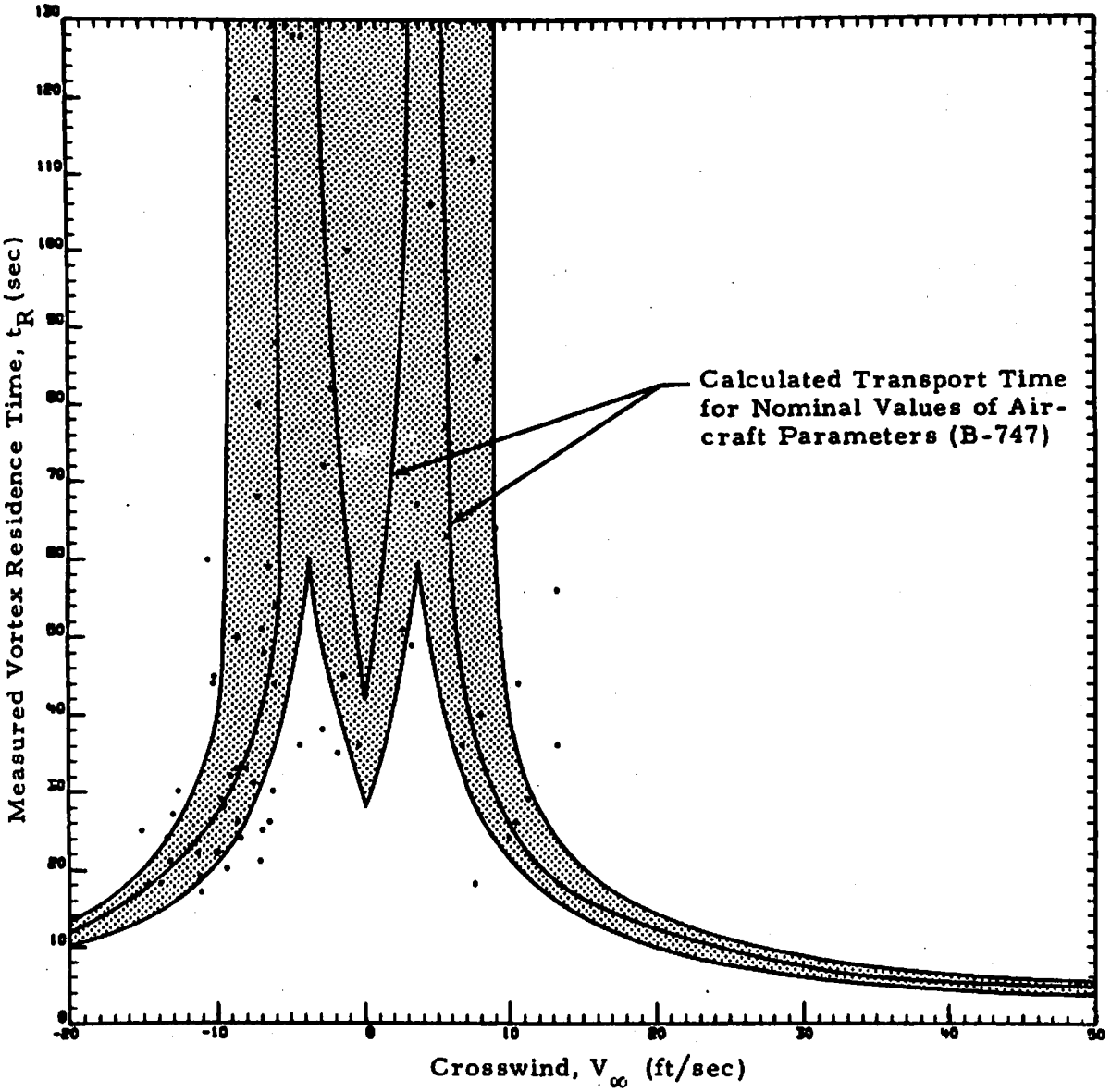

FIGURE 3-57 VORTEX RESIDENCE TIME FOR WIDE-BODY AIRCRAFT AS MEASURED BY GROUND WIND VORTEX SENSING SYSTEM Shaded area represents expected variations in calculated transport time from expected variations in aircraft parameters

83

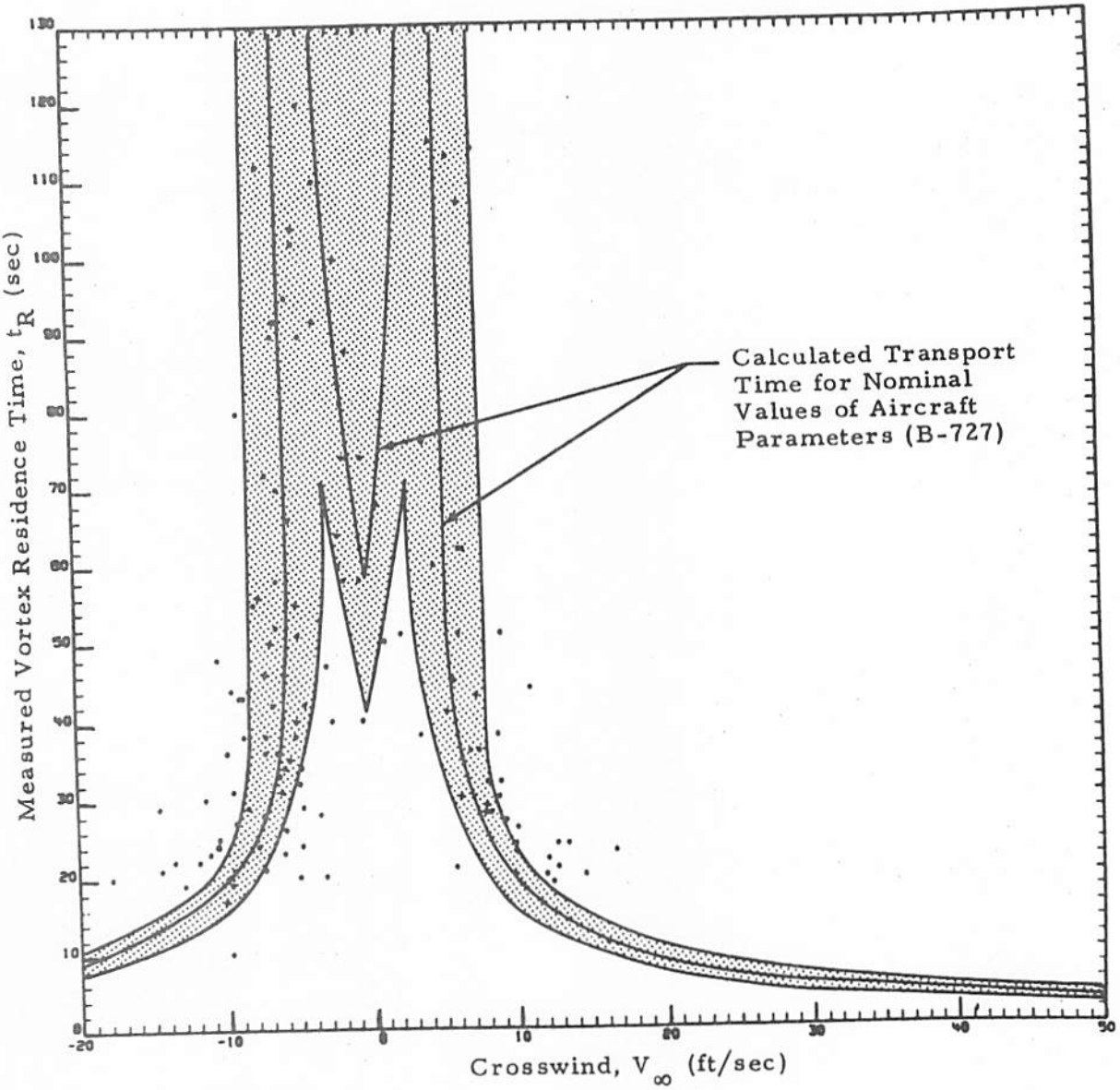

FIGURE 3-58 VORTEX RESIDENCE TIME FOR NARROW-BODY AIRCRAFT AS MEASURED BY GROUND WIND VORTEX SENSING SYSTEM Shaded area represents expected variations in calculated transport time from expected variations in aircraft parameters

each of the experimental points was measured at a distance of approximately 1000 ft from the point at which vortex transport was measured. This difference in the locatin of the measurement of crosswind and the measuremdnt of vortex transport accounts for the fact that some of the experimental points lie outside of the shaded area. A more general discusion of the crosswind uncertainty is presented in Section .

Reference I presents a good analysis of vortex residence time limited by transport time or by life time. Figure 3-59 indicates the percentage of the residence times which were life time limited. Most of the vortices with a residence time in excess of 40 sec experience vortex demise i the flight corridor, whereas most of the vortices with a residence time of 40 sec or less were transport time limited. However, the cases shown in Figure 3-59 represent only 30 percent of all the data; 50 percent of the recorded data had a residence time of less than 30 sec. The general conclusion tht trandpost is the dominant limitations for short residence times, and life time is the dominant limitation for long residence times is also supported by Figures 3-50 and 3-51.

3.4 VORTEX DEMISE

The demise of a vortex pair can occur from one of three forms. The first form of vortex demise is dissipative wake decay caused by viscous forces and is characterized by gradual weakening of the vortex strength. This decay would gradually lead to vortex demise if other forms of vortex demise did not destroy the vortex first; the vortex pair almost always is destroyed by one of two catastrophic demise mechanisms - core bursting or Crow instability. In the real atmosphere, demise mechanisms develop through coupling with atmospheric, aircraft-induced, and self-induced turbulence as well as with normal viscosity of air. These mechanisms effectively alter the organized vorticity of the vortex pair such that the encounter hazard to a following aircraft is abruptly and dramatically reduced. Such catastrophic wake demise is associated with the two phenomena of core bursting and Crow instability.

Before catastrophic wake demise, gradual weakening of the circulation of the vortex pair because of turbulent dissipation of vorticity occurs as

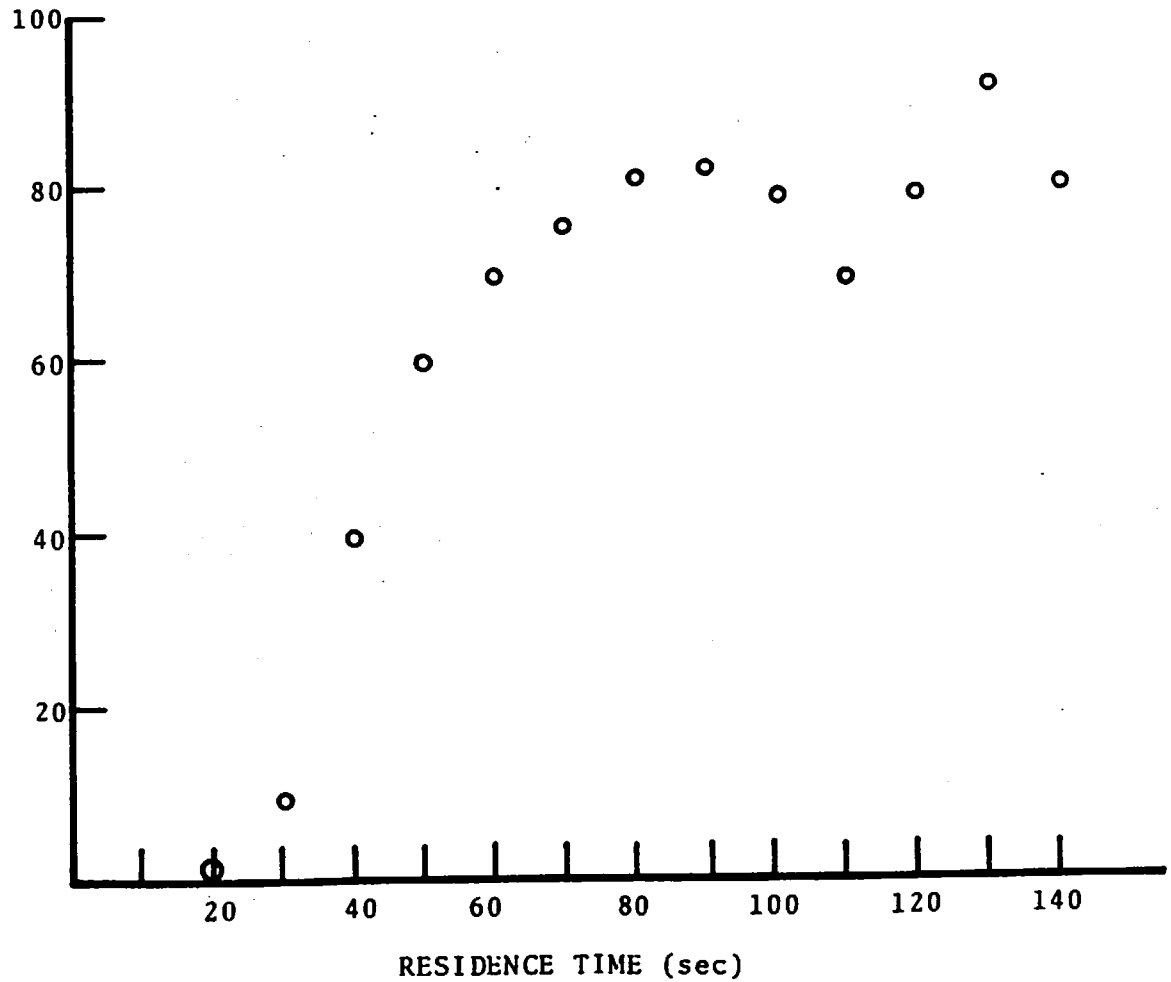

FIGURE 3-59. PERCENTAGE OF VORTICES WHICH DECAYED WITHIN SAFETY ZONE

98

the wake ages. The demise of the vortex is significantly accelerated after initiation of either of the two catastrophic demise modes. The demise modes act to alter the geometry of the vortices (reducing their danger to following aircraft), as well as accelerating the dissipation process in the residual wake, further reducing the danger associated with an encounter. Regardless of the mode of wake demise, the turbulent transport of vorticity away from the core region of the wake results in a weakening of the wake as it ages. At sufficiently long times, the wake is completely dissipated. Thus, harmless turbulence is the ultimate result of an aircraft passage through a given parcel of air.

3.4.1 Dissipative Wake Vortex Decay

Although not considered a significant vortex demise mechanism by itself, the dissipation or annihilation of vorticity caused by real fluid effects can have important consequences on the motion (and hence, the predicted location) of the wake before decay has occurred. For this reason, the dissipation process and its resultant effects on wake transport must be properly understood to develop a reliable predictive model for vortex behavior. This is particularly true in ground effect. Here, shear generated by vortex velocities at the ground can produce vorticity which mixes with and drastically affects the subsequent motion of a vortex.

The initial decay mechanism is one in which viscous forces cause the vortex core to expand without affecting vortex strength (c.f., discussion associated with Figs. 3-27 and 3-28 in Section 3.3.2.1). The vortex structure changes from that shown in Fig. 3-60(a) to that shown in Fig. 3-60(b). The vortex strength is the same for both figures. The expansion of the core with constant vortex strength causes a decrease in the peak tangential velocity as shown by Fig. 3-60(b) as well as by the equation for vortex strength of the Rankine vortex (equation (3.59)).

$$\Gamma = 2\pi r_c v_c \tag{3.188}$$

The decrease in peak velocity with vortex age from experimental measurements is shown in Figs. 3-61 and 3-62. The measurements were made at NAFEC (now the FAA Technical Center). It is noted that the numbers shown are peak recorded velocity for anemometers at 0.3-meter increments. For the B-747,

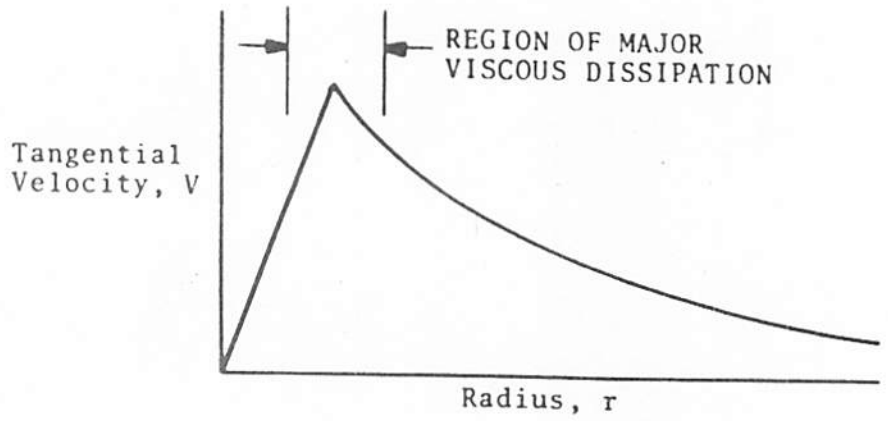

(a) Vortex Structure After Vortex Roll-Up

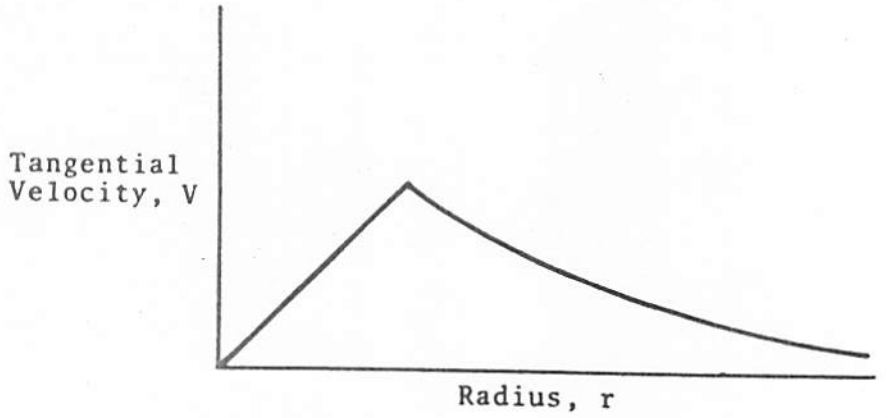

(b) Vortex Structure After Dissipative Decay

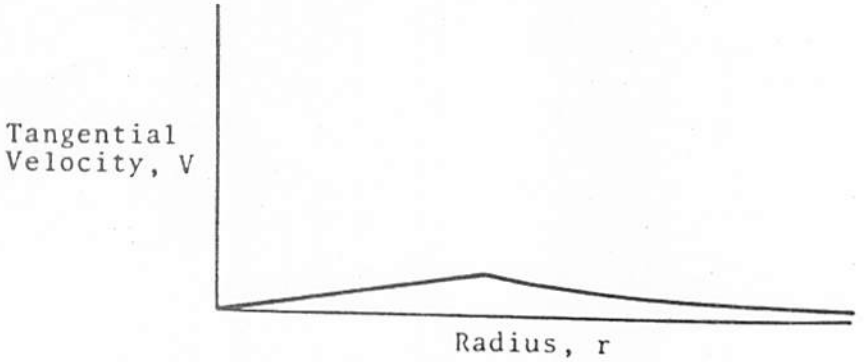

(c) Vortex Structure After Vorticity Detrainment
Stages of Vortex Dissipative Decay

FIGURE 3-60. VORTEX STRUCTURE WITH DISSIPATIVE DECAY.

88

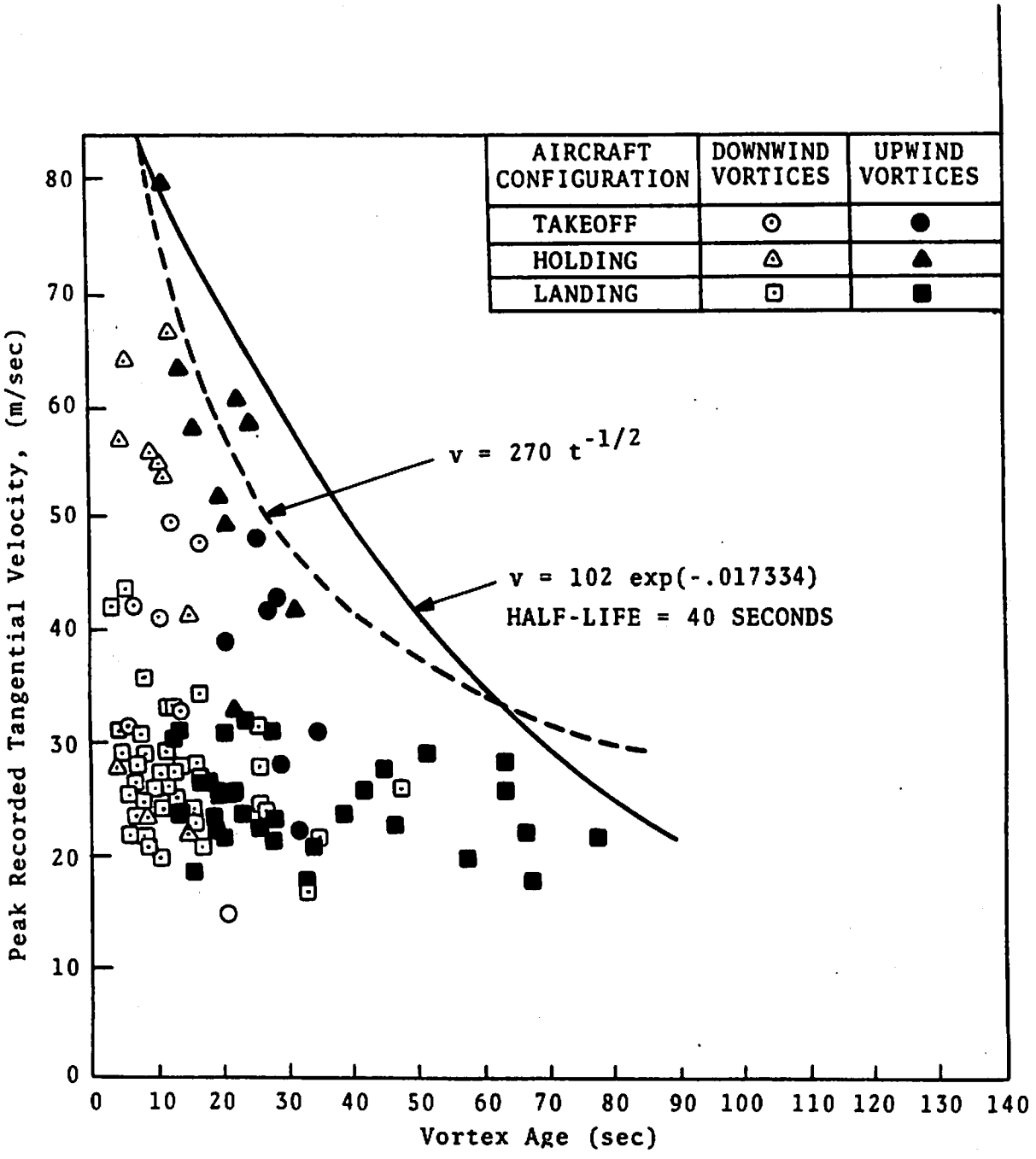

FIGURE 3-61. PEAK RECORDED TANGENTIAL VELOCITY VS AGE (ALL CONFIGURATIONS - B-747)

89

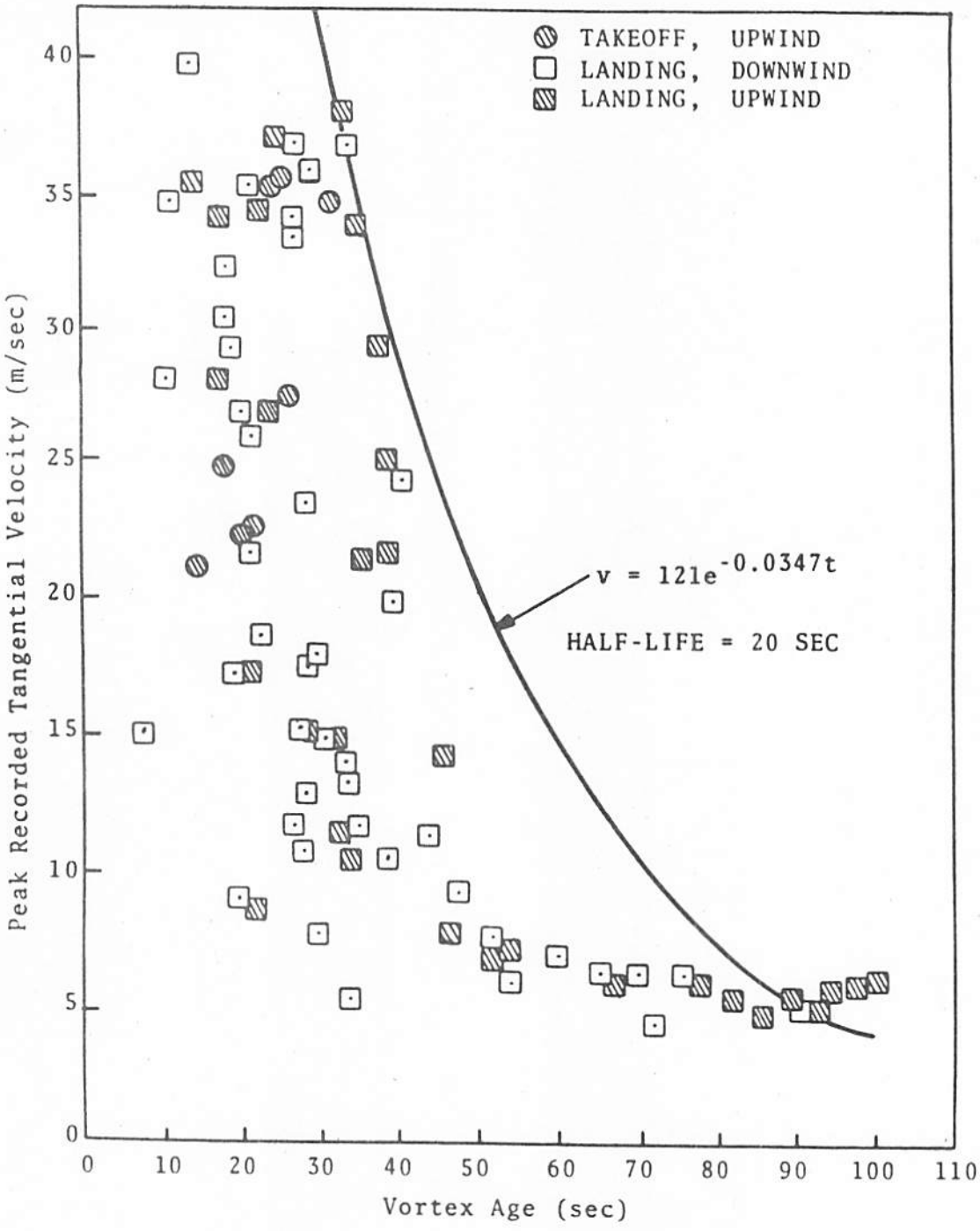

FIGURE 3-~~59~~ 62. PEAK RECORDED TANGENTIAL VELOCITY VS AGE (ALL CONFIGURATIONS - DC-9 - SERIES 10)

90

the fact that peak velocities are higher for takeoff and holding configurations than for the landing configuration is supported by the vortex structures (particularly the core size) shown in Figs. 3-15, 3-16, and 3-17.

Figure 3-61 shows theoretical curves for the decay of maximum tangential velocity. The inverse of the square root of time is from the model of Owens (ref. 21). The negative exponential form is based on the assumption that the derivative of the velocity with respect to time is proportional to the velocity.

3.4.2 Core-bursting

One major form of vortex instability is core-bursting or vortex breakdown. This mode consists of a sudden abrupt widening of the vortex core; in the case of a smoke-marked aircraft vortex, the widening is manifested by the disappearance of the tracer elements. The phenomenon has been observed in the laboratory and in flight tests.

Core-bursting has been observed under many different full-scale flight conditions (for example, ref. 42) although the reasons for its occurrence are not yet fully understood (ref. 51). Figure 3-63 shows an axially moving burst (vortex breakdown) from a field experiment. Smoke was injected into the vortex core from the generator aircraft for flow visualization.

Core-bursting manifests itself as a localized "burst," or sudden increase, in diameter of the vortex core, followed by rapid travel of a conical parcel of smoke down the vortex (vortex breakdown). There is usually little or no smoke left behind the traveling region, while the density of smoke within it increases as it moves down the core. This suggests that at least some of the smoke initially in the core is swept up by it. In the experimental work of ref. N, small balloons were released into the cores and showed vortex motion to be present after a visible vortex breakdown. In several cases, the balloons were still spinning in the vortex core at a vortex age of 150 seconds, which is well in excess of the observed core breakdown times. Core-bursting often occurs spontaneously at many positions along a vortex. In ref. N, this is attributed to variations in ambient turbulence along the axial direction of the vortex. The axially

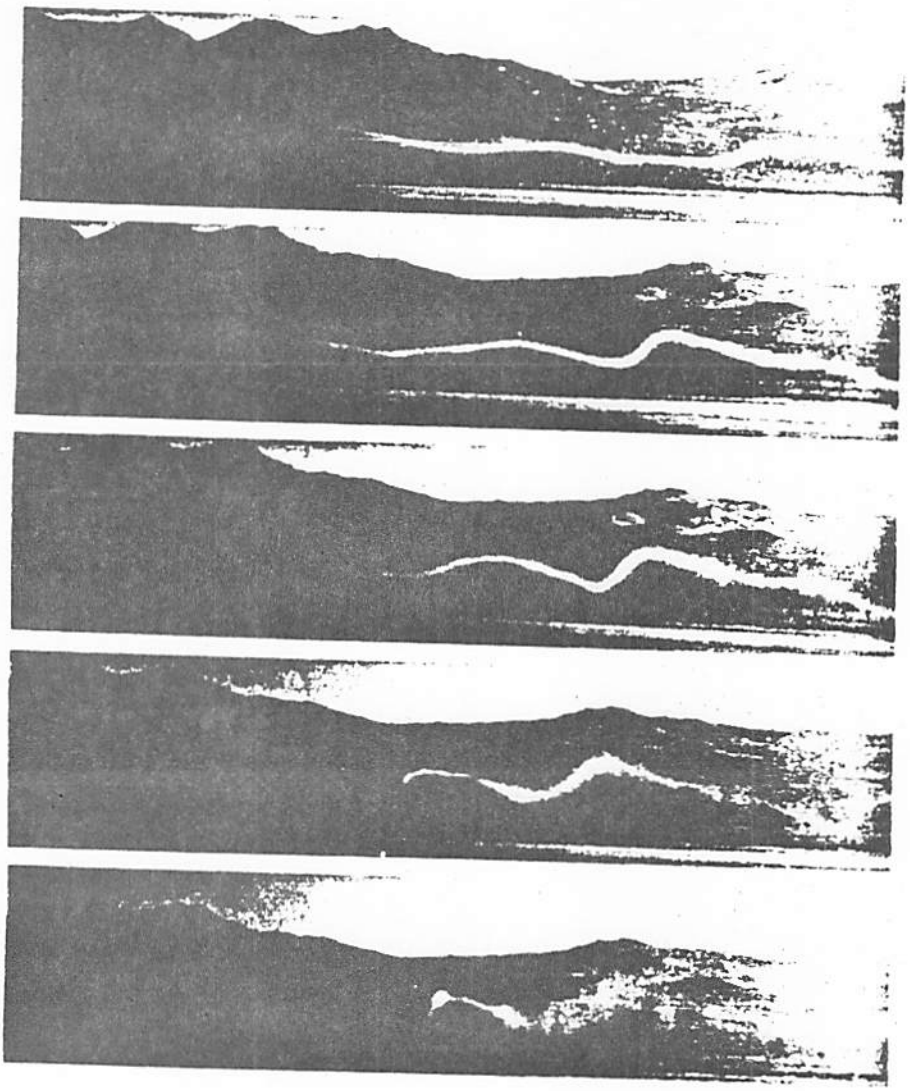

FIGURE 3-~~48~~ 63. VORTEX BREAKDOWN CAUSED BY CORE-BURSTING

92

moving bursts then quickly consume the remaining vortex segments. Initiation of core-bursting is apparently unrelated to the ambient meteorological conditions such as turbulence, stability, etc.

The qualitative details of the breakdown are still quite obscure. In the laboratory experiments of Sarpkaya (ref.52), the first effect seemed to be an axisymmetric disturbance under which the core expanded and contracted smoothly. Downstream a distinct spiral disturbance appeared which was then followed by a disorganized but roughly axisymmetric core widening, the final breakdown. In Tombach's flight test experiments (ref. 53), the same sequence of events seems to take place although the initial smooth axisymmetric bulging is not as distinct.

Several explanations of vortex breakdown have been proposed, and include the stagnation of the axial velocity (refs. 54 and 55), the conjugate jump theory (ref. 56), a stability approach (ref. 57), and momentum transfer due to ambient and mechanical turbulence (ref. N). None of these is entirely satisfactory, yet all contain common elements and all seem partially supported by experiment. It appears agreed that the rapid enlargement of the vortex core is accompanied by axial pressure gradients, and that the breakdown can only occur when the flow approaches a certain critical combination of axial and tangential flow profiles. Apparently, the magnitude of the triggering adverse pressure gradient required depends upon the proximity of the flow to its critical state. It is generally agreed that dissipation and core development will cause the core to approach the critical state, so that in most cases, the core will eventually develop to a state capable of breakdown.

It appears likely that the critical state can be described crudely as a function of the axial velocity on the centerline and the swirl ratio. The swirl ratio is the ratio of the maximum tangential velocity to the freestream speed. Core-bursting seems to be strongly related to the axial velocity in the vortex core. If the critical axial tangential flow conbination could be determined, then the breakdown prediction problem would reduce to testing for the critical state after computing the core development.

It appears that the core-bursting phenomenon is not related to an interaction between the left and right elements of the vortex pair, but rather to the development of the core itself, and this development is a function of the knematic viscosity controlling the core development. Observation by Tombach (ref. 42) have shown that, at the scale of his flight test in which vortices were generated by a single engine light airplane (Cessna 170), core-bursting occured before Crow instability in light atmospheric turbulence, while in high ambient turbulence the Crow instability invariably terminated the vortex life (because of the effect of turbulence on the onset of the Crow instability, rather than the effect of turbulence on core-bursting).

Thus, it is possible that at the same turbulence level, the time scales for core-bursting and Crow instability are related to some function of the airplane Reynolds number, which could be defined as $U_i b/Ö$, where U_i and b are the flight speed and span, and Ö the kinematic viscosity. On this basis, the vortices from small slow aircraft might be expected to dissipate principally because of core bursting while those from large fast aircraft are caused by Crow instability. Some supportive evidence is that most small-scale laboratory tests exhibit core-bursting (although Crow instability can certainly be excited), while very large-scale flight tests usually show sinuous instability.

Thus, it is possible (although not definitely substantiated) that Crow instability is the most frequent mode of decay for vortices characteristic of large transport aircraft. However under unusual or artificially perturbed circumstances, core-bursting may be important. Core-bursting is certainly the cause of vortex demise when a vortex pair tilts (e.g., because of wind shear as described in Section 3.3.4.1), and one vortex lingers after the other has been destroyed. As discussed in the next section, Crow instability requires the interaction of both vortices.

The nature and precise mechanism of vortex breakdown is still controversial. It is generally agreed that the breakdown is always associated with adverse pressure gradients, and apparently these may be either cause or effect. The conditions for breakdown to occur are related

principally to the swirl ratio and the magnitude of the axial flow. No general agreement on this critical function has been reached, but both Benjamin (ref. 56) and Mager (ref. 58) give similar results which can be represented as in Fig. 3-64. The axial velocity has been expressed as the ratio of the mean core axial velocity to the free-stream flow.

It should be noted that both supercritical and subcritical states are driven by dissipation toward the critical condition, so that in general, most cores will approach the breakdown state. Note that Mager defines a further dividing line in the swirl-number axial-velocity ratio diagram above which no breakdown is possible. If the proper conditions for breakdown were known, then it would still be necessary to be able to calculate core development to determine the core state. One of the controversial factors of the calculation is the viscous transfer constant and whether it is turbulent or laminar. It is certainly extremely important in any prediction scheme since turbulent dissipation would cause breakdown an order of magnitude more rapidly than Laminar flow.

3.4.3 Crow Instability

The Crow or sinuous instability is a better understood vortex annihilation phenomenon than is core-bursting. The mutual and self-induced velocity fields associated with a perturbed pair of vortices result in a periodic, sinusoidal oscillation of the pair which is unstable with time. The initial perturbation of the vortex pair is provided by atmospheric turbulence, which continues to act as an energetic forcing function to the instability during its growth.

The origin of the Crow instability (refs. 47, 57,and 59) is shown in Fig. 3-65(a). The figure shows the vortex pair with a small segment of the starboard vortex perturbed slightly inward by atmospheric turbulence. Vortex transport is a three-dimensional process; the motion of the entire port vortex is affected by each segment of the starboard vortex with the magnitude of the effect between two segments being inversely proportional to the distance between them. Because the magnitude of the tangential velocity is inversely proportional to distance from the vortex centroid, the inward perturbation of a small segment of the starboard vortex increases the downward induced velocity at the port vortex. Therefore, a portion of the

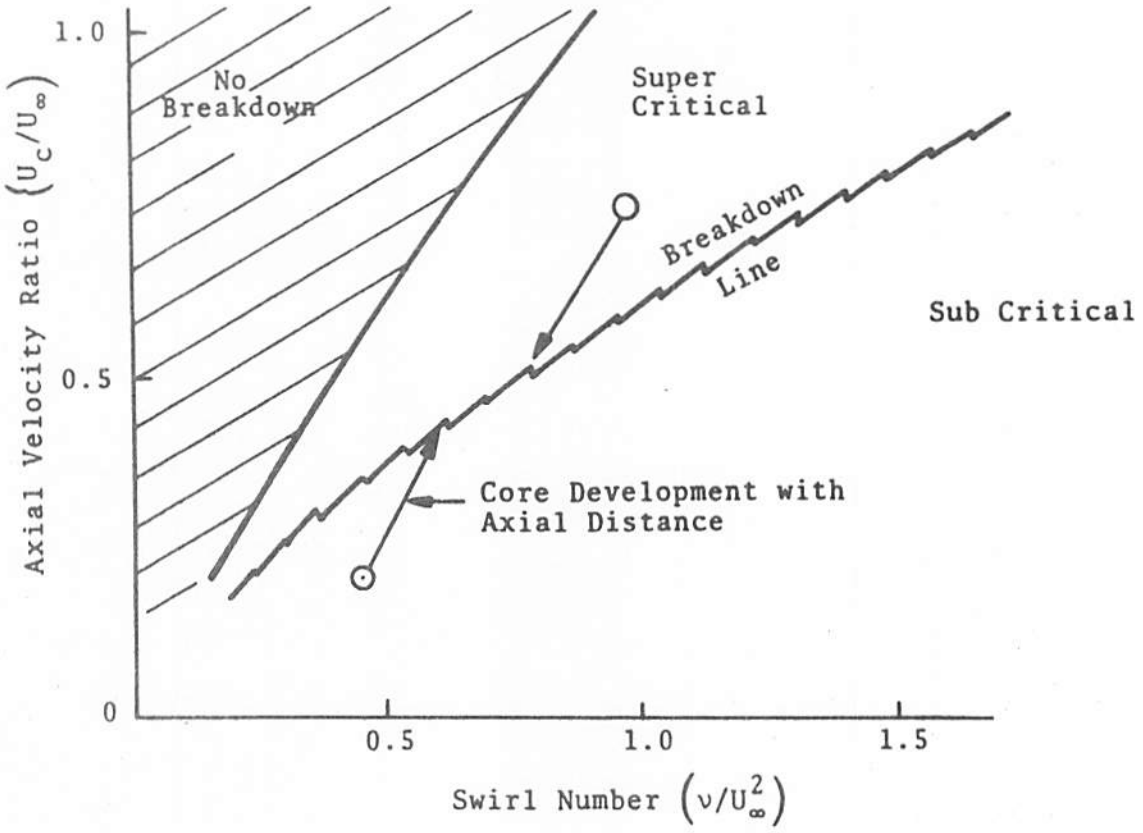

FIGURE 3-~~61~~ 67. ESTIMATED VORTEX BREAKDOWN DIAGRAM

96

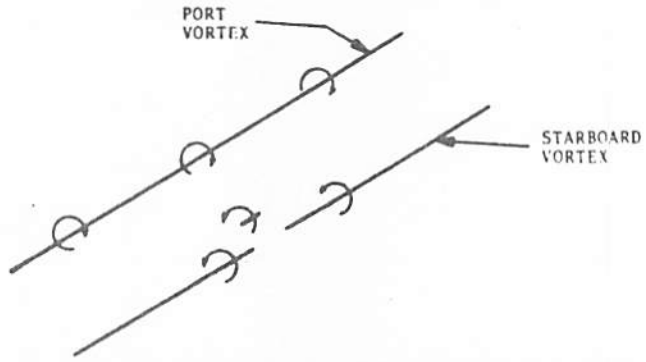

(a) ORIGINAL VORTEX PAIR WITH SMALL PORTION OF STARBOARD VORTEX PERTURBED BY ATMOSPHERIC TURBULENCE

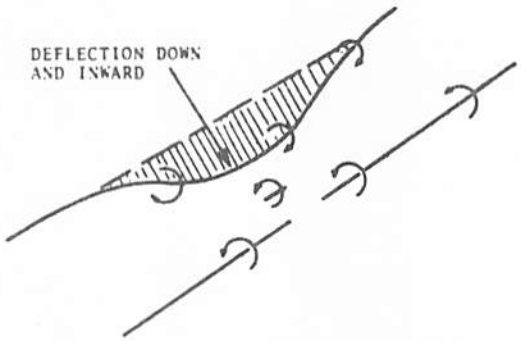

(b) EFFECT OF PERTURBATION OF STARBOARD VORTEX UPON PORT VORTEX

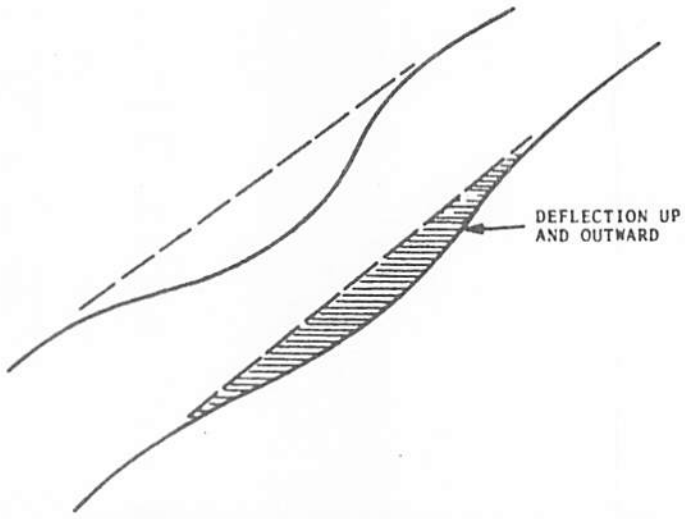

(c) EFFECT OF DEFLECTION OF PORT VORTEX UPON STARBOARD VORTEX (WITH ORIGINAL PERTURBATION REMOVED)

FIGURE 3-45. MECHANISM OF CROW INSTABILITY

97

port vortex is transported down at a faster rate than is the rest of the vortex. Because the starboard vortex field is circular, as the port vortex is transported down it encounters an inward velocity. Therefore, a portion of the port vortex is transported downward and inward as shown in Fig. 3-65(b).

Now remove the original perturbation (although not really necessary) and examine the effect of the deflection of the port vortex upon the starboard vortex. The distance between the port and starboard vortices at the point where the port vortex is deflected is greater than that for the undisturbed vortex. Therefore, the induced downward velocity (on the starboard vortex) is smaller opposite the deflected portion of the port vortex than it is where the vortices are undisturbed. In addition, the velocity field at the starboard vortex is outward and downward at the position opposite the deflected port vortex. Thus, in comparing the induced velocity field on the starboard vortex by the deflected and undeflected portions of the port vortex: (1) there is an outward component of velocity where the port vortex is deflected, and (2) the downward component of velocity opposite the deflected portion of the port vortex is less than that opposite the undeflected portion of the port vortex. Accordingly, the portion of the starboard vortex opposite the deflected portion of the port vortex is deflected upward and outward relative to the rest of the starboard vortex as shown in Fig. 3-65(c).

Although the initial deflections are small, the process continues in an unstable manner, causing the magnitude of the deflection to grow. The resulting instability manifests itself as a (roughly) sinusoidal oscillation of each of the two vortices. The two vortices oscillate in planes inclined at approximately 45 degrees to the vertical, roughly resembling a "V"-shaped trough, as shown in Figure 3-66. As the instability develops with time, the vortices move closer together at the bottom of the trough and further apart at the top. Eventually, the vortices touch at the bottom (called "linking") and cross connect such that they mutually annihilate themselves at the link points, and discrete vortex rings are formed from the remaining portions of the vortices between adjacent link points. Thus, because of the instability, the wake has been changed from a pair of parallel line vortices to a series of vortex rings. The geometry of the developing instability and

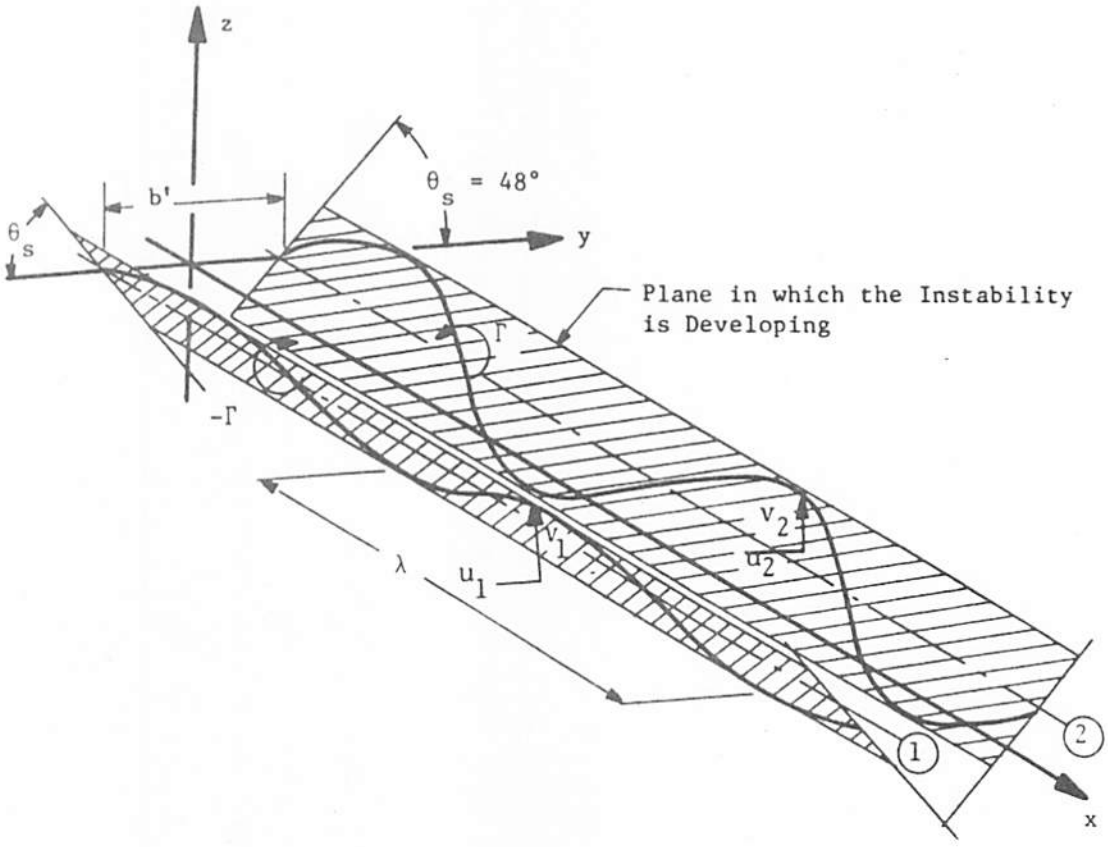

FIGURE 3-56. GEOMETRY OF THE OSCILLATING VORTEX PAIR. THE VORTICES ARE VIEWED FROM ABOVE, AND THE GENERATING AIRCRAFT LIES BEYOND THE UPPER LEFT-HAND CORNER OF THE FIGURE

99

the resulting vortex rings are a function of the undisturbed vortex pair spacing and circulation (the lift, span, and speed of the generating aircraft). Figure 3-67 shows the initiation and formation of vortex rings.

Upon formation of the vortex rings, the danger associated with vortex encounter is much reduced since the sustained rolling moment on an encounter aircraft because of a straightline vortex is no longer possible. Subsequent vortex breakdown within the rings themselves (usually initiated near the link points) quickly causes the dissipation and the overall loss of any remaining wake identity.

The time required for operation of the catastrophic vortex demise modes (after passage of the generator aircraft) has been examined experimentally (ref. 51). The general results of these experiments showed that core-bursting is apparently unrelated to ambient meteorology, while the time at which linking occurred for the Crow instability is a strong function of atmospheric turbulence, and corresponded well to the theory of Crow and Bate (ref. 59). In all cases, the Crow instability sets the upper limit on wake lifetime and hence is probably operationally significant. Turbulence hastens vortex demise through Crow instability by two mechanisms. First, turbulence causes an unsteady lift on the wing which results in a non-uniform vortex in the axial direction. Second, atmospheric turbulence provides the initial perturbation to start the Crow instability.

The time to link for the Crow decay modes can be expressed as a function of the properties of the undisturbed wake and the level of atmospheric turbulence, expressed as the rate of dissipation of turbulent energy, ε. Since atmospheric turbulence initiates the instability, the time to link may be expected to be a strong function of atmospheric turbulence. Thus for a given generator aircraft (fixed wake properties), the time to link can be directly determined from knowledge of ε in the region of interest.

Figure 3-68 shows representative times and distances downstream from various aircraft at which linking will occur. It should be mentioned that the values shown correspond only to the situation at which linking is just initiated and the vortex rings are formed. The additional short time

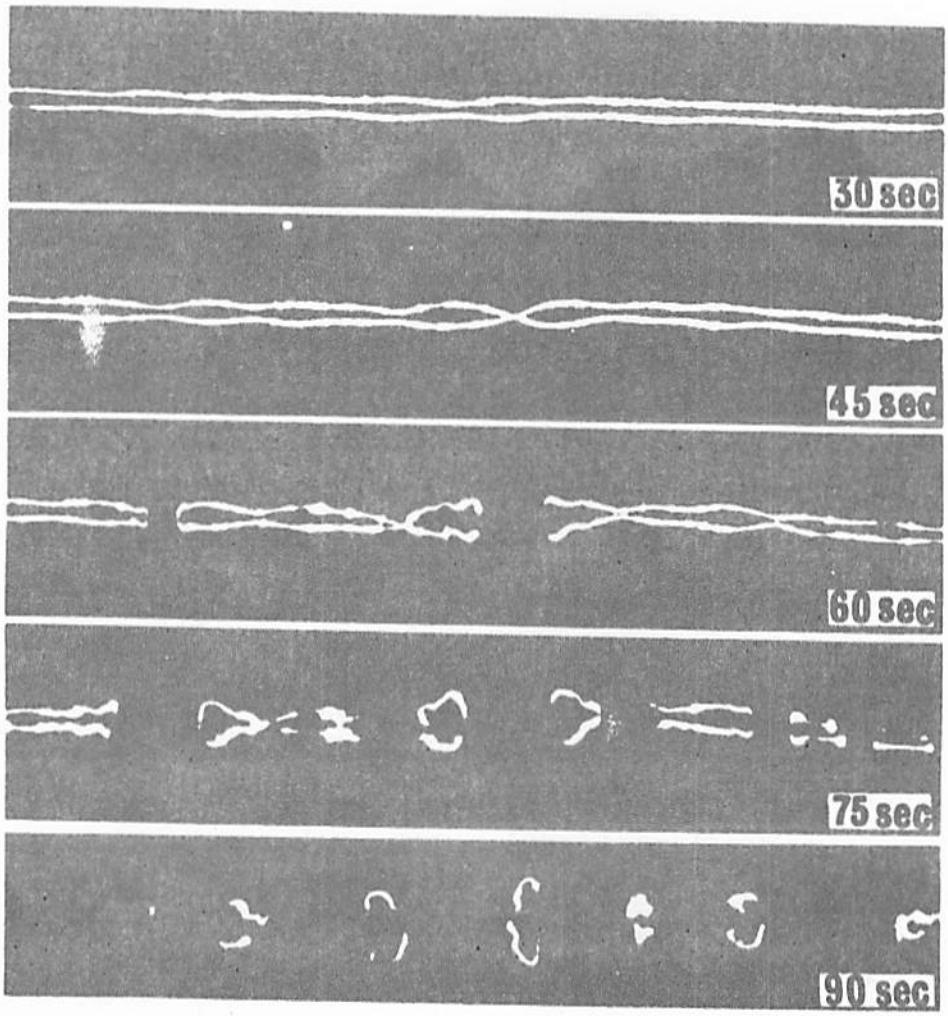

FIGURE 3-57. THE DEVELOPMENT OF THE CROW-LINKING PHENOMENON FROM AN OVERHEAD FLYING B-47

101

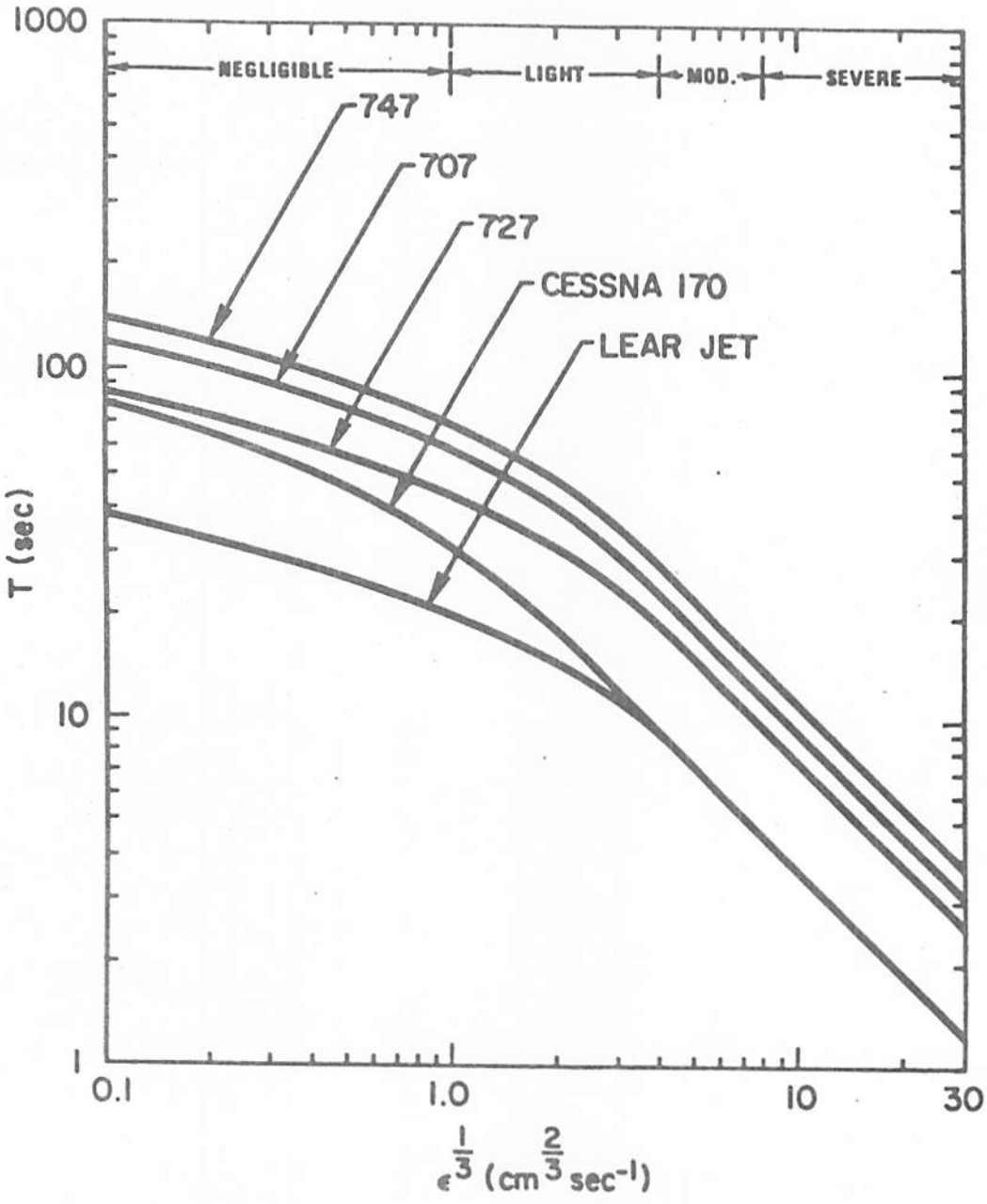

FIGURE 3-~~45~~ 68. TIME TO VORTEX LINKING, T, AS A FUNCTION OF ATMOSPHERIC TURBULENT DISSIPATION RATE, $\epsilon^{1/3}$.

102

required for complete destruction of the wake because of vortex breakdown on the rings has not been included. Also the values were computed at infinite altitude, so that ground effects were not included. The gross weight and speed of the aircraft were assumed for landing configuration although the vortex separation was for an unflapped, elliptically loaded wing. The numbers presented in the figure should thus be considered representative of vortex linking only and should not be interpreted to signify the termination of encounter danger. The values shown were derived using the theory of Crow and Bate, and therefore, do not represent actual measurements. In general, the Crow-Bate theory show that, in a given boundary layer, the net effect of ground proximity is to shorten wake lifetime, but by no more than 10 percent.

In general, turbulence increases as wind speed increases. Therefore, vortex lifetime may be expected to decrease as the wind speed increases. Such a criterion has been postulated by McGowan (ref. 60) and is shown in Fig. 3-69. Superimposed on the plot are B-747 (from ref. 27) and CV-880 data points (ref. 34) It is believed that the envelope is very conservative as the altitude is reduced, particularly for the downwind vortex in ground effect. (Section 8 examines the McGowan curve in the light of new data.)

It should be noted that wake decay near the ground is a complicated phenomenon which currently cannot be expressed analytically. Surface winds, wind shear, and turbulence sometimes act in concert to distort and stretch the vortices into highly convoluted shapes. The mutual interactions of the vortices and their images along with ground-generated dissipation and decay because of core-bursting and Crow instability further complicate the behavior of the vortices. (Recent measurements of vortex decay near the ground are discussed in Section 8.) Figure 3-47 showed an example of a situation during a low pass near the ground during an experimental field test with smoke-marked vortices. It can be seen that the prediction of the location and strength of the vortices at any given ground station along the aircraft flight path would be difficult to express in an analytical form. For this reason, the statistical analysis of the wake behavior will be quite important in the formulation of a reliable predictive model.

Reference E notes that rocking of the wings with spoilers extended reduces vortex life. Although no mechanism for this phenomenon is mentioned

in ref. E, it is likely that the rocking of the wings induces Crow instability. Rocking the wings by use of ailerons obviously changes the total lift as well as the lift distribution on each wing. Thus, in the direction of flight both the vortex strength and the vortex position will be non-uniform with respect to the direction of flight. As discussed earlier in this section, Crow instability is initiated by non-uniform vortex position. Usually, the non-uniform vortex position is initiated by turbulence, but in this case, it is initiated by shifts in the center of lift on the wing caused by wing rocking.

The early vortex demise caused by wing rocking is not operationally significant for three reasons. First, it produces and adverse ride quality which would be unacceptable to passengers. Second, significant repetitive shifts in wing loading could reduce the life of fatigue critical structural parts of the aircraft. Third, such rocking of the wings cannot be performed near the ground. Touching an engine or wing to the ground on landing can ruin a pilot's whole day.

3.4.4 Statistical Model of Vortex Demise

An accurate statistical model for vortex demise can serve several useful purposes. First, it allows a rational basis for extrapolation of vortex demise characteristics beyond the limits of experimental measurements. Two limits of experimental measurements are of particular importance: (1) the finite number of measurements precludes the direct measurement of very small probabilities, and (2) the finite detection threshold of vortex detection devices distorts the vortex demise measurements at low strength. A second purpose for a statistical vortex demise model is the characterization of the vortex demise by a small number of parameters whose variation with the cases selected can be used to determine the dependence of vortex demise upon meteorological conditions and aircraft type.

Reference L presents a statistical model of vortex demise. The salient features of that model are presented here. Several definitions are appropriate for the presentation of the model. Let H be defined as the hazard potential of the vortex. The hazard potential is defined as

$$H(r) = \frac{1}{r}\int_0^r \Gamma(r')\, dr \qquad (3.189)$$

where $\Gamma(r')$ is the vorticity contained within a circle of radius, r'. The hazard potential is a function of the distribution of vorticity as a function of radius and of some averaging radius over which the integral is performed. The averaging radius is ususally selected to correspond to half of the wing span of the following aircraft. Referring back to Fig. 3-60 in Section 3.4.1, it is seen that the vortex strength is equal for Figs. 3-60(a) and 3-60(b); however, the hazard potential is less for Fig. 3-61(b) than for Fig. 3-60(a). The derivation of the hazard potential function from considerations of aircraft upset is presented in Section .

The threshold vortex hazard potential, H_T, is the threshold value of the hazard potential above which the vortex is a hazard to following aircraft. The vortex is generally considered to be a hazard when recovery from a vortex encounter would require a roll rate exceeding some number, f, times the theoretical maximum roll rate of the aircraft. The initial hazard potential, H_0, is the value of the hazard potential at the time of the end of vortex roll-up.

For the statistical approach, the form of the decreasing probability function appropriate for describing vortex strength is

$$F(H_T,t) = \exp(-\alpha(t - d)^2) \qquad (3.190)$$

where H_T is a parameter of the equation. $F(H_T,t)$ is the probability that H is greater than H_T at time, t. The two parameters of the model, α and d, represent the asyptotic slope and the delay of the decay, respectively. The delay, d, is close to zero when the hazard threshold, H_T, is near the most probable initial strength, H_0 and becomes increasingly positive as H_T decreases below H_0. Physically, the delay may be viewed as the time required for the vortex to decay from its initial value of hazard potential, H_0, to the point where the hazard potential of the vortex equals the threshold hazard ptoential. The value of α

decreases as H_T decreases. Physically, this means that the probability that the vortex hazard potential exceeds its threshold value increases as the threshold value decreases.

Early in the anlysis of Ref. L, it was found that α was proportional to H_T for $H_T < H_0$, or

$$\alpha = C\, H_T \tag{3.191}$$

Although the assumption of $d = 0$ is not strictly applicable when H_T is significantly different from H_0, it is appropriate for many of the cases of interest, and it leads to a very simple analytical expression for the distribution function of the vortex hazard potential. Let the probability that the vortex hazard potential is greater than the threshold hazard potential be given by

$$F(H_T,t) = \int_{H_T}^{\infty} P(H,t)\, dH \tag{3.192}$$

where $P(H,t)$ is the probability density function of the hazard potential at time, t. Combining equations (3.190) and (3.192) gives

$$F(H_T,t) = \exp[-CH_T t^2] = \int_{H_T}^{\infty} P(H,t)dH \tag{3.193}$$

Differentiation with respect to H_T leads to

$$P(H,t) = Ct^2 \exp[CH_T t^2] \tag{3.194}$$

The ensemble average of vortex hazard potential at time, t, (i.e., the average hazard potential of all vortices measured at age, t) is given by

$$\bar{H}(t) = \int P(H,t)\, H\, dH \tag{3.195}$$

or combining with equation (3.194) gives

$$\bar{H}(t) = \frac{1}{Ct^2} \tag{3.196}$$

The ensemble mean hazard potential decays inversely with the square of the vortex age. It is noted that this model describes the decay of wake vortices with a single parameter, C, which depends upon aircraft type, meteorological conditions, and the averaging radius over which the hazard potential is calculated.

Figure 3-70 shows a comparison of the form of equation (3.194) with the actual probabilities obtained from experimental data. In Figure 3-60, the exponential decay lines of equation (3.194) agree exactly for a probability of 0.05 for H_T = 75 and 100 m^2/sec because those points were used to calculate the value of C. The straight-line fit to the 100 m^2/sec curve agrees very well for a probability of 0.05 but agrees less well for lower probabilities because of statistical fluctuations. The agreement is poorer for values of H_T of 75 and 50 m^2/sec because the assumptio of d = 0 is less reasonable.

The simple analytical model presented above suffers from several deficiencies, the most important of which is the lack of dealing adequately with the delay in the vortex decay, or more precisely, the time priod between aircraft pasage and the time at which the hazard potential equals the threshold hazard potential. A secondary problem is the lack of any systematic consideration of the initial vortex strength distribution. Therefore, the model is expanded in the following paragraphs to deal with these deficiencies.

The basic concept of the stochastic model is based on the observation that vortices often decay in two stages. During the first stage, the vortex strength remains roughly constant. During the second stage, the strengh decays rapidly. This concept is related to the vortex demise by one of the two catastrophic mechanisms (core bursting and Crow instability) discussed previously. This type of decay can be modeled mathematically by

$$H = H_0 \qquad t < t_c \tag{3.197}$$

$$H = H_0(t_c/t)^n \qquad t > t_c \tag{3.198}$$

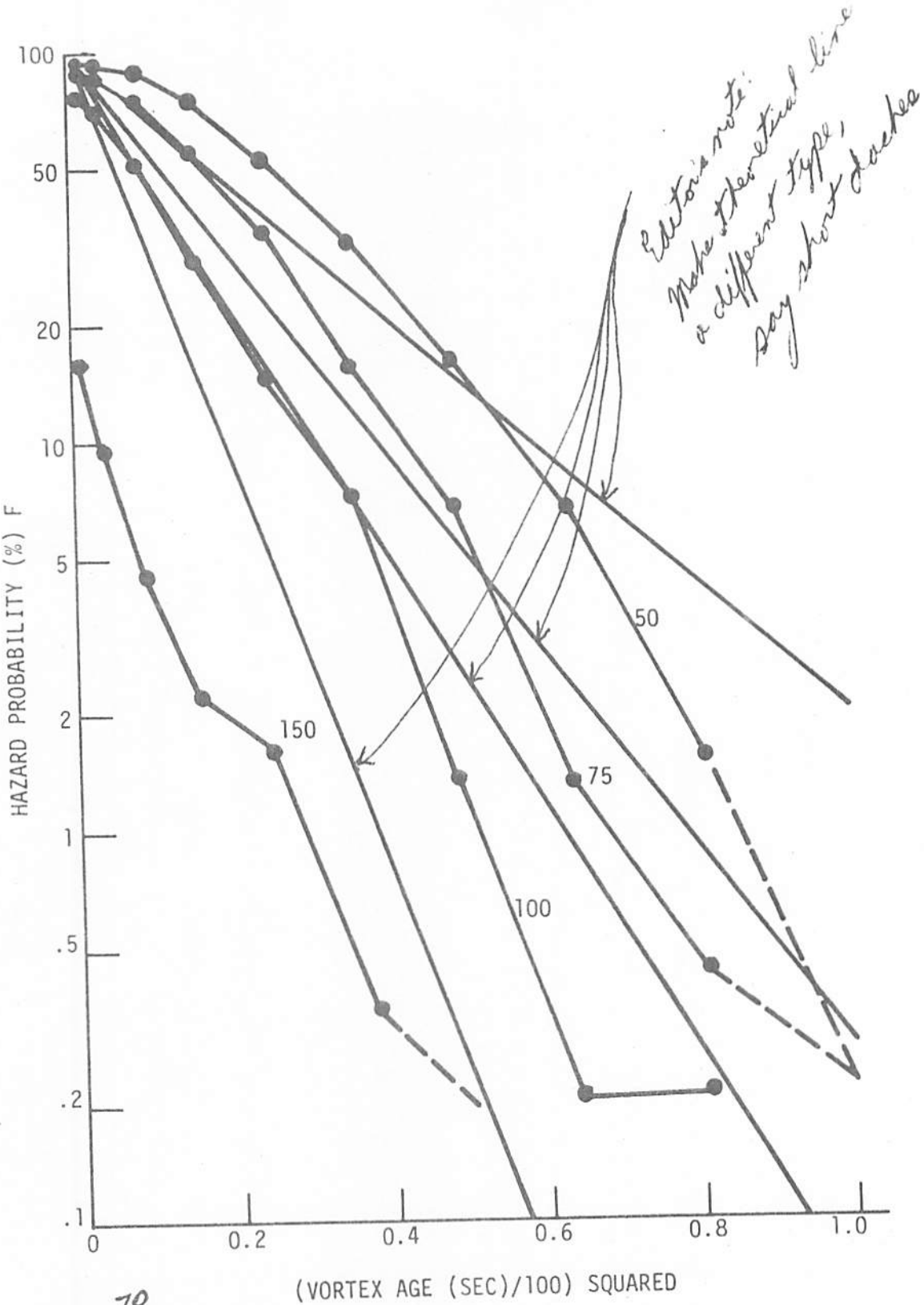

3-70

FIGURE 35. COMPARISONS OF MODEL HAZARD PROBABILITY (STRAIGHT LINES) WITH MEASUREMENTS (LINES WITH POINTS) FOR ALL B-707 VORTICES WITH 10-METER AVERAGING. THE VALUES OF Γ_T' (m^2/SEC) ARE INDICATED.

where H is the hazard potential for a particular aircraft and averaging radius, H_0 is the initial value of H, and t_c is the time at which catastrophic vortex demise begins. The vortex decay in time is governed by the power n. Equation (3.196) corresponds to n = 2. The stochastic feature of the model is introduced by assuming that the time at which catastrophic vortex demise begins is distributed in a normal distribution with a mean value t_0 and standard deviation σ. The probability density function for initiation of catastrophic vortex demise is

$$P(t_1) = \frac{1}{\sqrt{2\pi}\,\sigma} \exp[-(t_1-t_0)^2/2\sigma^2] \tag{3.199}$$

The three parameters of the model are thus n, t_0, and σ.

If the distribution in initial vortex strengths is ignored, the hazard probability $F(H_T,t)$ can be calculated explicitly in terms of the error function. From equation (3.198), for a given time, t, the vortex will be a hazard to a following aircraft if and only if

$$t_1 = t(H_T/H_0)^{1/n} \tag{3.200}$$

Let this value of t_1 be labeled t_{1T} because it is the limiting value of t_1 above which the vortex will be a hazard at time, t. Then, the hazard probability is given by the integral of $P(t_1)$ for all times greater than t_{1T}.

$$F(H_T,t) = \int P(t_1)\, dt_1 \tag{3.201}$$

This integral is related to the error function which satisfies the relationship

$$1-\mathrm{erf}(z) = \frac{2}{\pi}\int e^{-t^2} dt \tag{3.202}$$

Combing equations (3.200) through (3.202) leads to the expression

$$F(H_T,t) = \frac{1}{2}[1-\mathrm{erf}(t_{1T}-t_0)/\sqrt{2}\,\sigma \tag{3.203}$$

The results of this model assuming n = 2 and $\sigma = t_0/3$ are shown in Fig. 3-71. The values selected for H_T/H_0 correspond to the B-707 10-m results plotted in Fig. 3-70. The curves corresponding to H_T = 50, 75, and 100 m^2/sec are in reasonable correspondence with the measurements for low probabilities. The 30 m^2/sec curve, however, is off, perhaps because it is below the MAVSS detection threshold of perhaps because of the wrong value for n.

Several features of equation (3.203) and Figure 3-71 are worth noting. First, the shapes of the curves are similar and correspond simply to scaling the horizontal axis for different values of H_T/H_0. One way of looking at the dependence of F upon H_T/H_0 is to note that a given value of F corresponds to a particular value of the argument z of erf in equation (3.202)

$$z = [t(H_T/H_0)^{1/n} - t_0]/\sqrt{2}\,\sigma \qquad (3.204)$$

Equation (3.204) can be rearranged to give

$$t/\sigma = (t_0/\sigma + \sqrt{2}\,z)(H_T/H_0)^{-1/n} \qquad (3.205)$$

A second feature of the curves in Fig. 3-71 is that the asymptotic line for low probabilities is not straight but is slightly curved. This curvature is consistent with the asymptotic expression for the error function

$$[1-\mathrm{erf}(z)] \sim \frac{1}{\sqrt{\pi}\,z}\, e^{-z^2} \qquad (3.206)$$

The inverse z dependence in equation (3.206) causes the curvature.

Equation (3.203) can be used to calculate the time, t_F, required to reach a certain hazard probability. Listed below are the error function argument z values leading to specified hazard probabilities, F.

///

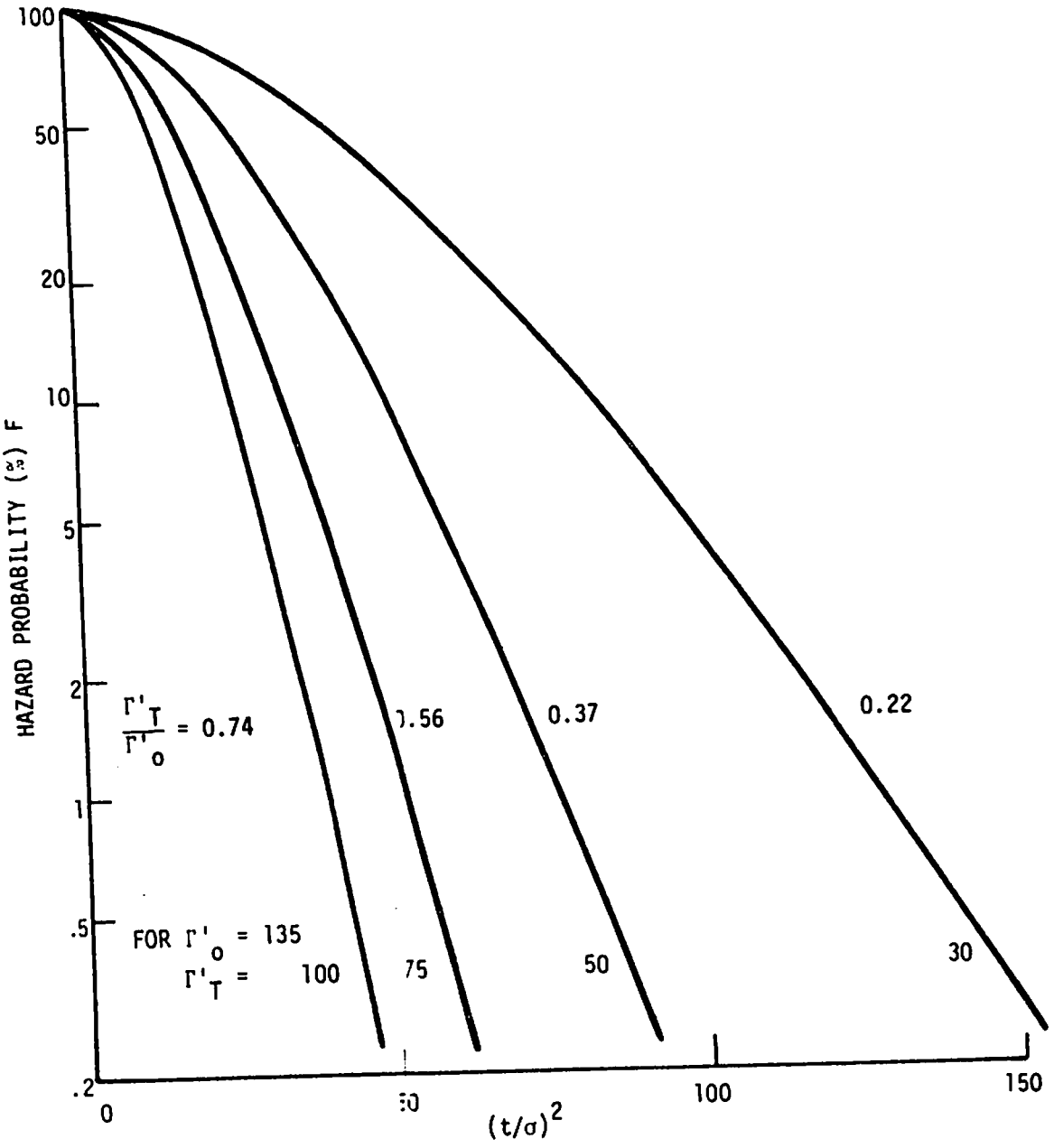

FIGURE 3-10. VORTEX DECAY FOR THE STOCHASTIC MODEL WITH $t_o = 3\sigma$ AND $n = 2$

F	z
0.2	0.59
0.1	0.91
0.05	1.16
0.02	1.45
0.01	1.65
0.005	1.82
0.002	2.03

Figure 3-72 shows a log-log plot of the dependence of $(t_F/\sigma)^2$ upon H_T/H_0 for three F values for the choice of parameters $\sigma = t_0/3$ and $n = 2$. For $n = 2$, the lines have a slope of -1. Changing the value of n simply changes the slope of the lines passing through the point where $H_T/H_0 = 1$. Changing the value of σ/t_0 moves the lines up or down.

The value of a model such as described above depends largely on the ability to determine realistic values of parameters used in the model. Reference L has used experimental data to determine the most appropriate values for these parameters and has generated an aircraft dependence of vortex hazard duration from these parameters as shown in Fig. 3-73. These values are based upon an assumed value of $H_T/H_0 = 1$. Other values of H_T/H_0 would, of course, change the results.

The ratio, H_T/H_0, has the physical meaning of being the ratio of the threshold hazard potential of the following aircraft to the intial hazard potential of the vortex of the generating aircraft. A value of $H_T/H_0 = 1$ means that the initial hazard potential from the vortex of the generating aircraft is just great enough to be a hazard to the following aircraft. The ratio, H_T/H_0, is therefore a function of the two aircraft types involved. For a B-737 following a B-747, $H_T/H_0 < 1$. Conversely, for a B-747 following a B-737, $H_T/H_0 > 1$. A potentially hazardous situation exists when $H_T/H_0 < 1$.

3.4.5 Statistical Description of Vortex Demise

A significant quantity of data related to vortex life time has been taken, and a standard format for the display of vortex life time has evolved. This standard format is shown in Fig. 3-74. Figure 3-74 shows $F(H_T,t)$ for strength thresholds of 150, 100, 75, 50, and 30 m^2/sec plotted against t^2. It shows in a single picture how the vortex hazard probability depends upon the vortex age and the assumed hazard threshold.

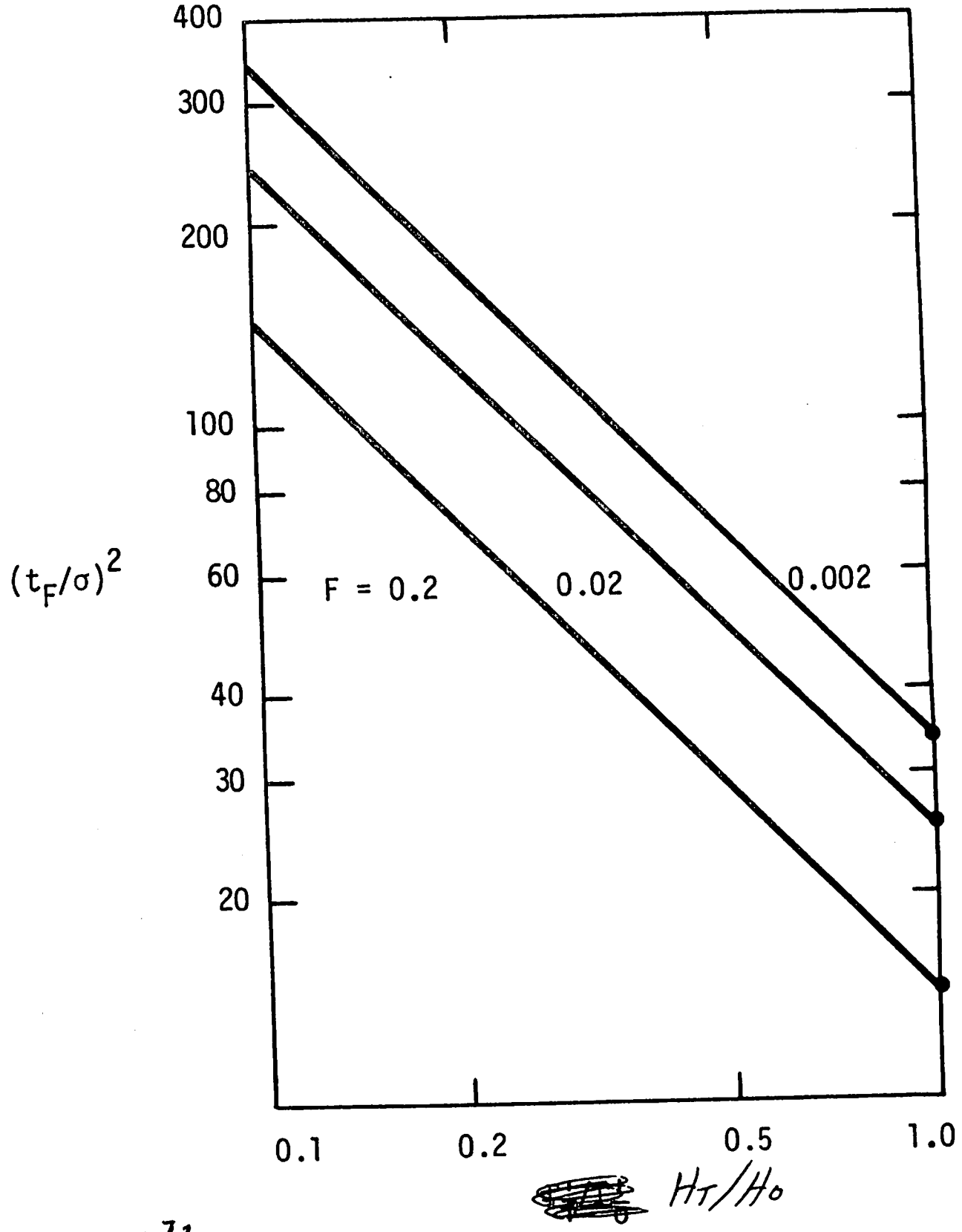

3-32

FIGURE 20. DEPENDENCE OF THE TIME TO REACH A PARTICULAR HAZARD PROBABILITY UPON THE HAZARD STRENGTH THRESHOLD

114

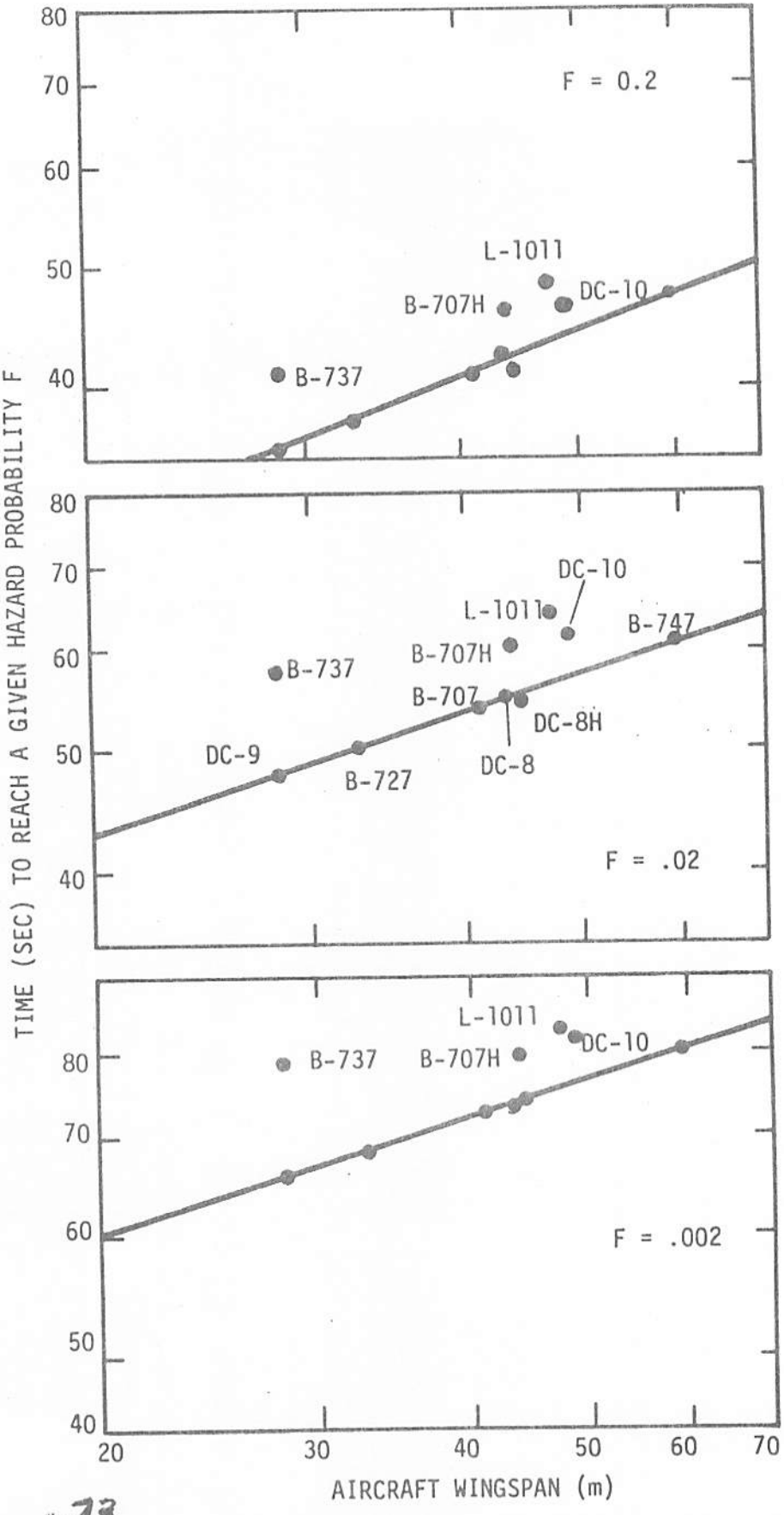

FIGURE 3-32. AIRCRAFT DEPENDENCE OF VORTEX HAZARD DURATION FOR $\Gamma'_T/\Gamma'_o = 1$

115

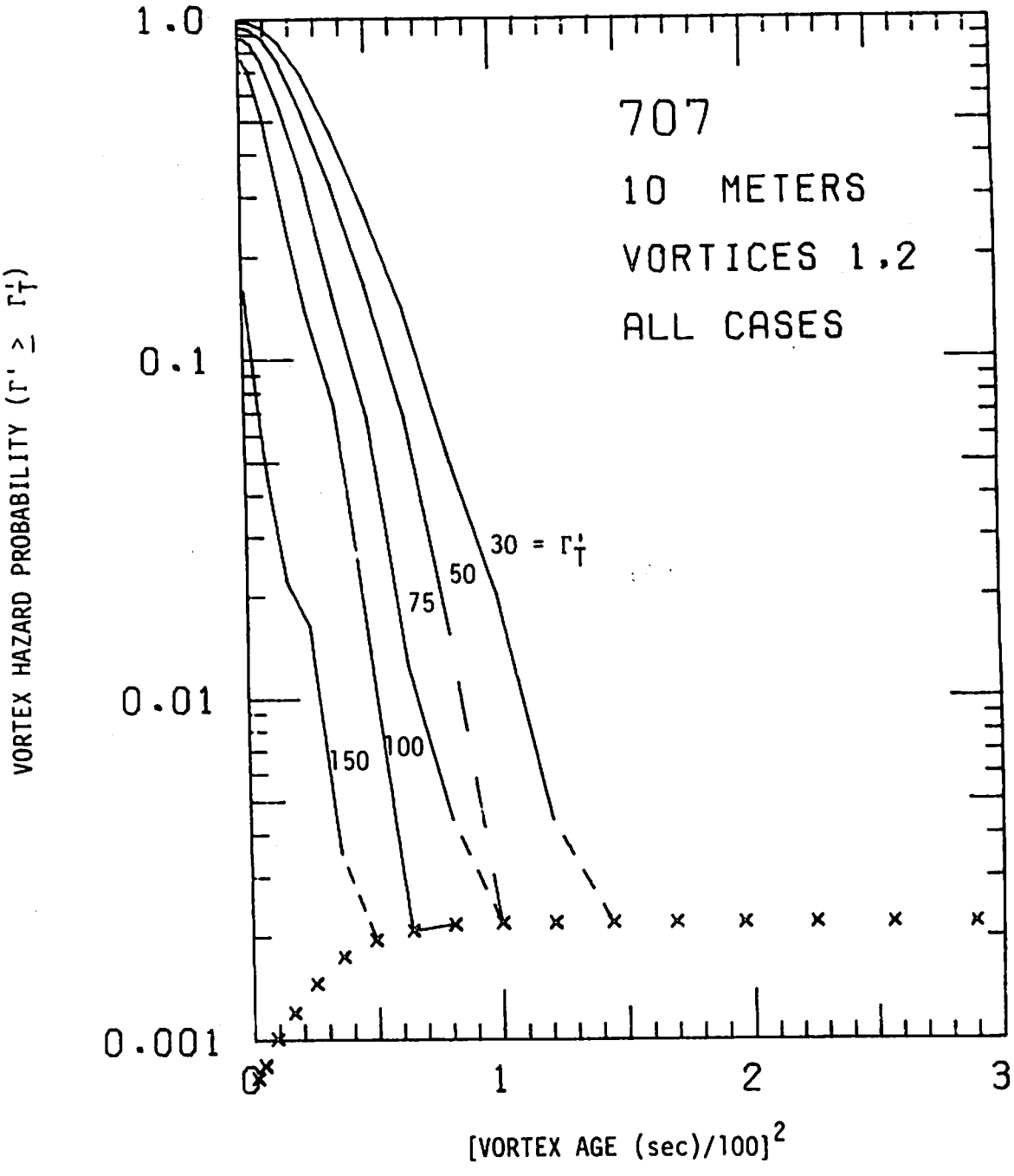

FIGURE 3-74. HAZARD PROBABILITY FOR 10-METER SEMISPAN VERSUS VORTEX AGE SQUARED FOR ALL B-707 VORTICES AND FIVE VALUES OF Γ_T' (m^2/sec)

Some of the details of Fig. 3-74 require explanation. The x's plotted in the figure correspond to the probability corresponding to one case in the sample for which the plot is generated. Since zero cannot be plotted on a logarithmic scale, the plots are terminated at the level of one case. If the probability drops to zero from a value higher than one case, a dashed line is drawn to the one-case value at the age where zero occurred. The single-case probability marked by x's rises with vortex age because the number of valid strength histories decreases with vortex age. Some of the long-lived vortices are transported out of the antenna array of the vortex detection system and thus are not tracked to their death. The number of cases reaches a steady level after about 80 seconds, when most of the valid measurements are those of vortices which have been declared dead.

Figures 3-75 and 3-76, taken from ref. L, show vortex life time probability plots for Boeing 747 aircraft. Figures 3-77 and 3-78 show similar data for the Boeing 727. Many more similar plots for other aircraft types and for different values of averaging radius are presented in ref. L.

Similar data from ref. M are shown in Fig. 3-79 for several selected aircraft types. Reference M also presents probability of vortex detection as a function of transport distance, as shown in Fig. 3-80. Such data are relevant for parallel runway operations, particularly when parallel runways are at close separations, such as at Atlanta, Denver, and San Jose.

Studies have shown that it is the wind speed (i.e., magnitude of the wind velocity) which correlates best with the demise of vortices. The McGowan curve (cf. Fig. 3-58) was generated to show this effect. Figure 3-81 shows the distribution of death times for the vortex having the longest duration for each pair for data measured at Heathrow and reported in ref. I. The data are divided into 2-knot increments. The lower the wind speed, the longer a vortex will survive on the average. As the wind increases, the average survival time of a vortex decreases as well as, to a certain extent, the maximum observed age. This trend certainly correlates well with the phenomenological descriptions of vortex demise presented in Sections 3.4.2 and 3.4.3

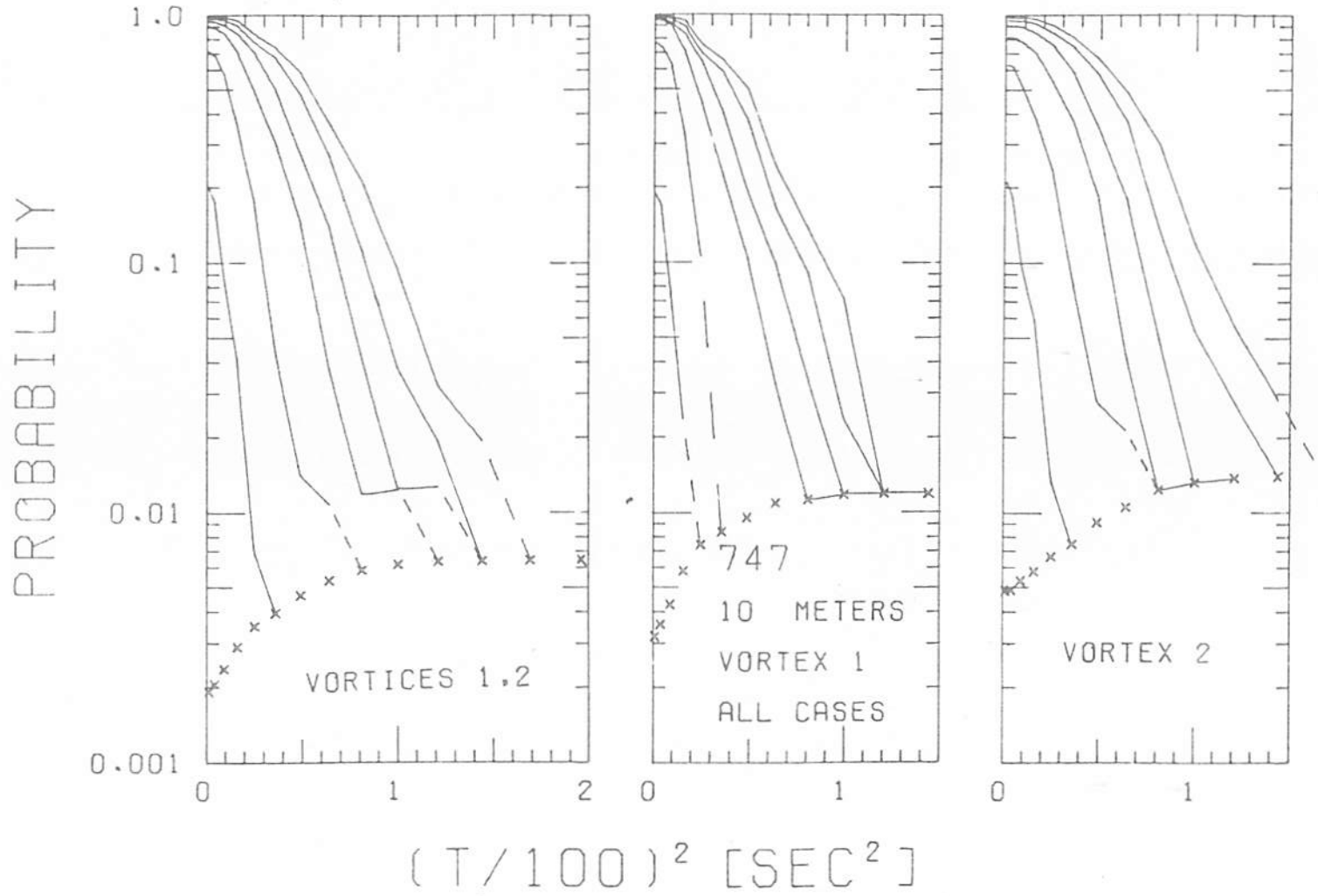

FIGURE 3-B5. PROBABILITY OF DECAY, B-747, VORTEX 1 AND 2, 10-m AVERAGING RADIUS

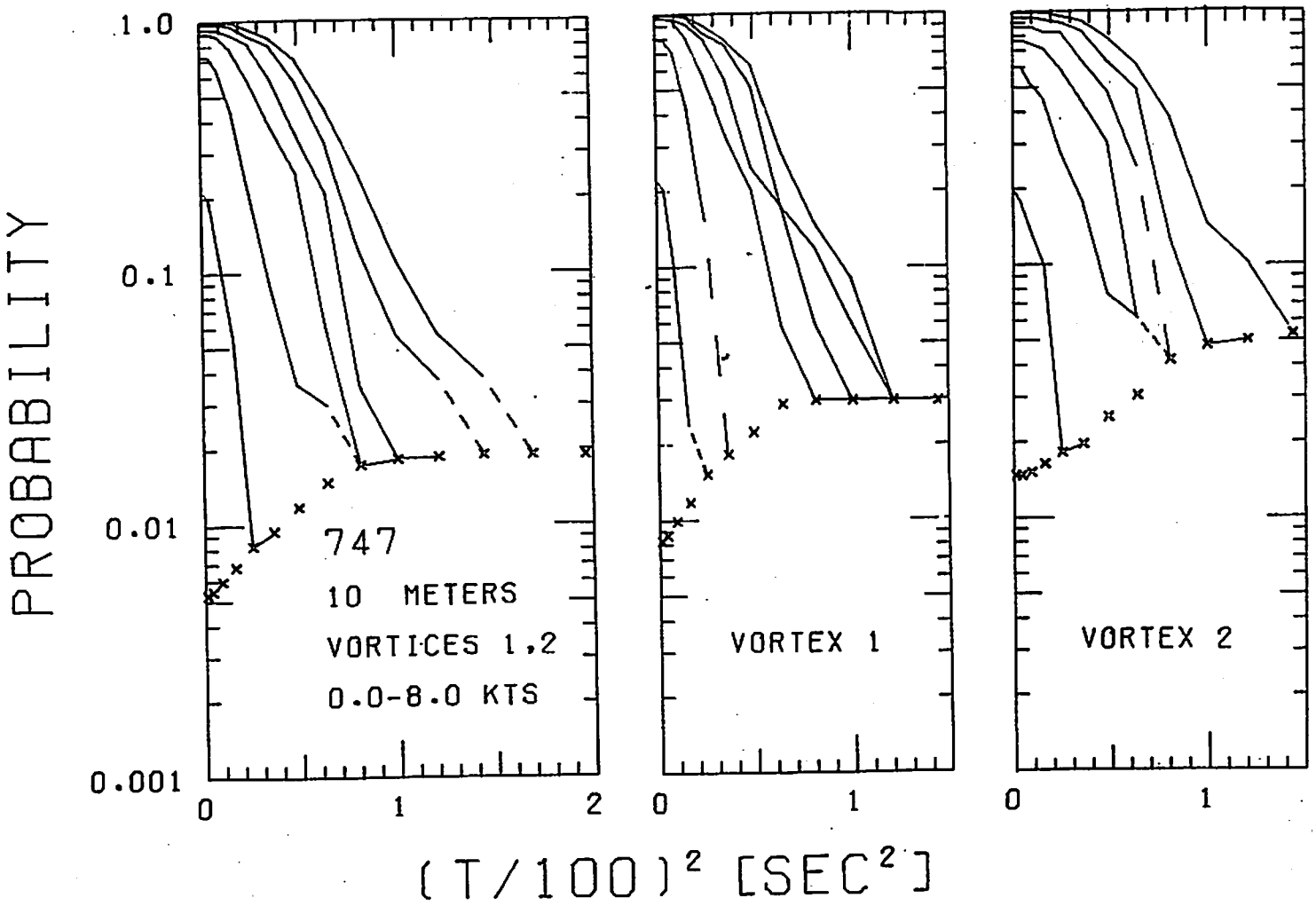

FIGURE 44. PROBABILITY OF DECAY, B-747, WINDS LESS THAN 8 KNOTS, 10-m AVERAGING RADIUS

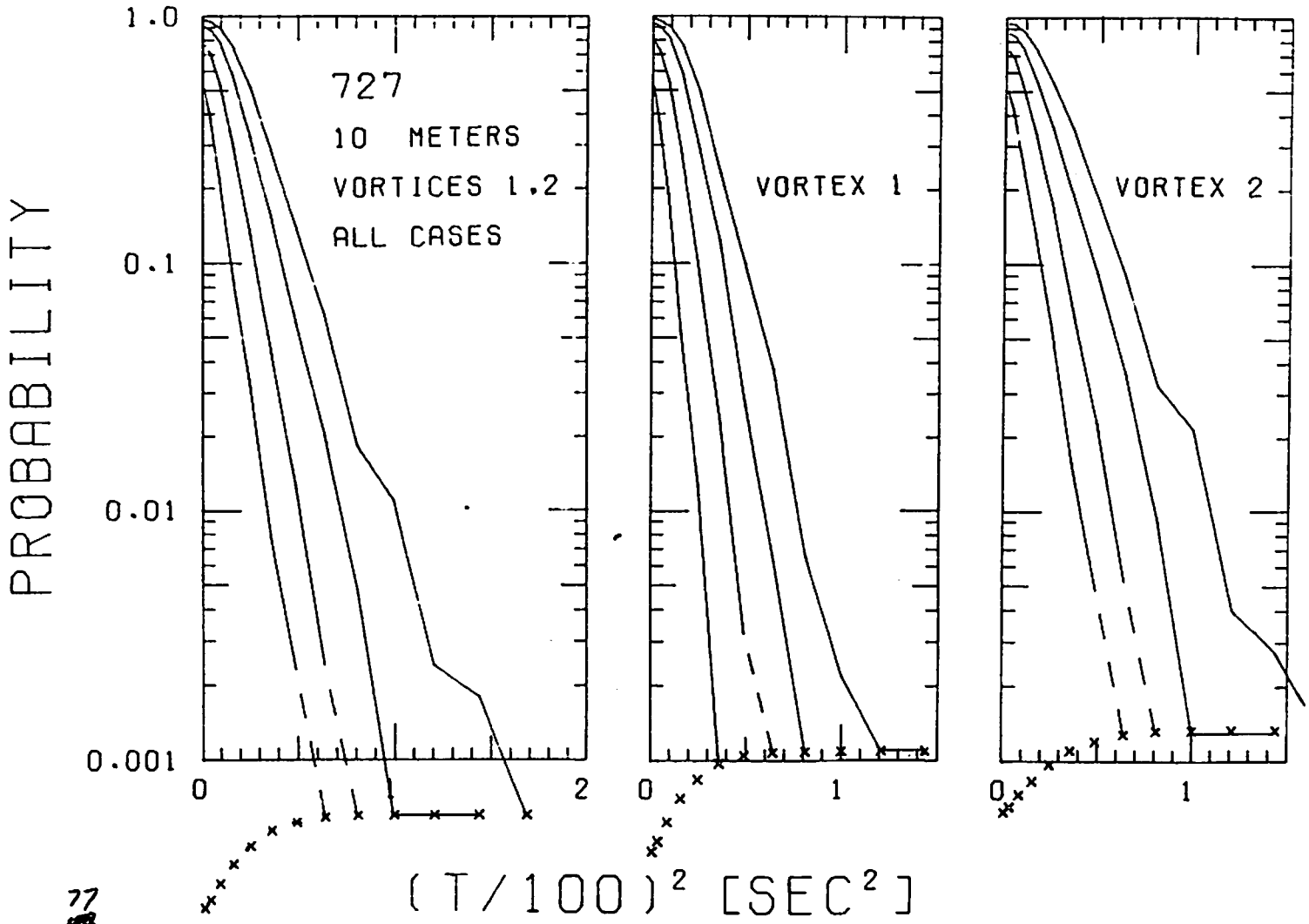

FIGURE 3-77. PROBABILITY OF DECAY, B-727, VORTEX 1 AND 2, 10-m AVERAGING RADIUS

021

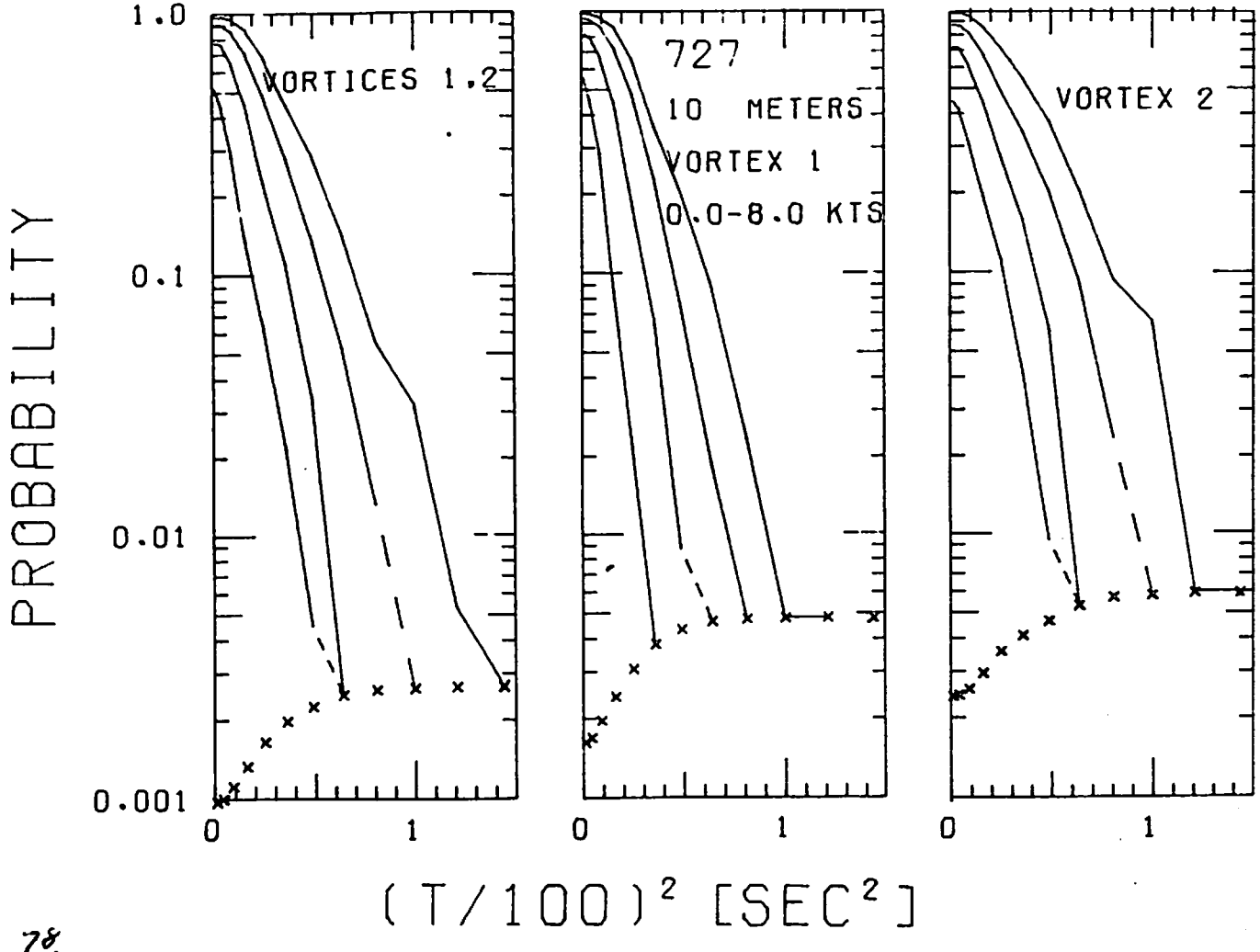

FIGURE 3-78. PROBABILITY OF DECAY, B-727, WINDS LESS THAN 8 KNOTS, 10-m AVERAGING RADIUS

121

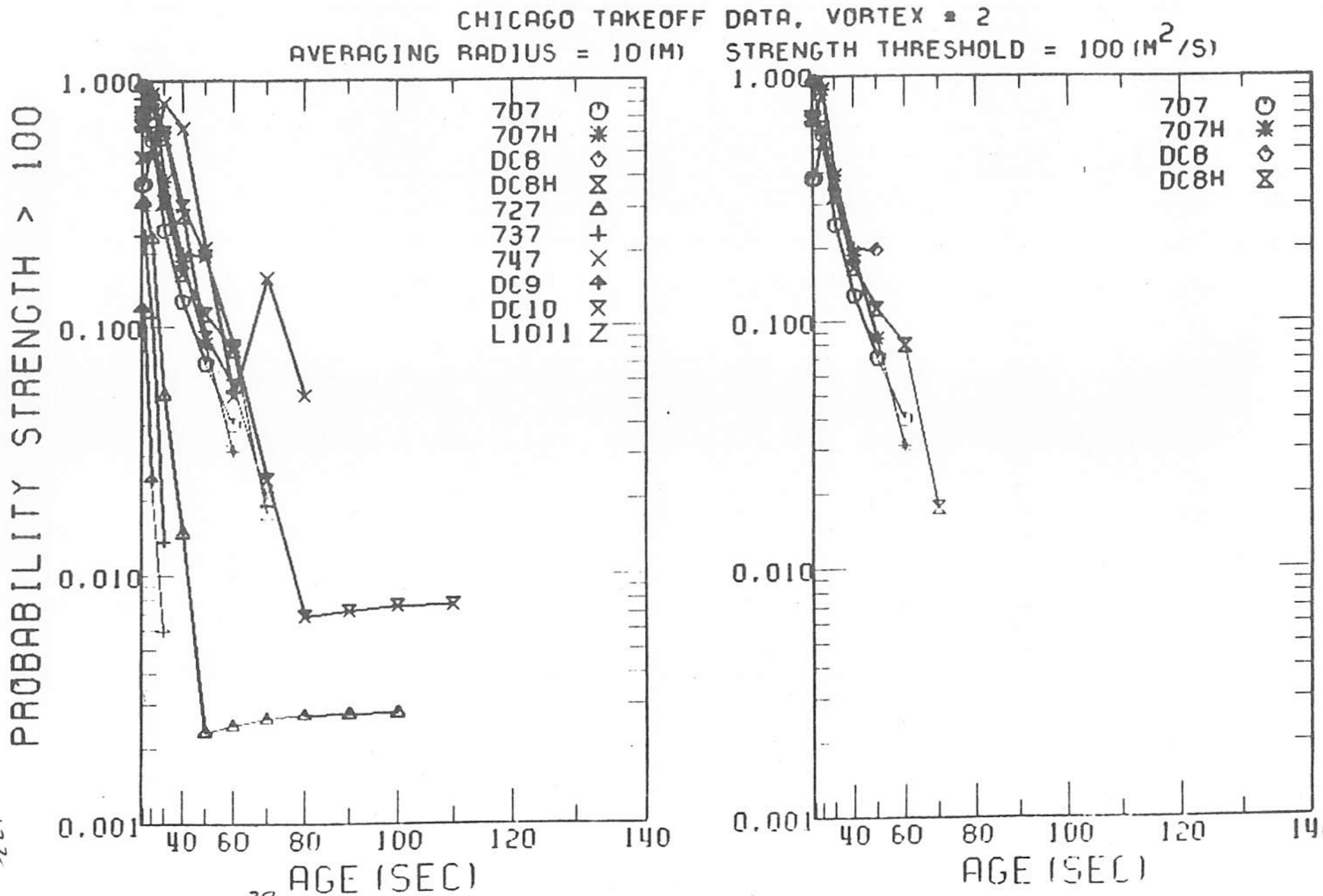

121

FIGURE 3 79

F's A-4

VORTEX DEMISE DATA FROM O'HARE TESTS

FIG C-1

~~Probability of Detecting a Vortex versus Distance From Runway Centerline (707)~~

SAS
ACTYPE=707

16:42 THURSDAY, NOVEMBER 29, 1984 20

PLOT OF PPROB*D SYMBOL IS VALUE OF DIR
PLOT OF PROBP*D SYMBOL IS VALUE OF DIR

Including Versus Excluding Intermediate Detection

P = positive Direction
S = negative Direction

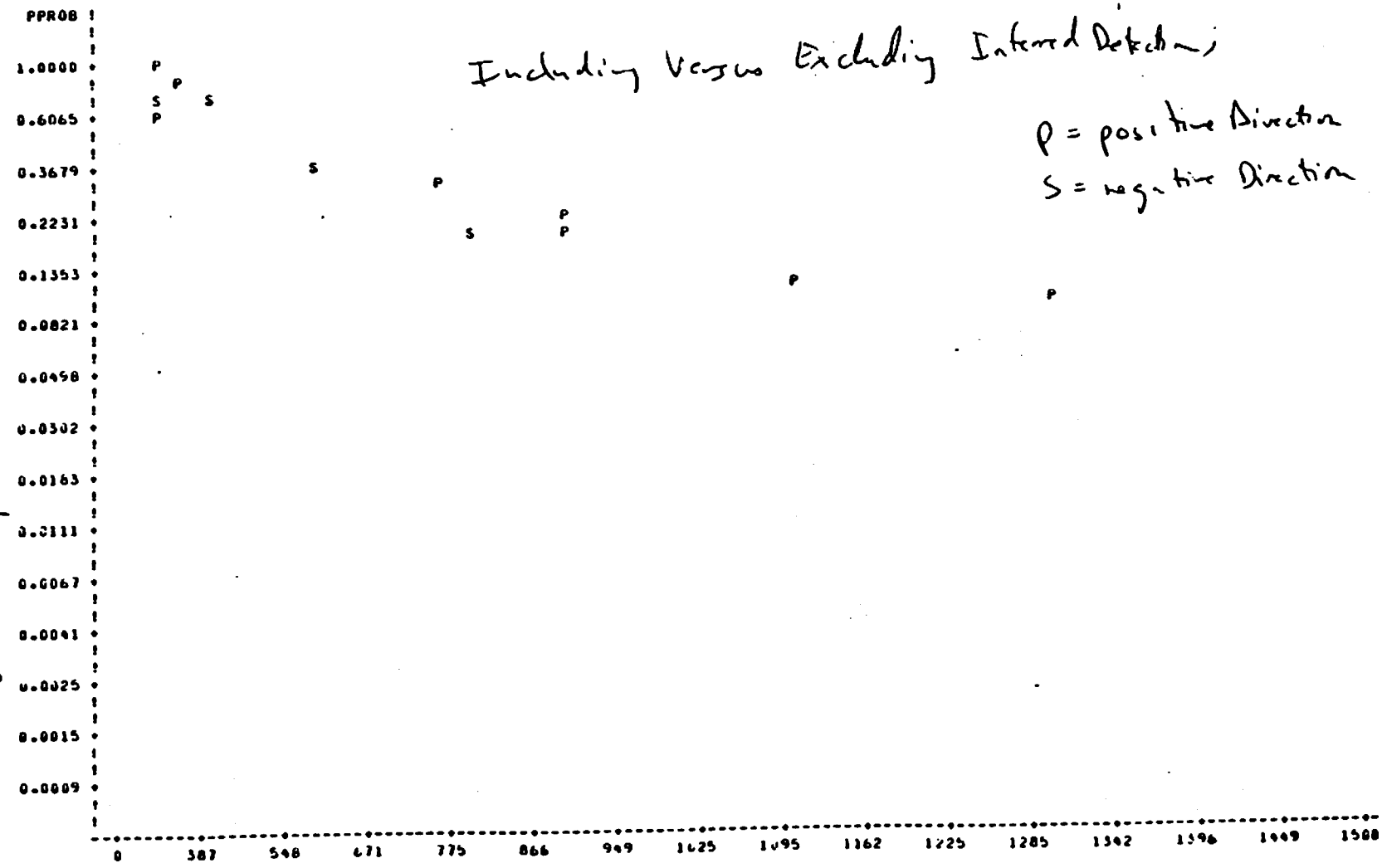

NOTE: 1 OBS HIDDEN

FIGURE 3-80 PROBABILITY OF DETECTING A VORTEX VERSUS DISTANCE FROM RUNWAY CENTERLINE (B-707)

121

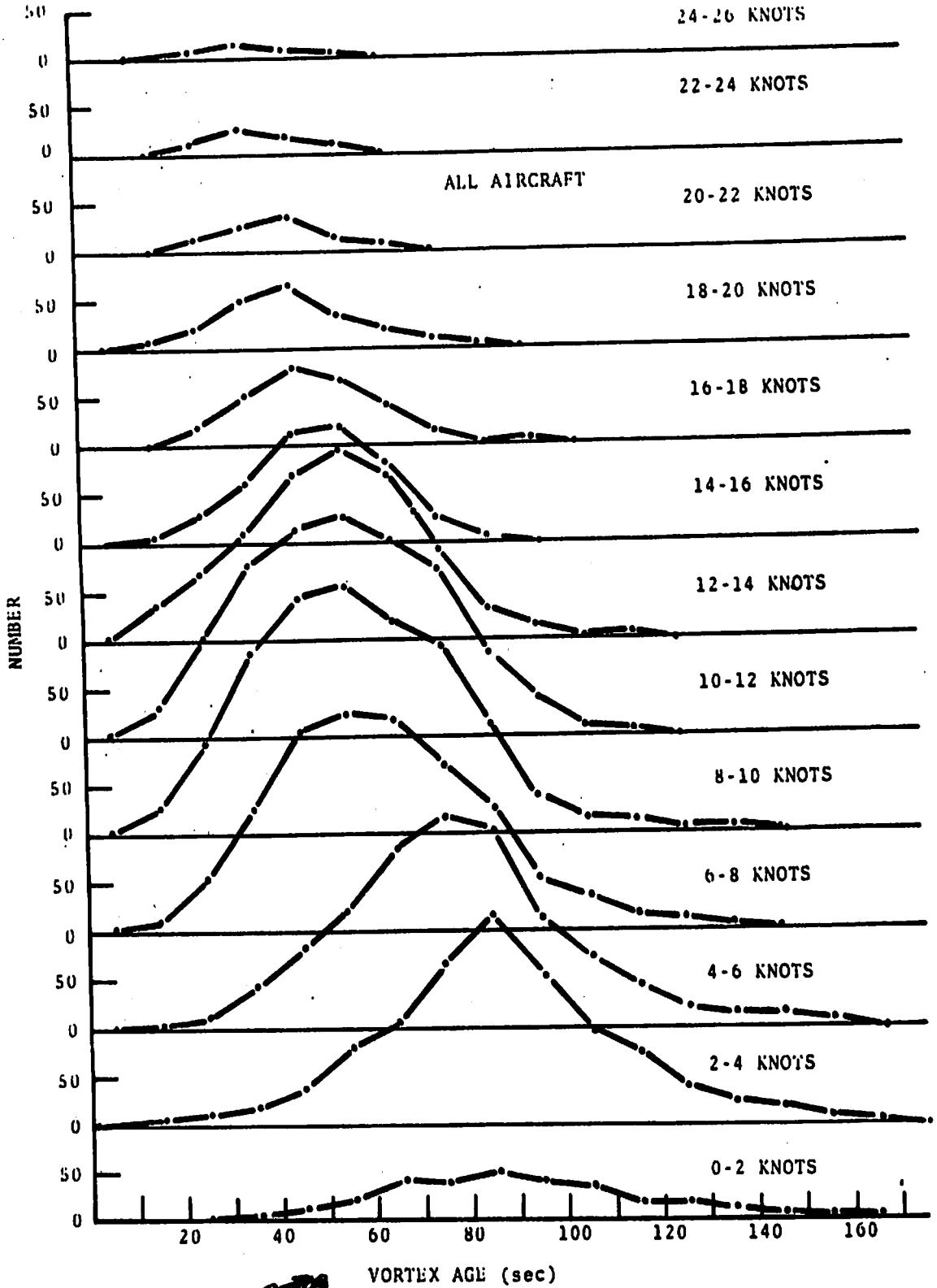

FIGURE 3-81. DISTRIBUTION OF VORTEX DEATH TIMES

124

3.5 METEOROLOGICAL VARIABILITY

As shown in Section 3.3.3 and 3.4, one of the strongest influences on both vortex transport and vortex demise is the ambient wind. Since wind varies over space and time, the accuracy with which the wind can be measured drives the accuracy with which vortex residence time can be calculated. The uncertainty with which wind can be measured has several operational implications for wake vortex avoidance systems and also has several programmatic implications for the development of an effective wake vortex avoidance system.

Operationally, there are several issues related to the accuracy with which wind can be measured. First, since an anemometer tower cannot be placed at the runway threshold, the difference between the wind at the point of measurement (i.e., the anemometer tower) and the point of interest (i.e., above the extended runway centerline) is a primary source of uncertainty for the wind affecting the vortex. Second, since the vortex corridor must be cleared of vortices at all points between the middle marker and the touchdown zone, there must be assurance that there is no point along the flight path at which crosswind will cause vortex stalling. Third, since some aircraft spacing criterion must be established prior to landing, the difference between the wind at the measurement time and at the landing time must be known.

From a programmatic point of view, the uncertainty in wind measurement drives the practical extent to which theoretical developments of vortex transport are warranted. For any model of vortex transport or demise, there will always be a difference between the values of the vortex parameters calculated from the model and measured values of the vortex parameters because of uncertainty in the measurement of wind. Therefore, the modeling of relatively minor phenomena related to vortex transport or demise is not warranted if the magnitude of their effect is significantly less than the magnitude of the effect of uncertainties in the wind. Stated alternatively, it is recognized that both vortex transport and vortex demise may be viewed as deterministic phenomena with significant random components superimposed on the deterministic phenomena. The random components must be treated statistically, and the formulation of statistical approaches to properly treat the random components is appropriate. Furthermore, it is programmatically not

appropriate to expend significant resources to define deterministic effects whose effect is significantly smaller than the random component. The appropriate programmatic development of a wake vortex avoidance system must emanate from an understanding of the relative magnitudes of deterministic phenomena and random phenomena and an appropriate balance of determinsitic and probabilistic models. One of the primary random phenomena is wind variability.

In the consideration of wind variability, the averaging period over which the wind average is taken is very important. For vortex transport and demise, the appropriate wind averaging time is 90 to 120 seconds, which is the approximate life time of the longer lived vortices. Figure 3-82, taken from Ref. O from work originally presented in Ref. P, shows the power spectral density of horizontal wind speed as measured at Brookhaven National Laboratory at alititudes of 91, 108, and 125 meters. The peak at 100 hours represents wind changes due to large scale meteorological phenomena such as the movemement of high and low pressure areas and frontal passage. The peak at 12 hours represents wind changes due to diurnal effects. The peak at 0.1 hours represents wind changes due to micrometeorological effects. For most meteorological work, the wind speed averaging period is generally taken as 15 minutes to one hour because averages of that time period filter out micrometeorological effects and are thus fairly characteristic of the atmosphere and do not exhibit significant variations for successive averaging periods.

However, for vortex phenomena, the averaging period of interest is approximately 1 to 2 minutes. Figure 3-82 shows that wind phenomena for that averaging period are clearly in the micrometeorological range and that significant variation among successive averaging periods can be expected. By Taylor's hypothesis (which states that variations of wind over time at a fixed point in space are equivalent to variations of wind over space at a fixed point in time, Ref. Q), this implies that significant differences between anemometers at different locations can be expected for averaging periods appropriate for vortex phenomena.

The expected magnitude of the wind error caused by the distance between the anemometer tower and the runway threshold can be estimated by comparing data measured by two or more anemometers separated by similar distances. Some

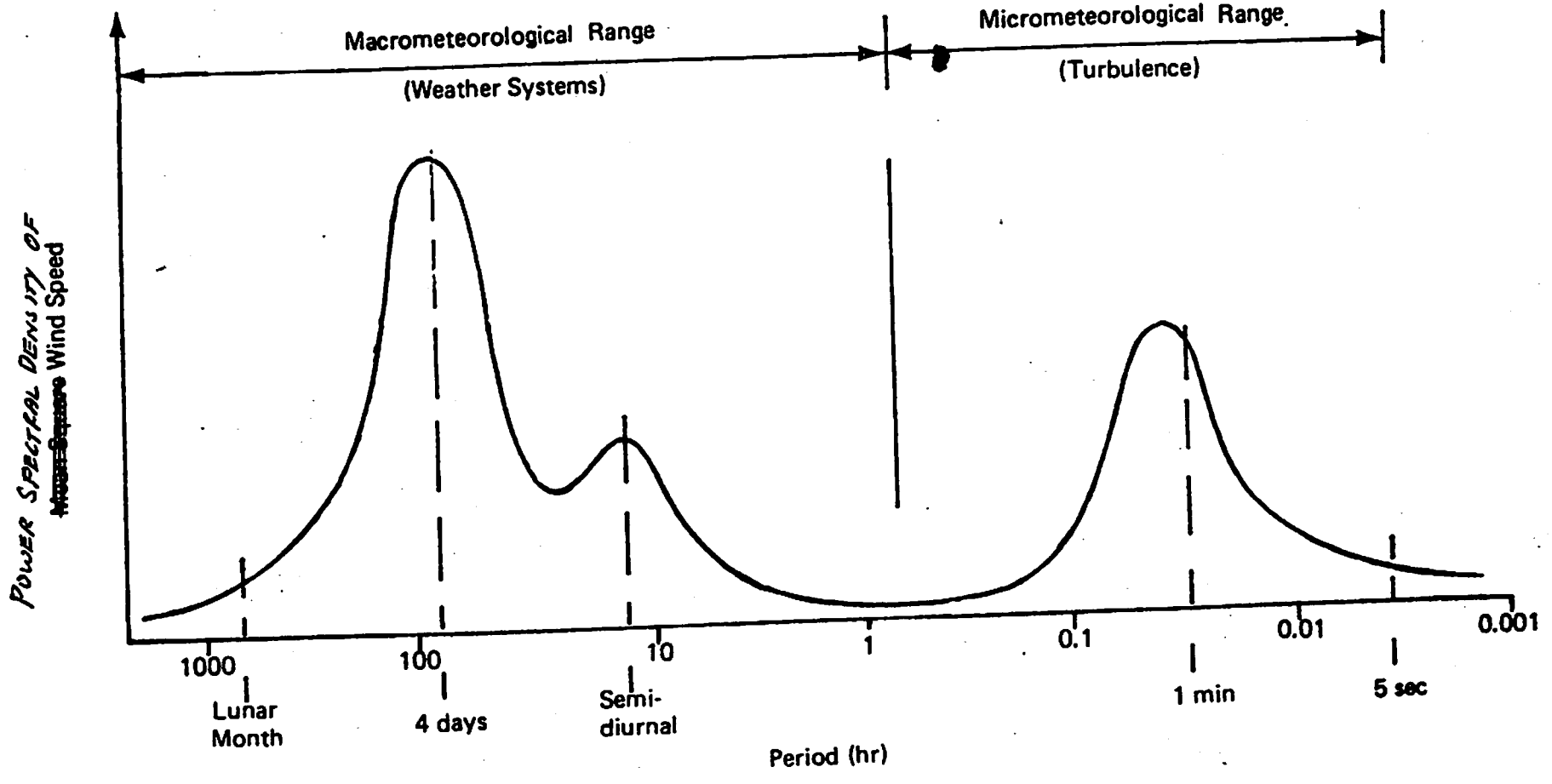

Figure 3-8. Power spectrum of horizontal wind speed FROM DATA MEASURED AT BROOKHAVEN NATIONAL LABORATORY.

data on wind variability with averaging times appropriate for vortex phenomena were measured at the vortex test site at Kennedy International Airport (JFK) in 1975. The overall layout of the test site is shown in Figure 7-1 in Section 7.1. Figure 3-83, taken from ref. K, compares the crosswind measured by Tower 1 with that measured by Tower 2 for 128-second averages. The two towers are at 400 ft on either side of the extended centerline of Runway 31L at JFK. Figure 3-84 shows similar data for crosswind measured by anemometers mounted on Tower 1 and Tower 3, which are separated by 2900 ft. It is seen that there is significant variation between the measurements made at the two locations.

Similar data was collected at O'Hare Airport (ORD) in 1977. Figure 9-2 in Section 9.1 shows the anemometer locations used at ORD for the verification of the Vortex Advisory System in 1977. The output of the anemometers was one-minute averages of wind speed and direction. Figure 3-85 shows the one-minute averaged crosswind to runway 14L as measured by anemometers 4 and 5 which are separated by feet. The one minute averages were taken at 15 minute intervals over eight days in January, 1977. Figure 3-86 shows similar data for anemometers 4 and 6 which are separated by feet. Again, it is seen that the variation between the anemometers can be significant and the magnitude of the difference increases as distance between the anemometers increases.

The results shown in Figures 3-83 through 3-86, overstate the magnitude of the problem of uncertainty in the wind speed as it relates to vortex residence time because no attempt has been made to separate the data according to the level of ambient turbulence. It has been shown in Section 3.4 that vortex life time is always short when ambient turbulence is high. Therefore, for vortex phenomena, uncertainty in wind measurement is important only when ambient turbulence is low. Figure 3-87, taken from Ref. R, shows significant spectral differences for day and night. Therefore, it is expected that the problem of wind variability might not be so severe for atmospheric conditions for which long vortex life would be expected. Development of figures similar to 3-83 through 3-86 for particular ranges of atmospheric turbulence (or atmospheric stability) is appropriate to determine the significance of this uncertainty for vortex phenomena.

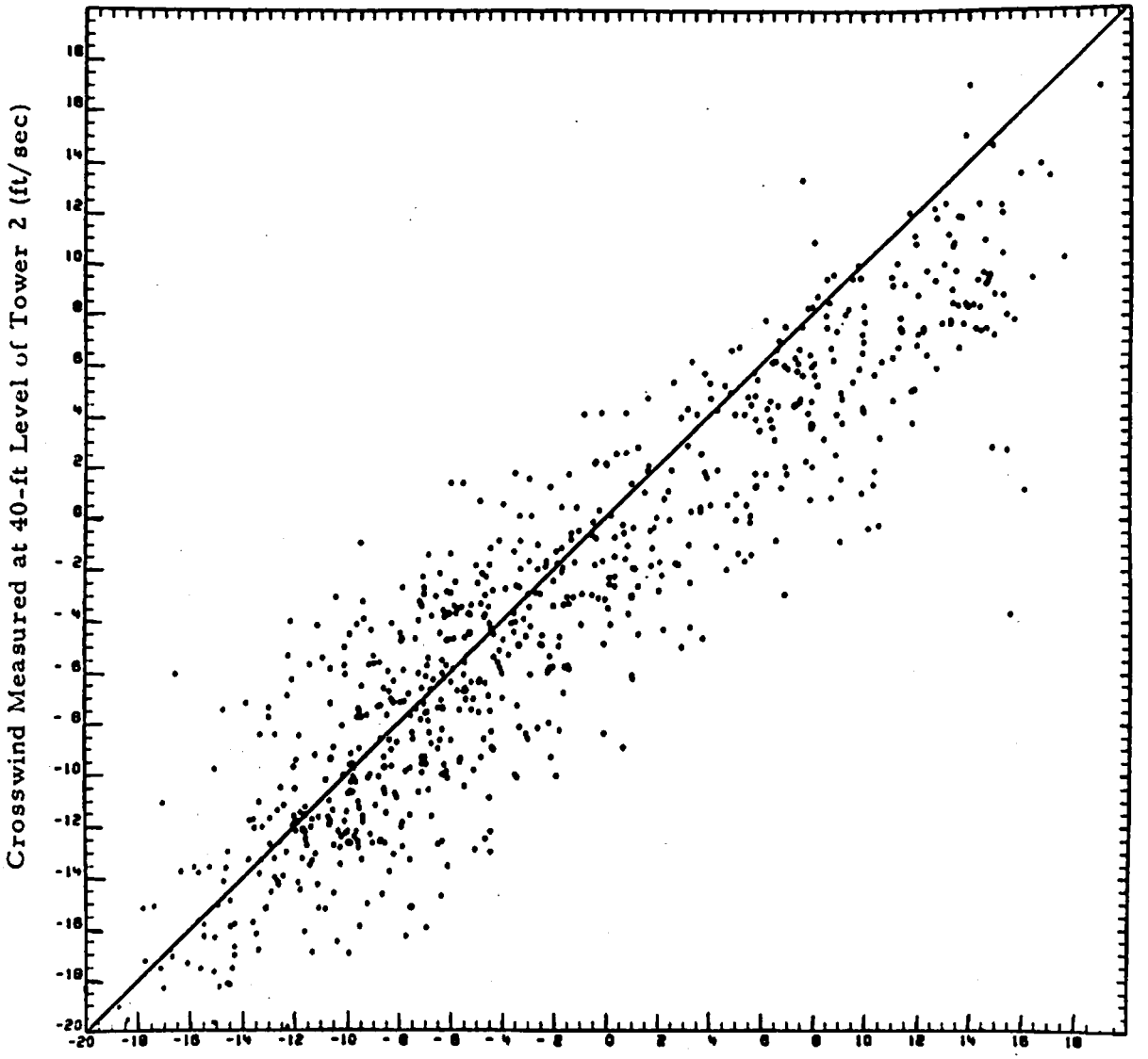

FIGURE 3-83. COMPARISON OF CROSSWIND MEASURED BY TOWER 2 WITH CROSSWIND MEASURED BY TOWER 1 AT JFK VORTEX TEST SITE

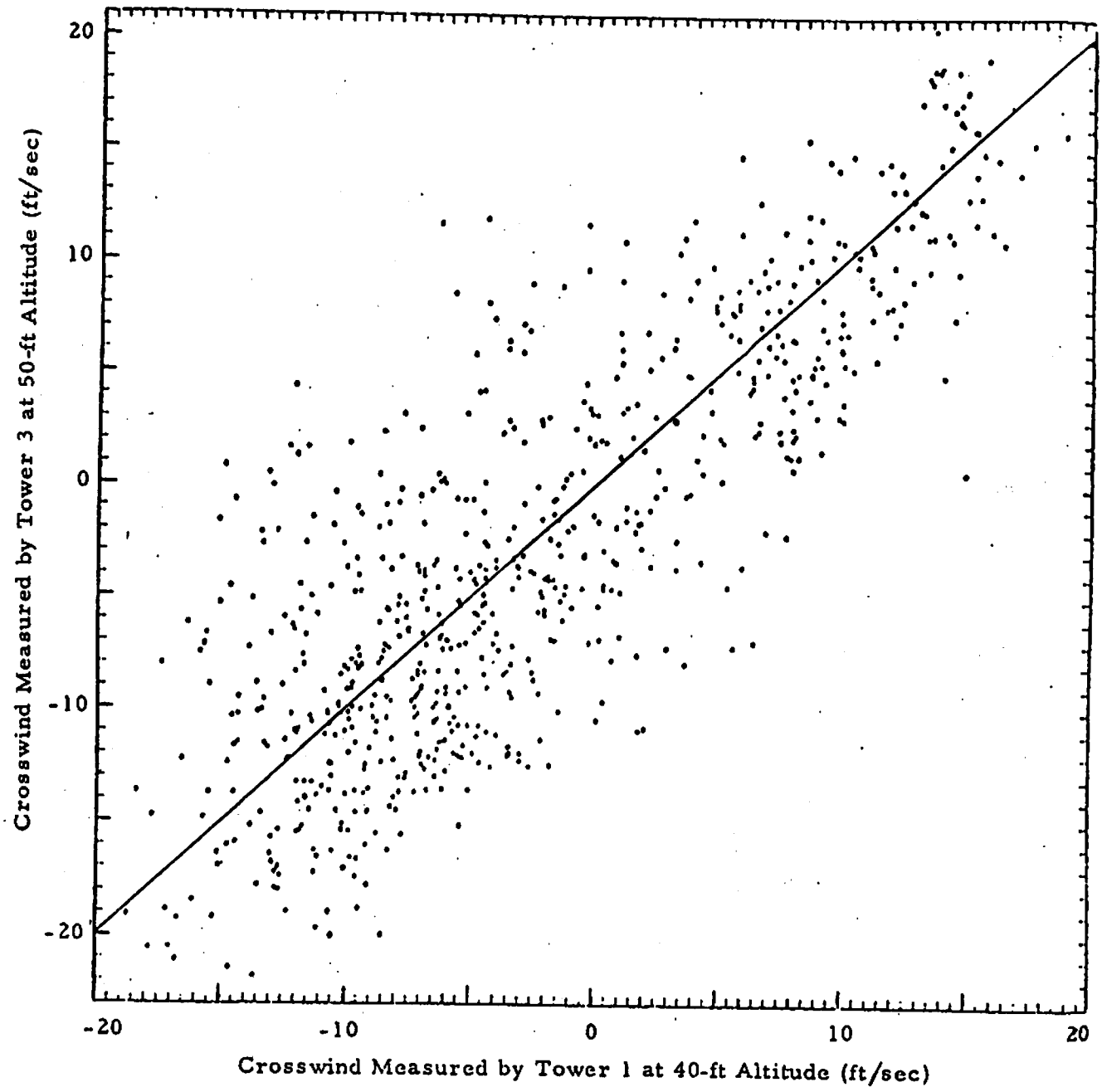

FIGURE 3-84. COMPARISON OF CROSSWIND MEASURED BY TOWER 1 AND BY TOWER 3 AT JFK VORTEX TEST SITE

Vortex Altitude (ft)
20
18
16
14
12
10
8
6
4
2
0

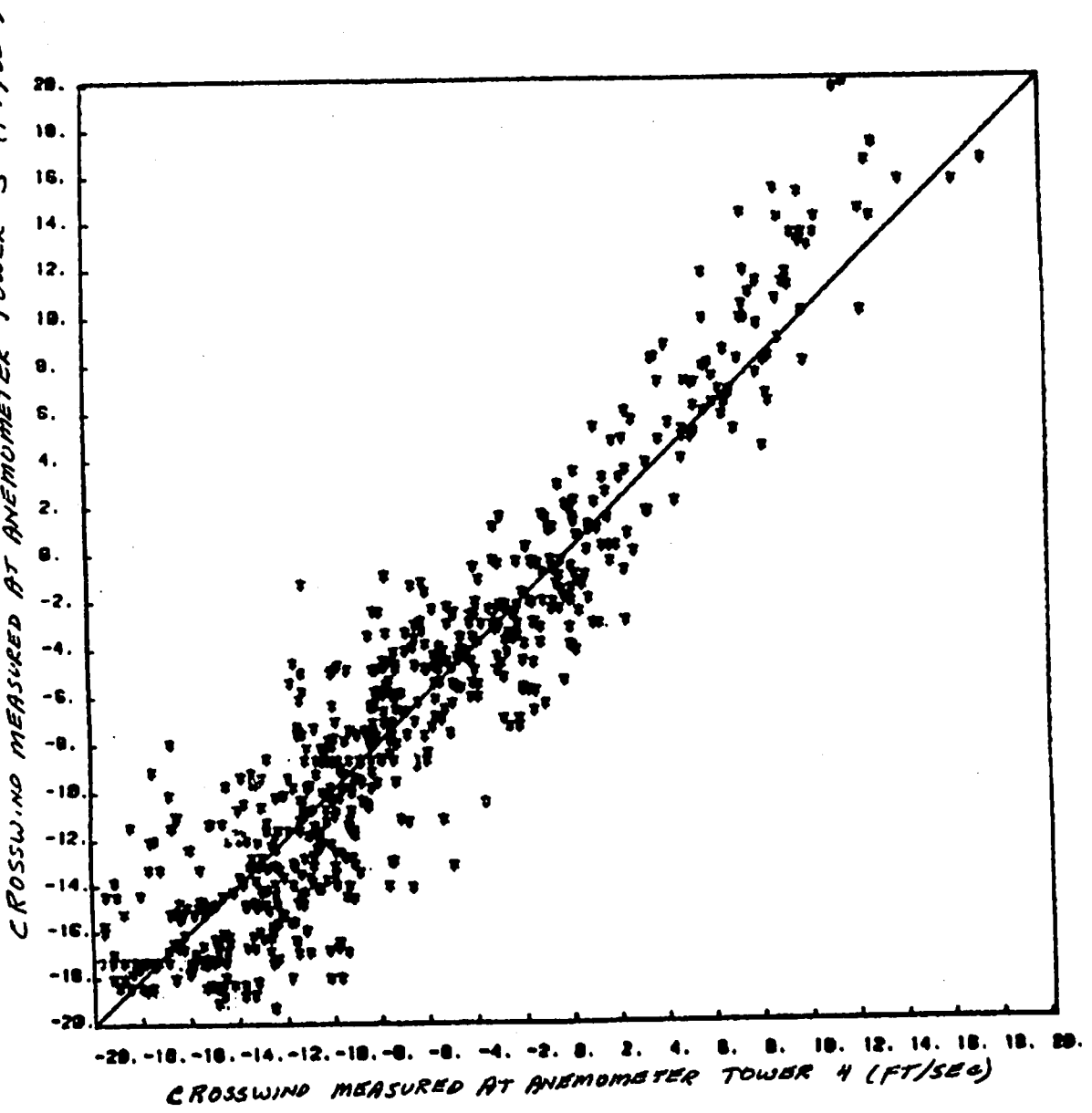

FIGURE 3-85 CROSSWIND TO RUNWAY 14L AS MEASURED AT ANEMOMETER TOWERS 4 AND 5 AT O'HARE INTERNATIONAL AIRPORT.

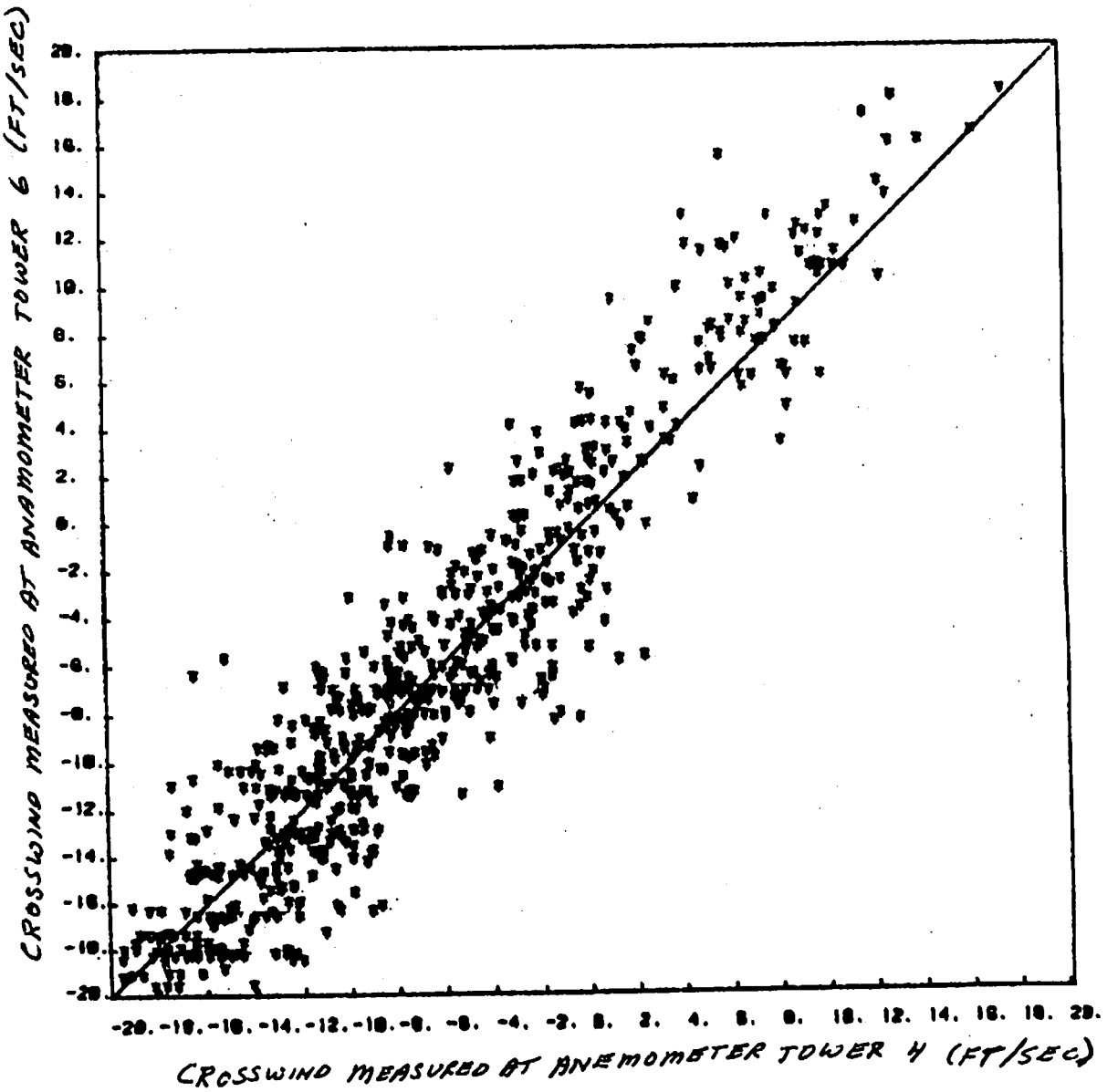

FIGURE 3-86. CROSSWIND TO RUNWAY 14 L AS MEASURED AT ANEMOMETER TOWERS 4 AND 6 AT O'HARE INTERNATIONAL AIRPORT.

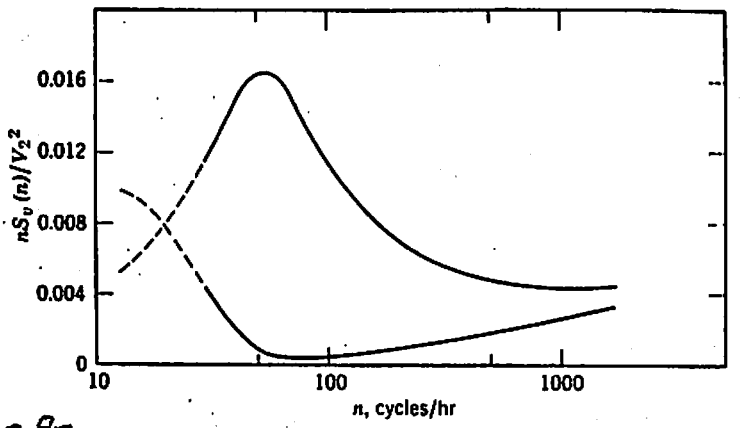

3-87

Fig. ~~3-12~~ Typical spectra of lateral velocity ~~at (a) Phoenix~~, divided by square of wind speed at 2 m. Upper curve, daytime; lower curve, night with gradual fluctuations of wind direction.

3.5 SUMMARY OF VORTEX METEOROLOGICAL EFFECTS

Table 3-3 presents a summary of vortex meteorological effects. The state of theoretical knowledge summarizes the degree to which the phenomenon is understood from a theoretical point. Theoretical knowledge includes the ability to accurately calculate the dependent parameters of the phenomenon if values of the appropriate independent parameters are known. The quantity of experimental verification indicates the degree to which the phenomenon has been observed experimentally and the degeree to which the theory related to the phenomenon has been verified. The operational significance of the phenomenon indicates the degree to which knowledge of the phenomenon will be necessary and/or helpful in an operational environment. The magnitude of the effect is a measure of the degree to which the phenomenon significantly affects vortex transport time and/or vortex life time, especially if it is an effect which can occassionally cause long life time. The deterministic or random rating is an indicator of whether the phenomenon can be considered to be deterministic or random. The followind paragraphs discuss some of the ratings given when the ratings are not immediately obvious.

The effect of crosswind on vortex transport is considered to be somewhat random because of the uncertainty of measuring crosswind at the region of vortex transport from an anemometer which is located at some distance from the region of vortex transport.

Vortex tilting is given a moderate rating for state of theoretical knowledge because we have some idea of the phenomena which cause vortex tilting. It is given a low to moderate rating on the quantity of experimental verification because experimental data has shown that the phenomenon exists, but there has been no definitive experimental data linking vortex tilting to any of the proposed mechanisms of vortex tilting. It is highly significant because of the long life time of the solitary vortex remaining as a result of vortex tilting.

The mechanism of vortex buoyancy has been modeled somewhat completely. However, its effect is low, and it is difficult to get good values of the independent parameters to use in the models.

Vortex decay is moderately significant because it affects vortex transport. It is not often a factor in vortex life time because one of the two catastrophic vortex demise mechanisms ususally occurs before decay can cause vortex demise.

Crow instability is given a moderate rating on state of theoretical knowledge and quantity of available experimental data because the phenomenon has been observed experimentally, and some theory exists for it. However, accurate predictions of vortex life time limited by Crow instability are not yet possible.

3.6 RECOMMENDATIONS FOR FURTHER WORK

Sections 3.3 and 3.4 have described the current (early 1985) state-of-the-art for vortex transport and vortex demise. In this section, deficiencies in the state-of-the-art are discussed. Primary emphasis is placed on state-of-the-art deficiencies which have operational significance, rather than those deficiencies which have only theoretical interest. For example, from a theoretical point of view, it is desirable to formulate a transport model that would include many effects on vortex transport. It may even be possible to validate such a model if the test conditions were chosen so that the wind velocity was very uniform and that the terrain was very flat. However, in an operational environment the model would not be very useful. Wind varies significantly over time and space, and the uncertainties associated with wind measurement exceed the uncertainties caused by the failure to include certain effects in a transport model. It is, of course, appropriate to attempt to improve understanding of vortex behavior by further analytical work. However, the limitations on reducing overall uncertainties should be realized. A discussion of wind measurement uncertainties is presented in Section _____.

3.6.1 Varying Altitude Considerations

As shown in Section 3.3.3.3, vortex transport is a function of aircraft altitude. Specifically, the crosswind at which the vortex stalls in the flight corridor is a strong function of altitude. Therefore, for a wide range of crosswind conditions, there is always some point along the a flight path at which the vortex will stall as the aircraft descends from

approximately 200 ft AGL at the middle marker to touchdown. Fortunately, there are two aspects to this phenomenon which tend to mitigate its severity.

First, as shown in Section 3.3.3.3, the vortex is theoretically curved near the ground for reasonably long transport times. Thus, the exposure time for any following aircraft would be small, and significant roll angles would probably not occur.

Second, vortex lifetime appears to be quite short for vortices generated in ground effect. Thus, for a given aircraft landing, vortex residence time is limited by transport time for the higher aircraft altitudes (e.g., 200 ft at the middle marker to 70 ft) and is limited by lifetime at the lower altitudes (e.g., below 70 ft).

In any case, it is shown that the current separation standards are safe and that vortices do not persist in the flight corridor for times as long as those defined by the current separation standards. However, for the reduction of current separation standards, this phenomenon must be understood better. In particular, the altitude at which residence time shifts from being transport limited to being life limited must be understood, and the factors (including aircraft characteristics and crosswind) which affect the transition altitude must be understood. The understanding must include an ability to determine residence time as a function of the coordinate distance as the aircraft flies from the middle marker to the touchdown zone.

3.6.2 Vortex Tilting

As discussed in Section 3.3.4.1, vortex tilting is operationally significant because of the long persistence of one of the vortices, which may stall in the flight corridor. The phenomenon is not well understood, but efforts to increase understanding are appropriate. In particular, it is desirable to identify the meteorological and aircraft conditions under which vortex tilting can occur and usually occurs. An automated data base which allow isolation of vortex trajectories for which tilting occurs from a large data base of vortex trajectories would be useful. The conditions which are common to tilted trajectories could then be identified.

One instrumentation improvement which would be helpful in the investigation of this phenomenon would be the automation of vortex tracking in the scanning laser Doppler velocimeter system. If scanning could be automated so that one scan always passes through the vortex core and two other scans pass near the vortex core, accurate measurement of vortex strength as a function of time would be significantly enhanced. Since two of the postulated mechanisms by which wind shear affects vortex tilting assume that wind shear augments the strength of the upwind vortex and decreases the strength of the downwind vortex, accurate measurement of vortex strength as a function of time would give some indication of the validity of the assumption and the efficacy of these two mechanisms in explaining vortex tilting.

3.6.3 Statistical Distribution of Vortex Residence Time

Section 3.3.5 contains a statistical description of vortex transport, and Section 3.4.4 contains a statistical description of vortex demise. However, for operational considerations, the statistics of extreme values (i.e., determining the probability that a vortex residence time will exceed a specified time or specifying a time for which it is known that the probability that a residence time will exceed that value is less than some specified probability) is relevant. It is noted that it is the vortex pairs which exhibit the longest residence times which are of primary interest in an operational environment. The statistics of extreme values is discussed in Section . It is appropriate to study vortex behavior statistically in terms of the statistics of extreme values.

3.6.4 Residence Time Prediction

As described in Section 3.3.3.2, aircraft parameters can have a very significant effect on vortex transport time. Therefore, it is almost impossible to predict aircraft transport time before aircraft passage. However, it is likely that if accurate estimates of vortex strength can be made shortly after aircraft passage, either by direct measurement or inferred from intial vortex descent rate, an early accurate prediction of the residence time of the vortex pair can be made. Kalman filtering is probably the most appropriate approach for making such a prediction. For this reason, Kalman filtering is discussed in Section . However, an attempt to make an early prediction of vortex residence time is appropriate

and, if successful, could be useful in an operational environment.

6. VORTEX SENSORS

The quest to capture and subdue the hazardous wake vortex has taxed the capabilities of men and their instruments. A simple swirling mass of air has proved to be an elusive quarry. Conventional detection and measurement techniques have proved only partially effective; newly developed remote-sensing instruments have fared better. Almost every conceivable technology has been tapped in the quest to protect the airways from the wake vortex danger. This section is a chronicle of the years spent chasing the wake vortex.

6.1 GENERAL SENSOR REQUIREMENTS

A wake vortex sensor must interact with some physical property of the vortex. The usefulness of the sensor depends upon how closely the property sensed is related to the property which is to be determined. For example, smoke injected into the vortex by the generating aircraft is very useful for marking the vortex location, but it provides virtually no information on vortex strength. The question of the appropriateness of a sensor is particularly important for sensors which are intended to monitor the decay of wake vortex hazard. The peoperty sensed may decay more quickly or more slowly than the actual hazard. The former case results in missed hazards while the latter leads to false alarms. These uncertainties have led to a strong emphasis in recent work on sensors which measure vortex strength.

6.2 SENSOR CHARACTERISTICS

In the following discussion of wake vortex sensors, five binary categories will be used to distinguish characteristics of the various sensors:

a. Remote/in situ: Can the sensor be located away from the point being sensed, or must it be located at the same point?

b. Active/Passive: Does the sensor project energy into the volume being sensed or does it simply extract energy already present?

c. Artificial Tracer/Natural Tracer: Does the sensor interact with something added to the vortex or with something occurring naturally within the vortex?

d. Operational/Research Only: Can the sensor be used during normal aircraft operations, or is it suitable only for special flight tests?

e. Airborne/Ground-based: Does the sensor have the potential for operation from an aircraft, or will it work only on the ground?

The first three categories are determined by the nature of the sensor's potential application. This section will concentrate on ground-based sensors. Apart from in situ sensors mounted on probe aircraft, very little work has been done on airborne wake vortex sensors.

The basic functions performed by wake vortex sensors are detection, tracking, and measurement. Each of these functions successively involves a higher order of complexity. Some sensors can detect and track but cannot measure. Normally, the most important vortex parameter to be measured is its strength. For those sensors which can measure strength, the detection and tracking functions were usually implemented first before strength measurement was attempted. Characterization of the detection function requires an understanding of miss and false-alarm rates as a function of detection threshold, vortex locations, and vortex properties. The tracking and measurement functions have the additional characteristic of accuracy. None of the wake vortex sensors have been completely characterized, but several of them can be represented by simple models which give a reasonable indication of their utility. The operational usefulness of sensors depends upon their sensitivity to operational variables such as meteorological conditions, generating aircraft type, and the presence of interference in the environment.

6.3 DESCRIPTION OF WAKE VORTEX SENSORS

The potential usefulness of each type of physical interaction is examined in turn, and the particular sensors based on the interaction are described and classified according to the criteria discussed in Section

6.2. Table 6-1 lists the sensors discussed and their classification. Unless specified otherwise, the sensor development work was carried out at TSC.

For the purposes of completeness, all of the sensors listed in Table 6-1 are discussed in this section. However, over the past several years, the Ground Wind Vortex Sensing System, the Monostatic Acoustic Vortex Sensing System, and the Scanning Laser Doppler Velocimeter System have emerged as the primary means of vortex sensing. Therefore, these systems are discussed in more detail than the other systems.

6.3.1 Mechanical Techniques

Mechanical sensors provide in situ measurements of wind velocity or pressure. Some of the other physical interactions can also provide equivalent local measurements and are conceptually included here. For example, an acoustic anemometer provides data very similar to that from a hot-wire anemometer.

In situ sensors have a fundamental limitation for sensing aircraft wake vortices. If the sensors are located at altitudes high enough to probe the center of the vortex, they cannot be used in an operational environment because of the hazard posed to aircraft. Conversely if they are low enough to be installed at airports, they measure only the peripheral region of the vortex and cannot verify the location and persistence of the vortex core.

6.3.1.1 Wind Sensors

In situ wind sensors provide a direct measurement of the vortex-velocity field at the point where the sensor is located. Some of the earliest and most detailed vortex measurements were made with instrumented towers which were tall enough to measure the complete flow field of a vortex as it drifts through the tower (refs. 27, 31-38). Although tall instrumented towers cannot be installed near airport runways, experience has shown that anemometers located near the ground can successfully detect and track wake vortices in runway-approach regions. Such a system, called the Ground Wind Vortex Sensing System (GWVSS), has produced much of the currently available data on wake vortex transport in the airport environment. First tested in 1972, the system was subsequently installed at

TABLE 6-1. WAKE-VORTEX SENSOR CLASSIFICATION

Technology	Sensor	Status			Type						Capability										
															Function†			Limitations††			
		Proposed	Tested	Used for Airport Data Collection	Remote	*In Situ*	Active	Passive	Artificial Tracer	Natural Tracer	Operational	Research Only	Airborne Potential	Ground Based Only	Detection	Tracking	Measurement	Dependence	Interference	Meteorological Dependence
Mechanical	Instrumented Tower	*	*			*		*		*		*		*			*			S
	GWVSS	*	*	*		*		*		*	*			*	*	*	P			S
	Pressure Sensor (local)	*	*			*		*		*	*			*	*	*				S
	Pressure Sensor (spatial average)	*				*		*		*	*			*	*					S
Acoustic	DAVSS	*	*	*	*		*			*	*			*	*	*	*		S	S
	MAVSS	*	*	*	*		*			*	*			*	*	*	*		S	S
	PAVSS	*	*	*	*		*			*		*		*	*	*		M	S	S
	Passive	*	*		*			*		*		*		*	*	*		M	S	S
	Infrasonic				*			*		*				*	?	?		?	?	?
Optical	Flow Visualization	*	*		*			*	*			*		*	*	*				S
	Infrared	*			*			*		*			*		*	*		?	?	?
	Ultraviolet	*	*		*			*		*		*	?	?	*	*		?	?	?
	Lidar	*	*	*	*		*			*	*		*		*	*	*			
Electromagnetic	Radar	*	*		*		*			*		*	?	?	*	*	P			M
	Radar	*	*		*		*		*			*	?	?	*	*	P			
	Electrostatic	*			*			*	*		*		*		*	*			S	
Combination	GWVSS + PAVSS	*			*	*	*	*		*				*	*	*				
	GWVSS + MAVSS	*			*	*	*	*		*				*	*		*			

†P = potential function requiring development

††S = some

M = much

142

Kennedy, Stapleton, Heathrow, O'Hare, and Toronto International Airports for data collecton (see Section 7).

The GWVSS consists of an array of single-axis anemometers installed on a baseline perpendicular to the aircraft path. Since the wake vortices induce winds near the ground which are perpendicular to the flight path, the anemometers are oriented to respond only to the perpendicular component of the wind (the crosswind). The theoretical crosswind at the ground produced by a pair of counter-rotating vortices is given by the expression

$$v_x = \frac{\Gamma}{\pi}\left[\frac{z_2}{z_2^2+(x-x_2)^2} - \frac{z_1}{z_1^2+(x-x_1)^2}\right] \qquad (6.1)$$

as a function of lateral position x, where x_1 and x_2 are the lateral positions of the two vortices, z_1 and z_2 are the altitudes of the two vortices, and Γ is the vortex circulation which is also designated as the vortex strength. Figure 6-1 shows the expected crosswind vortex signatures for three different vortex altitudes. It is assumed that the vortex-induced winds can be simply superimposed on the ambient crosswind.

The effects of the two vortices are easily distinguished since they are of opposite sign. When the vortices are at altitudes significantly less than their lateral separation, the peak vortex winds are located directly below the vortex centers. For altitudes greater than the vortex separation, the vortex signature deteriorjates because the winds from the two vortices tend to cancel; the signal amplitude diminishes more rapidly than 1/h and the signature no longer clearly indicates the vortex locations. The success of the GWVSS is the result of the normal behavior of wake vortices near the ground. After creation, the vortices descend toward the ground at a rate of 1 to 2 m/sec. According to classical theory (ref. 84), when the vortices approach the ground, they begin to separate and eventually reach an altitude of half of their initial spacing and a separation rate of twice their initial descent rate. Thus, the vortex motion produces the exact conditions needed to give good GWVSS signatures; namely, low altitudes and large lateral separations. The theory also predicts a maximum GWVSS crosseind of four times the initial descent rate; i.e., 4 to 8 m/sec.

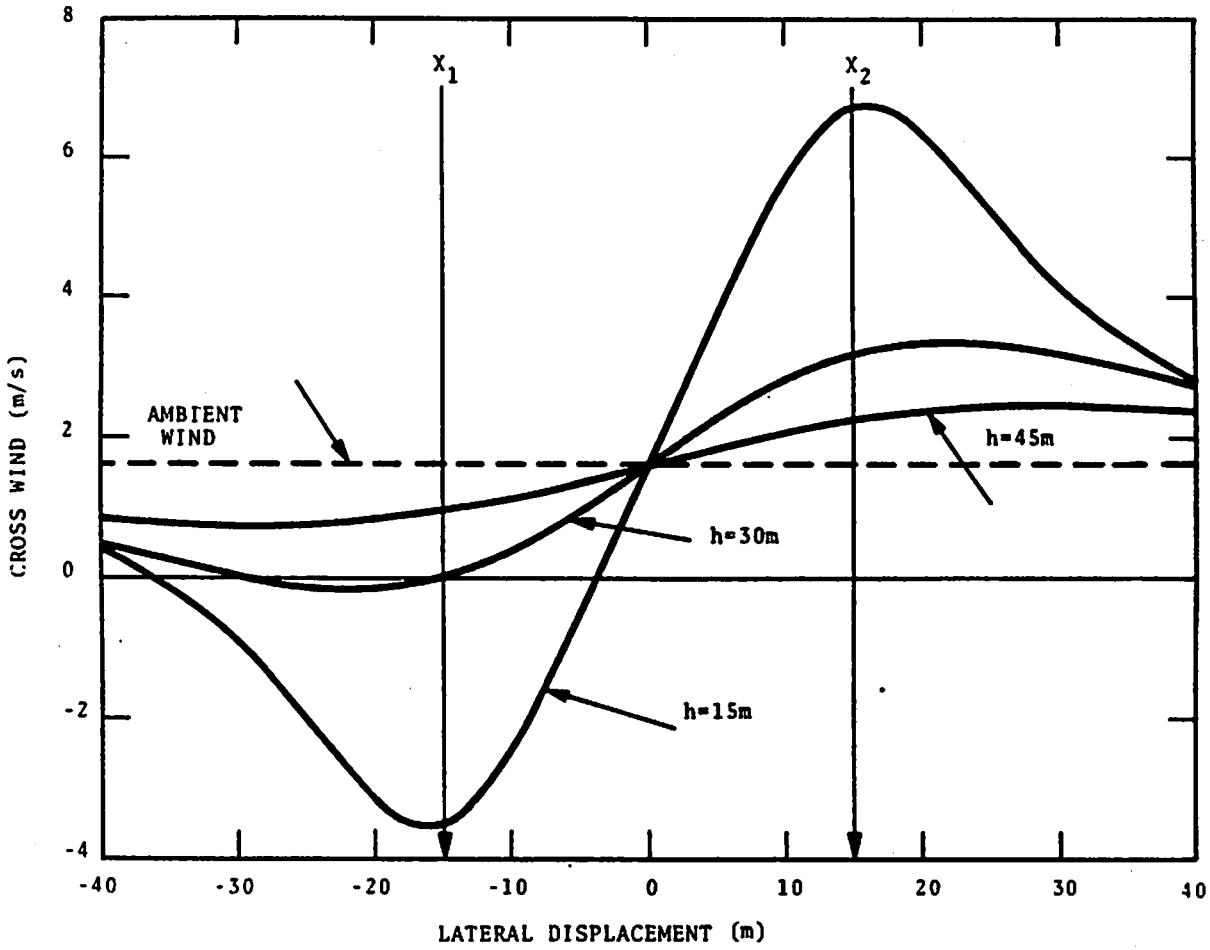

FIGURE 6-1. THEORETICAL GROUND LEVEL CROSSWIND VS. LATERAL POSITION. VORTEX STRENGTH = 300 m^2/sec, VORTEX SPACING = 30m, AMBIENT CROSS-WIND = +1.6 m/sec, AND VORTEX ALTITUDES = 15, 30, 45 m.

144

Figure 6-2 shows some experimental data from the Heathrow GWVSS installation (ref. 85). The wind measured simultaneously at each anemometer is presented as a bar graph obtained by successively sampling each anemometer output in turn. The motion of the vortices to the left is evidenced by the displacement of the vortex peaks at different times. The algorithm used to obtain the vortex positions from GWVSS data simply designates the location of the anemometer reading the highest crosswind velocity as the lateral position of one vortex and the location of the anemometer reading the lowest velocity as the position of the other vortex. Figure 6-3 shows the stepped vortex tracks obtained from this algorithm. When the vortex signals decay to the level of ambient turbulence, the vortex locations given by the algorithm become random. The termination of the vortex tracks can be made automatic by means of consistence requirements.

The accuracy of the GWVSS vortex locations was evaluated in 1972 flight tests at NAFEC. Figure 6-4 shows some data from those tests plotted as time histories of the crosswind at each anemometer. Comparisons with photographic tracks of smoke entrained in the vortices showed that the peak in the anemometer response accurately measures the time when the vortex is directly above the anemometer. Because the vortex peak becomes asymmetrical as the vortex ages, the stepped track of Figure 6-3 tends to display a bias compared to the actual vortex tracks. The peak response representing the vortex arrival typically occurs considerably before the middle of the total time the vortex position is assigned to a particular anemometer location.

A typical GWVSS installation is shown in Fig. 6-5. Fixed-axis propeller anemometers using dc generators are mounted on posts about 3 m high with lateral spacing of about 15m. The spacing between anemometers should be roughly equal to the expected minimum vortex altitude (about 3/8 of the wing span), so that vortices are not lost between sensors. The altitude of the anemometers is not critical but they should be well above any obstructions which could disrupt the wind flow. The 3 m height was selected to discourage unauthorized removal of the anemometers as much as for clearance to eliminate ground effects from the data. Proper orientation of the anemometers is important for reliable vortex tracking. A single anemometer skewed into the wind can falsely indicate the presence of a vortex at its location.

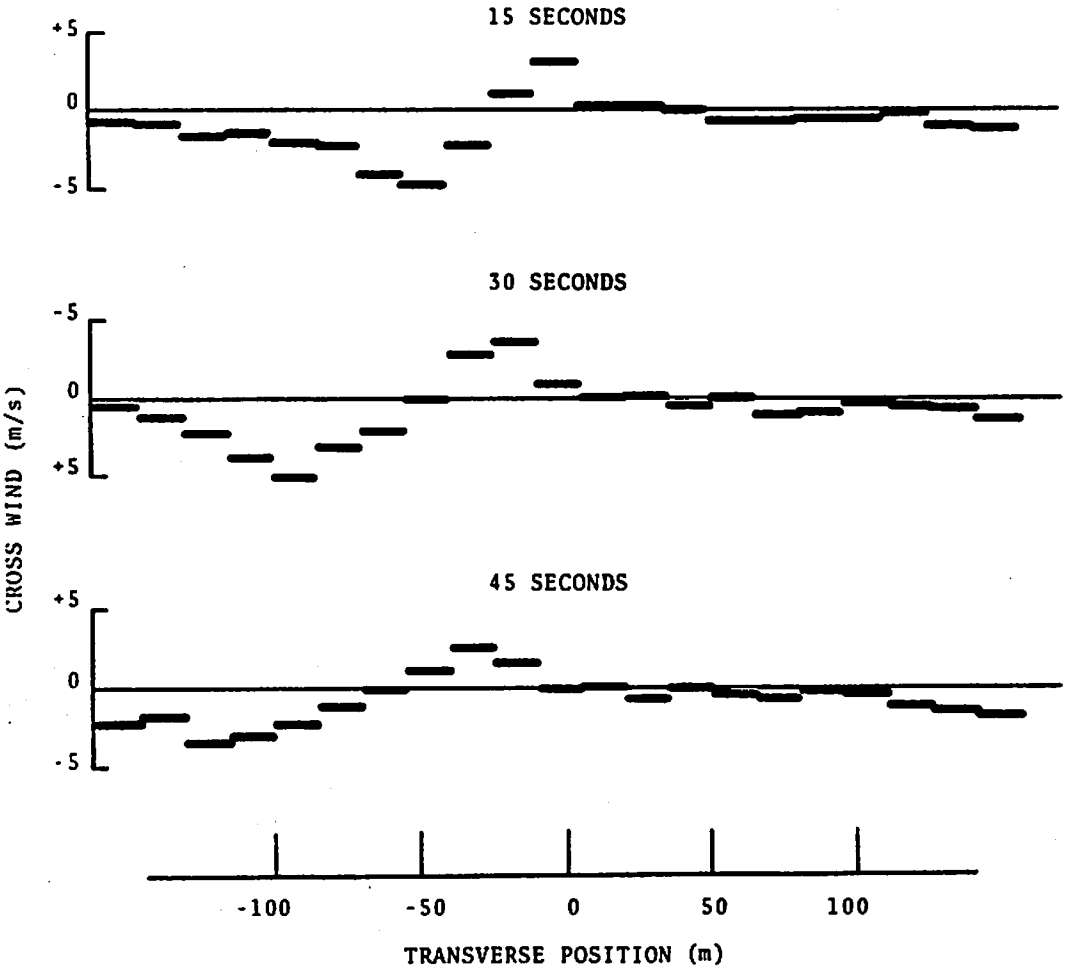

FIGURE 6-2. GWVSS DATA FOR A BOEING 707 AIRCRAFT. CROSSWIND PROFILES FROM THE INNER GWVSS BASELINE AT HEATHROW AIRPORT RUNWAY 28R ARE SHOWN FOR THREE ELAPSED TIMES AFTER AIRCRAFT PASSAGE AT 1123 HOURS ON 29 APRIL 1974.

146

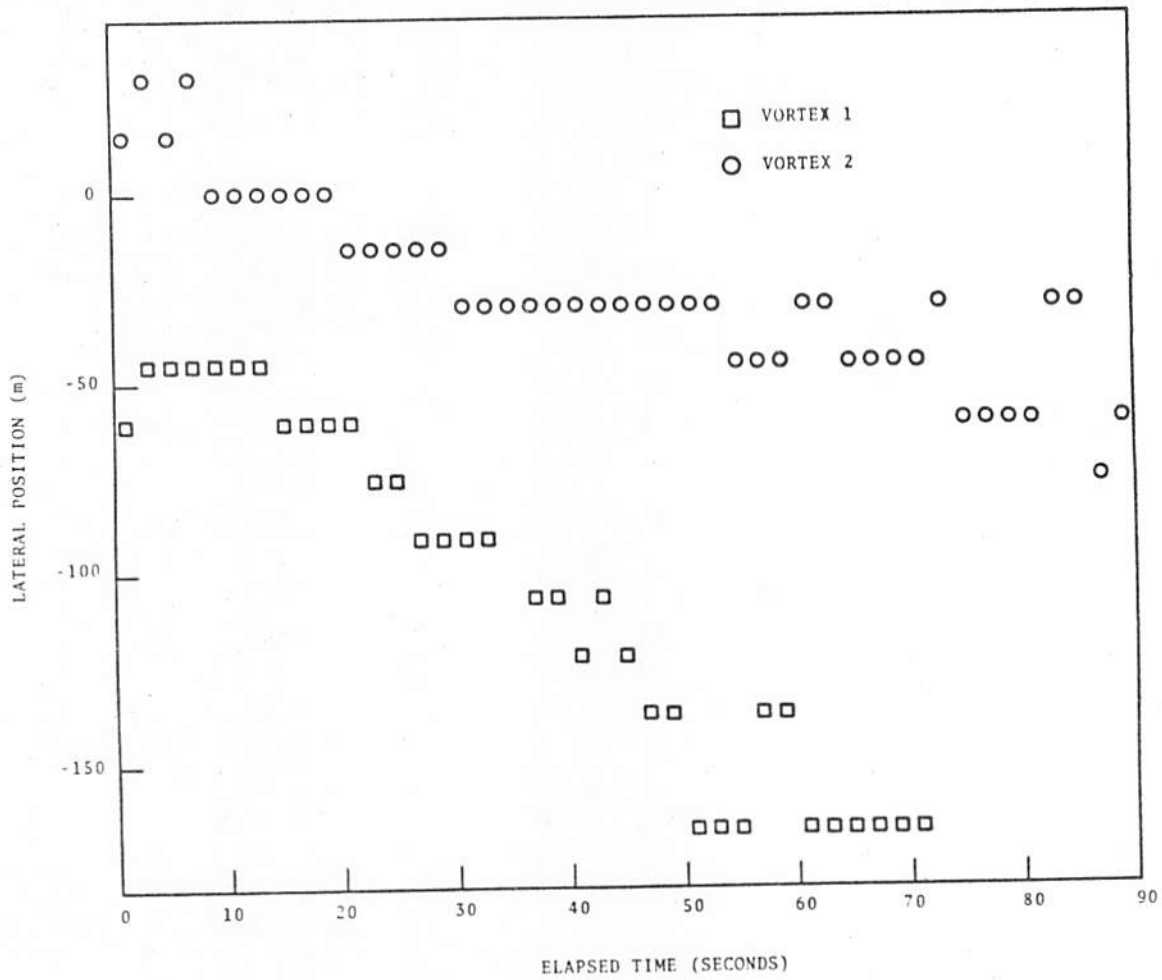

FIGURE 6-3. VORTEX TRACKS FROM THE INNER GWVSS BASELINE AT HEATHROW AIRPORT. THE DATA ARE FROM THE SAME RUN SHOWN IN FIG. 6-2.

147

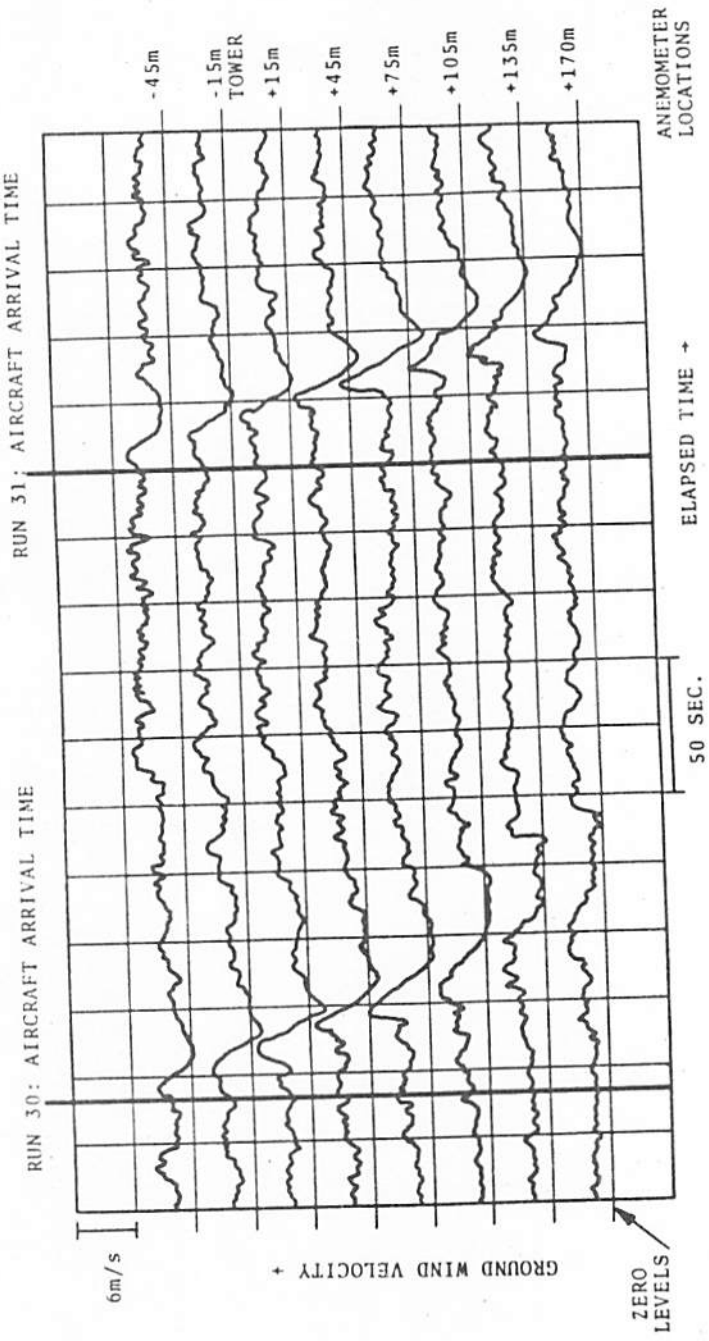

FIGURE 6-4. GWVSS TIME HISTORY DATA FROM A BOEING 747 AIRCRAFT IN HOLDING CONFIGURATION. TWO PASSES FROM THE 17 SEPTEMBER 1972 NAFEC CALIBRATION TESTS ARE SHOWN. DISTANCES ARE WITH RESPECT TO THE INSTRUMENTED TOWER. NOMINAL AIRCRAFT ALTITUDE WAS 60 m, AND LATERAL POSITION WAS - 45m.

148

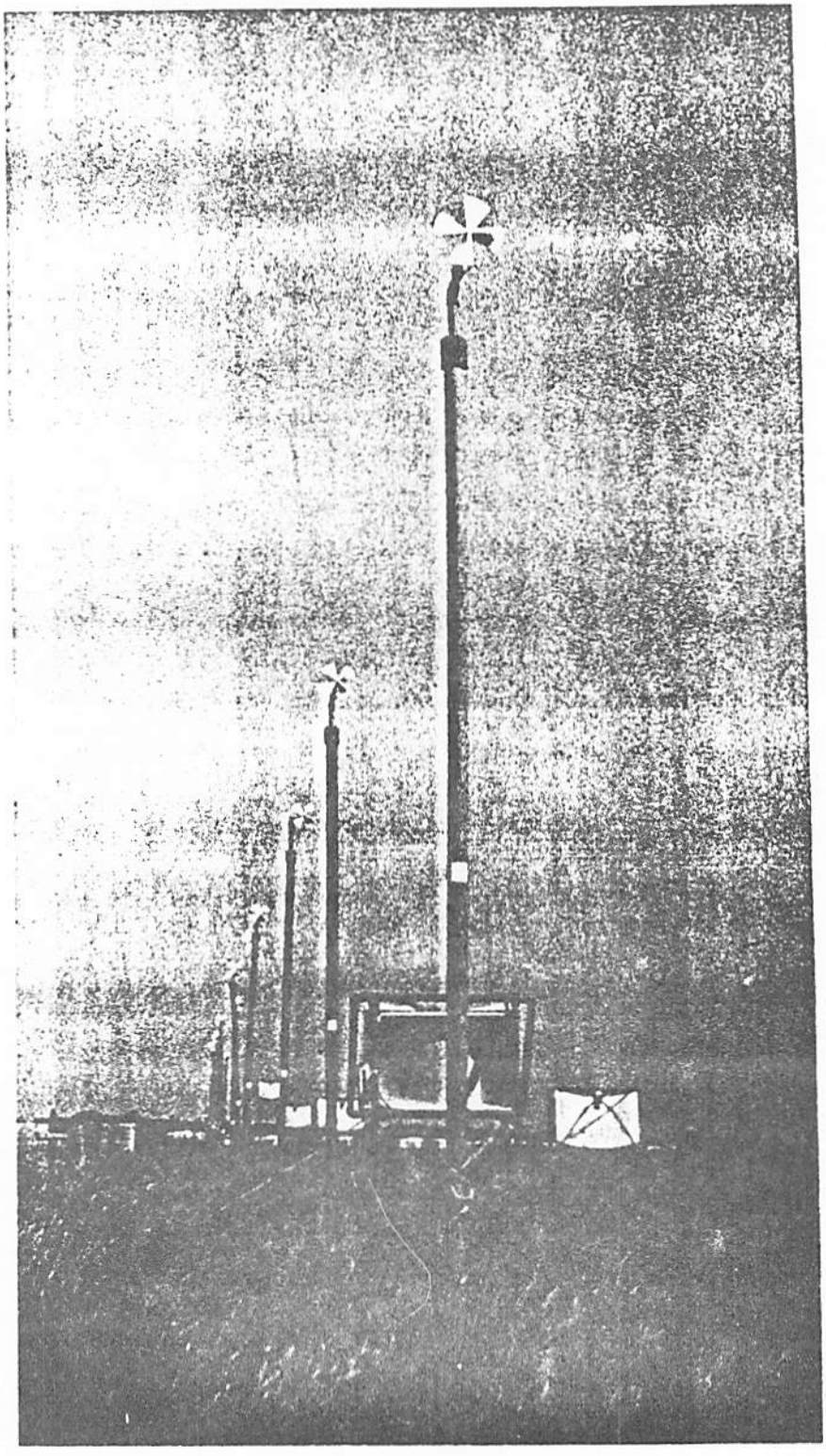

FIGURE 6-5. GWVSS INSTALLATION AT KENNEDY INTERNATIONAL AIRPORT

149

The GWVSS is well established as a reliable technique for obtaining the transverse positions of wake vortices located near the ground. However, the current tracking algorithm makes no use of the magnitude of the vortex signal which could perhaps give some indication of vortex height, z, or strength, Γ. The peak vortex signal from equation (6.1) is $\Gamma/\pi z$ for $h << (x_2-x_1)$. A basic limitation of the GWVSS is that the decrease or disappearance of a vortex signal could be caused by the decay of Γ, and hence a decay in hazard, or to an increase in h which could even increase the hazard to a following aircraft. The data-collection efforts using the GWVSS have usually included another vortex sensor sensitive to height to verify the disappearance of a vortex signal. At present, the boundary-layer effects on GWVSS vortex signatures are not well enough understood to allow the influence of Γ and h to be disentangled from GWVSS data alone.

From July 1976 through September 1977, GWVSS systems were used to collect data from 21,000 vortex pairs on the approaches to runways 14R, 27R, and 32L at O'Hare Airport (ref. J). Figure 6-6 shows the computer printout for runway 32L (on the left side of the figure) and 27R (on the right side of the figure). At each aircraft passage, a header line was printed identifying the runway, the aircraft type, the time code (day:hour:minute:second), the record number, and the sequence number for the respective runway. When two runways were operating simultaneously, the controlling clocks were adjusted so that the header line occupies a 2-second interval with respect to the other sensor line.

Immediately following each header line is a line of reference points (4.3.2.1,etc.) which is repeated every 60 seconds and is a reference for the sensor positions. the sensors are positioned at 50 foot intervals, and each character position corresponds to one of the sensor positions. The integers correspond to the sensor positions in hundreds of feet about the runway centerline.

The detection and tracking of the vortices were performed by comparing the voltage outputs of all of the anemometers in a complete ground wind line. The GWVSS location algorithm defined the position of the port (starboard) vortex to be at the location of the sensor with the lowest

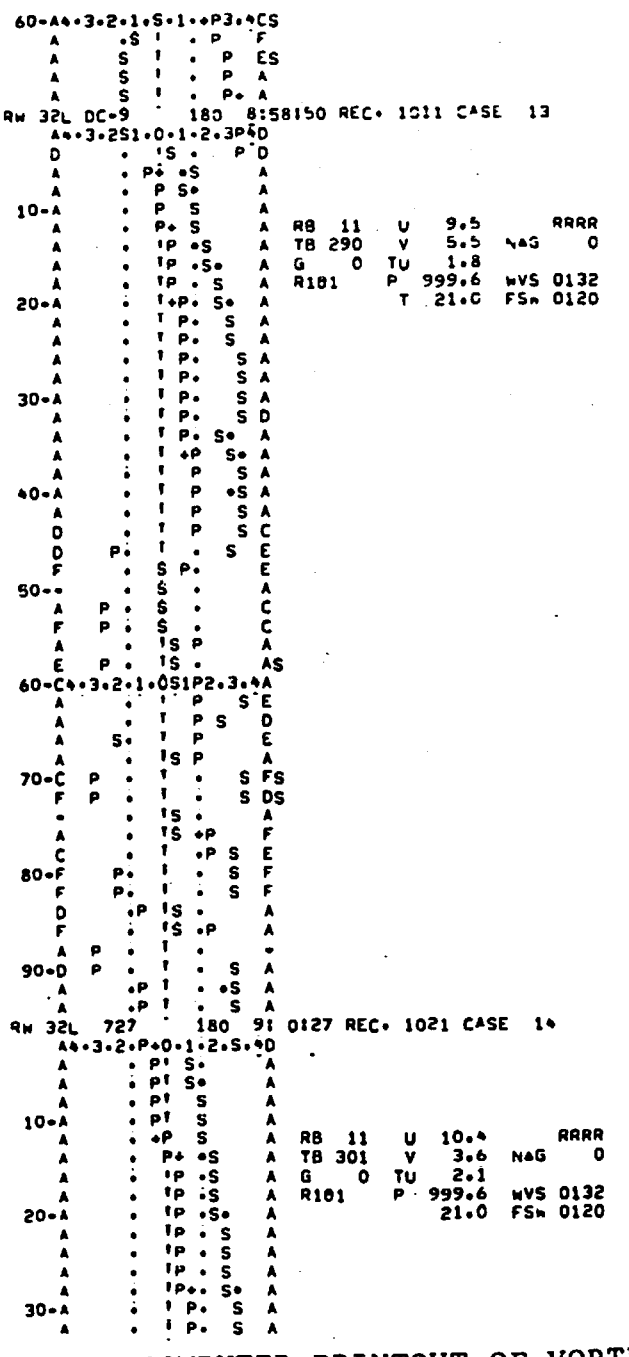

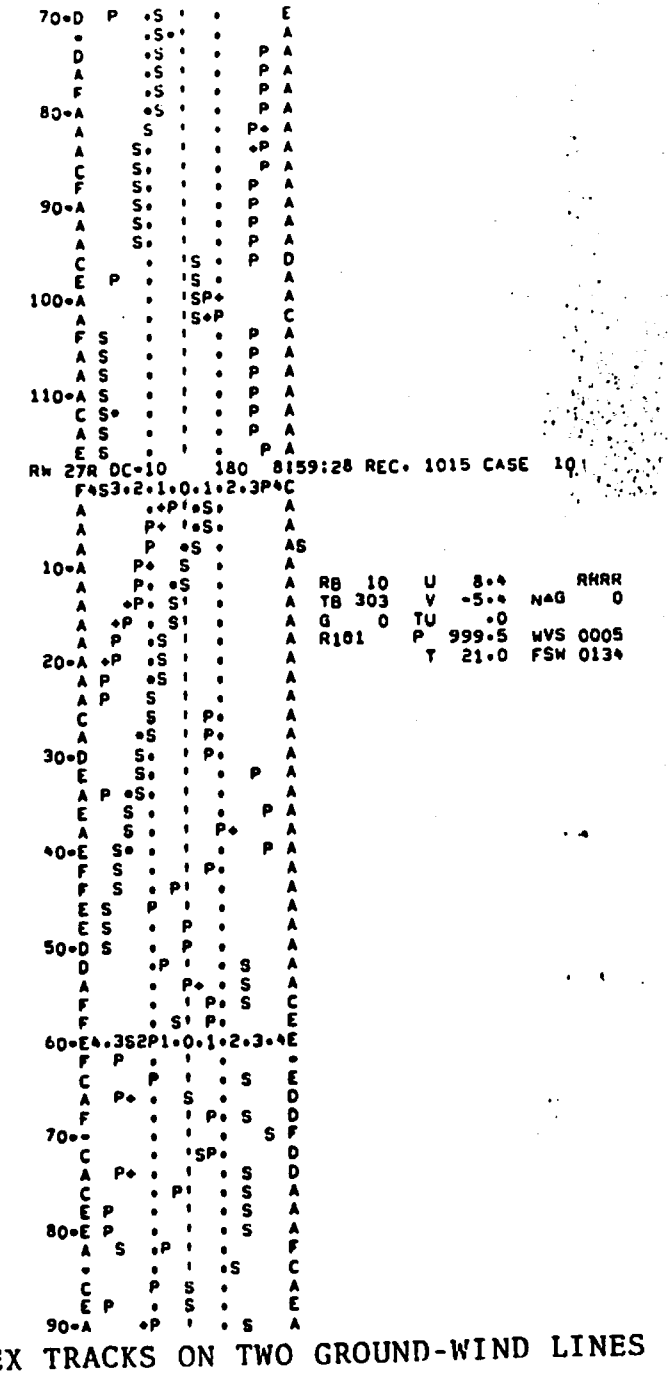

FIGURE ~~17~~. 6-6 COMPUTER PRINTOUT OF VORTEX TRACKS ON TWO GROUND-WIND LINES

(highest) vortage output. The algorithm made the following assumptions: (1) when no vortices were present, the statistics of each anemometer were identical to every other anemometer on a sensor line, (2) random fluctuations of wind were uncorrelated from sensor to sensor, (3) local amplitude deviations of the winds were much faster than the variations of the local wind fields attributed to vortices, and (4) the vortex signatures while transporting through the sensor line were distinctive and limited only by the sample rate.

The data were procesed in groups of eight frames or eight consecutive sets of anemometer outputs corresponding to two seconds of elapsed time. The location assigned to each vortex in a two-second interval was defined as the position of the sensor which was most frequently selected during the interval.

Each track is a time history of the prot and starboard vortices as indicated by the vortex location algorithm. A time axis is listed at 10-second increments immediately to the left of each track. The apostrophes in the center of each track represent the location of the extended runway centerline. The dots to the left and right of the apostrophes represent a ±150-foot vortex protected corridor (cf. Section 3.3.1.1.1). The vortex positions are printed at two-second increments with the port vortex assigned the character "P" and the starboard vortex the character "S". Whenever the indicated vortex location is distributed across two adjacent sensors, a "+" is associated with the port vortex, and a "*" is associated with the starboard vortex.

The alphabetic characters (A, C, D, etc.) running down the page on both sides of the tracks correspond to a validity weighting assigned to the port (left column) and starboard (right column) vortex selected location. The number of times a particular location was chosen during the two-second interval is an estimate of the confidence of the decision and was coded as follows:

Code	Number of Times a Location Chosen During A Two-Second Interval (Eight Samples)
A	8
C	7
D	6
E	5
F	4
-	< 4

When the chosen location contained less than four of the eight samples, a "-" code was listed, and no vortex location was indicated. This validity weighting was used as an aid in the data analysis when a decision must be made as to whether the observed signals truly represented the existence of a vortex or were due to fluctuations in the ambient wind.

6.3.1.2 Pressure Sensors - For the purposes of the discussion, the pressure signature associated with a wake can be represented by the Bernoulli equation (see ref. 84 for a more complete description):

$$\Delta p = -\rho v^2/2 \qquad (6.2)$$

where

Δp = the pressure change,

ρ = the air density, and

v is the magnitude of the air velocity.

In 1971, data were first collected (refs. 86 and 87) on the ground-level pressure and velocity signatures of wake vortices. Since the velocity was measured with a hot-wire anemometer which was not sensitive to direction, the vortex signatures were similar for both sensors. Subsequent work (ref. 88) concentrated on the pressure sensor because of its superior reliability. The first basic difficulty encountered with the simple pressure sensor was its inability to distinguish which vortex was being sensed. Under the conditions of the tests, both vortices gave negative signals, as expected from equation (6.2). The desire to discriminate between the two vortices led to a more complex configuration cosisting of a differential pressure sensor connected to two oppositely directed pitot tubes. This arrangement succeeded in providing opposite polarity signals

for the two vortices, but it also uncovered the fundamental problem of nonlinear response to the vortex winds. Because the air velocity v is a superposition of the vortex and ambient winds, the pressure signature given by equation (6.2) depends strongly on the ambient wind. This dependence was particularly troublesome under conditions where the ambient wind was predominantly perpendicular to the flight path; the vortex which added to the ambient wind usually gave much larger signals than the vortex which subtracted from the ambient wind. At this point in the development, it was concluded that a linear sensor should be used to measure the vortex crosswind signatures, so that the two vortices could be distinguished, and so that the ambient wind would not influence the measurement. The Gill propeller anemometer was found to have the required linear single-axis response and has been used in all GWVSS installations to date.

A vortex-warning detector using a pressure sensor has been proposed by Bedard (unpublished) of the NOAA Wave Propagation Laboratory. The basic concept is to average spatially the ground-level pressure along the direction of flight to reduce random noise while maintaining the response to the spatially coherent vortex. The pressure averaged over a 300-m distance is to be obtained by means of a pipe with periodically spaced leaks to the atmosphere. A complete vortex detector might consist of three such pipes placed on the approach-path centerline and 100 m to either side. Two differential pressure sensors would compare the average pressure in the center pipe to that in the two side pipes. In the absence of a vortex, all three pipes should measure the same pressure with a low noise level since they are exposed to the same averaged ambient wind. However, if a vortex is located near the centerline, both differential sensors will show a non-zero response apart from a few special null conditions which should last for only short periods of time. If both differential responses exceed a threshold, a vortex warning could be issued. The sensor will show a reduced response from a vortex which is skewed with respect to the runway centerline because the vortex is no longer coherent over the full length of the pipe. This feature may actually be desirable for protection against hazardous vortices since a strongly skewed vortex will also not interact coherently with an incoming aircraft. The noise level to be expected from the sensor is uncertain, but it is expected to increase with the square of the ambient wind, and also, to be very sensitive to obstructions such as large buildings or woods which could induce large-scale gradients in the surface wind.

6.3.2 Acoustic Sensors

A variety of acoustic sensors have been developed for the remote sensing of aircraft wake vortices. They all suffer from sensitivity to ambient noise. The major noise sources which limit the performance of acoustic sensors in the airport environment are aircraft operations and meteorological effects such as rain hitting the antenna and wind whistling around the antenna. At the current state of development, no acoustic sensor can be designated as an "all-weather" system.

The capabilities of an acoustic-sensing system are normally limited by the tradeoffs involved in antenna design. Since most sources of ambient noise and spurious reflections are located on the ground, antennas are designed to have low side response. The standard acoustic antenna consists of a transducer and horn at the focus of a parabolic dish. Low side response is achieved by surrounding the antenna with a shield which is covered on the inside with sound-absorbing material to eliminate internal reflections. One should note that mechanically scanned antennas such as used in radars are generally impracticable for acoustic antennas because of limitations posed by the slow speed of sound. Consequently, multiple beam antennas are often used to span an area, and can be constructed simply by using an array of transducers in the same dish. One of the limitations of the horn-dish-shield antenna configuration is that the feasible angular coverage of a single antenna is probably less than 50 degrees. Moreover, as the angular coverage increases, the side response also tends to increase, thus leading to lower signal-to-noise ratios.

One of the critical parameters for acoustic sensors is the frequency of operation. The acoustic absorption of air increases rapidly with frequency, and has a strongly peaked dependence on the absolute humidity (ref. 89). Acoustic absorption serves both to attenuate the desired vortex signals, and also, to reduce the ambient noise from distant sources. Proper selection of the frequency requires a balancing of the relative advantages of high frequency: smaller antennas and less ambient noise; and those of low frequency: longer range for a given signal loss and greater transducer efficiency. One pitfall in frequency selection should be noted. If the frequency chosen for a particular range is just satisfactory under normal

meteorological conditions, the humidity-absorption peak can severely degrade the range capabilities under conditions of low absolute humidity.

6.3.2.1 Active Acoustic Sensors - Sound waves interact with wake vortices via several scattering mechanisms. Turbulent fluctuations in the air cause some of the sound to be scattered in all directions. The scattered signals are Doppler-shifted by the mean velocity of the wind in which the turbulence is imbedded. The change in frequency, Δf, is given by

$$\Delta f = 2f_0(w/c_s) \sin(\theta/2) \qquad (6.3)$$

where f_o = the transmitted frequency,
θ = the scattering angle,
w = the mean velocity component of the wind in the direction bisecting the angle between the transmitted and received beams, and
c_s = the speed of sound.

The angular distribution of the acoustic energy scattered from turbulence depends upon the nature of the associated fluctuations (ref. 90). Figure 6-7 compares the expected scattering cross section for velocity and temperature (density) fluctuations with a Kolmogorov spectral distribution. The cross section decreases rapidly with angle and reaches a null at 90 degrees. An additional null occurs at 180 degrees scattering for velocity fluctuations. The positions of these nulls have influenced the design of Doppler Acoustic Vortex Sensing Systems (DAVSS). Although a bistatic (separated transmitter and receiver) acoustic sensor can respond to both velocity and temperature fluctuations, a monostatic (single location) sensor views 180 degrees scattering which can be produced only by temperature fluctuations. The characteristics of a monostatic acoustic sensor are, therefore, strongly dependent upon the distribution of thermal fluctuations in the wake, which may vary considerably with aircraft engine placement. Because of this uncertainty, the first DAVSS experiments (Refs. 91 and 92) employed bistatic configurations rather than the simpler monostatic configuration which would also provide greater velocity resolution according to equation (6.3).

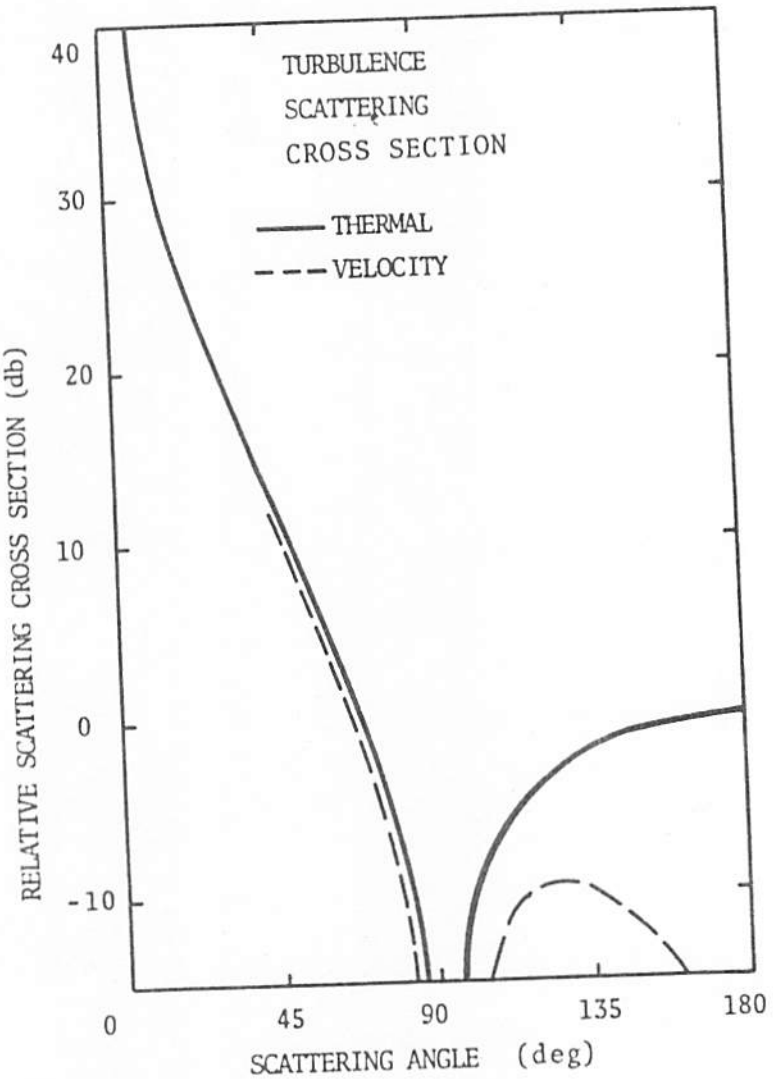

FIGURE 6-7. TURBULENCE-SCATTERING CROSS-SECTION VERSUS SCATTERING ANGLE.

157

Another mechanism for acoustic scattering is the modification of acoustic propagation by the non-fluctuating properties of the vortex. The dominant effect is a deflection or refraction of the sound propagating through the vortex core. The direction of propagation $\bar{n}$ is bent in the direction of vortex rotation according to the vector equation (ref. 93)

$$\frac{d\bar{n}}{ds} = -\bar{n} \times (\bar{\nabla} \times \bar{v}/c_s) \tag{6.4}$$

where s is the distance along the direction of propagation, and $\bar{\nabla} \times \bar{v}$ is the curl of the vortex flow field, is the vorticity which is large only near the vortex core. One can integrate equation (6.4) to obtain the maximum scattering angle

$$\theta_m = \Gamma/\pi c\bar{r} \tag{6.5}$$

where r is mean vortex radius weighted according to the radial variation in vorticity. The approximations leading to equation (6.5) become inaccurate as θ_m approaches 1.0 radian. The aircraft dependence of equation (6.5) lies in the two parameters Γ and r. For aircraft operating with the same coefficient of lift and wing shape (a reasonable approximation for a commercial jet transport), Γ is proportional to the wing span, b. The maximum scattering angle is then inersely proportional to r/b, the relative size of the core with respect to the wing span. A factor-of-three variation in θ_m has been observed (ref. 54) for different types of landing aircraft. The observed variation can be related to the proximity of engine-jet blast to the vortex core during the wake roll-up process (ref. 95). When the jet blast is near the origin of the vortex core (i.e., for aircraft with four wing-mounted engines), the vortex core is enlarged and the resulting maximum scattering angle is smaller than that for aircraft with engines far away from the vortex core (e.g., on the tail). Because of the strong variation in θ_m with aircraft type, a sensing system based on refractive scattering; e.g., the PAVSS, is highly sensitive to aircraft type. It is also incapable of measuring the vortex-wind distribution. Since the scattering is produced coherently by the vortex as a whole, Doppler shifts in the scattered signals characterize only the vortex transport velocity and not the wind velocity within the vortex. The scattering cross secction for refraction is much larger than that for

fluctuation scattering for two reasons. First, the entire incident beam is scattered, not just a fraction of it. Second, the beam is scattered into a plane, rather than a sphere of resultant propagation directons.

The refraction of sound in a vortex is not adequately described by equation (6.4) when the spatial variation in the acoustic propagation medium is significant over a distance of one acoustic wavelength, λ. When a vortex core is comparable in size to λ, it scatters sound in all directions, even at a 180-degree scattering angle.

Spatial resolution in active acoustic sensors is achieved by using narrow angular beams and/or short transmitted pulses. Since two dimensions must be specified to define a point in a plane, three basic configurations are available for resolving vortex location:

a. Two beam angles
b. One beam angle plus one pulse arrival time
c. Two pulse arrival times.

Figure 6-8 illustrates how each of these three configurations can be used to provide bistatic coverage of a plane perpendicular to the aircraft flight path. Each beam angle to be resolved requires a fan of narrow antenna beams. Each time to be resolved requires a wide beam antenna. The roles of transmitting and receiving antennas are interchangeable as far as spatial resolution is concerned. For the monostatic configuration, illustrated in Fig. 6-9, spatial resolution is achieved by range and beam angle measurements.

From the viewpoint of operational use, the monostatic configuration is superior to the bistatic configurations because it can be installed directly under the flight corridor to be monitored where the real estate is normally already available at airport sites. Moreover, the monostatic configuration minimizes the range to the vortex (and hence, the acoustic attenuation), and maximizes the spatial resolution for a given antenna beam width. The specific configuration of Fig. 6-9 is designed for monitoring wake vortices at the middle marker location of the approach corridor (1100 m from the runway threshold) using a maximum range of 100 m.

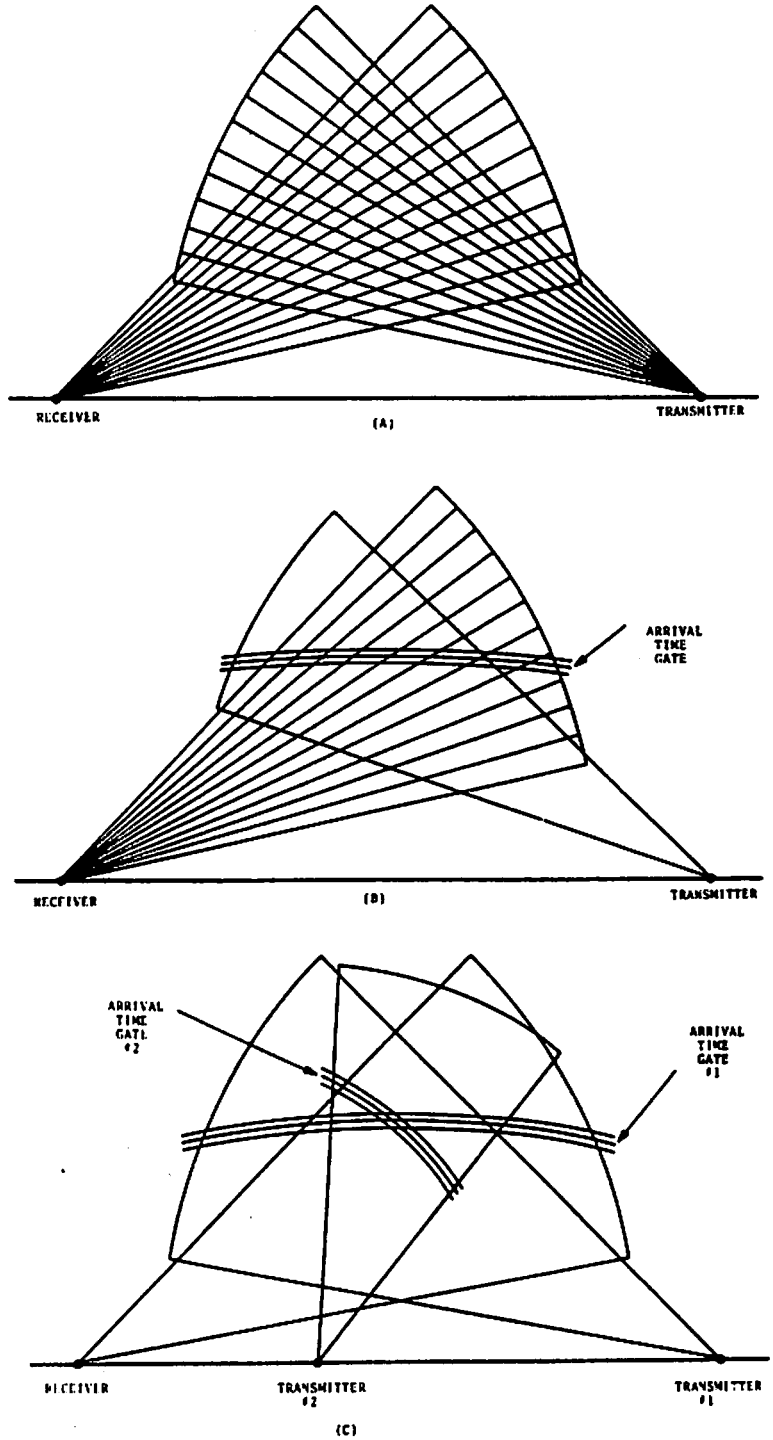

FIGURE 6-9. BISTATIC ACOUTIC SCATTERING CONFIGURATIONS. SPATIAL RESOLUTION IS OBTAINED BY: (A) TWO BEAM ANGLES, (B) ONE BEAM ANGLE AND ONE ARRIVAL TIME, AND (C) TWO ARRIVAL TIMES.

160

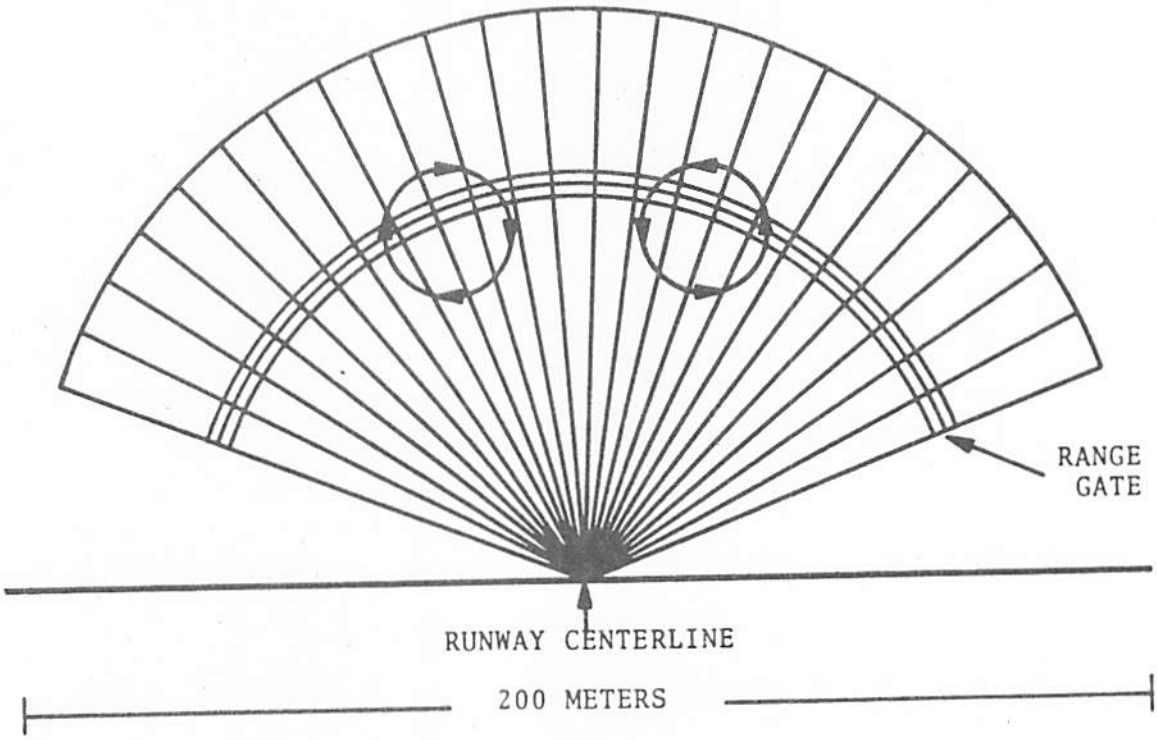

FIGURE 6-9. MONOSTATIC ACOUSTIC SCATTERING CONFIGURATION; VIEW ALONG THE FLIGHT PATH. THE VORTICES ARE SHOWN AT A TYPICAL AIRCRAFT ALTITUDE OVER THE MIDDLE MARKER.

161

6.3.2.2 Doppler Acoustic Vortex Sensing System - The term Doppler Acoustic Vortex Sensing System (DAVSS) does not refer to a particular sensor configuration, but rather to a host of sensor configurations sharing the common feature that the acoustic returns from turbulence within a vortex are spectrally analyzed to yield information on the velocity profile of the vortex. Doppler processing of the turbulence scattering signals is necessary for reliable vortex tracking even if the velocity information is not required. Since the turbulence is distributed throughout the vortex, the vortex center cannot be consistently identified by a maximum in the scattered signal. In fact, under some atmospheric conditions, the scattering from ambient turbulence is so large that even the presence of a vortex cannot be detected by the magnitude of the scattered signals.

The first DAVSS development work was done by the Xonics Corporation. In late 1970 and early 1971, they experimented with Doppler scattering from aircraft vortices at airport test sites. They then carried out two series of flight tests under FAA sponsorship at NAFEC in the fall of 1971 (ref. 91) and the spring of 1972 (ref. 92). Two types of experiments using bistatic configurations were carried out during these tests:

The first involved a detailed comparison of acoustic velocity measurements with those from hot wire anemometers mounted on a 43-m tower. A cw transmitter radiated into a narrow vertical beam near the tower. The scattered signals were received by an antenna with multiple beams which intersected the transmitted beam at various heights. The DAVSS and instrumented tower measurements showed reasonable agreement after suitable corrections were made for the different resolution of the two types of sensor. A model for the Doppler spectra expected from vortex scattering was developed to aid in the interpretation of the DAVSS data. The data from the tower comparison tests were also processed to yield vortex strength.

The second type of experiment was designed to explore the high altitude tracking capabilities of the DAVSS. Both configurations (a) and (b) in Fig. 6-8 were explored. The transmitter consisted of a phased array of

transducers. In configuration (a) eight beams were synthesized by proper phasing. The beams were scanned sequentially, two at a time using two distinct transmitted frequencies. The location of the wake vortices was determined by the beam(s) showing the greatest Doppler spread. Vortices were detected at altitudes as high as 400 m with configuration (a).

Late in 1972, work began on DAVSS monostatic configurations. Work at Xonics led to a demonstration of a monostatic DAVSS designed to track wake vortices in real time (ref. 96). TSC collected some monostatic acoustic wake vortex scattering data during the fall 1972 sensor calibration tests at NAFEC. The success of this simple data collection effort led to the development of the Monostatic Acoustic Vortex Sensing System (MAVSS) for studying the decay of wake vortex strength. The MAVSS is simply a particular DAVSS configuration, but it is discussed as a separate sensor because of its important role in data collection at airports.

In 1973, Avco Corporation built an engineered DAVSS with real time vortex tracking capability and the versatility to operate in any DAVSS configuration. The Avco DAVSS was installed in 1974 at Kennedy International Airport. Four antennas were placed in a bistatic configuration, and four in an incomplete monostatic configuration. Figure 6-10 shows the bistatic Avco DAVSS' configuration designed to monitor the landing glideslope window with two transmitting and two receiving antennas. Depending upon transmitter and frequency selections, it can be operated in the cw or pulsed mode and in the forward- or back-scatter modes. A comparison between the monostatic and bistatic vortex data showed the former to be much more useful because of large Doppler shifts (equation (6.3)), higher spatial resolution, and lower noise levels (because the receiving antennas were elevated farther above the horizon). As a result of these observations, the bistatic baseline was abandoned and the eight antennas were installed together to give the full 24-beam monostatic DAVSS coverage shown in Fig. 6-9. Figure 6-11 shows a photograph of this installation. The need for four 36-degree receiving antennas to sense a plane through the approach corridor is a cumbersome consequence of the previously mentioned angle limitations of horn dish antennas. It is unlikely that fewer than three antennas could span the corridor without a radical change in antenna design. One attempt to simplify the antenna configuration used three

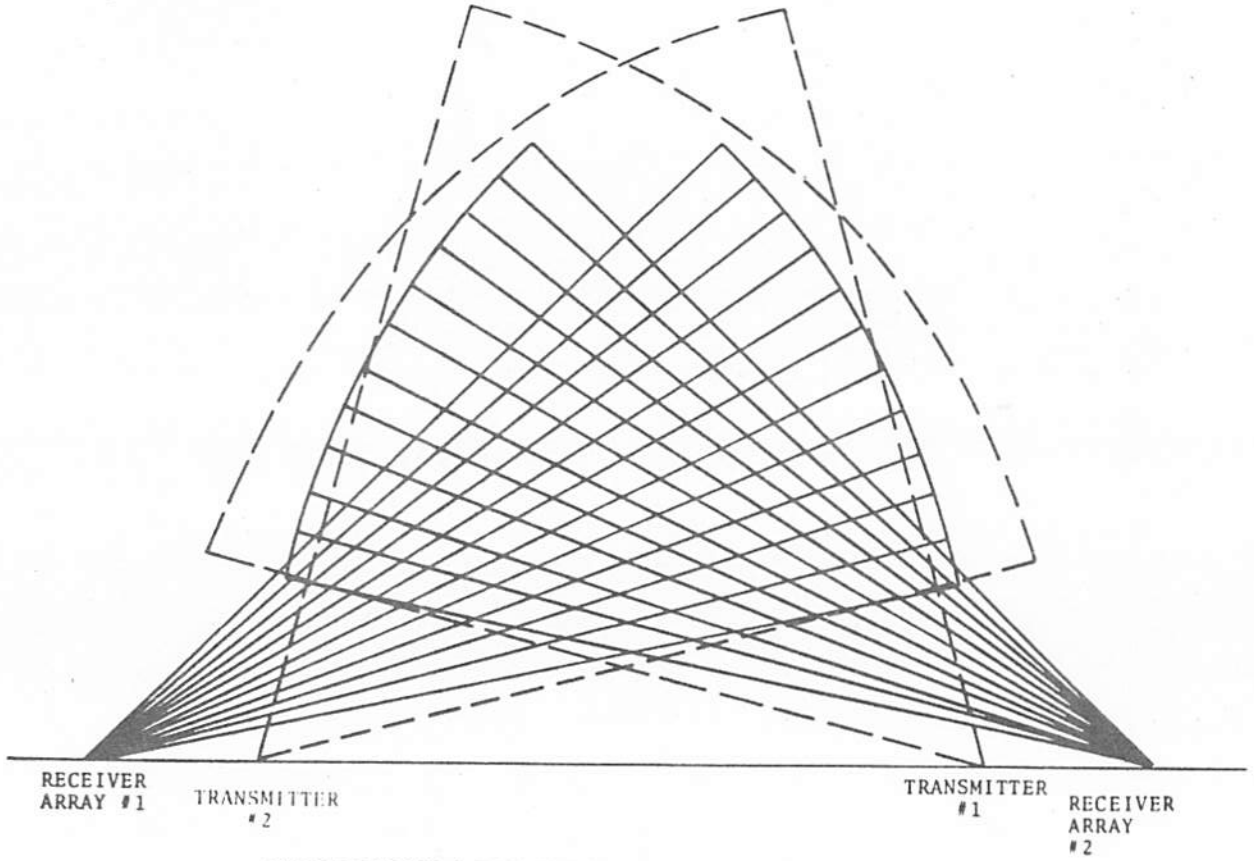

AVCO DOPPLER ACOUSTIC VORTEX SENSING SYSTEM
(DAVSS)

FIGURE 6-10. AVOCO DAVSS BISTATIC CONFIGURATION

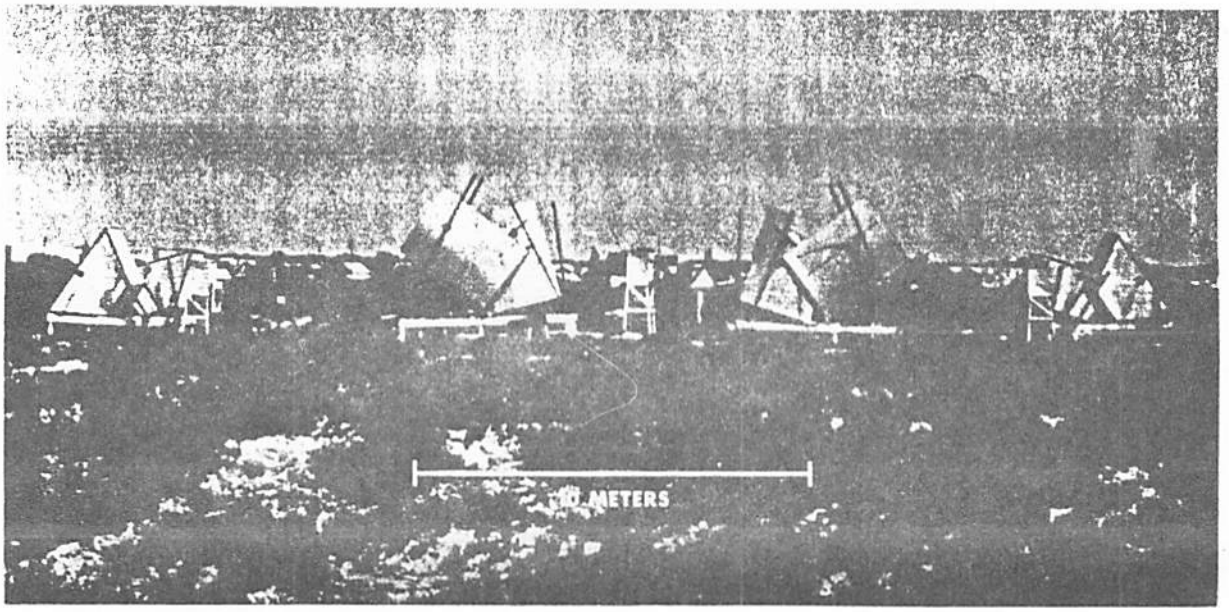

FIGURE 6-16. AVCO DAVSS MONOSTATIC INSTALLATION: VIEW ALONG THE FLIGHT PATH. THE CYLINDRICAL ANTENNAS ARE RECEIVERS WHICH RESOLVE 6 NARROW BEAMS WITH 6 DEGREES SPACING. THE TRAPEZOIDAL ANTENNAS ARE TRANSMITTERS WHICH PRODUCE FAN BEAMS.

165

50-degree fan-beam antennas (one vertical and one tilted to each side) to span the whole corridor. It was found that the tilted antennas had too much response to surface noise sources to give satisfactory performance.

In the Avco DAVSS, the received signals go to a computerized processor which produces real time displays and digital records of vortex locations. The processor simultaneously analyzes the signals from 24 receiver beams using a 6-frequency comb filter to characterize the Doppler spectrum of each signal. The spectral characteristics feed into a search algorithm which locates any vortices in the field of the antennas and determines their sense of rotation. The current algorithm also provides a crude estimate of vortex strength. Figure 6-12 shows some vortex tracks produced by the Avco DAVSS. The lateral position and altitude of the port and starboard vortices are plotted as a function of time after aircraft passage. In this run, the vortices are seen to drop toward the ground and separate as predicted by the classical theory in the case of a small crosswind. The port vortex drifts our of the sensor view, but the starboard vortex remains within the sensitive area until it dissipates.

6.3.2.3 Monostatic Acoustic Vortex Sensing System - The MAVSS antenna configuration illustrated in Fig. 6-13 was originally conceived as a simple test for studying the 180-degree acoustic-scattering properties of wake vortices. The Doppler shifts in this configuration depend only upon the vertical component of the wind in the sensitive volume. The test data showed scattered signals large enough to allow accurate measurement of the vertical wind profile of the aircraft wake (see Fig. 6-14). In fact, the analysis of the test data proved the simple MAVSS configuration to be a promising technique for studying vortex strength.

The MAVSS configuration is superior to the more complex DAVSS configurations for vortex measurement studies because the vortex measurements are not contaminated by the ambient wind which has little vertical component. Moreover, the simplicity of the MAVSS configuration allows a whole array of MAVSS antennas to be processed with the same effort required for a single DAVSS configuration. For example, the DAVSS NAFEC tower comparison tests gave vortex strength information similar to that from the MAVSS but required Doppler processing of twelve signals instead of one.

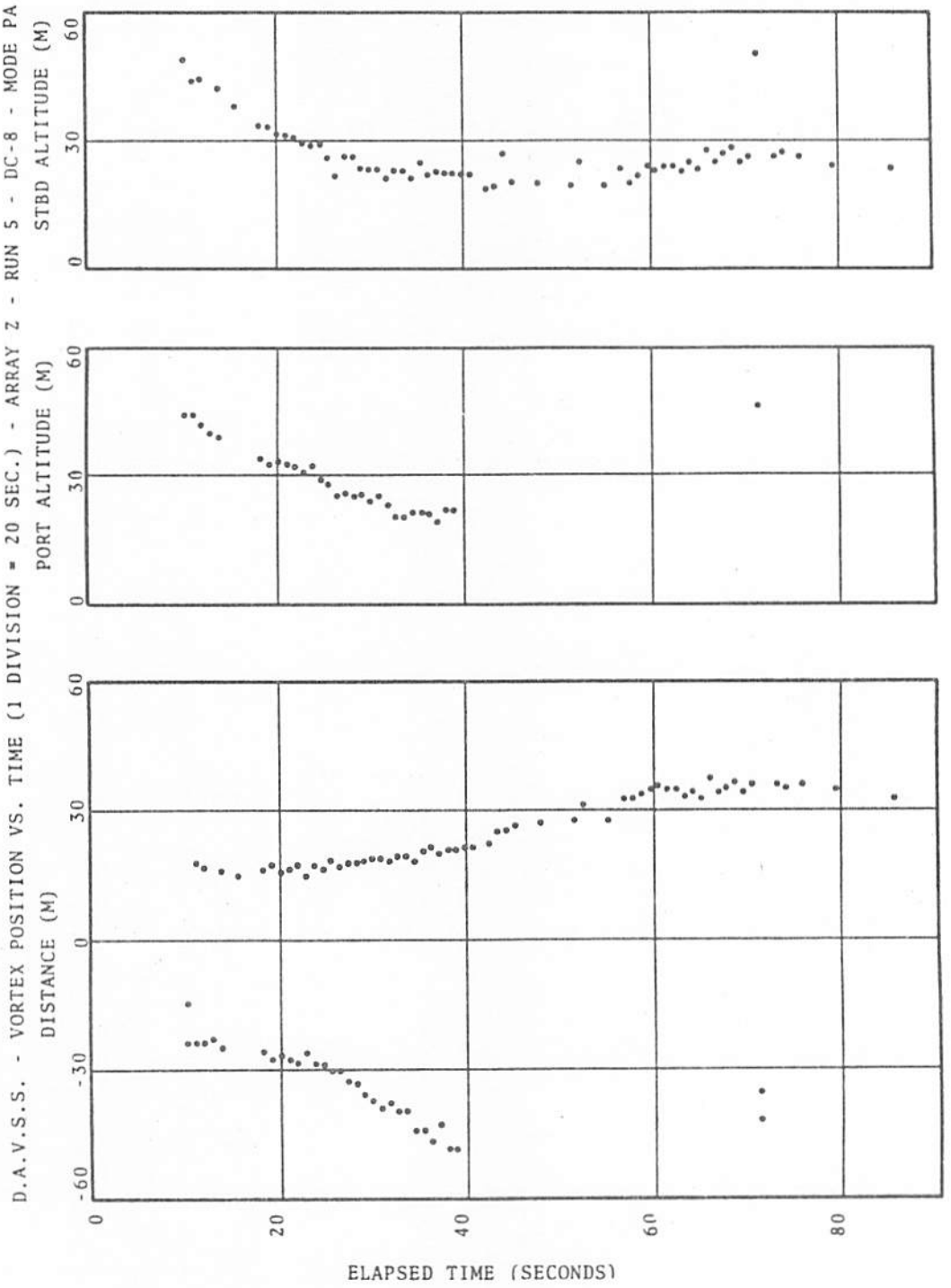

FIGURE 6-12. MONOSTATIC DAVSS VORTEX TRACKS, KENNEDY AIRPORT, RUNWAY 31R, DC-8 AIRCRAFT.

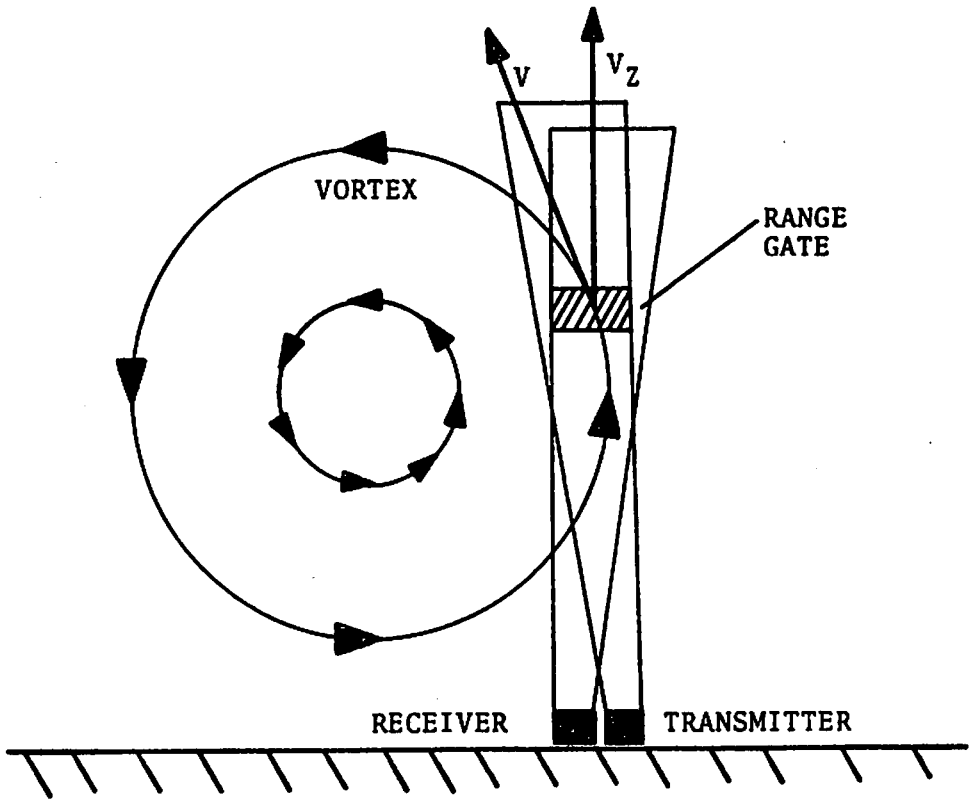

FIGURE 6-13. NARROW BEAM MONOSTATIC ACOUSTIC SENSOR.

168

The choice between the MAVSS and DAVSS configurations for data collection on vortex decay poses a dilemma. Since vortices are likely to drift laterally under most meteorological conditions, a MAVSS array laid out perpendicular to the flight path will usually give a more complete history of vortex decay than a single DAVSS located under the flight path. Unfortunately, a MAVSS array cannot measure the decay of vortices which do not drift at a significant speed. Since the primary wake vortex hazard is produced by the infrequent vortices which stall near the flight path, one is left with the difficult data collection question of collecting much data on vortices which are not in dangerous locations, or collecting skimpy data on vortices which remain in dangerous locations. An understanding of the influence of vortex motion on vortex decay is needed to resolve the dilemma.

The analysis of MAVSS data to yield vortex strength starts with the vertical velocity profile such as that shown in Fig. 6-14 for a B-707 aircraft. In the figure, the velocity at each range gate is plotted as a function of time after aircraft passage. The arrival times of the two wake vortices over the antenna can be located by the rapid reversal in the direction of the vertical wind. The vertical wind is negative between the vortices as one would expect. The height of a vortex is indicated by the range gate with the largest velocities. If one can estimate the transport velocity of the vortex past the antenna, the time data of Fig. 6-14 can be converted to a spatial picture under the assumption that the vortex decay is negligible during the time of passage. Figure 6-15 shows the results of such a transformation for the range gates where the vortex core is located. In this case, the range gate velocity is a direct measurement of the vortex tangential velocity averaged over the beam angle and range-gate resolution of the system.

The tangential velocity $v(r)$, where r is the vortex radius, completely describes a vortex which is axially symmetric. Other useful parameters can be derived from $v(r)$. The vortex circulation $\Gamma(r)$ is defined by

$$\Gamma(r) = 2\pi r v(r) \tag{6.6}$$

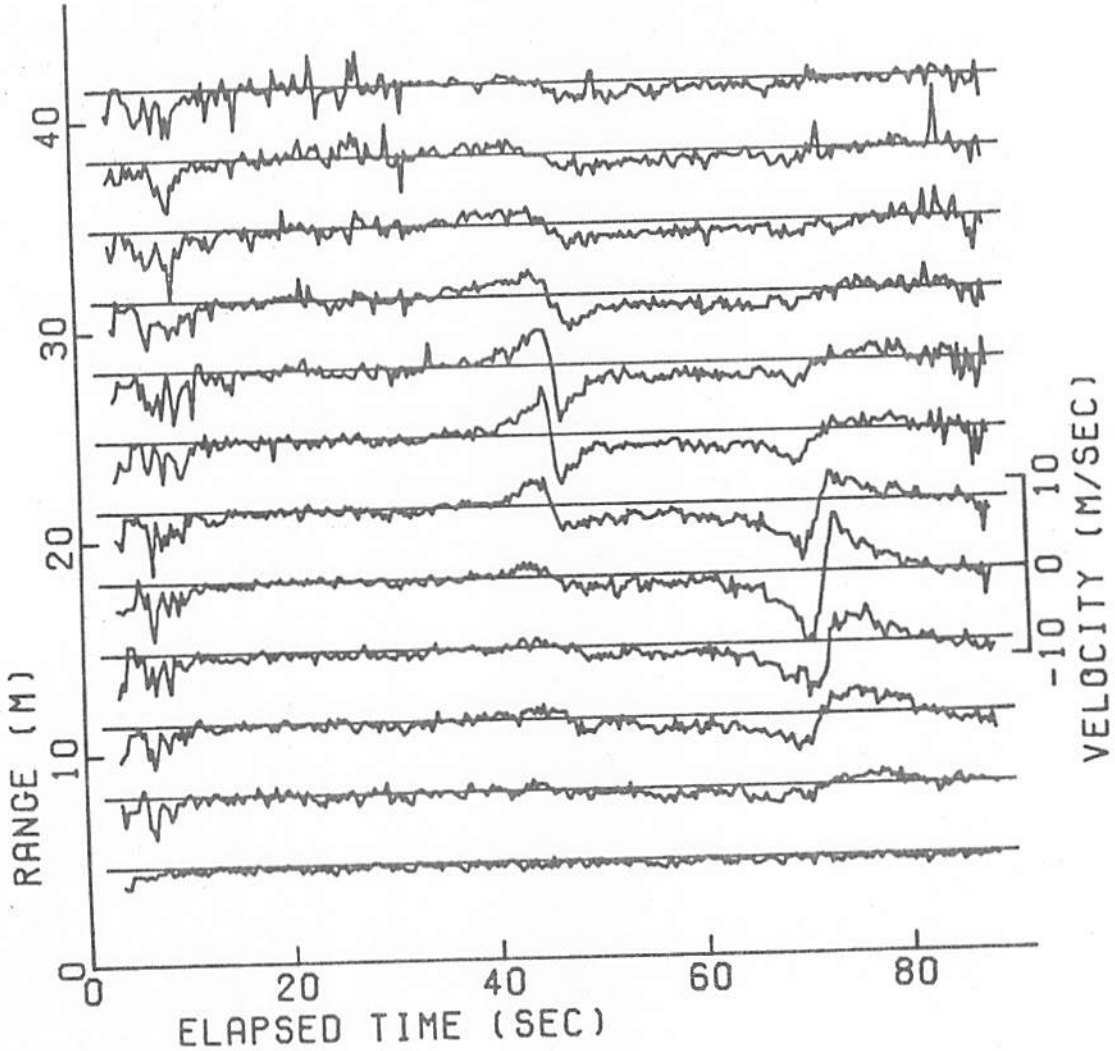

FIGURE 6-14. MAVSS WAKE VELOCITY PROFILE. B707 AIRCRAFT LANDING ON RUNWAY 31 R, KENNEDY AIRPORT, AT 1508 HOURS ON 13 NOVEMBER 1973. NOTE THE VORTEX ARRIVALS AT 46 AND 72 SECONDS. THE MAVSS ANTENNA WAS LOCATED 183 m FROM THE RUNWAY CENTERLINE.

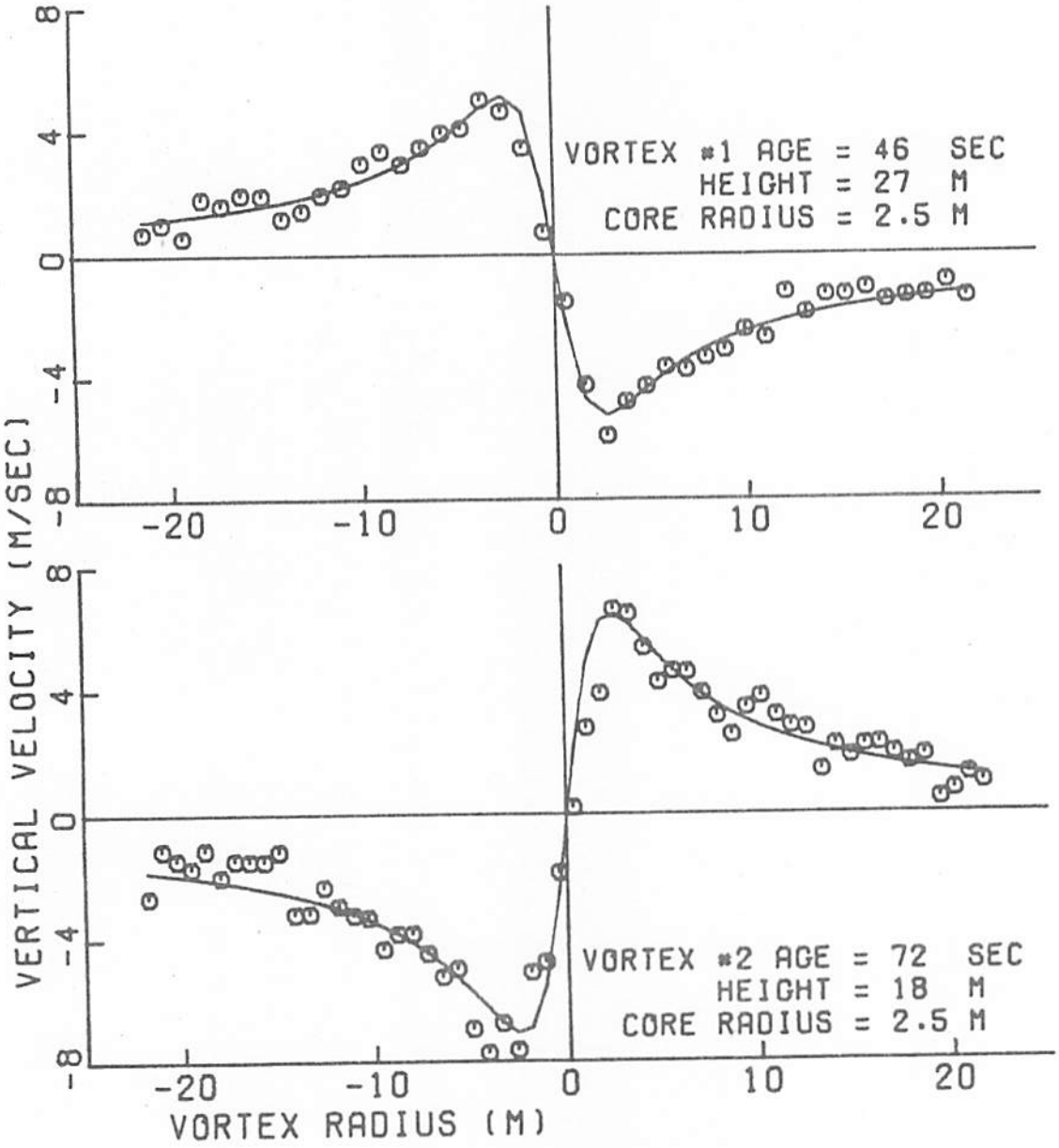

FIGURE 6-15. EXPANDED SCALE PLOTS OF THE DATA IN FIG. 6-13. THE VELOCITY IN THE RANGE GATE CONTAINING THE VORTEX CORE IS PLOTTED AGAINST DISTANCE FROM THE VORTEX CENTER FOR EACH VORTEX. THE SOLID LINES ARE THE RESULT OF A TWO-PARAMETER FIT TO THE CIRCULATION DATA IN FIG. 6-15.

Figure 6-16 shows the radial dependence of the circulation for the velocity data in Fig. 6-15. The circulation values for positive and negative radius are averaged to eliminate some sources of bias. The solid lines in Fig. 6-16 are a weighted least-squares fit to the data of the two parameter form:

$$\Gamma(r) = \frac{\Gamma}{1 + (r/r_c)^2} \tag{6.7}$$

where Γ = the circulation for infinite radius (also defined as the vortex strength), and

r_c = the vortex core radius.

This simple vortex model generally fits the MAVSS data reasonably well, and it has the virtue that r_c is both the radius of maximum velocity (equation 6.6) and of half-circulation ($\Gamma(r_c) = \Gamma/2$). The value of r_c obtained in the data-fitting is not necessarily related to the actual core radius. Only if the core radius is larger than the antenna beamwidth can one assign a physical significance to r_c. The vortex tangential velocity data can also be used to calculate the maximum rolling moment on a wing of span b centered in the vortex. The rolling moment can be shown to be proportional to

$$\Gamma'(b) = \frac{2}{b}\int_0^{b/2}\Gamma(r)\,dr \tag{6.8}$$

the average circulation up to radius 1/2 b. The value of $\Gamma'(b)$ approaches Γ as the span increases. The techniques of vortex parameterization discussed here assume that the vortex is isolated. The assumption is reasonable for old vortices which have had time to separate, but it leads to errors for fresh vortices which are still close together. (See Section 8.2.2.)

The measurement of wake vortex decay with the MAVSS uses an array of antennas which sequentially probe the vortices as they drift past. Figures 6-17 and 6-18 show some MAVSS data obtained from a four-antenna array. The vortex tracks in Fig. 6-17 are determined by the arrival time and altitude at each antenna. The time variations in the vortex parameters strength,

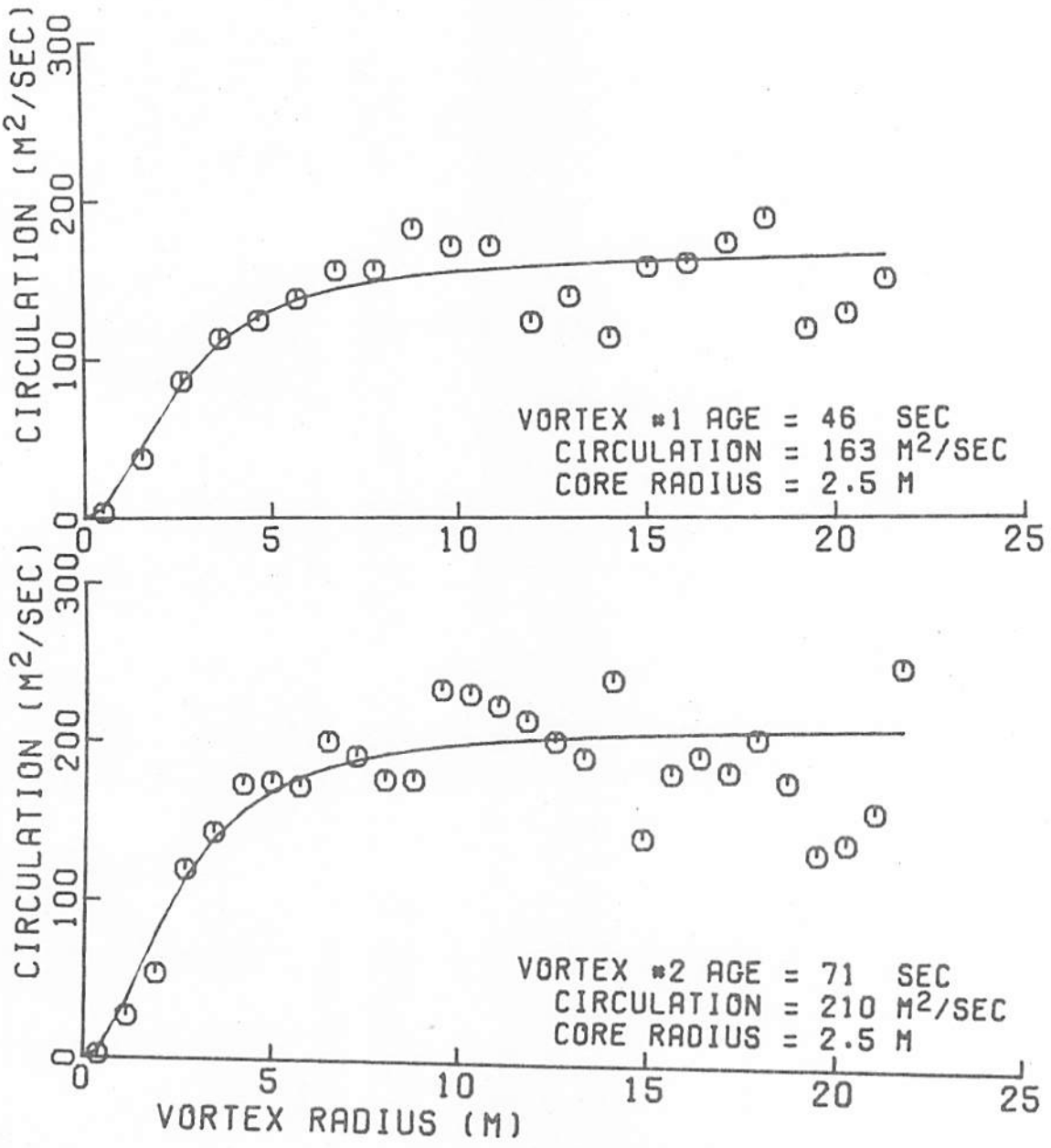

FIGURE 6-16. CIRCULATION VERSUS RADIUS FOR THE DATA IN FIG. 6-14.

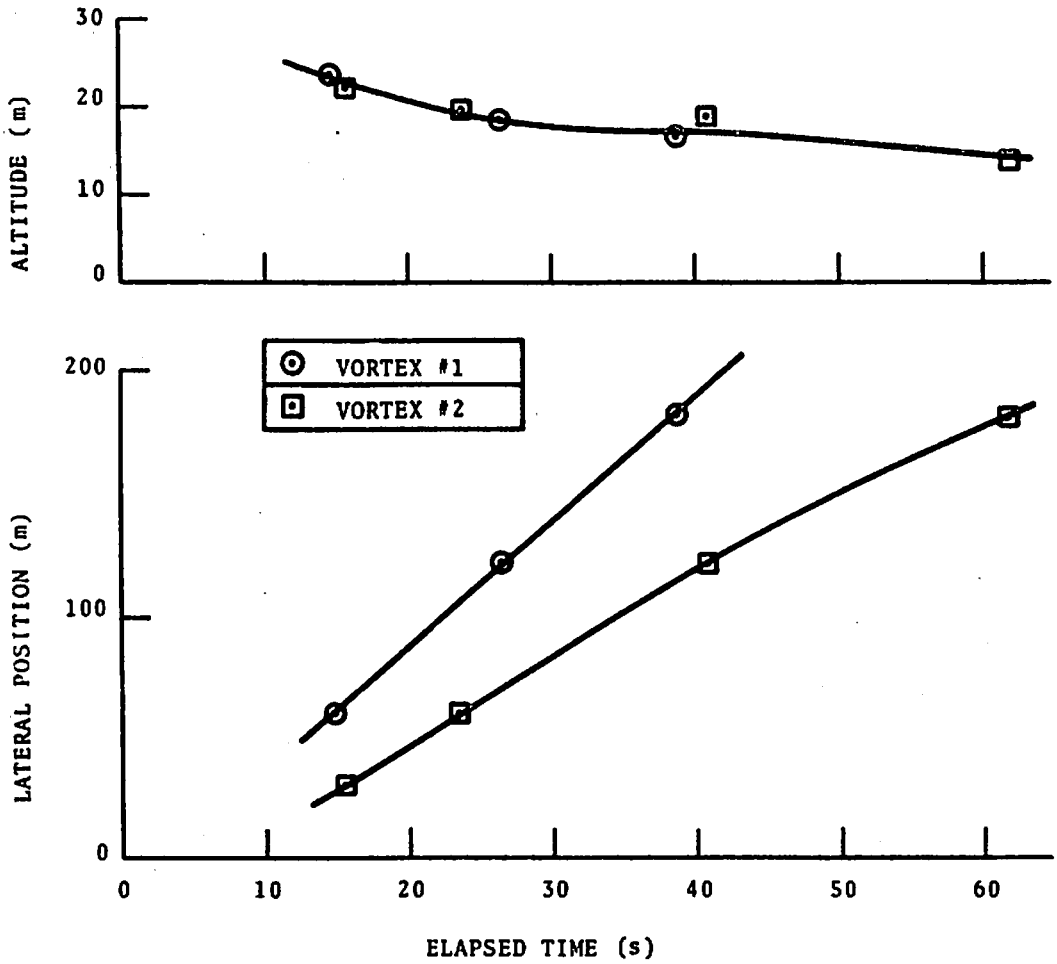

FIGURE 6-16. MAVSS VORTEX TRACKS: DC-8 AIRCRAFT, KENNEDY AIRPORT RUNWAY 31R, 1 JULY 1974 AT 1153 HOURS.

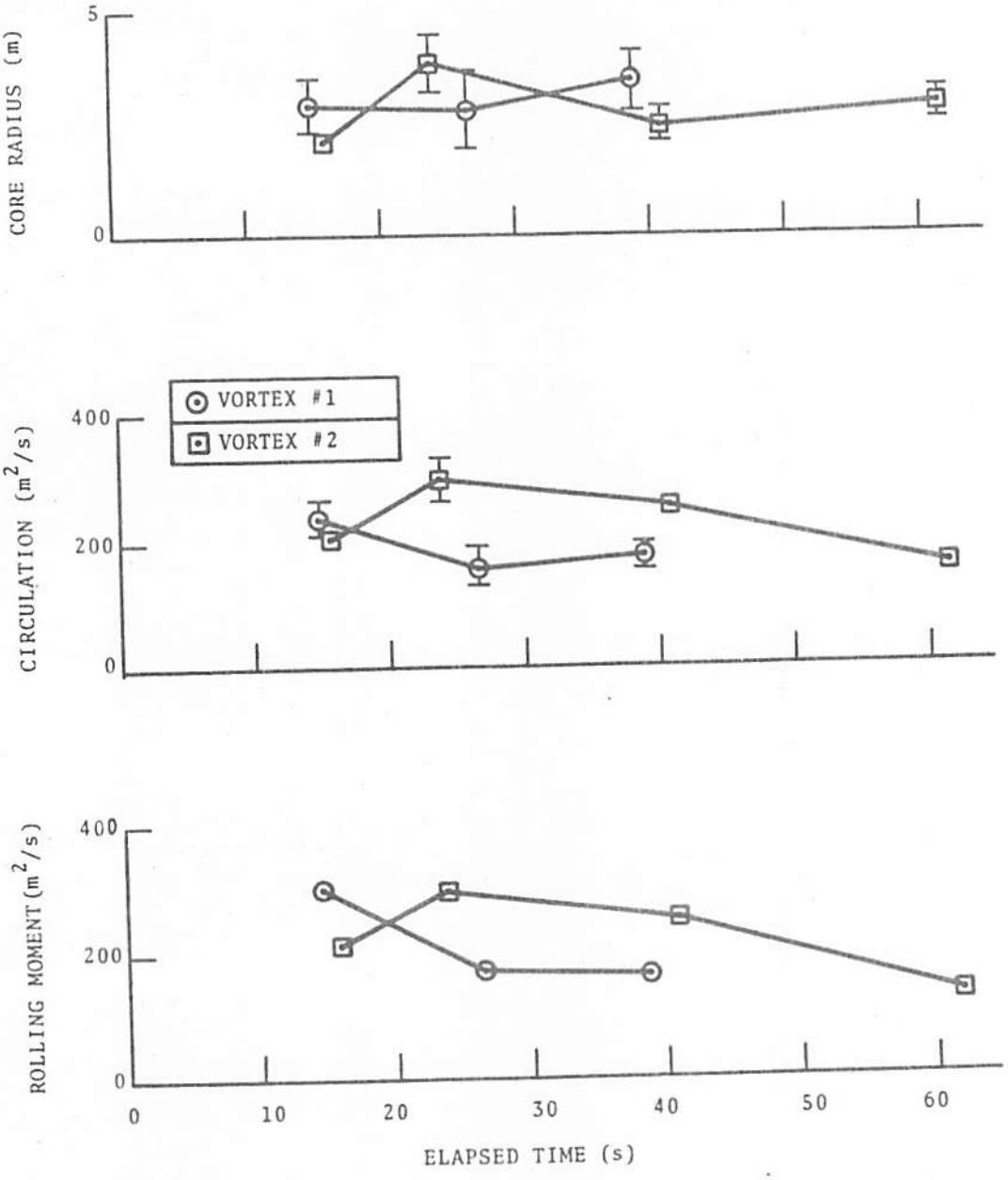

FIGURE 6-17. MAVSS VORTEX PARAMETERS VERSUS TIME FOR THE SAME RUN AS FIGURE 6-16. THE CORE RADIUS AND CIRCULATION ARE THE RESULT OF A WEIGHTED LEAST-SQUARES FIT; THE ERROR BARS INDICATE THE GOODNESS OF THE FIT. THE ROLLING MOMENT PLOTTED IS THE AVERAGE CIRCULATION Γ' FOR A WING SPAN OF 60 m.

Γ, core radius, r_c, and rolling moment Γ (b = 60 m) are shown in Fig. 6-18. The values of Γ' and Γ tend to agree for the large span b = 60 m. It should be noted, that the measurements for short times are less accurate because of interference from the other vortex, aircraft noise, and poorer estimates of the transport velocity.

The MAVSS configuration is essentially a meteorological acoustic sounder modified for wake vortex studies which require shorter ranges and higher resolution. Separate transmitting and receiving antennas, shown in Fig. 6-19, eliminate antenna-ringing which could obscure low-altitude returns up to perhaps 15 m. Each antenna consists of a 1.2-m square dish (0.8-m focal length) and a horn-driver transducer surrounded by the acoustic shield which can be seen in Fig. 6-19. A transmitted carrier near 3-Khz frequency is modulated by a 20-msec pulse (3.5-m resolution) with a smooth envelope to minimize the intrinsic frequency spread. The return signals are recorded and subsequently analyzed with a real-time spectrum analyzer. The mean frequency of the power spectrum is used in equation (6.3) to give the vertical velocity. The deviation of the spectrum about the mean is also calculated to indicate the reliability of the velocity measurement which can be degraded by noise and by strong velocity gradients. The rms deviation of the spectrum from the mean corresponds to about 1.2 m/sec for good data. In the absence of vortices, the pulse-to-pulse standard deviation in mean velocity is typically less than 0.6 m/sec.

Between July 1976 and September 1977, TSC collected data at Chicago's O'Hare Airport on the decay of wake vortex strength using the MAVSS as the primary measurement instrument. The results are presented in refs. S, T, and L. Reference S describes the MAVSS principles of operation, the hardware developed, and the data reduction methods employed. Reference T describes the analysis of MAVSS data to examine whether landing B-707 and DC-8 aircraft need to remain divided into Heavy and Large categories on the basis of the wake vortex hazard. Reference L describes the statistical methods used to understand wake vortex decay as well as a statistical presentation on vortex demise on all common jet trnasport aircraft. The statistical data presented in Section 3.4.5 in this document are taken from the MAVSS data presented in ref. L.

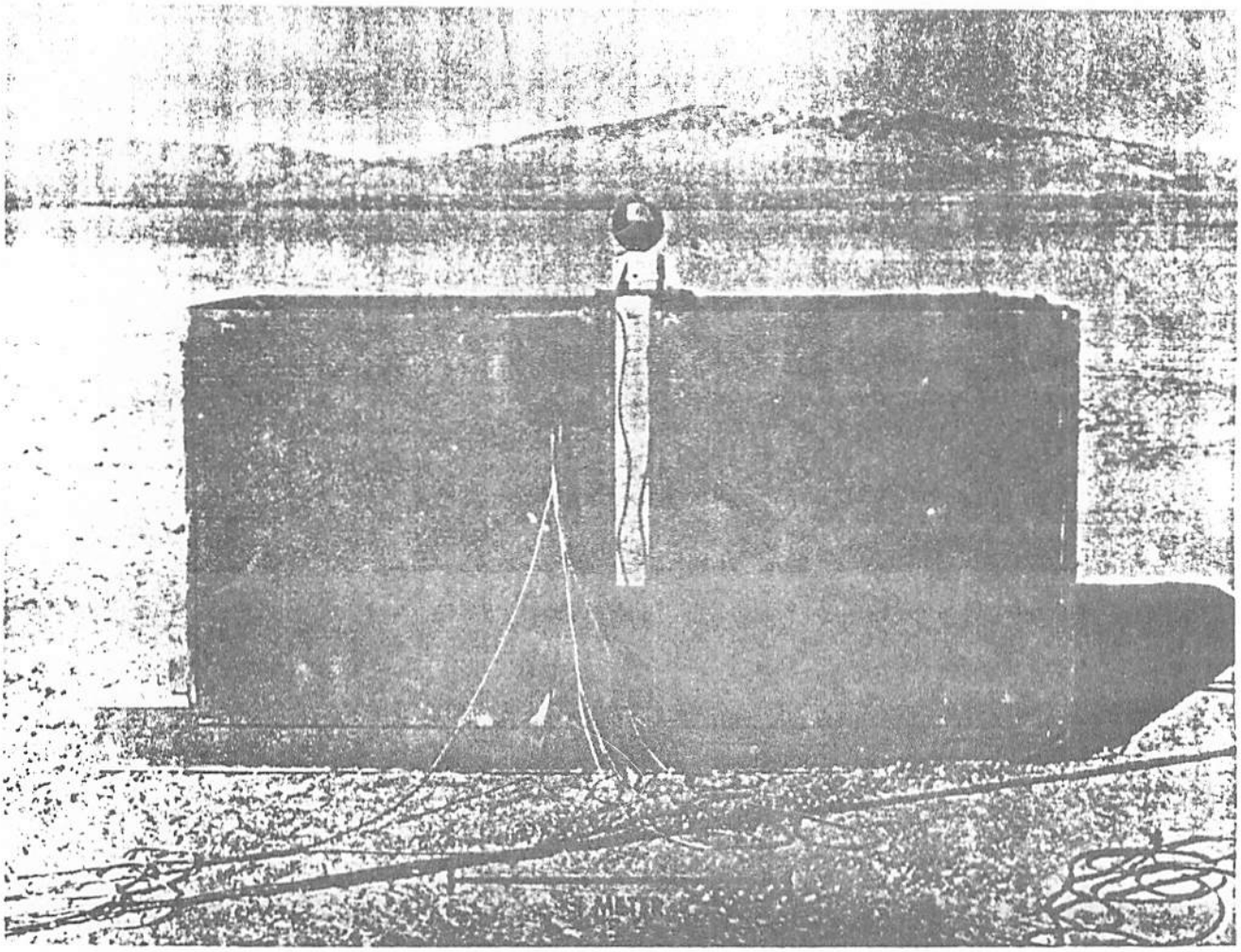

177

FIGURE 6-19. MAVSS ANTENNA

6.3.2.4 Pulsed Acoustic Vortex Sensing System - The Pulsed Acoustic Vortex Sensing System (PAVSS) makes use of refractive scattering to locate a wake vortex by means of time delays. The first refractive signals from aircraft wake vortices were observed in the winter of 1971 (ref. 97). In the spring of 1971, the basic PAVSS tracking system shown in Fig. 6-20 was tested. This configuration is essentially a forwardscattering version of that shown in Fig. 6-7c. The sensitive area is scanned by one wide fan-beam transmitter and two wide fan-beam receivers. The antenna response extends down to the horizon, so that two signals are received, one directly along the ground and one scattered from the vortex. Since refractive scattering is produced by a bending of the propagation path in the direction of vortex rotation, only one of the two vortices will be seen by a particular transmitter-receiver pair (see Fig. 6-20).

Figure 6-21 shows a picture of PAVSS signals received from one receiver in Fig. 6-20. The CRT intensity indicates the received acoustic intensity. The picture is scanned rapidly in the vertical direction in synchronization with the transmitter pulses (5 msec long with a 60 msec period). A slow horizontal scan gives the dependence of the signals as a function of the time after aircraft passage. The direct signal appears as a horizontal band near the bottom of the picture. The vortex signal is vertically displaced (delayed) with respect to the direct signal by an amount which depends upon the vortex location, and hence, varies with time. The time delay in arrival of the scattered signal determines that the vortex lies on an ellipse with foci at the transmitter and receiver. The exact vortex location can then be determined by the intersection of ellipses from two different transmitter-receiver pairs (see Fig. 6-22).

Comparisons with the NAFEC tower in the summer of 1971 (ref. 86) showed that the PAVSS gave reasonably accurate vortex locations. The PAVSS was then developed to its final configuration by the winter of 1972 (ref. 88). Frequencies in the 2 to 3 kHz range and pulse widths of 2 to 3 msec are used. Three antennas are placed on either side of the runway centerline. Each alternately transmits and receives, so that both vortices can be detected. The multiplicity of antennas is needed to give the desired spatial coverage while maintaining reasonable location accuracy. The tracking limitations of the PAVSS are discussed below.

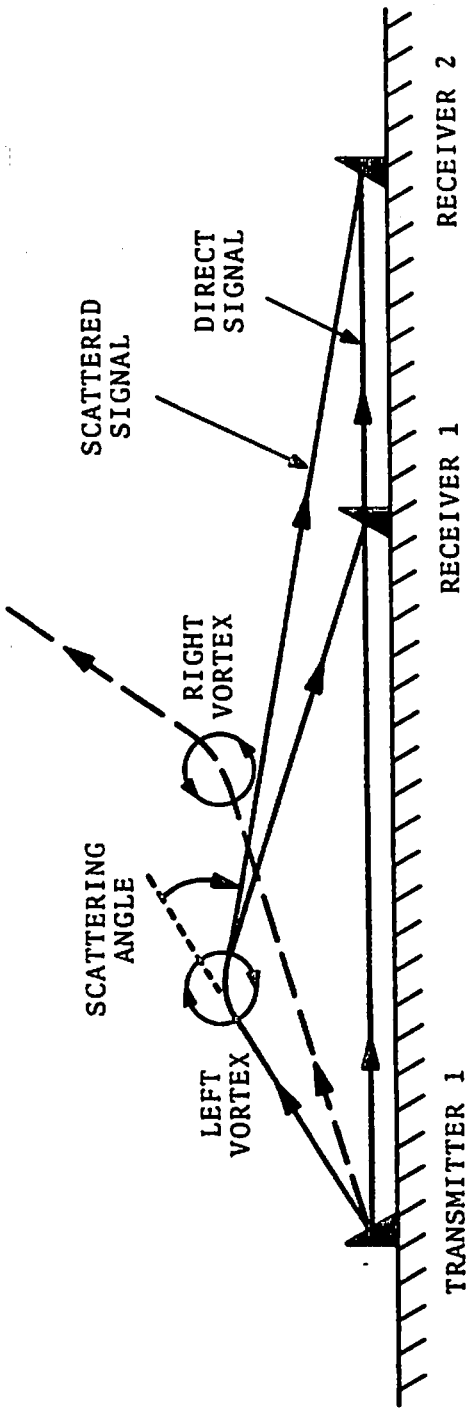

FIGURE 6-~~19~~ 20. SIMPLE PAVSS CONFIGURATION. NOTE: THE RIGHT VORTEX SCATTERS SOUND AWAY FROM THE GROUND AND WILL NOT BE DETECTED.

179

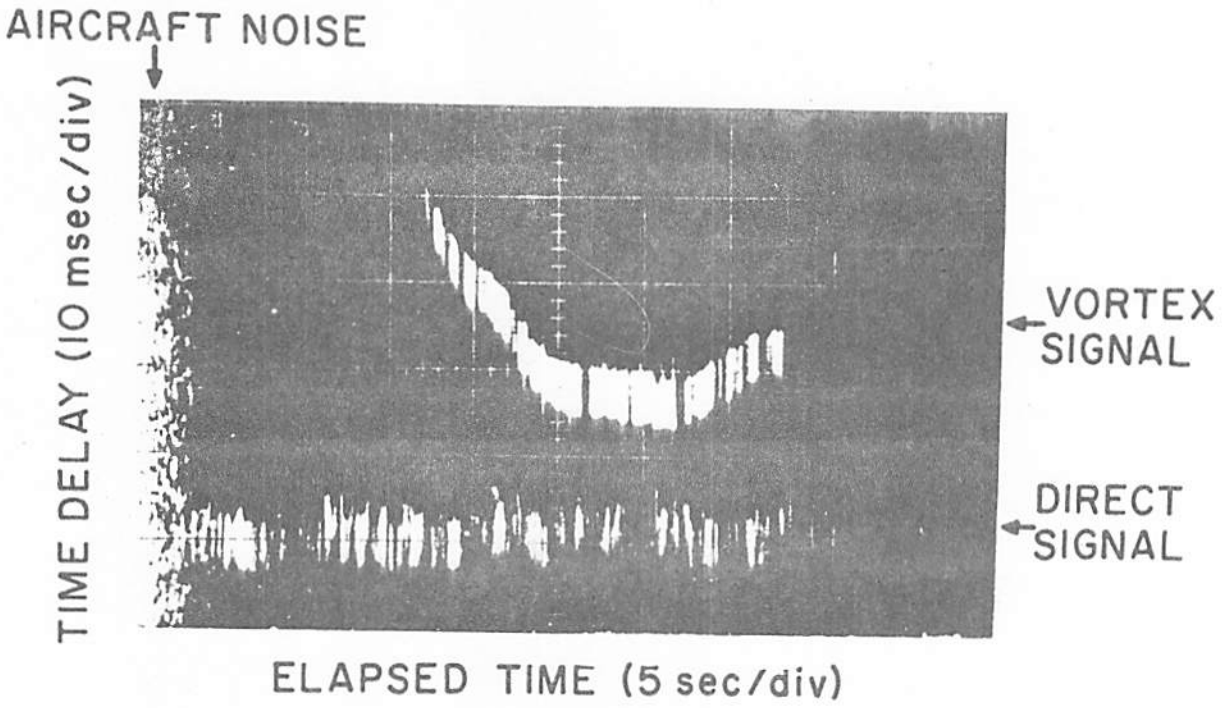

FIGURE 6-~~20~~ 21. PAVSS SIGNALS FOR A B-747 AIRCRAFT LANDING ON RUNWAY 22L, LOGAN AIRPORT, 3 JUNE 1971. TRANSMITTER-RECEIVER SEPARATION = 138 m.

180

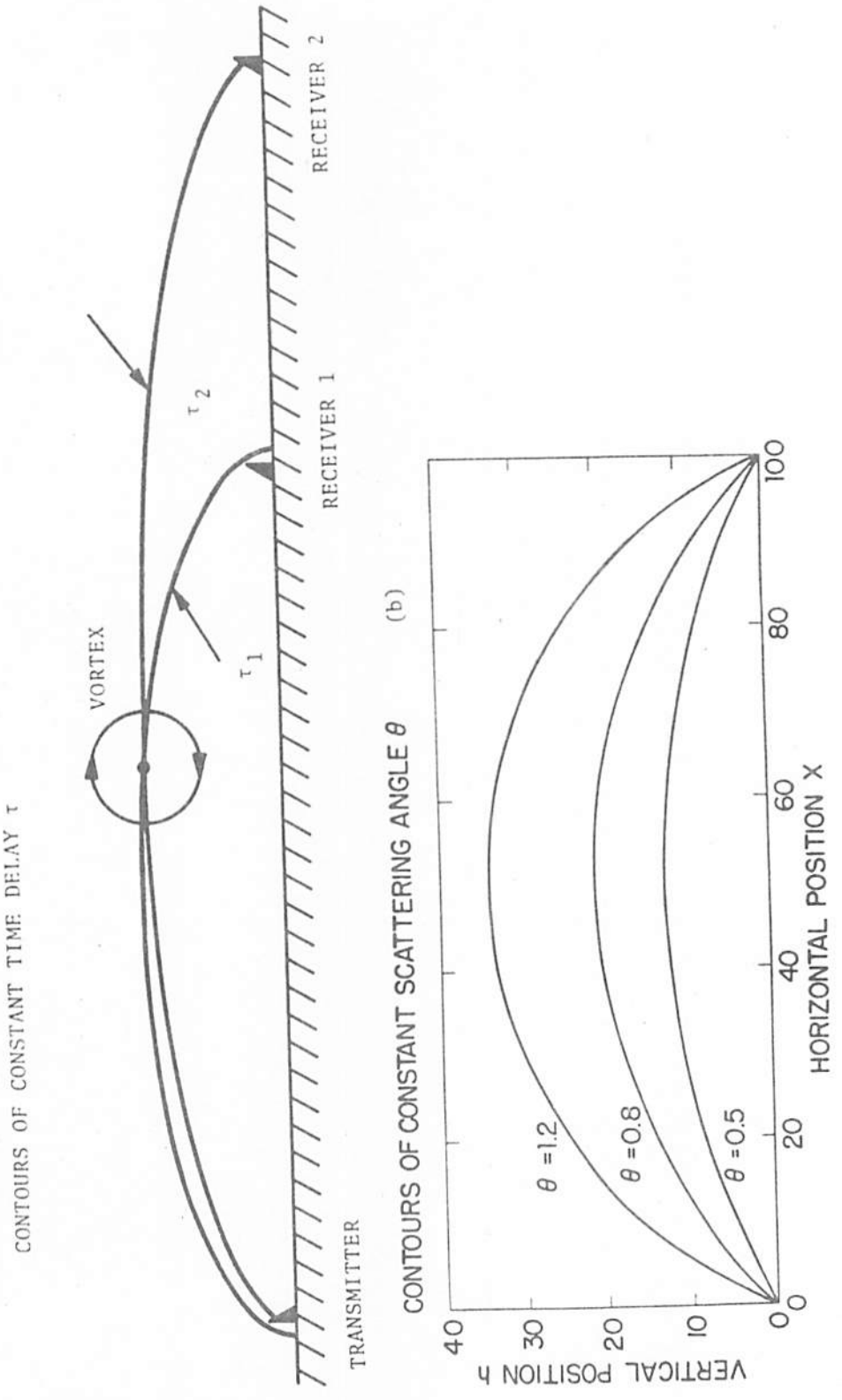

FIGURE 6-22. (A) VORTEX LOCATION BY THE INTERSECTION OF CONSTANT TIME-DELAY ELLIPSES FOR TWO TRANSMITTER-RECEIVER PAIRS. (B) CONTOURS OF CONSTANT SCATTERING ANGLE (RADIANS) FOR THE TRANSMITTER-RECEIVER ONE PAIR. THE DISTANCE UNITS ARE ARBITRARY.

181

PAVSS development continued with calibration tests at NAFEC during the fall of 1972, studies of take-off vortices at Logan Airport during the winter of 1973, and the demonstration of realtime tracking using a minicomputer during the spring of 1973. The calibration tests further verified that the PAVSS gives accurate vortex locations when properly configured for the altitudes of interest. Increasing the antenna separation to 800 m was found to increase the PAVSS altitude range to 200 m.

Avco Corporation built an engineered version of the PAVSS which could measure vortex locations in real time simultaneously at two different distances from the runway threshold. The sysem was installed at Kennedy Airport during the spring of 1974. Figure 6-23 shows the wide-beam antenna used in the Avco PAVSS. (The antenna array can also be seen in Fig. 6-5). Figure 6-24 shows some vortex tracks obtained from the Avco PAVSS.

The ability of the PAVSS to detect and track wake vortices is strongly dependent upon the scattering angle θ defined in Fig. 6-20. Because the refractive scattering angles are small, the two ellipses in Fig. 6-22a are very flat. Consequently, the horizontal position determined by their intersection can have large errors for small errors in the time delay measurements. The vortex height is much less influenced by timing errors, and therefore, is given more accurately by the PAVSS. The timing errors in the signal delay measurements are typically several msec. Errors of this size lead to a horizontal position accuracy which is useless unless one of the scattering angles is greater than 0.5 radian. Smaller values of θ also lead to difficulty in separating the direct and scattered signals since the time delays are proportional to θ^2 for small θ. The difficulty is illustrated in Fig. 6-24 where the vortex signals are lost for a time when the port vortex altitude is so low that the resultant scattering angles and time delays are too small.

The maximum vortex-scattering angle θ_m (equation (6.5)) determines the area where a vortex can be detected. Figure 6-22b shows the detection limits for three values of scattering angle. The useful tracking area is roughly the region between the 0.5-radian contour and the θ_m contour. As discussed previously, the values of θ_m range from 0.5 to 1.2 radians

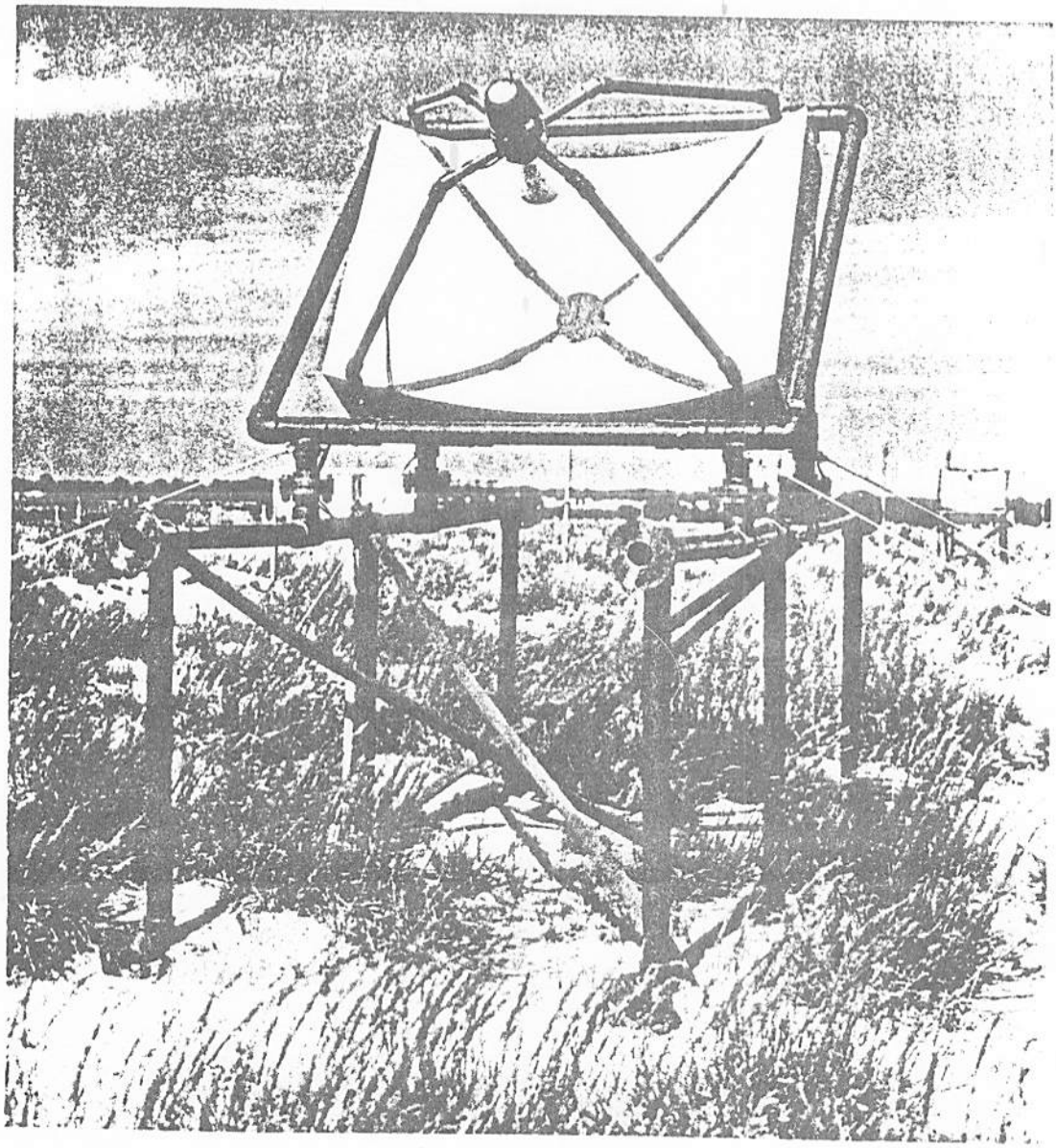

FIGURE 6-~~22~~ 23. AVCO PAVSS ANTENNA. DISH PARAMETERS: FOCAL LENGTH = 0.51 M, WIDTH = 1.32 M, AND HEIGHT = 0.91 M.

183

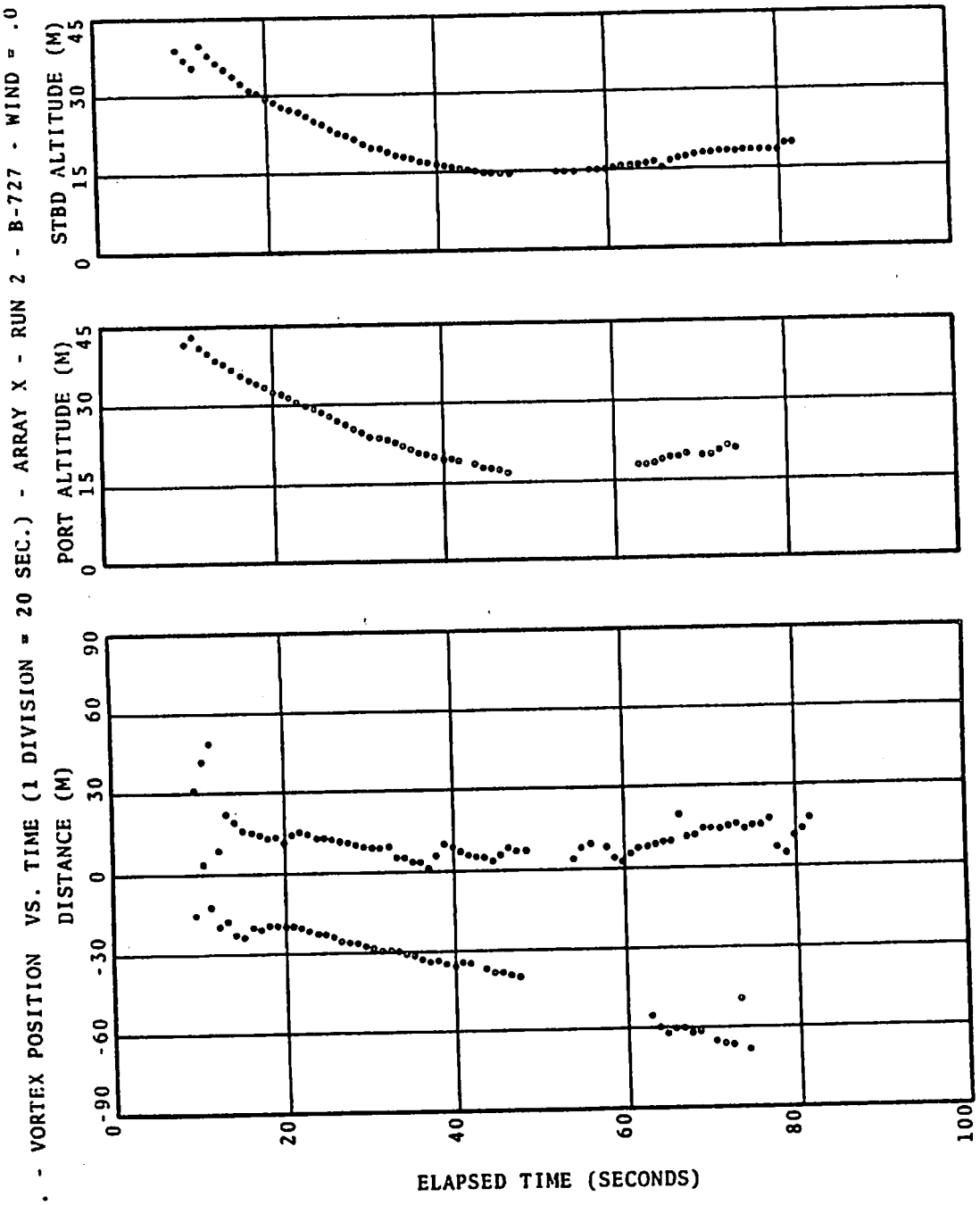

FIGURE 6-~~23~~ 24. VORTEX TRACKS OBTAINED WITH THE AVCO PAVSS: B-727 AIRCRAFT LANDING ON KENNEDY AIRPORT RUNWAY 31R AT 0810 HOURS ON 2 JUNE 1975.

184

for different types of aircraft (ref. 94). The PAVSS is thus very useful for B-727 vortices (θ_m = 1.2 radians) and is worthless for B-707 vortices (θ_m = 0.5).

6.3.2.5 Passive Acoustic Sensors - Some wake vortices generate a swishing sound with energy in the spectral range of 1 to 5 kHz. The sound is heard from vortices with very tight cores such as those from landing B-727 and DC-10 aircraft. Because the sound is extremely variable in time and does not occur consistently even for the most likely aircraft, no development work has been done to exploit this signal. One should note that the vortex-generated noise can interfere with the proper operation of the DAVSS and MAVSS sensors. MAVSS data show that the sound is generated in the vortex core.

Dedard at NOAA (unpublished) has proposed the possibility of detecting a wake vortex by the infrasonic radiation it generates. The concept has not been explored; however, infrasonic microphones have been used to explore the near-field pressure signature of vortices near the ground. The technique is identical to the pressure measurements of Section 6.3.1.2 except that the dc component of the signal is lost, thus producing less easily interpreted signatures.

6.3.3 Optical Techniques

Optical techniques have the general advantages of high resolution and long range. They are degraded by conditions of low visibility. Infrared sensors are less affected than those using visible light.

6.3.3.1 Passive Optical Techniques - Wake vortices can become visible if they contain a sufficient density of light-scattering particles. Under certain natural conditions (high altitude flight or high humidity), water vapor condenses in the wake vortices and remains trapped until the vortices dissipate. The effect is familiar to anyone who observes contrails. Under normal atmospheric conditions, particles must be added to make vortices visible. Two techniques have been developed for dedicated flight tests. In the first, smoke grenades or smoke generators are mounted on an aircraft in an appropriate spot to mark the core of the wake vortex. In the second, smoke grenades are mounted on a tower through which the wake drifts after

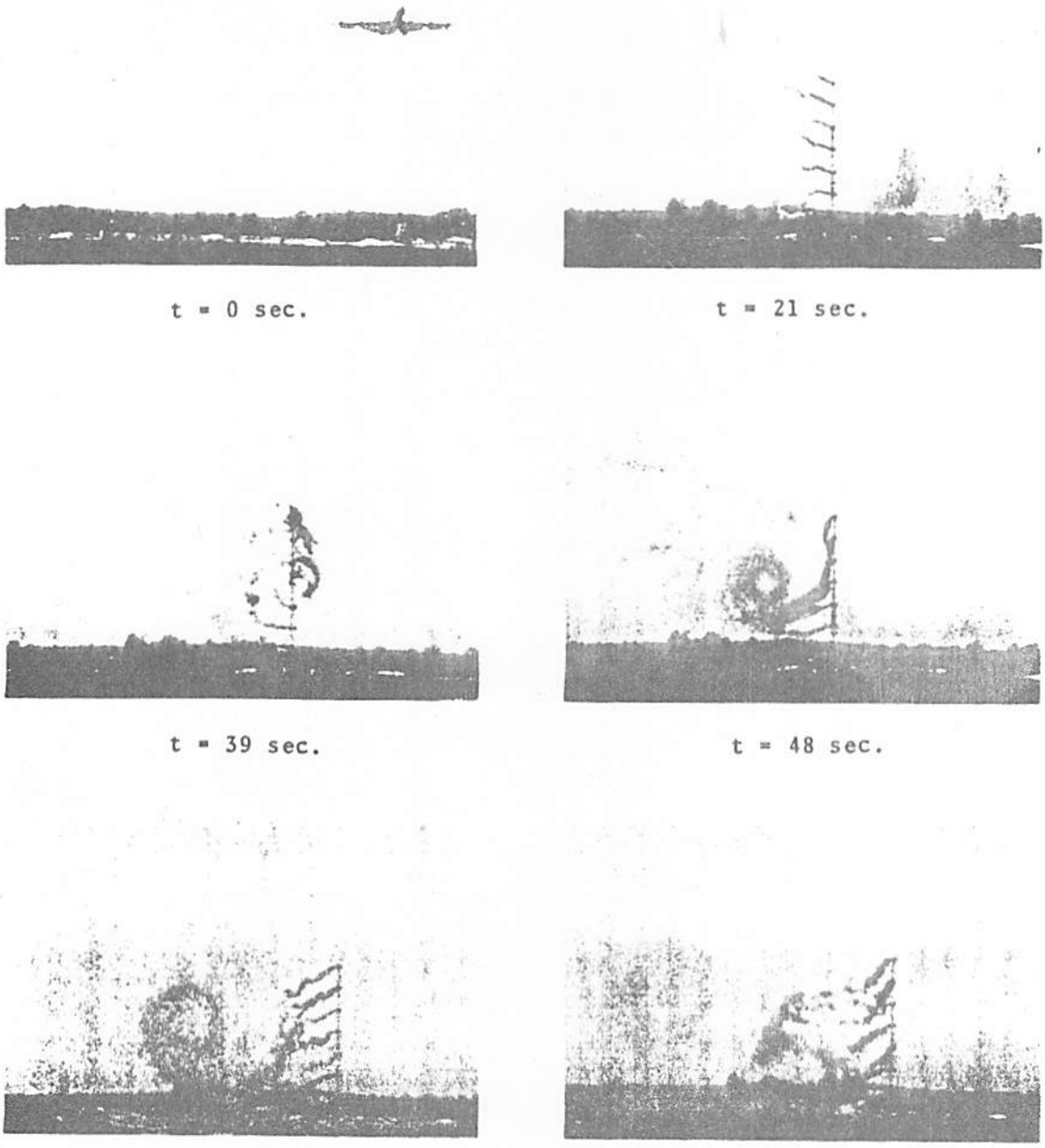

FIGURE 6-25. FLOW VISUALIZATION OF WAKE VORTICES FROM A B-707 AIRCRAFT. TOWER HEIGHT = 43 m, CAMERA DISTANCE = 600 m.

186

the aircraft has passed. Figure 6-25 shows some photographs of the second technique, which was used to provide an absolute reference for the other sensors in the 1972 NAFEC calibration tests. The proper interpretation of the photographs in Fig. 6-25 requires careful corrections for the effects of the ambient wind.

Several proposals have been made to detect wake vortices by passive infrared scanners. The technique is based on the excess radiation from the aircraft wake which contains heat, H_2O, and CO_2 from the engine exhaust. Appropriate wavelength filtering could allow an infrared sensor to be very sensitive to this excess radiation. The infrared signature of the wake is likely to give the general vortex locations, but it is uncertain how easily it can indicate vortex decay. Some experimental data will be needed to allow a definitive assessment of infrared vortex-sensing feasibility.

During the 1972 NAFEC calibration tests, a UV photographic sensor was tested (ref. 98). The sensor apparently makes use of sunlight scattered from nitrogen compounds in the wake. No feasibility information is available.

6.3.3.2 Scanning laser Doppler Velocimeter System - The Scanning Laser Doppler Vortex Sensor (SLDVS) is an optical vortex sensor which operates in the far infrared at the CO_2 laser wavelength of 10.6 microns. The SLDVS works by focusing a laser beam at a given region in space, collecting the laser energy backscattered by natural aerosol in the atmosphere, and measuring the difference between the frequency of the transmitted beam and the frequency of the backscattered beam as being the Doppler shift resulting from the component of the aerosol velocity along the laser beam line-of-sight. By controlled scanning of the focal volume, the velocity field of the vortex may be mapped. The selection of the 10.6 micron wavelength offers the advantages of high available power, low personnel hazard, long range in fog, and feasible heterodyne detection.

6.3.3.2.1 SLDVS historical development - The basic research in the development of laser Doppler systems was initiated during the early 1960s at the NASA Marshall Space Flight Center (MSFC). The initial emphasis was to find an acceptable technique for measuring wind tunnel flow fields about models without obstructing the flow. The resulting success with the

technique led researchers to investigate the feasibility of applying the technology to measure atmospheric flow fields and turbulence, particularly the turbulence which was known to be hazardous to aviation. Initial feasibility was demonstrated in 1969 when successful measurements of the vortices from a DC-3 aircraft were made. This success led to continued systems studies and testing which showed the feasibility of practically applying the technique for detecting, tracking, and measuring aircraft vortices. In 1972, the FAA requested NASA to accelerate this applied research activity to provide assistance in understanding the aircraft wake vortex problems. The result of the extensive research into the application of the laser Doppler principle to atmospheric flow-field problems led to the design and development of the SLDVS (ref. 100). The SLDVS was used at the JFK Airport to detect, track, and measure the vortices generated by aircraft in the approach corridor of runway 31R between September 1974 and May 1975.

Subsequent to the JFK work, a mobile SLDVS was developed by Lockheed. The real time data processing capability was more limited than for the NASA SLDVS, but it was easily moved and had a more versatile beam scanner. It was used to collect wake vortex data at a variety of airports (ref. 101) and at some special B-747 vortex tests conducted at a California dry lake (see Section 10) as well as several measurements of atmospheric phenomena unrelated to wake vortices.

In 1977, a version of the Lockheed SLDVS system, but with greatly expanded computer capability, was delivered to DOT/TSC. As described below, the system was used at several vortex test sites. Figure 6-26 shows an exterior view of the SLDVS unit at O'Hare Airport. Figure 6-27 shows a view of the optical components of the SLDVS. During the 1981-1984 hiatus in the vortex program, the DOT/TSC unit was used by the U. S. Army at Redstone Arsenal, Alabama, for measurement of flight velocities of Tow missiles. In 1985, the system was extensively refurbished, including being packaged in a larger mobile container and replacing the original PDP-11/05 computer with a PDP-11/34.

In the 1982-1985 time period, Lockheed significantly advanced the state-of-the-art for LDV systems. They have built, tested, and used a compact LDV unit shown in Figure 6-28. This system has been used to measure wind profiles in support of a test on the effect of crosswind on the trajectories

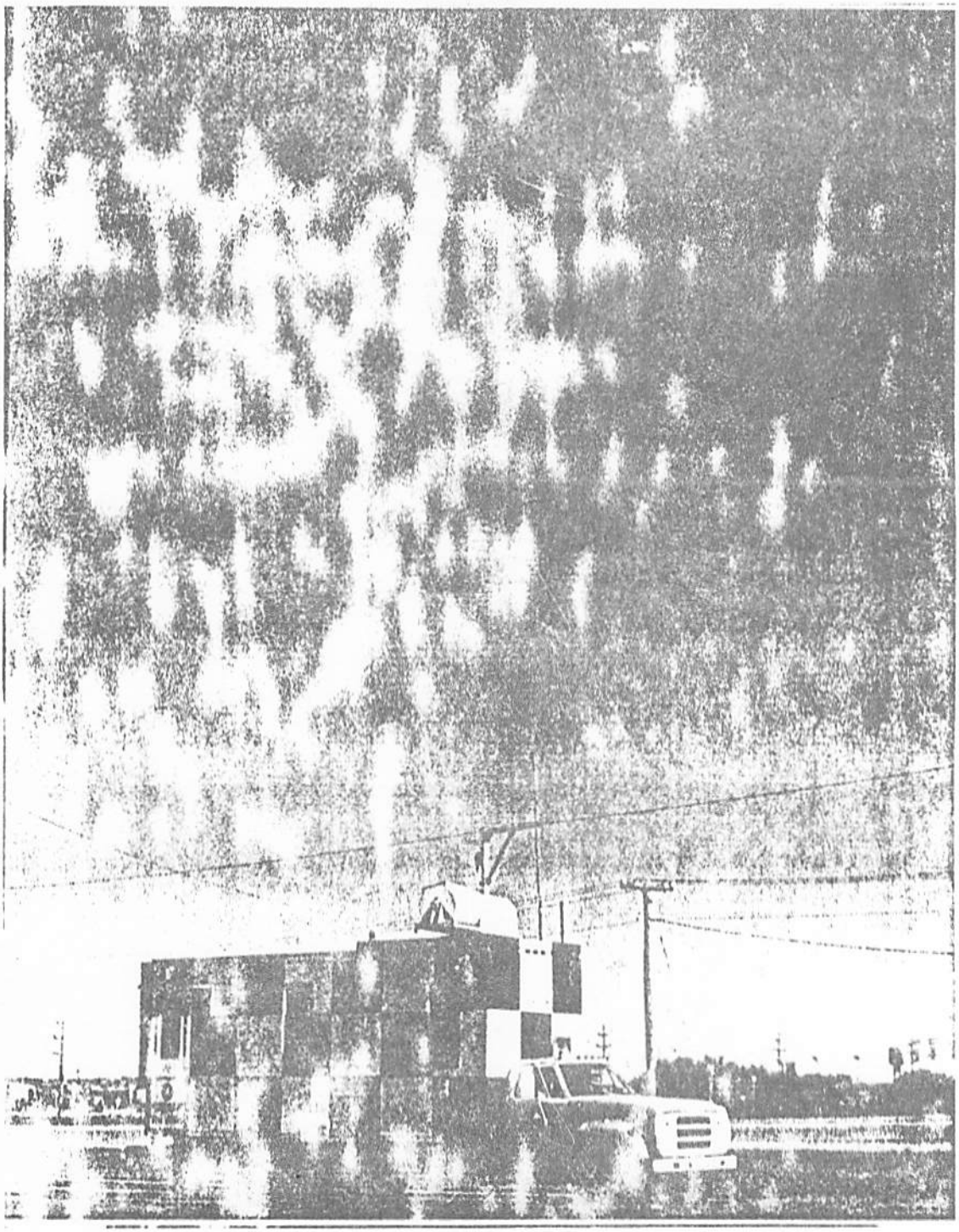

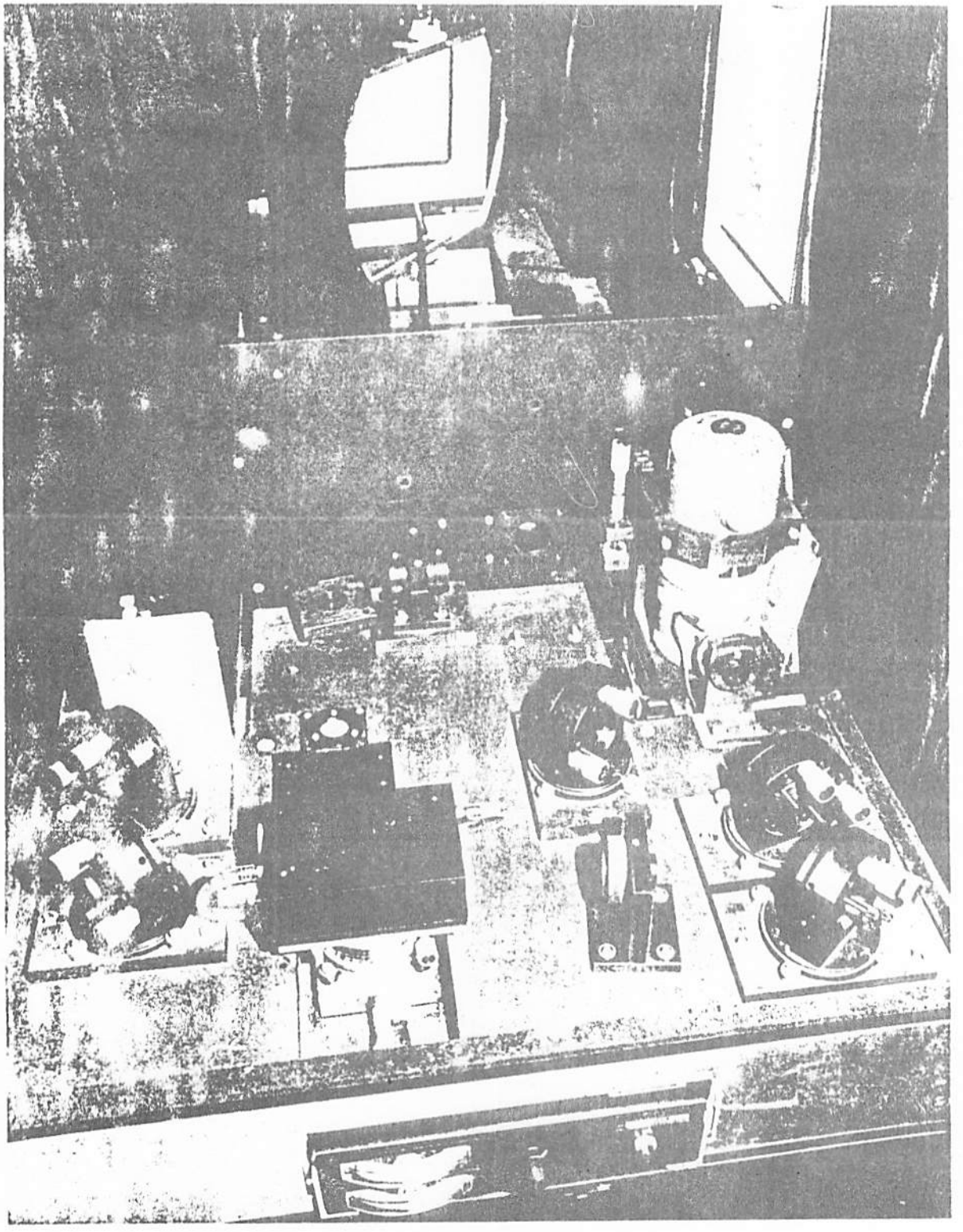

Fig. ~~2-10~~ 6-27 The TSV/LDV Interferometer

190

DESCRIPTION
- SIZE: 1m x 0.5m x 0.3m
- WEIGHT: 120 LBS
- LASER: 10 WATT, 10.6μ METER
- DETECTOR: MERCURY CADMIUM TELLURIDE
- INTERFEROMETER: MODIFIED MACH ZEHNDER (SEVERAL DIFFERENT ARRANGEMENTS AVAILABLE)
- INVAR HONEYCOMB STRUCTURE

SCANNER: EITHER ROTATE GERMANIUM WEDGE OR GIMBAL ENTIRE ASSEMBLY

TELESCOPE: 25 cm APERTURE f/2 SCHWARTZCHILD
CONFIGURATION: INVAR TUBE STRUCTURE

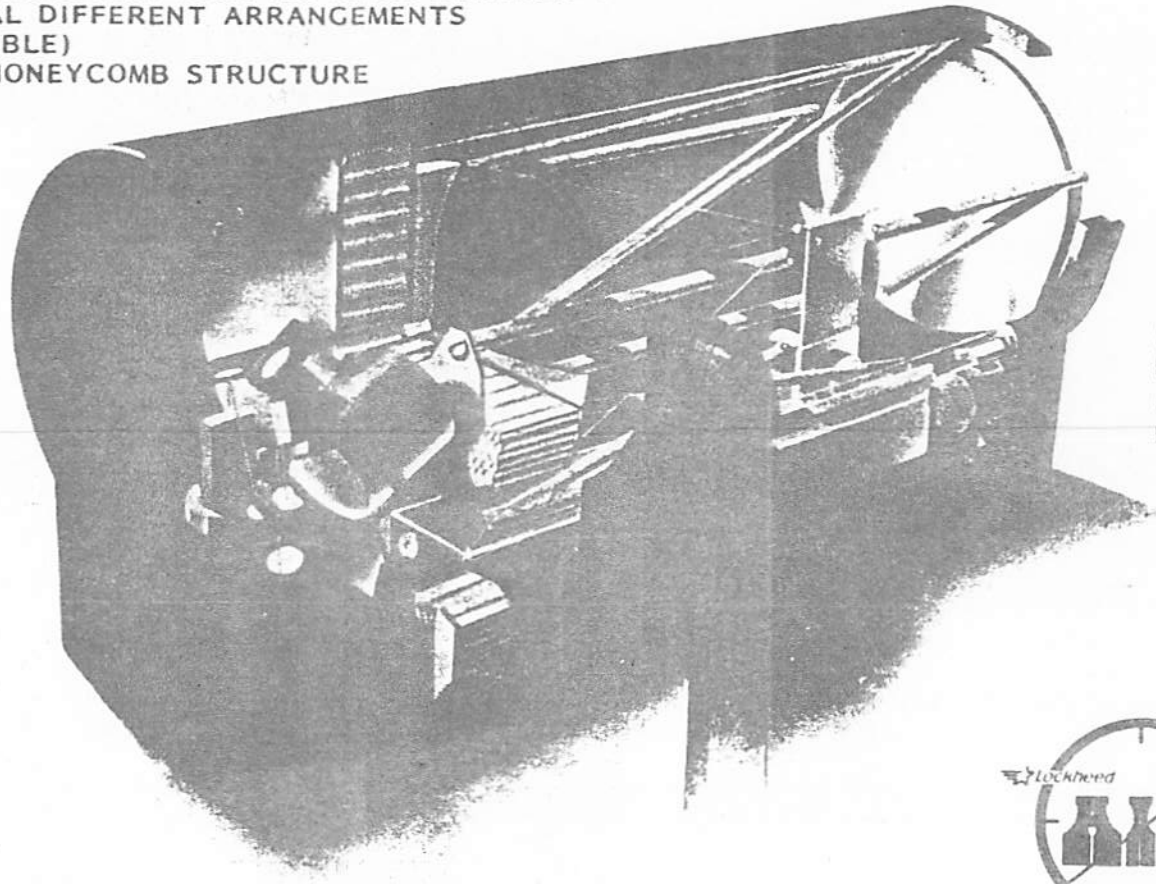

STRUCTUALLY DESIGNED FOR M-113 TYPE ENVIRONMENT

APPLICATIONS:
- REMOTE WIND PROFILE
- MISSILE VELOCITY
- SLED VELOCITY
- OBSCURANT

~~ACTIVE~~
~~INFRARED~~
~~MEASUREMENT~~

FIGURE 6-28 COMPACT LASER DOPPLER VELOCIMETER SYSTEM BUILT BY LOCKHEED

of free flight rockets. By the use of an array processor, Lockheed has increased the data rate of measurement of the line-of-sight component of velocity from 70 measurements per second to 2000 measurements per second. In addition, advanced processing of the data used to generate the characteristic line-of-sight velocity has resulted in higher quality (i.e., smoother) data than previously available.

In mid 1985, plans for upgrading the DOT/TSC SLDVS are in process. Upgrade plans include automated tracking of vortex pairs (i.e., automated adjustment of scan limits to follow the moving vortex pair) and automated algorithms for identifying vortices and plotting vortex trajectories.

6.3.3.2.2 SLDVS vortex measurement experience - The JFK installation used in 1974-1975 consisted of two SLDVS units, each scanning in range and elevation perpendicular to the localizer (ref. 102). They were positioned near the middle marker, 762 m from the end of runway 31R, approximately 122 m on either side of the extended runway centerline. A vertical plane across the approach corridor was scanned to determine the tracks of the aircraft vortices. The detected vortices were then monitored and displayed as they moved across the scan plane. The tangential velocity profile of the vortex was also measured and recorded for later data evaluation. The area covered by the scanning patterns of the two SLDVS units at JFK is shown in Fig. 7-1 in Section 7.1.

SLDVS testing was performed at JFK in two separate test periods. The first series of test was carried out during the time between September 7, 1974, when the equipment was installed, and December 13, 1974, when the system was placed in a standby condition. The second series of tests was performed from March 3, 1975, when the systems were returned to an operatinal status, through June 2, 1975, when the systems were returned to MSFC. At the conclusion of the second test period, vortex data had been recorded on 1619 aircraft landings. An analysis of these data is presented in ref. K.

The TSC SLDVS has also been used for vortex measurement programs involving many landings at Toronto (ref. U), Boston Logan Airport (ref. V) and at O'Hare in Chicago (ref. W). At O'Hare, data from more than ten thousand vortex trajectories were recorded. The O'Hare measurement program involved five day per week operation for twenty two months. It has also been used for

vortex tests at Moses Lake (ref. X), China Lake, Dryden Flight Research Center, and Redstone Arsenal, Alabama (ref. Y). The measurement program at Redstone Arsenal measured the wakes of helicopters.

6.3.3.2.3 SLDVS hardware description - The basic SLDVS consists of a very stable single-frequency CO_2 laser, Mach-Zehnder interferometer, transmit-receive optics, infrared detector, range-angle scanner, velocity-frequency analyzer, data-algorithm processor/display, and recorders. Four SLDVS units have been used for vortex measurements: the two NASA systems used for the JFK tests, the Lockheed system, and the DOT/TSC system built by Lockheed. The following discussion will describe the characteristics of the TSC system.

The SLDVS optical system is shown schematically in Figure 6-29. A horizontally polarized, 20 watt continuous wave CO_2 laser beam (10.6 μm wavelength) emerges from the laser (1) and is deflected 180 degrees by mirrors (2) and (3). The approximately 6 mm diameter beam then passes through a Brewster window (4) and a CdS quarter waveplate (5) which converts it to a circular polarization. The beam impinges on the secondary mirror (6) and is expanded and reflected into the 30-cm diameter primary mirror (7) and then focused into the atmosphere. The distance from the primary mirror to the focal point in space is controlled by the distance between the secondary mirror (6) and the primary mirror (7). Energy reflected from aerosol at the focal volume (9) is collected by the primary mirror (7), collimated by the secondary mirror (6), and passed through the quarter waveplate (5). The quarter waveplate changes the polarization of this aerosol-backscattered radiation from circular to vertical linear polarization. The vertically polarized beam is approximately 78% reflected off the Brewster window (4) and is directed by the mirror (10) to the collecting lens (11). A small portion of the original beam is reflected from the secondary mirror (6) back through the quarter waveplate (5) instead of being reflected off the primary mirror (7) and being directed out into space. This small portion of the beam is also reflected by the Brewster window (4) and the mirror (10) onto the collecting lense (11). It serves as a local ocsillator or reference beam for determining the Doppler shift of the backscattered radiation. After passing through the collecting lens (11), the two beams (beam backscattered from the ambient aerosol and the reference beam reflected directly from the secondary mirror) are photomixed on the detector (12) in a heterodyne configuration. The

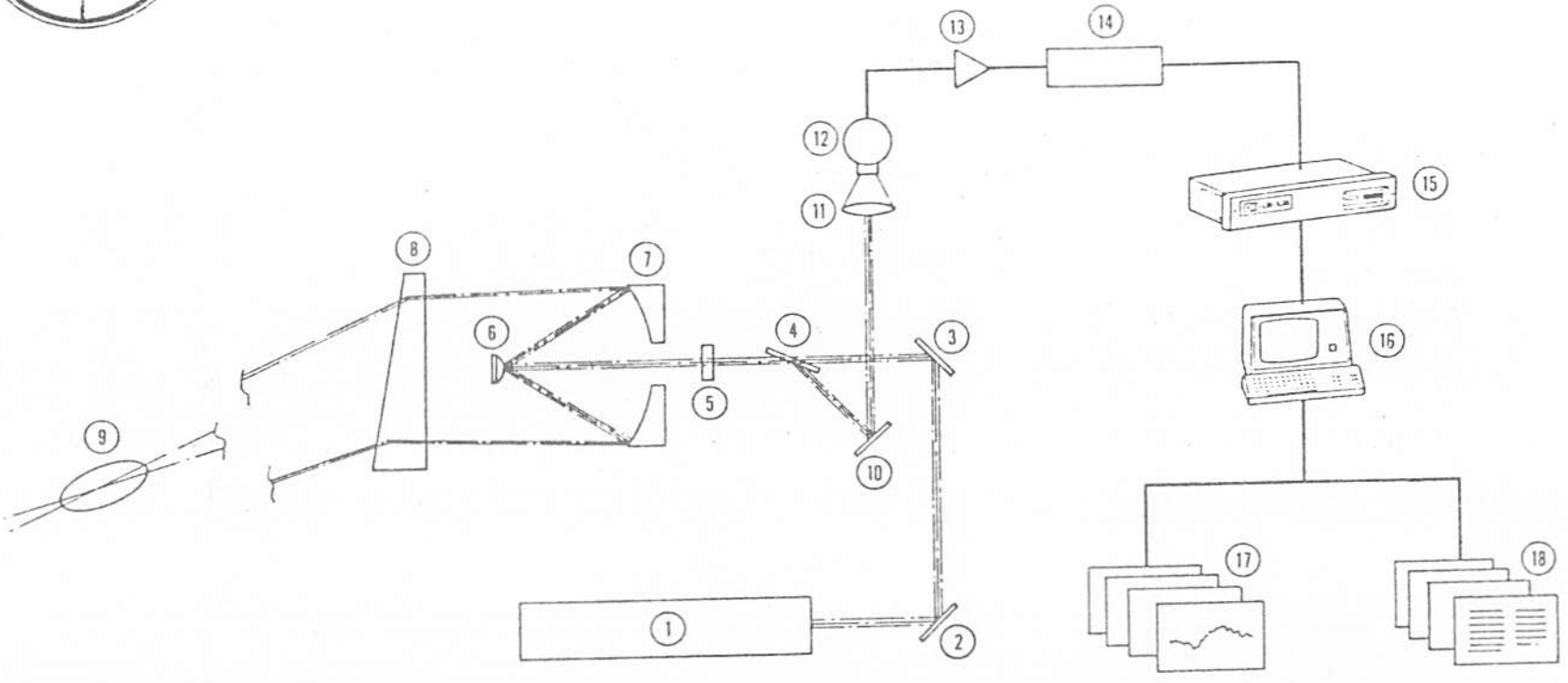

(1) CO_2 Laser
(2) Mirror
(3) Mirror
(4) Brewster Window
(5) Quarter Wave Plate
(6) Secondary Mirror
(7) Primary Mirror
(8) Beam Directing Germanium Wedge
(9) Focal Volume
(10) Mirror
(11) Lens
(12) Photodetector
(13) Preamplifier
(14) High Speed A/D Converter
(15) Array Processor for Spectral Analysis
(16) PDP-11/23 Computer
(17) Wind Plots
(18) Wind Tables

~~LOCKHEED-HUNTSVILLE~~

FIGURE 6-29 SCHEMATIC DIAGRAM OF LASER DOPPLER VELOCIMETER

electrical output of the detector (12) is amplified with a 5 MHz bandwidth, 30 dB gain low noise type preamplifier (13) and fed into a spectrum analyzer (14). The spectrum analyzer displays Doppler frequency (abcissa) versus returned signal strength (ordinate). The spectrum analyzer determines the signal intensity for each of one hundred frequency bines (i.e., Doppler shifted frequency) which span the frequency from minimum to maximum selected values. The signal displayed on the spectrum analyzer output is illustrated in Figure 6-30. The PDP-11 computer (15) identifies the frequency band which has the highest signal intensity, determines the Doppler frequency shift of the maximum intensity signal, and converts this spectrum analyzer output into a direct velocity readout.

The spatial resolution of the SLDVS is achieved by focusing the continuous wave laser beam at the desired range, D. For ranges much larger than the optics diameter, d, the focal volume diameter is approximately λF where $F = D/d$ is the f-number of the focus distance, and λ is the 10.6 micron wavelength of the laser radiation. The length of the focal volume is approximately equal to $F^2\lambda$, and therefore, is much larger than the focal width for the usual values of F. For example, at 100 m range, the diameter of the beam at the focal point is approximately 1 cm, and the focal volume length is approximately 7 meters. Since the length of the focal region increases as the square of the range, there is a limiting range beyond which the SLDVS give poor range resolution.

Because the length of the focal volume increases as the square of the range, the maximum useful range for such a beam diameter is roughly 500 m for the data processing technique currently used for the TSC system. It is expected that some of the advanced spectrl processing techniques developed and implemented by Lockheed on other applications, but not yet applied to vortex detection, will significantly expand the maximum useful range of the SLDVS. The focusing technique for achieving spatial resolution also suffers from the fact that the response does not fall off rapidly outside the focal region (ref. 99). This limitation can cause some difficulty in signal processing if the concentration of scattering aerosol varies along the beam.

The question may be asked: Why not use a pulsed laser to achieve range

electrical output of the detector (12) is amplified with a 5 MHz bandwidth, 30 dB gain low noise type preamplifier (13) and fed into a spectrum analyzer (14). The spectrum analyzer displays Doppler frequency (abcissa) versus returned signal strength (ordinate). The spectrum analyzer determines the signal intensity for each of one hundred frequency bines (i.e., Doppler shifted frequency) which span the frequency from minimum to maximum selected values. The signal displayed on the spectrum analyzer output is illustrated in Figure 6-30. The PDP-11 computer (15) identifies the frequency band which has the highest signal intensity, determines the Doppler frequency shift of the maximum intensity signal, and converts this spectrum analyzer output into a direct velocity readout.

The spatial resolution of the SLDVS is achieved by focusing the continuous wave laser beam at the desired range, D. For ranges much larger than the optics diameter, d, the focal volume diameter is approximately λF where $F = D/d$ is the f-number of the focus distance, and λ is the 10.6 micron wavelength of the laser radiation. The length of the focal volume is approximately equal to $F^2\lambda$, and therefore, is much larger than the focal width for the usual values of F. For example, at 100 m range, the diameter of the beam at the focal point is approximately 1 cm, and the focal volume length is approximately 7 meters. Since the length of the focal region increases as the square of the range, there is a limiting range beyond which the SLDVS give poor range resolution.

Because the length of the focal volume increases as the square of the range, the maximum useful range for such a beam diameter is roughly 500 m for the data processing technique currently used for the TSC system. It is expected that some of the advanced spectrl processing techniques developed and implemented by Lockheed on other applications, but not yet applied to vortex detection, will significantly expand the maximum useful range of the SLDVS. The focusing technique for achieving spatial resolution also suffers from the fact that the response does not fall off rapidly outside the focal region (ref. 99). This limitation can cause some difficulty in signal processing if the concentration of scattering aerosol varies along the beam.

The question may be asked: Why not use a pulsed laser to achieve range

195

FIGURE 6-30. SAMPLE SPECTRUM OUTPUT

196

resolution, as in Doppler radar and Doppler acoustic sensors, instead ot using the complicated focusing system of the SLDVS? The answer is that, for a specific desired spatial resolution, the single pulse velocity resolution at λ = 10.6 microns is a factor of 100 worse than for a 3 kHz Doppler acoustic sensor. Moreover, it may not be possible to integrate over many pulses, as in a Doppler radar, because the cohenent times of the scattered signal is limited by diffusion of the aerosol scatterers.

The scanner is the cylindrical device on the roof of the SLDVS in Fig. 6-26. It consists of a fixed mirror which directs the vertical beam horizontally along the scanner and amovable mirror which is gimballed about two axes to direct the beam at a desired direction in space. As described above, range scanning is obtained by controlling the position of the secondary mirror. The function of the scanner is to move the beam axis and the location of the focal volume in such a way that (a) the coordinates of the illuminated region are known at all times; (b) a given region of space may be examined in an efficient systematic manner; and (c) the nature of the scan program may be conveniently altered to suit a variety of applications. The scan pattern currently used for vortex detection and tracking is shown in Fig. 6-31. Although four ranges are shown, up to eight ranges may be selected. Currently, the LDV operator views a cathode ray tube display in the SLDVS and adjusts scan limits to keep the vortex within the scan field of view. However, in mid 1985, initial planning to automate the scan control is in progress. The scan pattern shown in Figure 6-31 is the pattern currently used for vortex detection. The SLDVS is capable of other scan patterns which are shown in Fig. 6-32.

A set of typical velocity profiles measured by the SLDVS is shown in Fig. 6-33. The purpose of the test for which the profiles were measured was the evaluation of vortex alleviation techniques (ref. E). Therefore, profiles for both non-alleviated and alleviated conditions are shown. The SLDVS measures the absolute value of velocity, shown negative in Fig. 6-33. Therefore, the velocity data show only one sign. A vortex trajectory as measured by the SLDVS is shown in Fig. 6-34. Vortex trajectories measured by the NASA systems during the JFK tests are shown in Fig. 6-35.

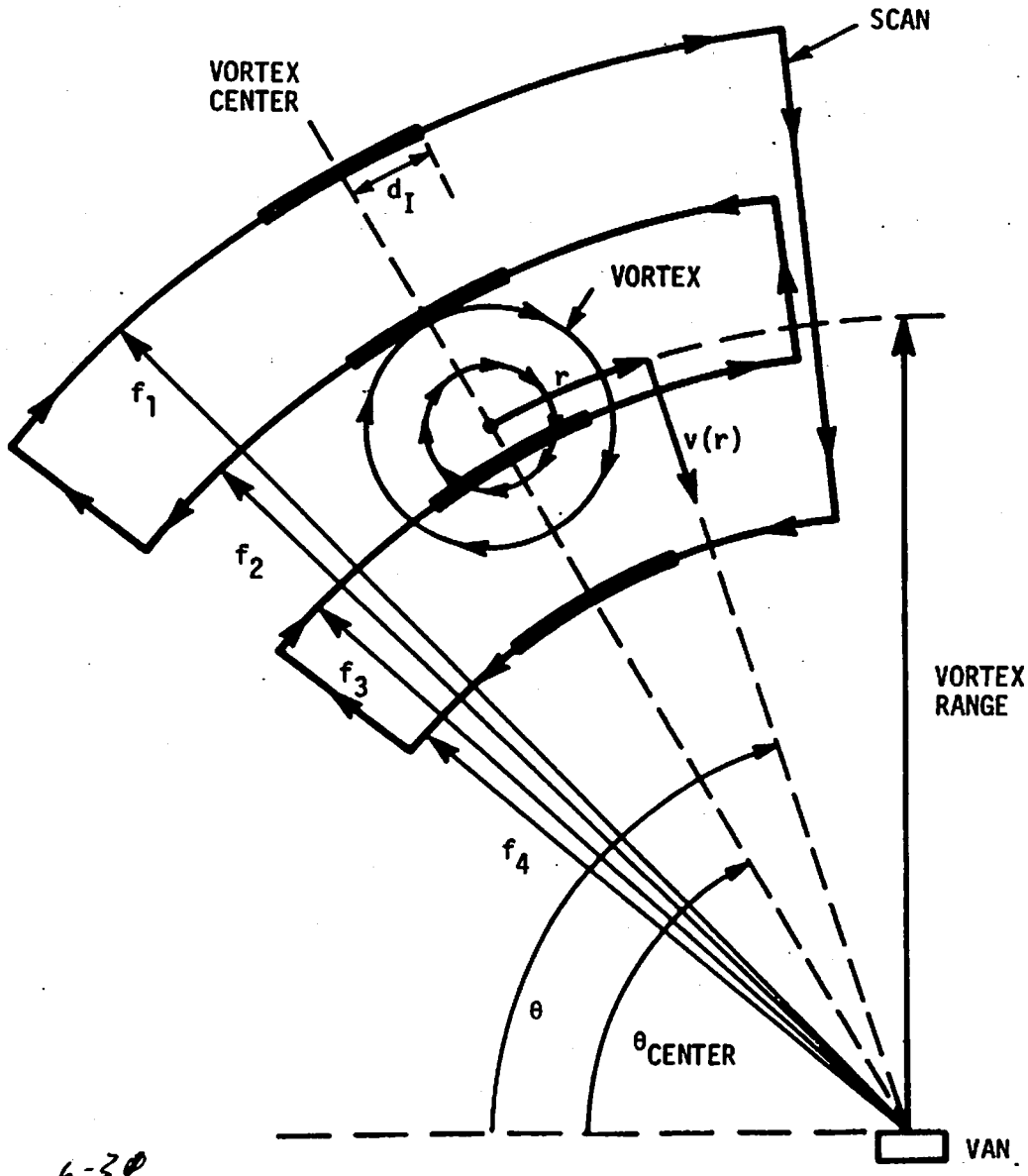

FIGURE 6-30. GEOMETRY FOR PROCESSING ONE SCAN FRAME OF LDV DATA

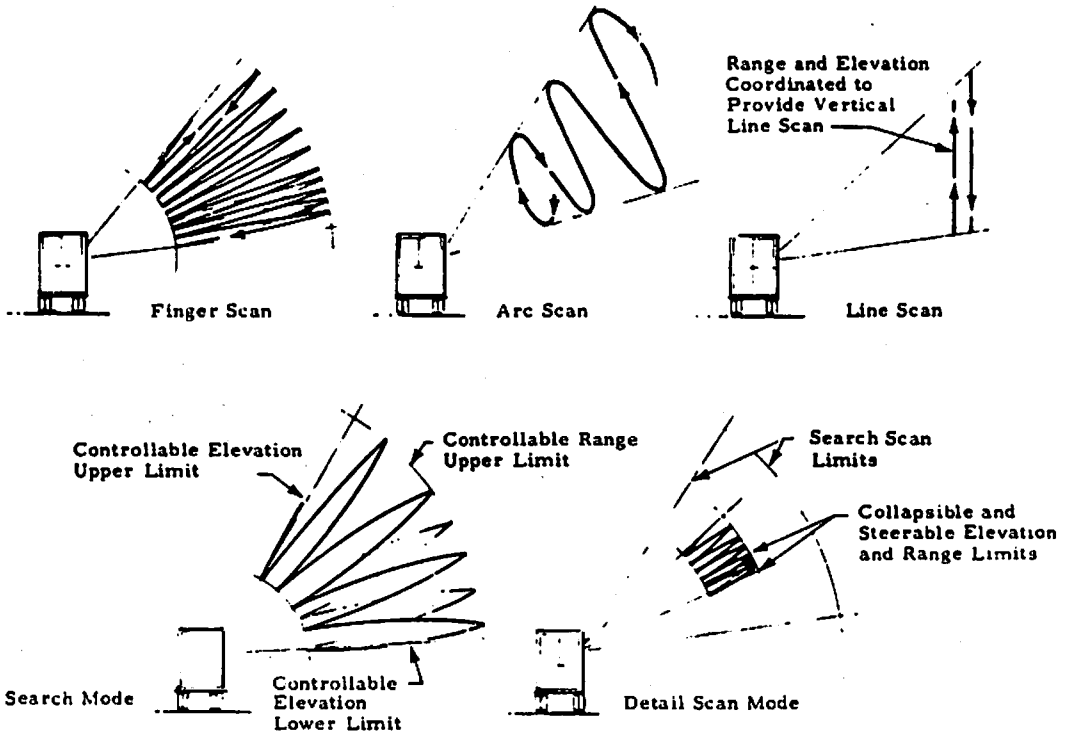

FIGURE 6-~~26~~ 32. SCHEMATIC REPRESENTATION OF THE BASIC SCANNING MODES 197

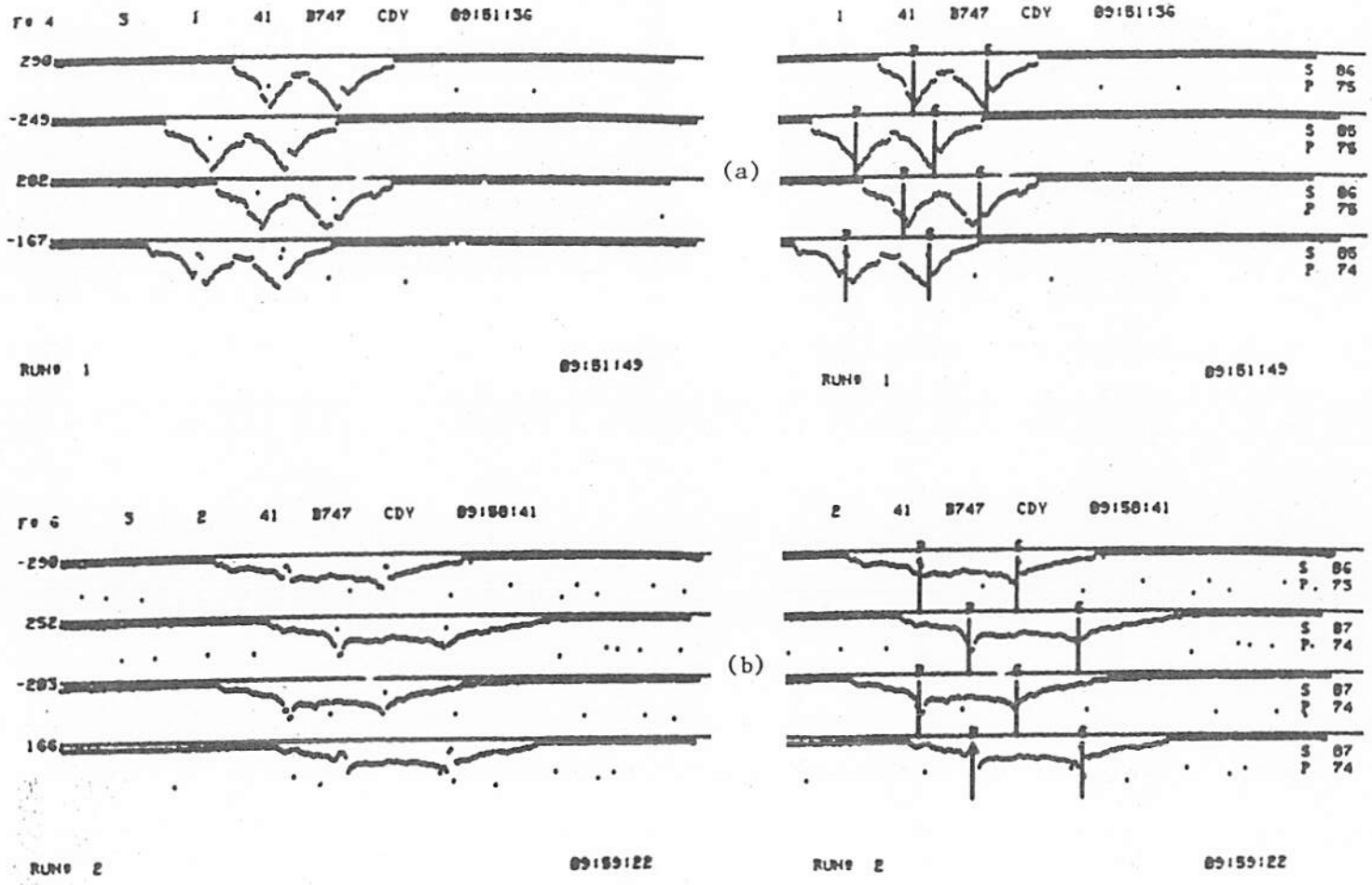

FIGURE 5. PLAYBACK CRT DISPLAY: (a) NON-ALLEVIATED (RUN 1, 2/10/79) (b) ALLEVIATED (RUN 2, 2/10/79). THE SELECTED VORTEX CENTERS ARE LISTED ON THE RIGHT.

SCAN

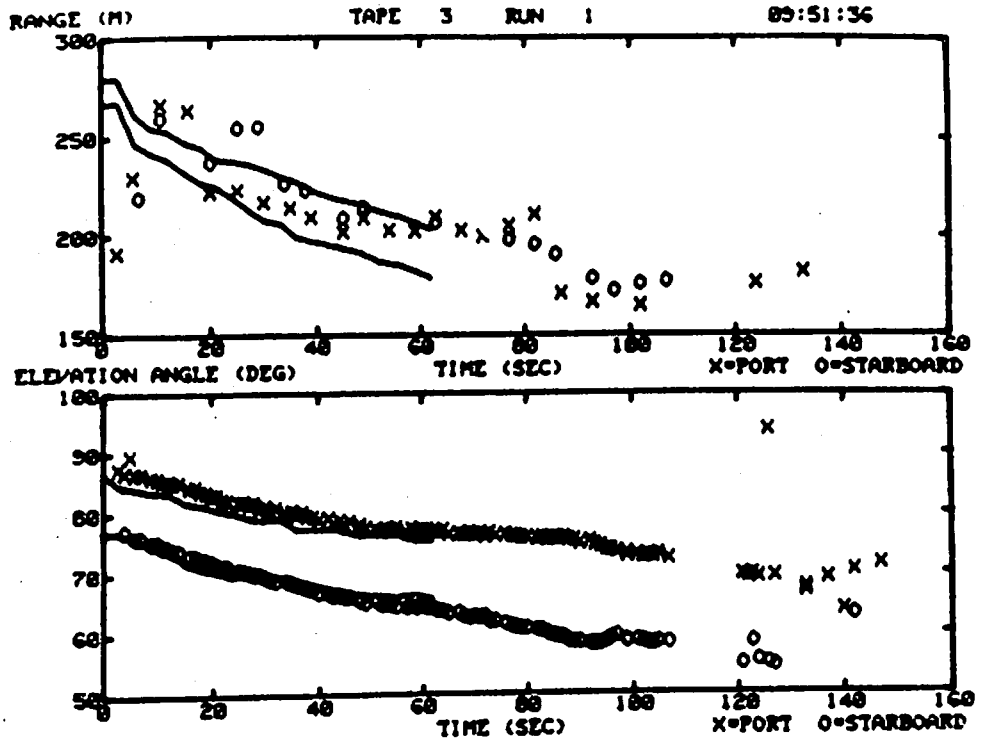

(a)

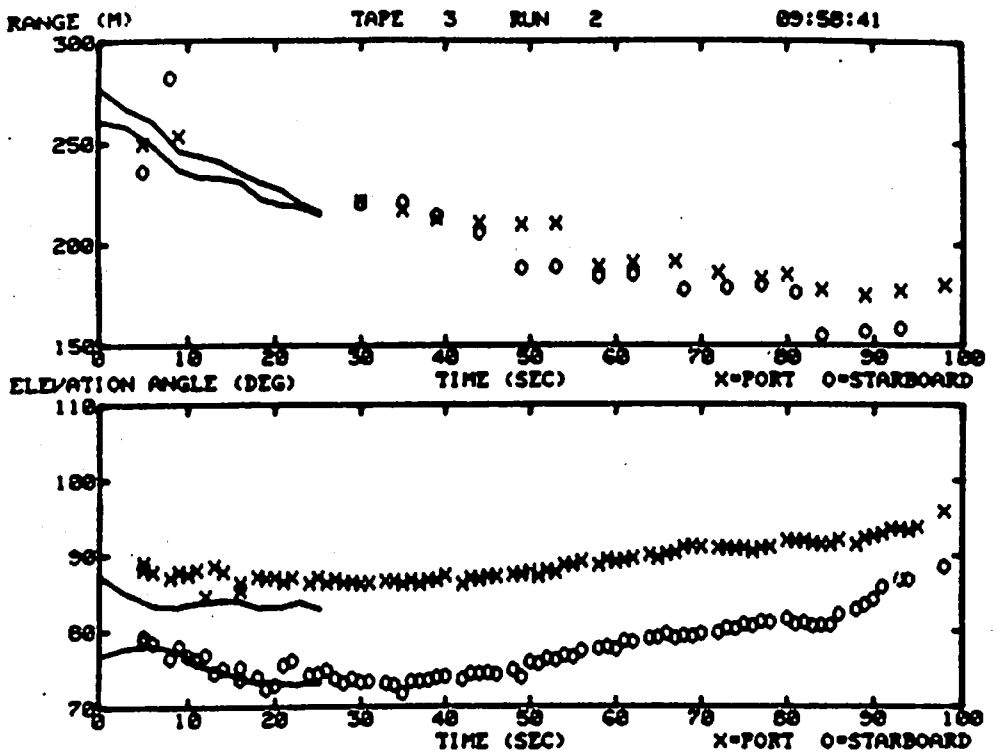

(b)

6-34

FIGURE 11. POLAR COORDINATE VORTEX TRAJECTORIES: (a) NON-ALLEVIATED (RUN 1, 2/10/79) (b) ALLEVIATED (RUN 2, 2/10/79)

6.3.4 Electromagnetic Techniques

Although the radar cross sections of natural aerosol in wake vortices are too small for the use of conventional radar systems (ref. 97), some observations (ref. 103) of Doppler shifts caused by wake vortices have been made using chaff and snow as scatterers. It has been proposed that wake vortices could be detected by means of electrostatic charge injected by an aircraft into the wake. Such charge may occur naturally via the discharge electrodes on aircraft wings, but it could also be intentionally injected, perhaps putting opposite polarity on the two vortices. No experimental data are available on the electric potentials near wake vortices. An airborne electrostatic sensor might be capable of detecting electrostatically marked vortices from a preceding aircraft.

6.3.5 Combination Techniques

A combination of techniques may be more useful than a single one if the strengths and weakensses are complementary. Two combination techniques have been suggested during the wake vortex sensor development.

The first combines the PAVSS and the GWVSS. If the lateral position of a vortex is known from the GWVSS, the vortex height could be accurately determined by a pair of PAVSS antennas. Such a system would still be subject to the aircraft type limitations of the PAVSS.

The second combines the MAVSS and the GWVSS to yield a direct measurement of circulation for vortices stalled near the runway centerline. The circulation within an area is computed directly as a line integral around the area. The MAVSS is ideally suited for measuring the velocity line integral along a vertical line. The measured line integrals are in reasonable agreement with the theoretical values based on the vortex strength measurement. Two MAVSS antennas would measure the vortex line integrals along the sides of the area. The GWVSS sensors would complete the integral between the two MAVSS antennas. For low altitude vortices, the top of the area makes no significant contribution to the line integral.

6.3.6 Future Sensor Development

Perhaps the most important goal in future sensor development is to establish a satisfactory method of measuring the strength of stalled vortices. If such a measurement could be made, a stalled vortex could be penetrated by a following aircraft if there were assurance that its strength were sufficiently small. To that end, a DAVSS strength algorithm could be implemented, and the MAVSS-GWVSS combination could be tested. Improved SLDVS strength algorithms could also be developed. The improved methods of deriving the line-of-sight velocity developed by Lockheed over the past several years will greatly aid the development of strength algorithms using the SLDVS.

Another goal is to gain an understanding of the boundary layer processes influencing GWVSS signatures. A better understanding of the GWVSS is needed because it is currently the most likely sensor candidate for incorporation into any vortex avoidance system because of its simplicity and ability to operate for long periods of time with minimal maintenance. Improved processing for GWVSS data and careful comparisons with data from the MAVSS sensor may lead to valid measurements of vortex decay using GWVSS data alone. Such a development would substantially increase the usefulness of the large GWVSS data base already collected.

6.4 AIRBORNE WAKE VORTEX DETECTION

Active and passive remote sensing systems have been assessed (ref. 104) to determine the feasibility of detecting aircraft trailing vortices using instrumentation on board an aircraft. It was found that a modification of the front end receiver of a 10 GHZ weather radar system or a change of frequency to 35 GHz may allow vortex identification over a range of several kilometers. A 10.6 micron coherent Doppler optical radar and passive radiometric techniques in the 8 - 14 micron region indicate promise. Incoherent lidar, Raman shift techniques, fluorescence scattering, acoustic radar, and ultraviolet emissions were shown not to possess sufficient sensitivity.

9. MATHEMATICAL AND STATISTICAL METHODS APPLICABLE TO VORTEX TECHNOLOGY

This section presents mathematical methods which have been developed and used in other areas of technology, have not been previously applied to vortex technology, but show significant promise for application to vortex technology. They are presented here to introduce them to the vortex technical community in order to stimulate their further application to vortex technology and to the conceptual design of an effective wake vortex avoidance system.

9.1 Statistics of Extreme Values

In many applications of probabilistically defined phenomena, the rare event is often of much more significance than the common event. Examples of this include rare random failures of critical mechanical components, structural failure, and rarely occurring concentrations of air pollutants. In a wake vortex avoidance system, statistics on normal vortex behavior may be easily obtained. However, in order to assure absolute safety, the extremes of vortex residence time are of much more significance than a statistical definition of normal vortex behavior. The statistics of extreme values provides a rational basis for statistical description of vortex behavior for extremely long residence times.

This section presents a general description of the statistics of extreme values and its application to vortex technology. For a theoretical description of the statistics of extreme values, the reader is referred to references Z through B'. Although the statistical concepts presented here have not previously been applied to vortex technology, they will be described in terms of vortex technology. This section should not be contrued as being the ultimate application of the statistics of extreme values to vortex technology, but should only be construed as being an introduction of the subject.

The statistics of extreme values may be used to address three types of issues related to vortex technology:

> Given a data base consisting of a historical set of n measurements of vortex residence time, what is the probability that the mth largest value of the set will be exceeded i times in N additional measurements?

For a given set of n measurements of a random variable, the largest value measured in the n measurements is also a random variable. Given M sets of measurements of a random variable, what is the probability distribution function of the largest value of the random variable measured in each set? In vortex terms, if vortex residence times are measured over a fixed number of landings, what is the probability distribution function of the longest residence time measured in a time period of one hour?

Given a data base consisting of a historical set of n measurements of vortex residence time, what is the residence time for which the probability of occurrence is less than a defined number, P? For example, given a set of 10,000 vortex measurements, what is the residence time which has a probability of occurrence of less than 10^{-6}?

Ostensibly, it would be desirable to determine the "worst case". Statistically, however, such a "worst case" does not exist since for any "worst case" measured from a finite sample, it would always be possible that a greater worst case could be measured from a sample of equal size, and a greater "worst case" could almost always be found if a second sample of sufficient size were generated. Therefore, the cases with extremely small probabilities are examined, but they are not considered a "worst case".

Before the results of the statistics of extreme values are presented, the manner in which they might be applied to a WVAS are presented. Two levels of WVAS are envisioned. The first level is a meteorological WVAS with meteorological measurement, but without a vortex sensing system which would track vortices for each landing aircraft. The second level is a full WVAS with meteorological measurement and with a vortex sensing system which would track vortices for each landing aircraft and would provide a warning to following pilots when a vortex is active in the flight corridor between the middle marker and the touchdown zone. The implementation of either system would occur over a period of time as data bases sufficient to support either system are assembled.

At each site, the full WVAS would be initiated with the current 4/5/6/7 nmi. separation standards, and a data base consisting of measured vortex residence times would be established. Data bases for various bands of crosswind similar to those presented in Fig. 3-71 would be assembled. After a sufficient data base had been assembled, full implementation of the full

WVAS could occur. For the full WVAS, vortex tracking for each landing aircraft would be performed, and a visual warning would be provided to following pilots when a vortex is active in the flight corridor between the middle marker and the touchdown zone. If the following pilot reaches the middle marker with the warning on, he would then execute a missed approach. For a given band of crosswind, the aircraft separation distance would be chosen so that the probability of a missed approach would be less than some small probability (e.g., < 0.001). Thus, the historical data base is used with the statistics of extreme values to provide a rational basis for selecting separation distances which will assure that the probability of a missed approach is less than some defined value. As time passes, the data base will become larger, so that the appropriate separation distance can be defined more precisely. Additionally, it may be possible to partition the data base by additional meteorological parameters, such as atmospheric stability.

For the meteorological WVAS, the data bases established for the full WVAS would be used to establish appropriate separation distances so that the probability of vortex encounter is very small (e.g., < 10^{-7}). It is expected that the separation distances for the meteorological WVAS would be greater than they would be for the full WVAS, but that the meteorological WVAS would be used at airports with lower traffic than the airports with a full WVAS.

As illustrations of the statistics of extreme valuesg, three examples are presented: (1) the probability that vortex residence time will exceed a specified value for a single aircraft landing; (2) the probability that vortex residence time will exceed a given value i times during one hour of airport operation, and (3) the probability distribution function of the greatest vortex residence time over a period of one hour. For examples of the use of the statistics of extreme values for vortex applications, the vortex residence time distributions shown in Fig. 9-1 will be used. The data shown in Fig. 9-1 are not divided into bands of crosswind, although such division of data would probably be done for an operational system.

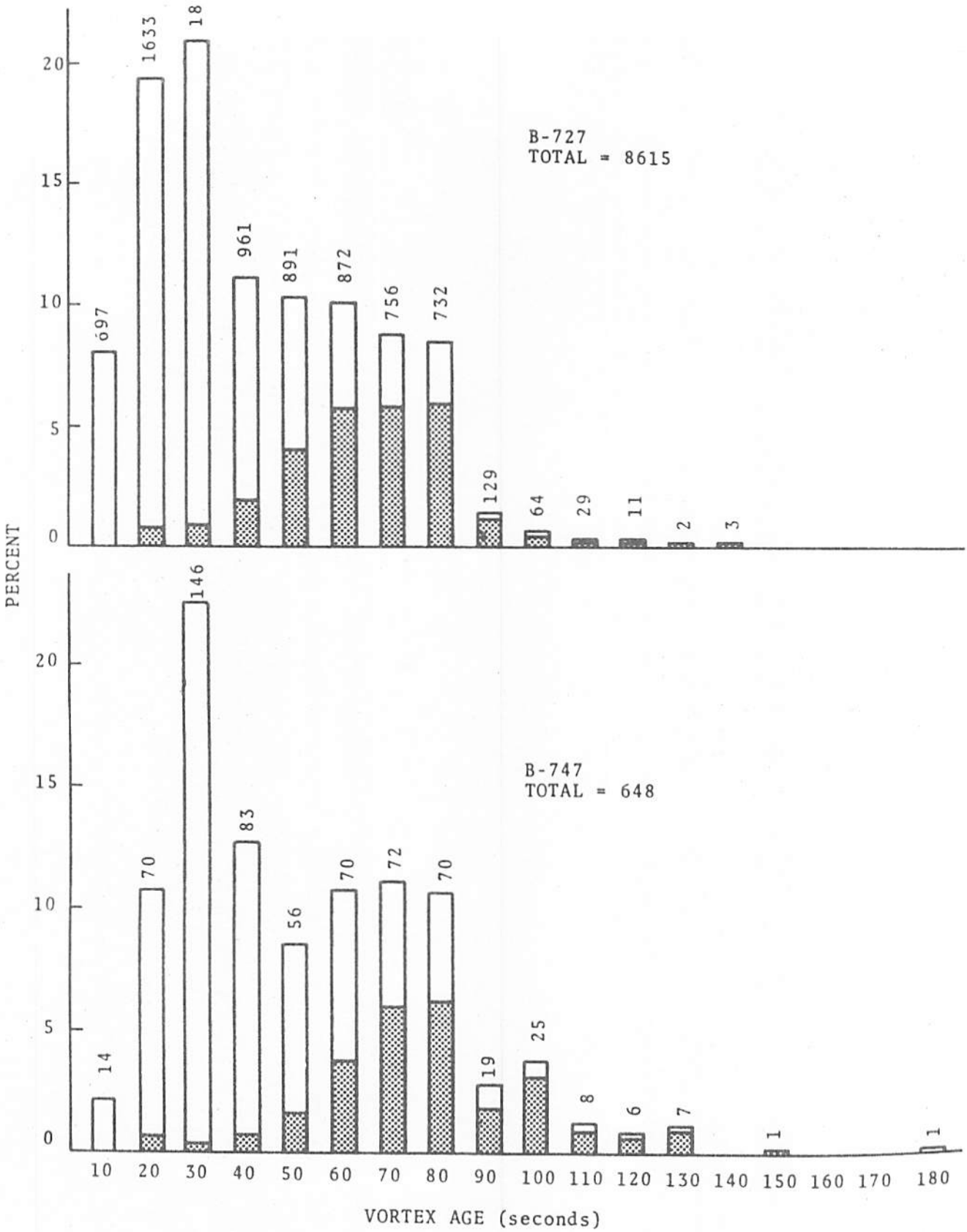

9-1

FIGURE 5. RESIDENCE TIME DATA FOR B-727 (TOP) AND B-747 (BOTTOM) AIRCRAFT

268

Given a set of n initial samples of a random variable, P(i,n,m,N) is the probability that the mth largest sample of the original set will be exceeded i times in a second sample of size, N. For example, given a data set of n vortex residence times, P(i,n,m,N) is the probability that in a future set of N measurements of residence time, the residence time of i vortex pairs will exceed the mth largest value of the original set. From ref. S,

$$P(i,n,m,N) = \frac{\binom{n}{m}\, m \binom{N}{i}}{(N+n)\binom{N+n-1}{i+m-1}} \tag{9.1}$$

which can be simplified to

$$P(i,n,m,N) = m\frac{(i+m-1)!}{i!\ m!}\ \frac{n!}{(n-m)!}\ \frac{N!}{(N-i)!}\ \frac{[(N+n)-(i+m)]!}{(N+n)!} \tag{9.2}$$

One of the distributions of interest in vortex technology is the overall probability distribution that a vortex residence time will exceed a specified value for a single aircraft landing. Figure 9-2 shows that probability for the B-727 data and for the B-747 data shown in Fig. 9-1. For the B-747, the number of samples in the original sample set is n = 648; the number of samples in the second sample set is N = 1 for a single aircraft landing. It is desired to know the probabilty that i = 1 from the second sample set will exceed the mth largest value from the original sample set.

As a second example, the probability that vortex residence time will exceed a given value i times during one hour of airport operation is desired. Let it be assumed that one hour or airport operation consists of 20 B-747 landings. Then in equation 9.2 , N = 20. Figure 9-3 shows the probability that the given residence time will be exceeded n times for 20 landings.

The drawback of the preceeding analysis is that it does not permit extrapolation beyond the greatest observed value of the finite data set, nor does it permit consideration of probabilities less than the reciprocal of the number of observations in the data set. Hence, it does not permit determiniation of vortex residence times of extremely small probabilities.

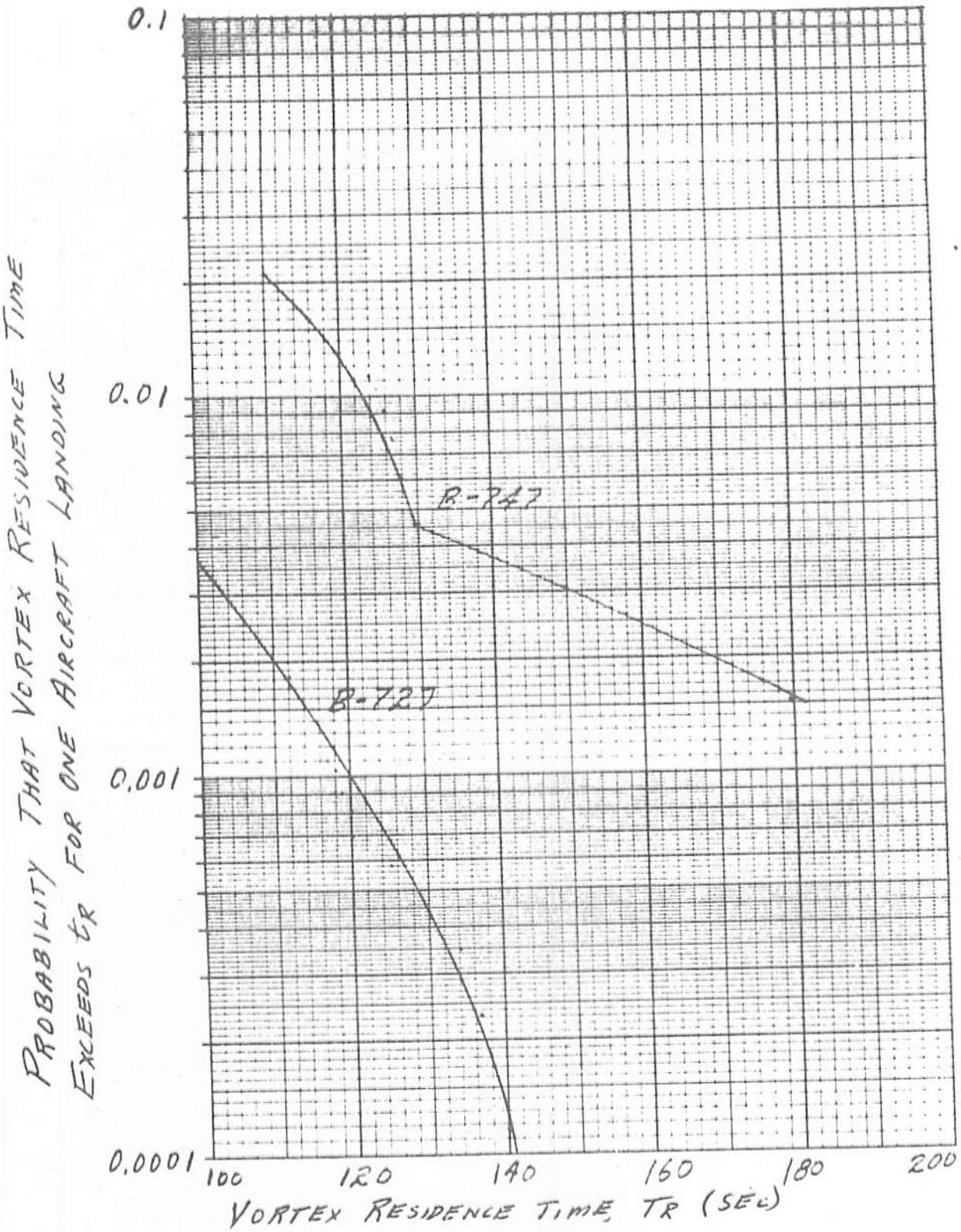

FIGURE 9-2 PROBABILITY THAT VORTEX RESIDENCE TIME EXCEEDS A GIVEN VALUE FOR ONE AIRCRAFT LANDING

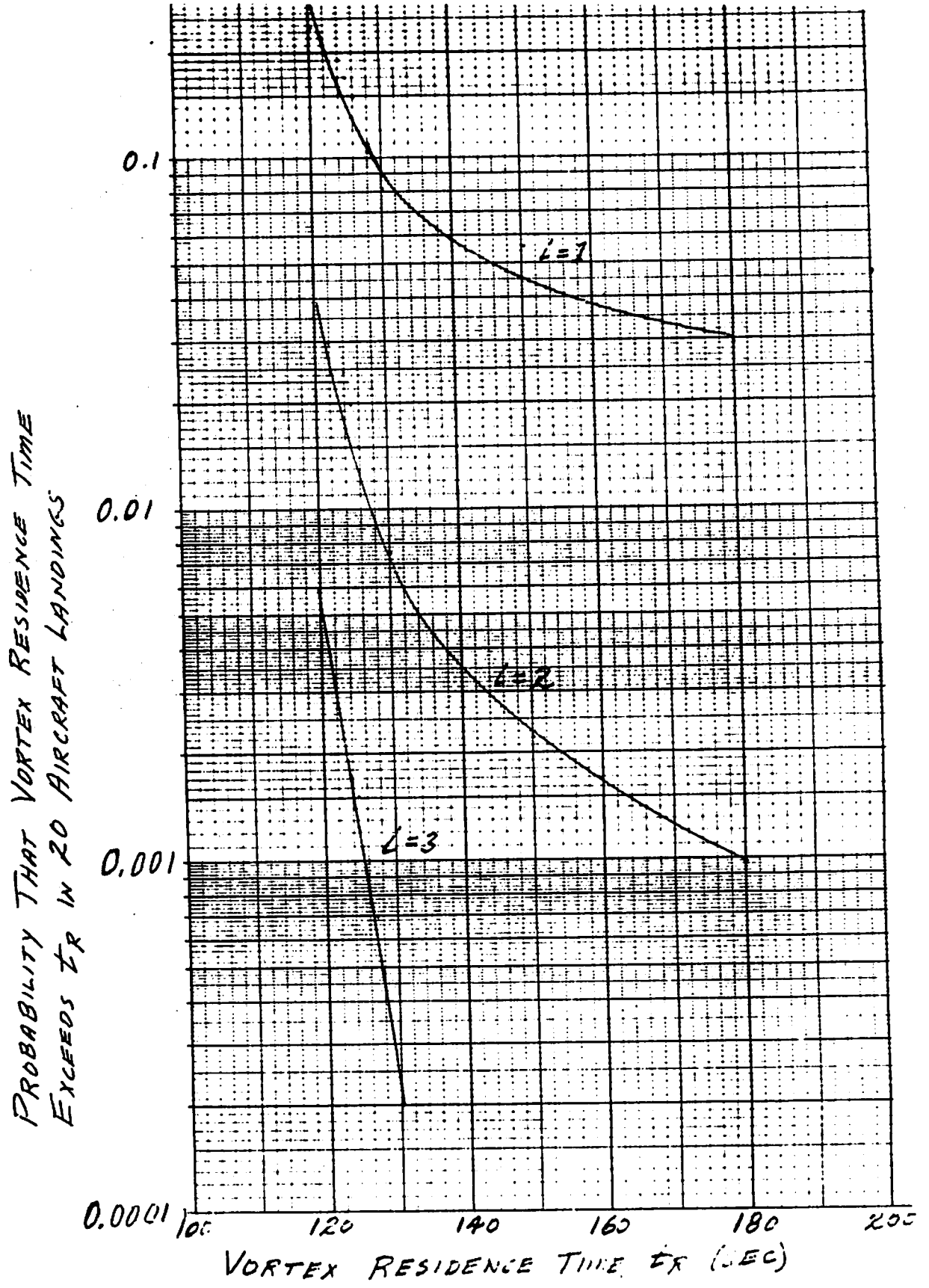

FIGURE 9-3. PROBABILITY THAT VORTEX RESIDENCE TIME EXCEEDS A GIVEN VALUE i TIMES FOR 20 AIRCRAFT LANDINGS.

In general, if a given random phenomenon conforms to a given mathematical form of a probability distribution function, it is not necessarily true that the phenomenon will conform to that mathematical form for extreme values. The statistics of extreme values can be developed without knowledge of the general form of the probability distribution function.

For this development, the B-747 data presented in Fig. 9-1 is used. Let it be assumed that the data consists of 16 hours of 40 landings per hour and that it is desired to obtain the overall probability distribution function for the greatest vortex residence time in a period of one hour (i.e., 40 landings). Figure 9-4 shows the decreasing probability distribution function of the maximum vortex residence time expected from 20 landings. It is noted that even though the maximum residence time which occurred in the data set was 180 sec, the distribution function includes the possibility of residence times in excess of 180 sec.

9.1 Kalman Filtering

The second mathematical technique which is applicable to vortex technology is Kalman filtering. There are three aspects to Kalman filtering:

Given a set of p measurements related to the measurement of n unknown quantities ($p > n$), with each of the measurements containing uncertainty because of measurement noise, make a best estimate of the values of the unknown quantities and specify the uncertainty in the estimate. This is called optimal estimation

Given a dynamic process for which equations of the process are known but are subject to random inputs and measurements which are subject to measurement inaccuracies (i.e., noise), make a best estimate of the values of the state variables as a function of time. If measurements before and after time, t, can be used to make an estimate of the value of the state variables at time, t, this is called optimal smoothing. The uncertainty in the estimate is also given.

Given the same situation as above, suppose that measurements are available up to time, t, but that projections of values of state variables at time, $t+t_1$ are desired. The class of Kalman filtering termed "optimal prediction" will make a best estimte of the state variables at time, t, based on the dynamic equations of the system and measurements up to that time. Optimal prediction will then predict a best estimate of the state variables at time, $t+t_1$, based upon the dynamic equations. The prediction will include a definition of the uncertainty at t and at $t+t_1$.

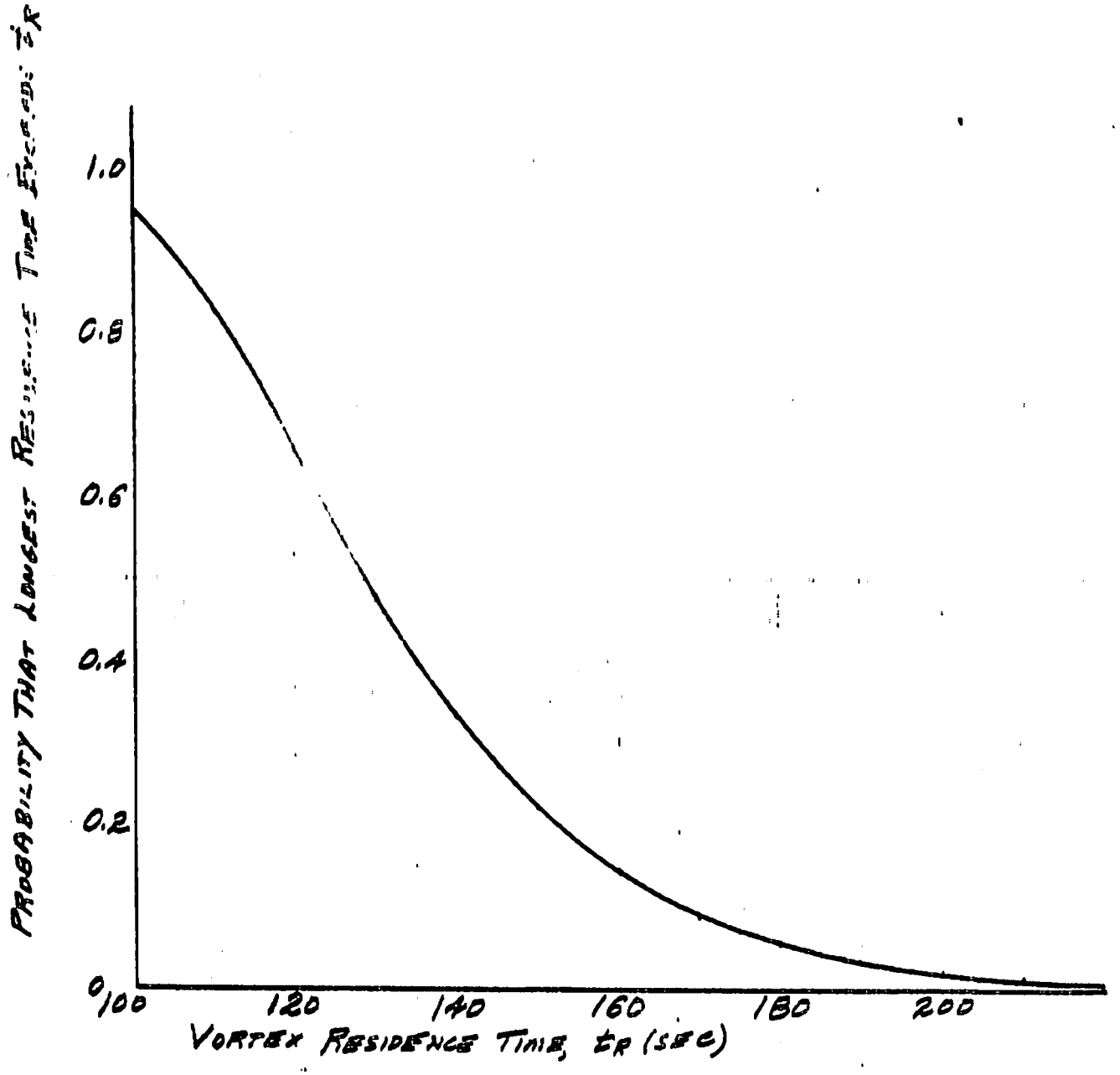

FIGURE 9-4 PROBABILITY DISTRIBUTION FUNCTION OF THE GREATEST VORTEX RESIDENCE TIME IN 20 B-747 LANDINGS

Kalman filtering is used in dynamic processes for which forcing functions contain a random component and for which measurements contain some measurement uncertainty. Kalman filtering is a rational method for combining the known analytical relationships with measurements to generate a best estimate for the values of the state variables of the system. This section presents the concepts of Kalman filtering and the applications of Kalman filtering to vortex technology. An excellent introductory description of the mathematics of Kalman filtering is given in ref. C'.

There are several potential applications of Kalman filtering to vortex technology. These include:

Most vortex detectors consist of an array of sensors at discrete locations normal to the extended runway centerline. Consequently, vortex tracking consists of determination of the discrete times at which the vortex passes over a given sensor in the array (as for monostatic acoustic sensors) or identification of the sensor closest to the vortex (as for groundwind vortex sensing systems). Kalman filtering would permit smoothing of the vortex trajectory from available data.

Kalman filtering uses data from all available measurements with the weighting applied to each measurement being inversely proportional to the uncertainty of the measurement. Thus, it can integrate data from several vortex sensors (i.e., SLDVS, MAVSS, GWVSS) into one best estimate of the vortex trajectory. For the GWVSS, initial accuracy may not be good because of vortex altitude; however, the GWVSS accruacy improves as the vortex approaches the gound. Therefore, the relative weight given to the GWVSS would increase as the vortex pair approaches the ground.

Because Kalman filtering uses measurements made over a period of time and is able to use all data to make better estimates as more data are obtained, parameters such as vortex strength and crosswind may be inferred from vortex trajectory data.

In an operational environment, Kalman filtering has several potential uses.

As described above, Kalman filtering will permit the inferrence of vortex strength from the vortex trajectory. Because of individual variations in aircraft weight, the initial vortex strength will be unknown in the operational environment. Therefore, Kalman filtering can be used to infer vortex strength soon after aircraft passage and make an early estimate of vortex residence time. As vortex transport proceeds, the estimate of residence time can be continually updated to give a running estimate of vortex residence time. This gives controllers and pilots an early warning of particular cases for which residence time may be long. For example, suppose an operational vortex detection system consists of a MAVSS and a GWVSS. The MAVSS would make a measurement of the initial descent rate soon after aircraft passage, and the GWVSS would simultaneously measure ambient crosswind. From this information, an initial estimate of vortex transport time could be made. As time passes, updates of projected vortex transport time would be made. All of this is contained within the mathematical structure of Kalman filtering.

For each time increment, Δt, Kalman filtering consists of two steps: an initial estimate of the state variables based upon an analytical expression for the dynamic process and a final estimate based upon measurement. At time, t, there exists a voctor, x_i, which is the best estimate of the values of the state variables of the dynamic process. There also exists a covariance matrix of the state variables, which is a measure of the uncertainty associated with each of the state variables. The first step uses an analytical expression for the transition from time, t, to time $t+\Delta t$.

$$X_{i+1} = \Phi x_i + G\omega \tag{9.3}$$

where

X_{i+1} = the vector of the estimated state variables at time, $t+\Delta t$,
x_i = the vector of the best estimate of the state variables at time, t
Φ = the transition matrix relating the state variables at time, t, to the states variables at time, $t+\Delta t$,
G = the transition matrix relating the values of the forcing function matrix to the state variables at time, $t+\Delta t$,
ω = the forcing function, which contains a random component.

The transition equation generates an initial best estimate of the values of the state variables at time, $t+\Delta t$, as well as a covariance matrix which represents the uncertainty in the values of the state variables at time, $t+\Delta t$. Let P be the covariance matrix (i.e., measure of uncertainty) of the state variable vector at time, t. Let Q be the covariance matrix (i.e., measure of randomness) of the forcing function, ω, at time, t. Then it can be shown that the covariance matrix of the best estimate, X_{i+1}, is

$$M = \Phi P \Phi^T + GQG^T \tag{9.4}$$

Because the forcing function, ω, has a random component, the uncertainty in the state variable vector, X_{i+1}, is greater than the uncertainty in the state variable vector, x.

After the best estimate at $t+\Delta t$ is made from the transition equation, a measurement is made. After measurement, the best estimate of the state vector is

$$x_{i+1} = X_{i+1} + PH^T R^{-1}(z_{i+1} - HX_{i+1}) \tag{9.5}$$

In equation (9.5) z_{i+1} the measurement which is related to the state variables by the known relationship

$$z = Hx + \nu \tag{9.6}$$

where z = vector of measurements made

H = a known matrix which relates the n-component state vector to the p-component measurement vector.

ν = measurement noise

R = covariance matrix of the measurement noise

After measurement, the uncertainty in the estimate of the state vector, x_{i+1}, is given by the covariance matrix

$$P = M - MH^T(R+HMH^T)^{-1}HM \tag{9.7}$$

Measurement decreases uncertainty. Therefore,

$$P < M \tag{9.8}$$

Equations (9.3) through (9.7) are used iteratively to derive a best estimate of the state vector as a function of time.

In the measurement equation, R is the covariance matrix of the measurement noise. If one of the measurement parameters is unavailable, then the "noise" for that measurement is set very large, and the measurement is essentially ignored. Kalman filtering uses all available information with the weight put on each available piece of information being inversely proportional to its uncertainty.

REFERENCES NOT NECESSARILY IN PREVIOUS STATE-OF-THE-ART REPORT

A. Hallock, J. N., "Monitoring the Movement of Wake Vortices at Kennedy and Stapleton Airports," In: Proceedings of 5th Annual Symposium of Society of Flight Test Engineers, 1974, p. 4/7-4/12.

B. McWilliams, I. G., "Hazard Extent About Aircraft Wake Vortices--An Analytic Approach," In: Proceedings of Aircraft Wake Vortices Conference, Trasnportation Systems Center, FAA-RD-77-68, June 1977, pp. 23-30.

C. Crow, S. C., "Stability Theory for a Pair of Trailing Vortices, AIAA J., Vol. 8, No. 12, Dec. 1970, pp. 2172-2179.

D. Atias, M. and D. Weihs, "Motion of Aircraft Trailing Vortices near the Ground," Journal of Aircraft, v.21, n.10, OCT 1984, pp. 783-786.

E. Burnham, D. C., "B-747 Vortex Alleviation Flight Tests: Ground-Based Sensor Measurements", DOT-FAA-RD-81-99, U. S. Department of Transportation/Transportation Systems Center, Cambridge MA, Feb 1982.

F. Brashears, M. R., A. D. Zalay, L. C. Chou, and K. R. Shrider, "Development of Predictive Wake Vortex Transport Model for Terminal Area Wake Vortex Avoidance," FAA-RD-76-94, Lockheed Missiles & Space Company, Inc., Huntsville AL, May 1976.

G. Hallock, J. N., W. D. Wood, and E. A. Spitzer, "Vortex Advisory System," In: Proceedings of 7th Conference on Aerospace and Aeronautical Meteorology," Nov 1976, pp. 162-166.

H Hallock, J. N., "Monitoring the Movement of Wake Vortices at Kennedy and Stapleton Airports," In: Proceedings of Aircraft Wake Vortices Conference, Transportation Systems Center, FAA-RD-77-68, June 1977, pp.23-30.

I. Hallock, J. N., B. P. Winston, D. C. Burnham, T. E. Sullivan, I. G. McWilliams, and W. D. Wood, "Joint US/UK Vortex Tracking Program at Heathrow International Airport," FAA-RD-76-58-II, vol. 2, Transportation Systems Center, Cambridge MA, Nov. 1977.

J. Sullivan, T. E., J. N. Hallock, and B. P. Winston, "Analysis of Ground-Wind Vortex Sensing System Data from O'Hare International Airport," FAA-RD-80-133, U. S. Department of Transportation/ Transportation Systems Center, Cambridge MA, Sept. 1980.

K. Eberle, W. R., M. R. Brashears, A. D. Zalay, K. R. Shrider, and D. A. Love, "Aircraft Wake Vortex Characteristics from Data Measured at John F. Kennedy International Airport," FAA-RD-78-47, Lockheed Missiles & Space Co., Inc., Huntsville AL, March 1978.

L. Burnham, D. C. and J. N. Hallock, "Chicago Monostatic Acoustic Vortex Sensing system, Volume IV: Wake Vortex Decay," DOT-TSC-FAA-79-18, IV, U. S. Department of Transportation/Transportation Systems Center, Cambridge MA, July 1982.

M. Yarmus, J. C., D. C. Burnham, A. Wright, and T. Talbot, "Aircraft Wake Vortex Takeoff Tests at O'Hare International Airport," DOT-TSC-FAA-84-??, U. S. Department of Transportation/Transportation Systems Center, Cambridge MA, Nov. 1984.

N. Tombach, I., P. B. S. Lissaman, J. B. Mullen, and S. J. Barker, "Aircraft Vortex Wake Decay Near the Ground," FAA-RD-77-46, AeroVironment, Inc., Pasadena CA, May 1977.

O. Dickson, R. E., "An Atmospheric Turbulence Model for the Dynamically Aimed Free-Flight Rocket (DAFFR) Error Analysis," Technical Report RD-82-1, U. S. Army Missile Command, Redstone Arsenal AL, Oct. 1981.

P. Van der Hoven, I., "Power Spectrum of Horizontal Wind Speed in the Frequency Range from 0.007 to 900 Cycles per Hour," Journal of Meteorology, v. 14, n. 4, April 1957, pp. 160-164.

Q. Slade, D. H. (Editor), "Meteorology and Atomic Energy," U. S. Atomic Energy Commission, Office of Information Services, 1968, p. 94

R. Lumley, J. L. and H. A. Panofsky, The Structure of Atmospheric Turbulence, Interscience Publishers, New York NY, 1968, p.176.

S. Burnham, D. C. and J. N. Hallock, "Chicago Monostatic Acoustic Vortex Sensing system, Volume I:," DOT-TSC-FAA-79-18, I, U. S. Department of Transportation/Transportation Systems Center, Cambridge MA, Date to Come

T. Burnham, D. C. and J. N. Hallock, "Chicago Monostatic Acoustic Vortex Sensing system, Volume II:, Decay of B-707 and DC-8 Vortices," DOT-TSC-FAA-79-18, II, U. S. Department of Transportation/ Transportation Systems Center, Cambridge MA, Sept. 1981.

U. Sullivan, T., J. Hallock, B. Winston, I. McWilliams, and D. Burnham, "Aircraft Wake Vortex Takeoff Tests at Toronto International Airport". Report No. FAA-RD-78-143, Research and Special Programs Administration, Transportation Systems Center, Cambridge MA, Feb. 1979.

V. Boston Logan Report

W. Hallock, J. N., "Vortex Advisory System Safety Analysis, Volume III: Summary of Laser Data Collection and Analysis," FAA-RD-78-68, III, U. S. Department of Transportation/Transportation Systems Center, Cambridge MA, Aug. 1979.

X. Moses Lake test

Y. Burnham, D. C. and S. A. Teager, "Preliminary Measurements of Helicopter Wake Vortex Velocity Profiles," DOT-TSC-FA527-PM-85-7 (Preliminary Version - Subject to Change), U. S. Department of Transportation, Transportation Systems Center, Cambridge MA, March 1985.

Z. Roberts, E. M. "Review of Statistics of Extreme Values with Applications to Air Quality Data, Part I, Review," Journal of the Air Pollution Control Association, v. 29, n.6, June 1979.

A'. Roberts, E. M. "Review of Statistics of Extreme Values with Applications to Air Quality Data, Part II, Applications," Journal of the Air Pollution Control Association, v. 29, n.6, July 1979.

B'. Gumbell, E. J., Statistical Theory of Extreme Values and Some Practical Applications, National Bureau of Standards, Applied Mathematics Serices 33, Washington, D. C., 1954.

C'. Bryson, A. and Ho, Y. C., Applied Optimal Control, John Wiley & Sons, New York, NY, 1975.